

Phenol-pyrazole ligands in the design of manganese(III) compounds:

Synthesis, structural characterization and study of the magnetic
properties.

PROEFSCHRIFT

Ter verkrijging van

de graad van Doctor aan de Universiteit Leiden,

op gezag van Rector Magnificus professor mr.P.F.van der Heijden,

volgens besluit van het College voor Promoties

te verdedigen op donderdag 22 oktober 2009

klokke 16.15 uur.

door

Marta Viciano Chumillas

geboren te Valencia, Spanje in 1980

Promotiecommissie

Promotor Prof. Dr. J. Reedijk

Prof. Dr. L. J. de Jongh

Co-promotor Dr. S. Tanase Grecea

Overige leden Dr. E. Bouwman (Universiteit Leiden, The Netherlands)

Prof. Dr. M. Julve (Universitat de València, Spain)

Prof. Dr. M. Drillon (Université Strasbourg, France)

Prof. Dr. J. Brouwer (Universiteit Leiden, The Netherlands)

Prof. Dr. J. M. van Ruitenbeek (Universiteit Leiden, The Netherlands)

This work has been supported financially by the European Networks MAGMANet, Network of Excellence (No. 515767) and QueMolNa (No. MRTN-CT-2003-504880).

Printed by Wöhrmann Print Service, Zutphen , The Netherlands, 2009.

Quan surts per fer el viatge cap a Ítaca,
has de pregar que el camí sigui llarg,
ple d'aventures, ple de coneixences.
Has de pregar que el camí sigui llarg,
que siguin moltes les matinades
que entraràs en un port que els teus ulls ignoraven,
i vagis a ciutats per aprendre dels que saben.
Tingues sempre al cor la idea d'Ítaca.
Has d'arribar-hi, és el teu destí,
però no forcis gens la travessia.
És preferible que duri molts anys,
que siguis vell quan fondegis l'illa,
ric de tot el que hauràs guanyat fent el camí,
sense esperar que et doni més riqueses.
Ítaca t'ha donat el bell viatge,
sense ella no hauries sortit.
I si la trobes pobra, no és que Ítaca
t'hagi enganyat. Savi, com bé t'has fet,
sabràs el que volen dir les Ítaques.

*(Part of Ítaca, song of L. Llach
based on a poem of K. Kavafis)*

A mis padres

Contents

List of abbreviations

Chapter 1	Introduction	7
Chapter 2	A family of mononuclear compounds: $[\text{Mn}(\text{HphpzR})_2\text{X}]$ ($\text{R} = \text{H}, \text{Me}, \text{Et}, \text{Ph}; \text{X}^- = \text{Cl}^-, \text{Br}^-$)	37
Chapter 3	Mononuclear compounds as building blocks for the design of trinuclear manganese(III) compounds with the $[\text{Mn}_3(\mu_3\text{-O})(\text{phpzR})_3]^+$ core	61
Chapter 4	From 1-D to isolated trinuclear compounds: impact of the co-ligand and the carboxylate on the core $[\text{Mn}_3(\mu_3\text{-O})(\text{phpzR})_3]^+$	89
Chapter 5	Manganese(III) compounds of high nuclearity	107
Chapter 6	Coordination versatility of 3(5)-methyl-5(3)-(2-hydroxyphenyl)-pyrazole with Co(III), Ni(II) and Cu(II) ions	123
Chapter 7	Summary, concluding remarks and perspectives	137
Appendix A	HF-EPR spectroscopic studies for $[\text{Mn}(\text{HphpzR})_2\text{X}]$ ($\text{X}^- = \text{Cl}^-, \text{Br}^-$) as complementary technique to magnetic susceptibility and specific heat techniques	145
Appendix B	Crystallographic information for compounds of Chapter 5	159
	Samenvatting	165
	Resumen	171
	Curriculum vitae	175
	List of publications	176
	Acknowledgements	177

List of abbreviations

H ₂ phpzH	3(5)-(2-Hydroxyphenyl)-pyrazole
H ₂ phpzMe	3(5)-(2-Hydroxyphenyl)-5(3)-methylpyrazole
H ₂ phpzEt	3(5)-(2-Hydroxyphenyl)-5(3)-ethylpyrazole
H ₂ phpzPh	3(5)-(2-Hydroxyphenyl)-5(3)-phenylpyrazole
H ₂ salen	N, N'-bis(salicylidene)ethylenediamine
DPPH	2,2-Diphenyl-1-picrylhydrazyl radical
IR	Infrared Spectroscopy
ESI-MS	Electrospray Mass Spectroscopy
NMR	Nuclear Magnetic Resonance
UV/VIS/NIR	Ultraviolet-Visible-Near Infrared
(HF)EPR	(High Field or High Frequency) Electron Paramagnetic Resonance
CV	Cyclic Voltammetry
SQUID	Superconducting Quantum Interference Device
AC	Alternating Current
DC	Direct Current
PPMS	Physical Property Measurement System
TGA	ThermoGravimetric Analysis
<i>g</i>	Electron gyromagnetic factor (2.002 for a free electron)
<i>A_N</i>	Hyperfine splitting parameter (G)
<i>k_B</i>	Boltzmann constant, $1.3806580 \times 10^{-23} \text{ JK}^{-1}$ ($0.69503877 \text{ cm}^{-1}\text{K}^{-1}$)
<i>N</i>	Avogadro's number, $6.022 \times 10^{23} \text{ mol}^{-1}$
β (μ_B)	Bohr Magnetron, $9.274 \times 10^{-24} \text{ JT}^{-1}$ ($4.66864374 \times 10^{-5} \text{ cm}^{-1}\text{G}^{-1}$)
χ_M	Molar magnetic susceptibility ($\text{cm}^3\text{mol}^{-1}$)
<i>B</i> (η)	Brillouin function
<i>J</i>	Magnetic exchange parameter (cm^{-1})
ZFS	Zero-Field Splitting
<i>D</i> , <i>E</i>	Zero-Field Splitting parameters, axial and rhombic components (cm^{-1})
<i>C_m</i>	Magnetic heat capacity ($\text{JK}^{-1}\text{mol}^{-1}$)
<i>C_l</i>	Lattice heat capacity ($\text{JK}^{-1}\text{mol}^{-1}$)
<i>R</i>	Gas constant, $8.314472 \text{ JK}^{-1}\text{mol}^{-1}$
<i>M</i>	Magnetization
<i>S_m</i>	Entropy ($\text{JK}^{-1}\text{mol}^{-1}$)
θ_D	Debye temperature (K)
λ	Molecular field constant
θ	Curie-Weiss temperature
SMM	Single-molecule magnet
<i>S_T</i>	Spin ground state

Chapter 1

Introduction*

The aim of the thesis is the synthesis of mainly manganese complexes with phenol-pyrazole ligands. The chapter starts with the goal and outline of the thesis. To justify the use of phenol-pyrazole ligands, this chapter concludes with an overview of the role of pyrazole-based ligands in the formation of transition-metal clusters. The ability of the pyrazole ligand to provide a pathway for magnetic exchange interactions is highlighted.

* Parts of this chapter will be submitted for publication: Viciano-Chumillas M., Tanase S., de Jongh L.J., Reedijk J.

1.1. Introduction

In the last decades, many efforts have been made to control matter at the molecular level, in a length scale range of 1–100 nm. Researchers have progressively developed, characterized and addressed new materials that can be used for technological applications, such as in medicine, electronics, catalysis, etc.¹ Two main approaches are taken to miniaturize the size of the materials, the first of which is the so-called “top-down” approach, which comes down to the fragmentation of already known materials. This approach is based on miniaturizing techniques, such as machining, templating or lithographic techniques.² The disadvantages are the lack of atomic-level control and the limitations of the size. The other approach is called the “bottom-up”, which is based on self-assembly of molecular precursor building blocks into larger structures. The advantages are the lower costs as compared with the “top-down” approach and the good control to scale the dimensions.^{3,4}

Materials reduced to the nanoscale can show new physical properties, associated with quantum effects, enabling unique applications.^{3,5,6} One of these properties is associated with magnetism. In this sense, a new field entitled *molecular magnetism* has emerged in the last years.^{3,5,6} This is an interdisciplinary field, where chemists design and synthesize new magnetic molecules and physicists develop techniques to understand in more detail their novel magnetic properties.⁷ The key property of a bulk magnet is that, below a critical, magnetic ordering temperature, T_C , it exhibits spontaneous magnetization. It means that it remains magnetized after the removal of magnetic field. Molecule-based magnets, *i.e.* magnets made from molecules, constitute a broad emerging class of new materials that extend the properties typically associated with magnets to include some advantages such as low-density, transparency, electrical insulation, solubility, biocompatibility and the possibility of low-temperature fabrication.^{3,5,6}

The origin of the magnetic moments in molecular magnetic materials, just as in bulk, is the unpaired electrons of transition-metal ions, rare-earth ions or organic radicals of which the molecules are composed. Transition-metal ions and rare-earth ions require a magnetic or diamagnetic ligand to be stabilized in a molecular unit. Therefore, the magnetic properties of molecular polymetallic systems derive from the intramolecular exchange interactions between the paramagnetic metal ions through the bridging ligands. In particular, to design polymetallic clusters, small ligands are necessary to provide efficient bridges and to determine the growth of the cluster. Often these ligands are monoatomic ligands, such as O^{2-} , S^{2-} , F^- , *etc.*, or ligands with a single donor atom, like OH^- , OR^- , which are known to transmit the magnetic interactions effectively. In addition, blocking or terminal ligands are required to prevent the growth of the cluster and to avoid the formation of polymeric structures.

Two strategies for the synthesis of polymetallic clusters have been largely developed depending on the choice of the polydentate ligand. One strategy is just serendipity, in which flexible ligands are used, such as pyridonate⁸ or carboxylate ligands,⁹ which have been the most studied bridging ligands. The identity of the final products is very difficult to predict, because of the large variety of orientations and binding modes of the ligand that impose little or no geometric effect.¹⁰ The other strategy is based on a more rational design that can be performed by using rigid ligands, such as cyanide,¹¹ or polytopic picolinic-hydrazone ligands.¹² In the latter case, the ligand imposes the geometry of the cluster and the results are more predictable.^{13,14} Synthetic strategies involve the use of preformed simple molecules, *i.e.* building blocks with a tendency of self-assembly to form more complex molecules. Some examples of building blocks are hexacyanidometalates,¹⁵⁻¹⁷ trinuclear manganese complexes,⁹ or mononuclear manganese(III) salen complexes.¹⁸

In the design of polymetallic clusters, parameters like the pH of the solution, the solvent or the metal to ligand ratio, can also determine the variety of products. However, the choice of a suitable polydentate ligand remains essential, since two requirements need to be fulfilled: the ability to bridge more than one metal ion and to provide a suitable intramolecular pathway for magnetic exchange interactions.

1.2. Aim of this thesis

The purpose of this thesis research is to develop new synthetic strategies to obtain molecular-based magnetic materials, exploring the coordination chemistry of phenol-pyrazole ligands as bridging ligands. Carboxylates and Schiff-base derivative ligands are widely studied for the formation of polymetallic complexes.^{9,18} However, the synthesis of polymetallic clusters containing new ligands is still rather limited. Many pyrazole-based ligands have the ability to bridge two metal ions and to provide an effective magnetic-exchange pathway between them. The chemistry and the magnetic properties of dinuclear pyrazolate compounds are well understood.¹⁹⁻²² However, the research focused on polynuclear compounds,^{23,24} especially dealing with high-nuclearity clusters is still developing.²⁵ Variations in the substituents on the pyrazole ring can control the distances between the metal ions and the electronic and magnetic properties. Therefore, a phenol moiety has been introduced as a substituent on the pyrazole ring to increase the number of possible coordination sites. Only a few examples of polymetallic clusters have been reported until now with phenol-pyrazole ligands and most of them have been obtained in the course of this thesis project.²⁶⁻³¹ Following earlier promising results in our group,^{30,32} a family of phenol-pyrazole

ligands has been synthesized with the main difference on the substituent in the fifth position of the pyrazole group (Figure 1.1).

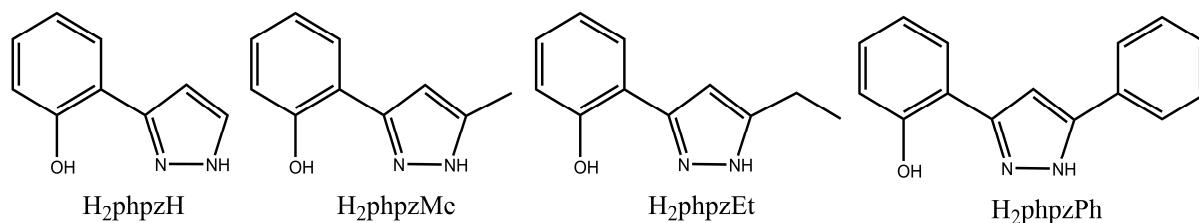


Figure 1.1. Phenol-pyrazole ligands (H_2phpzR ; $R = H, Me, Et, Ph$) employed in this thesis.

The ligand is crucial in the organization of the paramagnetic metal ion. Nevertheless, the choice of the magnetic carrier is essential, since the origin of the magnetic moment resides in the electrons. In this thesis project, the manganese metal ion has been chosen to explore its coordination chemistry, because of some special advantages. Manganese displays a large variation in oxidation states, *e.g.* manganese(II) (d^5), manganese(III) (d^4) and manganese(IV) (d^3) for the formation of complexes. Most of these types of manganese cations behave as a hard Lewis acid. So they are well stabilized by O-donor ligands. In most of the manganese complexes, the manganese(II) and manganese(III) ions are high-spin with a large number of unpaired electrons.³³ Besides the paramagnetic nature of the manganese ion in various oxidation states, another crucial characteristic is the negative Ising type of anisotropy that the manganese(III) ion displays due to the Jahn-Teller distortion, which can provide additional interesting magnetic properties.^{7,34}

In the following section of the present chapter, the choice of phenol-pyrazole ligands in this thesis as bridging ligands is justified with an overview of polynuclear metallic clusters containing pyrazole-based ligands.

In Chapter 2, the synthesis and the magnetic and thermal properties are presented of a family of mononuclear manganese(III) compounds with the general formula $[Mn(HphpzR)_2X]$ ($R = H, Me, Et, Ph$; $X^- = Cl^-, Br^-$). The influence of the type of ligand is reflected in the crystal packing and the magnetic properties of the compounds.³⁵

Chapter 3 deals with the use of some of the mononuclear compounds presented in Chapter 2 as building blocks to form trinuclear manganese(III) compounds with the $[Mn_3(\mu_3-O)(phpzR)_3]^+$ core. The chapter contains a study of the magneto-structural correlations of all the oxide-centred trinuclear manganese(III) compounds reported in the literature.³⁶ In Chapter 4, the impact of the co-ligands on the trinuclear compounds with the core $[Mn_3(\mu_3-O)(phpzR)_3]^+$ is described.³⁷

Chapter 5 is devoted to some high-nuclearity manganese(III) clusters. The formation and the stability of the core and the magnetic properties depending on the type of phenol-pyrazole ligands and the reaction conditions are discussed.

Chapter 6 describes the coordination versatility of H₂phpzMe ligand with transition-metal ions other than the manganese(III) ion.³⁸

Chapter 7 presents the summary and conclusions of this work, as well as some future prospects.

In Appendix A, HFEPR studies are described, dealing with two mononuclear manganese(III) compounds presented in Chapter 2 to determine the sign and magnitude of the zero-field splitting parameters. In Appendix B, crystallographic data of the compounds presented in Chapter 5 is reported.

Parts of this thesis have been published (Chapter 2, 3, 4 and 6),³⁵⁻³⁸ or will be submitted for publication (Chapter 1 and Chapter 5).

1.3. Coordination versatility of pyrazole-based ligands towards high-nuclearity transition-metal clusters

1.3.1. Introduction

The choice of the bridging ligand is crucial in the formation of polynuclear cluster compounds. In this thesis, phenol-pyrazole ligands have been chosen because as had been established with numerous polynuclear compounds,^{23,24} pyrazole ligands fulfil both conditions, they can bridge more than one metal ion and they provide a suitable intramolecular pathway for magnetic exchange interactions. In the present section, the coordination versatility of pyrazole-based ligands towards the formation of polymetallic compounds,²⁵ especially dealing with high-nuclearity clusters is illustrated.

1.3.2. Pyrazole

Pyrazoles are five-membered heterocyclic aromatic rings consisting of three carbon atoms and two nitrogen atoms at the positions 1 and 2 (Figure 1.2). The N(1)-H has an acid character due to the proton, whereas the N(2) has a basic lone pair in the sp² orbital. Therefore a basic character is present. Tautomerism exists in the case of symmetrical substitution, or non-substitution on the ring, unless the substituent is in position 1, because the rupture of the N-C bond is more difficult than that of the N-H bond. Five-membered heterocycles, such as pyrazoles, are π -excessive. As a consequence they are poorer π -acceptor and better π -donors than six-membered heterocycles. Hence, they can act as a hard donor site.^{39,40} Numerous

synthetic routes have been used to obtain pyrazole-based ligands. However, two routes are the most important: the condensation of a 1,3-diketone (1,3-dicarbonyl) with hydrazine derivatives and the 1,3-dipolar cycloaddition of diazoalkane with alkynes.⁴¹

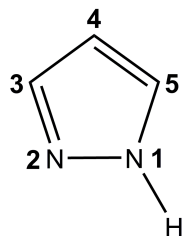


Figure 1.2. Pyrazole (Hpz).

Pyrazoles can behave either as monodentate or as bidentate ligands, after deprotonation of the N(1)–H group. The pyrazolato anion can act as an endo- (η^2), or an exo-bidentate ($\eta^1-\eta^1$) bridging ligand in the form of the pyrazolato anion (Figure 1.3). This coordination ability or nucleophilicity is controlled by the nature of the metal ion and the substituents on the pyrazole ring. Substituents at the 3- and 5-positions modify the steric properties, whereas substituents at the 4-position, can mainly change the electronic properties.

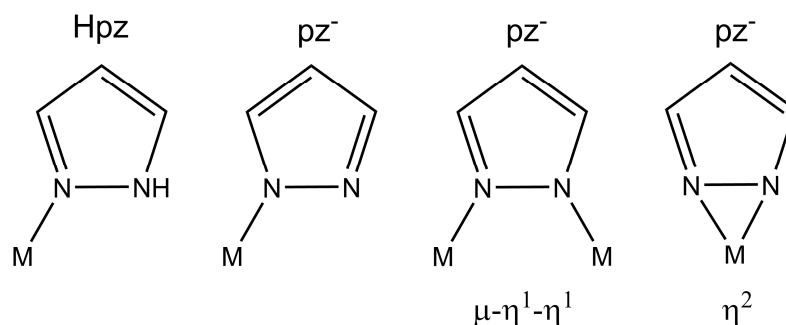


Figure 1.3. Common coordination modes of the pyrazole ligand and the corresponding anionic ligand.

The study of the coordination chemistry with pyrazole ligands began in 1889 with the report of a silver pyrazole complex, $[\text{Ag}(\text{pz})]_n$.⁴² Much later, Trofimenko *et al.* stimulated the research with the introduction of poly(pyrazolyl)borate chelating ligands in coordination chemistry.⁴³⁻⁴⁶ After this discovery, numerous papers and reviews have been written illustrating the rich coordination chemistry of pyrazole-based ligands.^{39,40,47-50} In the literature, three main reviews have been reported dealing with polynuclear compounds²³⁻²⁵. The first review was published in 1997 illustrating the catalytic activity of polynuclear heteroatom-bridged pyrazole complexes.²⁴ Two other reviews have appeared more recently.^{23,25} One of them deals with di-, oligo- and polynuclear transition-metal complexes with substituted pyrazole ligands having chelating side arms.²³ The other review describes metal-cluster compounds with pyrazole-based ligands.²⁵

1.3.3. Clusters with pyrazole-based ligands

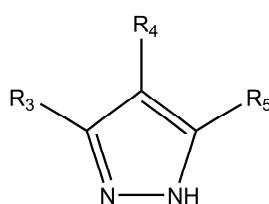
1.3.3.1. Introduction

In this section, the aim is to provide an overview of the pyrazole-based ligands used to form transition-metal clusters. In addition, the ability of pyrazole to provide a pathway for magnetic exchange interactions is highlighted. Only in the last decade, a significant development has been achieved in the coordination chemistry with pyrazole ligands to form polynuclear clusters. Three main reviews dealing with polynuclear complexes have already appeared.²³⁻²⁵ Hence, pyrazoles substituted at *N1* position, polymers and dinuclear compounds are not discussed.

As described above, the pyrazole and the pyrazolato anion have numerous coordination modes, providing versatile coordination chemistry. The most common modes are shown in Figure 1.3. Deprotonated pyrazoles can link two metal ions resulting in a metal-metal distance between 3.5–4.5 Å. Changes in the substituents of the pyrazole ring can induce changes in the intermetallic distances, hence controlling the magnetic exchange interactions. Therefore, the compounds discussed in this text are grouped depending on the type of substituents in the pyrazole ligand.

1.3.3.2. Pyrazole ligands with non-coordinating substituents

A significant number of cluster compounds containing pyrazole ligands has been obtained to date.²⁵ Most of the cluster compounds incorporate the pyrazole ligand or the pyrazole ligand with non-coordinating substituents, such as Br, NO₂, Me, Mes (2,4,6-trimethylphenyl), *etc.* in the 3-, 4-, or 5-position of the pyrazole ring (HR-pz). In this section, a summary is presented of these cluster compounds reported in the literature. Figure 1.4 shows some of the pyrazole ligands discussed in this section.



Ligand	R ₃	R ₄	R ₅	Ligand	R ₃	R ₄	R ₅	Ligand	R ₃	R ₄	R ₅
HL1a	H	H	H	HL1e	H	I	H	HL1i	H	H	^t Bu
HL1b	H	Me	H	HL1f	H	NO ₂	H	HL1j	H	H	4-F-Ph
HL1c	H	Cl	H	HL1g	H	CHO	H	HL1k	Me	H	Me
HL1d	H	Br	H	HL1h	H	H	Mes	HL1l	CF ₃	H	CF ₃

Figure 1.4. Some of the discussed pyrazole ligands with non-coordinating substituents.

Trinuclear complexes are the most common clusters with pyrazole ligands or pyrazole derivatives containing non-coordinating substituents, in which the compound can adopt two different types of structure. The first type is a linear structure which can be formed when the pyrazole is deprotonated and it bridges the metal ions as shown in Figure 1.5a, whereas other ligands are found at the terminal positions, *i.e.* halogens, acetylacetonate, non-deprotonated pyrazoles or cyclopentadienyl ligands. Some examples are reported with nickel(II),^{51,52} cobalt(II),^{53,54} palladium(II) ions,⁵⁴ and palladium(II)/cobalt(II) mixtures.⁵⁴ Weak antiferromagnetic interactions are observed between the paramagnetic metal ions in all the cases.

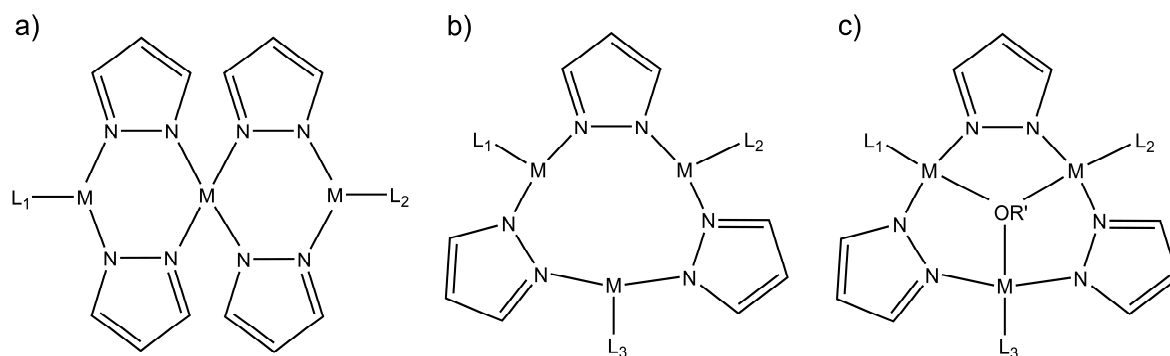


Figure 1.5. Trinuclear types of pyrazole-bridged compounds.

The second possible type of structure that trinuclear compounds can adopt is the triangle, in which the transition-metal ions are at the vertexes of a triangle (Figure 1.5b,c). Monovalent group 11 ions (copper(I), silver(I) and gold(I)) and mercury(II) ions form compounds with a general formula $[M(R-pz)]_3$ (Figure 1.5b).⁵⁵⁻⁶² In some cases, the distance between the trinuclear units is small, forming dimers of trimers.⁶³⁻⁶⁶ Luminescence properties were studied in some of this type of complexes.^{61,67} Trinuclear heterobimetallic gold(I)-silver(I) compounds have been synthesized with 3,5-diphenylpyrazole and other type of bridging ligands.^{68,69} Compounds with the general formula $[M_3(R-pz)_6]$ are formed with divalent metal ions, *i.e.*, palladium(II),⁷⁰ platinum(II)⁷¹ or platinum(II/III) ions.⁷¹

$[M_3-\mu_3-O(R')]^m+$ ($R' = H, Me, m = 4, 5, 7$) centred triangles have been reported with several transition-metal ions, such as iron(III), cobalt(II/III) and copper(II) ions (Figure 1.5c). The compound $X_4[Fe_3(\mu_3-O)(L1f)_6Cl_3]Cl_2$ ($X^+ = HNEt_3^+, Bu_4N^+, PPh_4^+$) has a structure which resembles the basic carboxylates because of the presence of six pyrazole ligands.⁷² Mössbauer spectra, magnetic susceptibility and EPR studies have revealed the presence of antiferromagnetic interactions between the iron(III) ions and the achievement of a ground state of $S_T = 1/2$. In this case, the pyrazole ligands mediate stronger antiferromagnetic interactions than the analogous carboxylates.⁷² Another example is $[Co_3(\mu_3-OH)(L1a)_4(dbm)_3] \cdot 2THF$ (Hdbm = dibenzoylmethane) that is a mixed-valence

cobalt(II/III) compound with a μ_3 -hydroxide bridge for which catalytic activity in the oxidation of the hydrocarbons has been reported.⁷³ Numerous compounds have been synthesized with copper(II) ion. Many of them have been reported by Raptis and co-workers,⁷⁴⁻⁸⁰ who have studied the influence of non-coordinating substituents on the pyrazole ring and of the terminal ligands, L, present in the triangle. The general formula of these complexes is $[\text{Cu}_3(\mu_3\text{-OR}')(\text{R-pz})_3\text{L}_3]^{m+}$ ($\text{R}' = \text{H, Me}$; $\text{L} = \text{Cl}^-, \text{Br}^-, \text{Hpz}, \text{RCO}_2^-, \text{HL1g}, \text{H}_2\text{O}, \text{EtOH}$; $\text{R-pz}^- = \text{L1a}^-, \text{L1f}^-, \text{L1h}^-$ and $m = 0, 1, 2$).⁷⁴⁻⁸⁹ Most of the trinuclear centred copper(II) triangles are synthesized from a copper(II) salt and the pyrazole ligand in a molar ratio 1/1 or 1/2 in the presence of base and using different counter ions.⁷⁴ Other possible synthetic routes are: the substitution of the terminal ligand, L, or the centred anion, in a preformed trinuclear compound, or the addition of a bridging ligand such as carboxylate, an acid, a base or NaBr.^{74,77,78,81,83} The control of the pH is crucial in the formation of new triangles, since numerous species often exist in solution. In some cases, compounds of higher nuclearity, or even polymers are obtained, in which the trinuclear structure can be retained.^{79,81-85} Another synthetic route to obtain trinuclear-centred copper(II) compounds is by oxidation of mononuclear copper(I) complexes.⁸⁶ Apparently, the introduction of substituents in the 4-position of the aromatic ring does not affect the formation of trinuclear copper(II) complexes. However, the use of 3,5-substituted pyrazoles precludes the formation of the triangle, because of the steric effects of such side groups in the ligand. In these cases, mononuclear or dinuclear copper(II) complexes are obtained.^{77,82} So far in only one case with substituents at the 3,5-positions, the trinuclear structure is retained.⁸⁷ Following similar procedures as those described for the synthesis of O(R')-centred copper(II) triangles ($\text{R}' = \text{H, Me}$), but with different amounts of the counter ion, the formation of new compounds with the formula $[\text{Cu}_3(\mu_3\text{-X})_2(\text{R-pz})_3\text{X}_3]^{2-}$ ($\text{X}^- = \text{Cl}^-, \text{Br}^-$ and $\text{R-pz}^- = \text{L1a}^--\text{L1f}^-$) can be achieved (Figure 1.6).^{74-77,79} Trinuclear copper(II) compounds with two types of bridging ligands, such as hydroxide and chloride ligands for $[\text{Cu}_3(\mu_3\text{-OH})(\mu\text{-Cl})\text{Cl}(\text{L1a})_3(\text{HL1a})_2]$,⁹⁰ and oxide and perchlorate ligands for $[\text{Cu}_3(\mu_3\text{-O})(\text{L1a})_3(\text{HL1a})_3(\mu_1, \mu_2\text{-ClO}_4)] \cdot \text{CH}_3\text{OH}$,⁹¹ have also been reported.

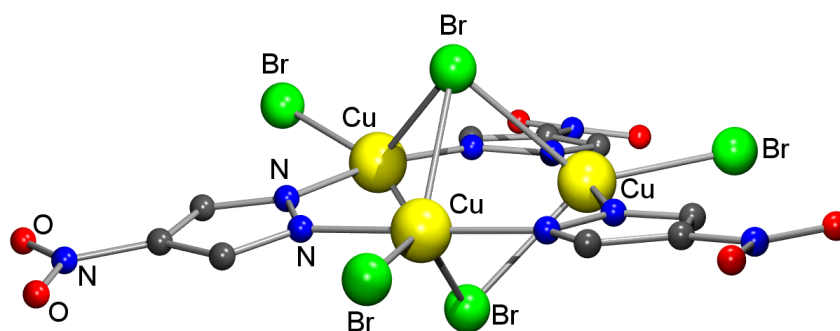


Figure 1.6. Molecular structure of the anion $[\text{Cu}_3(\mu_3\text{-Br})_2(\text{L1f})_3\text{Br}_3]^{2-}$.⁷⁵

The introduction of substituents on the pyrazole ring does not induce any significant structural differences, such as Cu...Cu distances or Cu- μ_3 -O(R') (R' = H, Me) distances in the trinuclear copper(II) core. The main difference is the distortion of the Cu- μ -Y-Cu angle from going to μ -O²⁻, OH⁻, μ -X (X⁻ = Cl⁻, Br⁻). Magnetic susceptibility and EPR studies have been performed for some of the compounds (Table 1.1). Strong antiferromagnetic interactions between the copper(II) ions are operative in the case of the compounds with a Cu- μ_3 -Y-Cu angle of *ca.* 120° (Y²⁻ = O²⁻). Apparently, a decrease in magnitude of the antiferromagnetic exchange interaction is observed when the Cu- μ_3 -Y-Cu angle decreases (Y⁻ = OH⁻) and ferromagnetic interactions become operative when the Cu- μ_3 -Y-Cu angle is *ca.* 80° (Y⁻ = Cl⁻, Br⁻). This change of the magnetic behaviour can be explained by the principles of the orbital complementarity and overlapping.⁷⁵ Small values of the magnetic susceptibility at low temperature are common in O(R)-centred copper(II) triangles.^{87,90} This phenomenon can be described by the presence of antisymmetric exchange between the copper(II) ions in view of the magnetic susceptibility and EPR studies.⁸⁷

Electrochemical studies have been performed for the compounds containing the core [Cu₃(μ_3 -O(R'))(R-pz)₃L₃]^{m-/+} (R' = H; R-pz⁻ = L1a⁻, L1c⁻, L1d⁻, L1g⁻, L1f⁻; L = Cl⁻, NCS⁻, py, CH₃CO₂⁻, CF₃CO₂⁻ and *m* = 1, 2).^{76,88} A shift of the redox potentials has been observed depending on the substituents at the fourth position of the pyrazole ligand and also on the terminal ligand, L.^{76,88} The catalytic activity of some trinuclear copper(II) compounds has been tested in the cyclopropanation of styrene⁸³ and in the peroxidation of alkanes.^{84,85}

Mononuclear and trinuclear complexes with pyrazole ligands have been used as starting materials to achieve compounds of higher nuclearity by addition of bridging ligands, such as carboxylate, pyridazine or nitrate ligands.^{55,79,92,93} Also, pyrazole-based ligands have been used to bridge mononuclear compounds to form tetranuclear copper(II) compounds,⁹⁴ or to bridge two trinuclear units thus forming hexanuclear copper(II) compounds.⁸⁰

Tetranuclear copper(II) compounds can also be synthesized from the copper(II) salt, the pyrazole ligand, another type of ligand and a base. As a result, the pyrazolate anion bridges two dinuclear units.^{95,96} An example is the compound with the formula [Cu₄(L1a)₄L₂]ClO₄ (HL = 1,3-diamino-2-propanol), in which the dinuclear unit is formed by two copper(II) ions bridged by a pyrazolato ligand and by 1,3-diamino-2-propanol.⁹⁵ Another example is the compound [Cu₄L₂(L1a)₄(CH₃OH)₂](ClO₄)₂ (L = 1,1-di-(2-pyridyl)-1-methoxymethanol).⁹⁶ Magnetic susceptibility studies define both compounds as dinuclear complexes with weak antiferromagnetic interactions between the dinuclear copper(II) units, ascribed to the countercomplementary behaviour of the bridging pyrazole that decreases the value of the magnetic exchange imposed by the other bridging ligand.^{95,96} One more example is the

compound $[\text{Cu}_4\text{F}_2(\mu_4\text{-F})(\text{L1j})_5(\text{HL1j})_4]$ that contains a $\mu_4\text{-F}$ bridge between the four copper(II) ions that interact antiferromagnetically.⁹⁷ A tetranuclear zirconium(IV) compound is obtained by conversion of a dinuclear compound in wet toluene.⁹⁸ Tetranuclear heterobimetallic compounds with palladium(II) ions have also been reported.^{70,99} Some of the tetranuclear compounds that are reported in the literature were minor side products that were only characterized by X-ray crystallography.^{100,101}

Table 1.1. Magnetic and structural data for trinuclear copper(II) compounds.

Compound	Cu–Y–Cu <i>a</i>	Cu ₃ – μ_3 -Y <i>b</i>	<i>J</i> /cm ⁻¹ <i>c</i>	<i>g</i> ^{<i>d</i>}	<i>g</i> ^{<i>e</i>}	Ref
(PPN) ₂ [Cu ₃ (μ_3 -O)(L1a) ₃ Cl ₃]	119.59 119.59 120.82	n.r.	-500	2.1	n.r.	74
(PPN) ₂ [Cu ₃ (μ_3 -OH)(L1a) ₃ Cl ₃]	118.54 117.26 104.38	0.524	n.r.	n.r.	n.r.	74
[Cu ₃ (μ_3 -OH)(L1a) ₃ (MeCO ₂) ₂ (HL1a)]	118.0 115.5 102.6	0.563	< 0	n.r.	<i>g</i> _{xx} = 2.015 <i>g</i> _{yy} = 2.050 <i>g</i> _{zz} = 2.200	83
[Cu ₃ (OH)Cl ₂ (L1a) ₃ (py) ₂] \cdot py	102.2 113.3 70.93	n.r.	-148 -23	2.17	n.r.	90
[Cu ₃ (OH)(L1a) ₃ (HL1a) ₂ (NO ₃) ₂] \cdot H ₂ O	112.0 115.0 116.4	0.478	< 0	n.r.	2.1	86
[Cu ₃ (μ_3 -OH)(L1a) ₃ (HL1a) ₂ (Me ₃ CCO ₂) ₂] (Me ₃ CCOOH) ₂	116.32 111.98 108.40	0.567	-117.7 -90.3 -90.3	2.047	n.r.	89
(Bu ₄ N) ₂ [Cu ₃ (μ_3 -Cl) ₂ (L1a) ₃ Cl ₃]	86.05	n.r.	+28.6	2.07	<i>g</i> _⊥ = 2.05 <i>g</i> _∥ = 2.11	74, 75
(Bu ₄ N) ₂ [Cu ₃ (μ_3 -Br) ₂ (L1f) ₃ Br ₃]	77.41- 81.07	n.r.	+3.1	<i>g</i> _⊥ = 2.46 <i>g</i> _∥ = 2.42	<i>g</i> _⊥ = 2.01 <i>g</i> _∥ = 2.08	75
[Cu ₃ (μ_3 -OMe)Cl(L1h) ₃ (HL1h) ₂]Cl	105.77 105.09 101.87	n.r.	-100	2.19	<i>g</i> _⊥ = 2.21 <i>g</i> _∥ = 1.47	87
[Cu ₃ (μ_3 -OMe)(L1h) ₃ Br(HL1h) ₂]Br	107.43 104.61 104.40	n.r.	-103	2.20	<i>g</i> _⊥ = 2.19 <i>g</i> _∥ = 1.59	87

^a Cu–Y–Cu angle (Y = O²⁻, HO⁻, Cl⁻, Br⁻); ^b Distance of μ_3 -Y from the Cu₃ plane; ^c The *J* values describe the magnetic exchange interactions depending on the geometrical parameters of each compound; ^d *g*-values obtained from the fitting of the magnetic susceptibility data; ^e *g*-values obtained from EPR measurements; n.r. = not reported; ligand abbreviations HL1a–HL1f are given in Figure 1.4; PPN⁺ = bis(triphenylphosphoranylidene)ammonium cation.

The reaction of CuX₂ (X⁻ = Cl⁻, Br⁻, NO₃⁻) with 3(5)-*tert*-butylpyrazole (HL1i) and sodium methoxide in methanol affords the heptanuclear compounds [$\{\text{Cu}_3(\text{HL1i})_6(\mu_3\text{-X})(\mu_3\text{-OH})_3\}_2\text{Cu}\}\text{X}_6$ (X⁻ = Cl⁻, Br⁻, NO₃⁻).^{102,103} The use of a ligand with larger steric hindrance at

the 3,5-positions of the pyrazole ring precludes the formation of the heptanuclear species and affords a trinuclear compound (as described above).⁸⁷ The use of other salts, like CuF_2 yields other products with different nuclearity.¹⁰⁴ The heptanuclear copper(II) compounds are double-cubanes in which a vertex of a copper(II) ion is shared and it is coordinated by six hydroxide ligands. Antiferromagnetic interactions between the copper(II) ions were found in all of the compounds and the magnetic exchange interaction is in the order of correlations made on the Cu–O–Cu angle (so-called Haase correlation)¹⁰⁵ for $[\text{Cu}_4(\mu_3\text{-OR})_4]^{4+}$ and $[\text{Cu}_2(\mu\text{-OH})]^{3+}$ species, leading to a ground state of $S_T = 1/2$.^{102,103}

$[\text{Fe}_8(\mu_4\text{-O})_4(\text{L1a})_{12}\text{Cl}_4]$ is an octanuclear iron(III) compound which has a Fe_4O_4 cubane structure, where the inner iron(III) ions are connected with the outer iron(III) ions through pyrazole bridges and in which the chloride ligands are at terminal positions.¹⁰⁶ This compound is the first example of an all-iron(III) cubane. Electrochemically four reductions are observed, where the last one is not reversible, but no oxidation process is detected.¹⁰⁶ The compound has an unusual stability due to the $[\text{Fe}_4\text{O}_4]^{4+}$ core. Replacement of the terminal chloride ligands with other ligands and the introduction of the fourth substituent on the pyrazole ring (HL1b and HL1c) were reported.¹⁰⁷ These compounds exhibit similar redox properties, demonstrating that the $[\text{Fe}_4\text{O}_4]^{4+}$ core is redox active.¹⁰⁷ Strong antiferromagnetic interactions between the iron(III) ions are present in the compound $[\text{Fe}_8(\mu_4\text{-O})_4(\text{L1a})_{12}\text{Cl}_4]$. The fit of the experimental magnetic data indicates strong antiferromagnetic coupling between the inner and the outer iron(III) ions ($J = -50.55 \text{ cm}^{-1}$), and much weaker coupling is observed between the iron(III) ions within the core ($J = -2.1 \text{ cm}^{-1}$).¹⁰⁷ The stronger antiferromagnetic interactions between the inner and the outer iron(III) ions are in agreement with the larger Fe–O–Fe angles, *ca.* 119° , as compared with the Fe–O–Fe angles of the inner core, *ca.* 98° . DFT studies were performed to confirm the parameters obtained with the fit of the experimental magnetic susceptibility data.¹⁰⁷ A gallium(III) analogue has also been synthesized.¹⁰⁸ Other examples of octanuclear clusters can be found involving molybdenum(V/VI)¹⁰⁹ or zinc(II) ions.¹¹⁰ The compound $[\text{Ni}(\text{bma})(\text{H}_2\text{O})_3][\text{Ni}_8(\text{OH})_6(\text{L1a})_{12}] \cdot 6\text{DMSO}$ (bma = bis(2-benzimidazolymethyl)amine) consists of an anionic structure composed from an octanuclear nickel(II) unit, $[\text{Ni}_8(\text{OH})_6(\text{L1a})_{12}]^-$ and the cation formed by a mononuclear nickel(II) entity, $[\text{Ni}(\text{bma})(\text{H}_2\text{O})_3]^+$. In the former case, the eight nickel(II) ions form a cube and the Ni \cdots Ni \cdots Ni angles are around 90° . Antiferromagnetic interactions are present between the nickel(II) ions in the octanuclear anion leading to $S = 0$, but the ground state of the molecule is $S_T = 1$, resulting from the mononuclear counter ion. DFT calculations were performed to estimate the magnetic exchange interactions.¹¹¹

A dodecanuclear copper(II) cage with the formula, $[\text{Cu}_{12}(\mu_4\text{-Cl})_4(\mu_3\text{-Cl})_2(\text{HL1k})_6(\text{L1k})_4(\text{tBuPO}_3)_6(\text{tBuPO}_2\text{OH})_2]$ is formed by combination of phosphonates and pyrazoles as ligands, in which two hexameric units are linked to each other and are stabilized by hydrogen bonding. This compound displays weak antiferromagnetic interactions between the copper(II) ions.¹¹²

The combination of two pyrazole moieties, *i.e.* bispyrazole ligands, has been used to form tetranuclear copper(II) compounds¹¹³ and also porous coordination polymers with palladium(II), platinum(II), silver(I) or copper(I) ions.¹¹⁴⁻¹¹⁷

1.3.3.3. Pyrazole ligands with substituents containing donor atoms

Substituents with donor atoms on the pyrazole ring can increase the number of possible metal-binding sites that may lead to polynuclear type of compounds. Commonly, the substituents are placed at the 3- and 5-positions of the aromatic ring. Variation of the side arm chain lengths gives some control over metal-metal separation, while the number and type of side arm donor sites allow determining electronic and coordinative properties.^{48,118} Recently, a review has been published by Meyer and co-workers, dealing with polynuclear transition metal complexes with compartmental pyrazolate ligands.²³ A main part of this review has been dedicated to dinuclear compounds and therefore they have not been included in this section.

Pyrazole ligands with N-donor substituents, amines

Figure 1.7 shows the ligands used for the compounds described in this section. An important part of this research has been developed by Meyer and co-workers,¹¹⁹⁻¹³⁴ who have studied the coordination ability of the 3,5-bisubstituted pyrazole ligands, with chelating side arms, mainly with N-donor atoms. They mainly differ in the chain lengths of the chelating side arms and the number of donor sites.

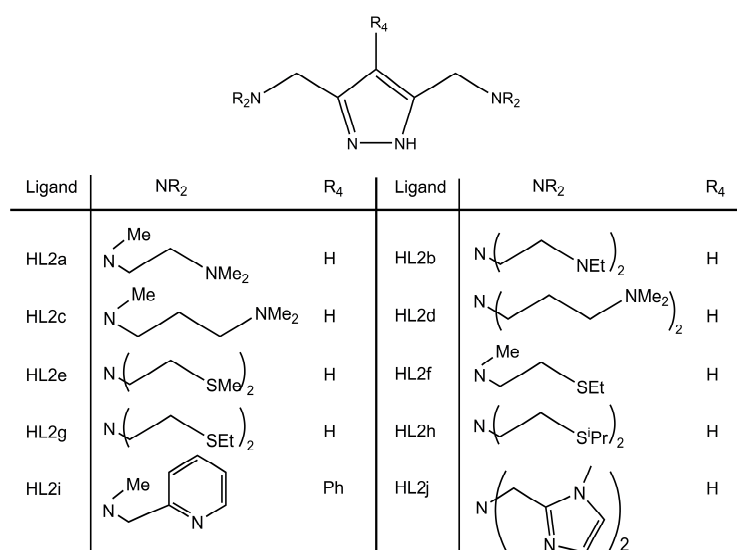


Figure 1.7. Pyrazole-based ligands with N-donor substituents, amines.

Tetranuclear nickel(II) compounds with the general formula $[\text{Ni}_4\text{L}_2]^{6+}$, have been synthesized with stoichiometric amounts of the metal salt, the pyrazole-based ligand (HL = HL2c–HL2h, see Figure 1.7), the base and the appropriate amount of the bridging ligands, *i.e.* azide and/or carboxylates. The similar central core of these structures is formed by dinuclear nickel(II) units, $[\text{Ni}_2\text{L}]^{3+}$, that are connected by azide and carboxylate bridges (Figure 1.8).^{123–128} Also, the formation of 1-D chains is possible with the assembly of the dinuclear nickel(II) units.^{123,131} In Table 1.2 the values of the magnetic exchange interactions for the tetranuclear nickel(II) compounds discussed are shown. In most of the tetranuclear compounds, overall antiferromagnetic interactions are present between the nickel(II) ions (high-spin) leading to a ground state of $S_T = 0$, except for the first four compounds of Table 1.2, in which ferromagnetic interactions between the nickel(II) ions are dominant.¹²⁴ Ferromagnetic exchange constants between nickel(II) ions are found in the presence of end-on azido bridges. In the case of end-to-end azido bridges, the Ni–N₃–Ni torsion angle and the Ni–N–N angle are crucial to determine the value of the exchange constant between the nickel(II) ions, as established by common magneto-structural correlations based on the azide bridge.^{124–128} Besides exploring azide as bridging ligand, other ligands, such as urea¹²⁹ and cyanide¹³² have been used in combination with HL2a and HL2b ligands, respectively. With urea as a ligand, a tetranuclear nickel(II) compound is formed, in which the presence of two low-spin nickel(II) ions and two high-spin nickel(II) ions that interact ferromagnetically, is confirmed by magnetic susceptibility studies.¹²⁹

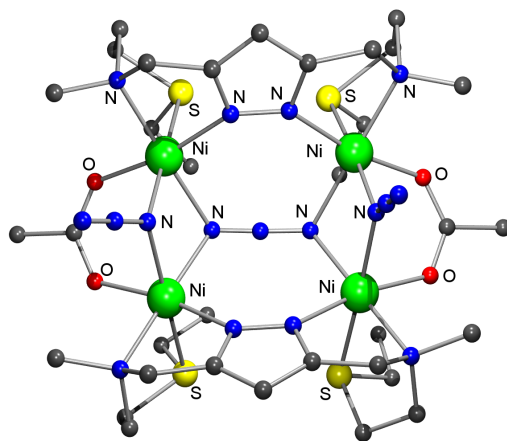


Figure 1.8. Molecular structure of the cation, $[\text{Ni}_4(\text{L2f})_2(\mu\text{-}1,1\text{-N}_3)_2(\mu_4\text{-}1,1,3,3\text{-N}_3)(\text{O}_2\text{CMe})_2]^+$.¹²⁵

The coordination ability of the HL2a ligand towards other metal ions, such as copper(II) or zinc(II) ions was also explored. The pyrazolato ligand bridges the two metal ions and in some cases, the dinuclear structures, $[\text{M}_2\text{L2a}]^+$ ($\text{M} = \text{Cu}(\text{II})$ and $\text{Zn}(\text{II})$), are linked by carbonates taken from the air,^{119,122} μ_4 -peroxido,¹³⁰ phosphato¹²¹ or oxazetidinylaceto.¹²⁰ An octanuclear copper(I) compound, that can be described as a $[(\text{MesCu})_4(\mu_4\text{-O})]^{2-}$ ($\text{Mes} = 2,4,6\text{-}$

trimethylphenyl) anion with two dinuclear copper(I)-pyrazole clamps containing the HL2i ligand has also been reported.¹³⁴

Table 1.2. Magnetic data for tetranuclear nickel(II) compounds.

Compound ^a	J / cm^{-1} ^b	g	Ref.
$[\text{Ni}_4(\text{L2c})_2(\mu\text{-}1,1\text{-N}_3)_2(\mu\text{-}1,3\text{-N}_3)_2](\text{ClO}_4)_2 \cdot 2\text{CH}_4\text{O} \cdot 0.5\text{H}_2\text{O}$	+1.8; +4.2	2.21	124
$[\text{Ni}_4(\text{L2c})_2(\mu\text{-}1,1\text{-N}_3)_2(\mu\text{-}1,3\text{-N}_3)_2](\text{ClO}_4)_2 \cdot 2\text{C}_3\text{H}_6\text{O} \cdot \text{C}_5\text{H}_{12}$	+2.5; +2.5	2.16	124
$[\text{Ni}_4(\text{L2c})_2(\mu\text{-}1,1\text{-N}_3)_2(\mu\text{-}1,3\text{-N}_3)_2](\text{BPh}_4)_2 \cdot 2\text{C}_3\text{H}_6\text{O}$	+3.4; -1.0	2.22	124
$[\text{Ni}_4(\text{L2d})_2(\mu\text{-}1,1\text{-N}_3)_2(\mu\text{-}1,3\text{-N}_3)_2](\text{BPh}_4)_2 \cdot 2\text{C}_3\text{H}_6\text{O}$	+0.9; -5.8	2.27	124
$[\text{Ni}_4(\text{L2d})_2(\mu\text{-}1,1\text{-N}_3)_2(\mu\text{-}1,3\text{-N}_3)_2](\text{BPh}_4)_2$	+2.0; +4.7	2.19	124
$[\text{Ni}_4(\text{L2g})_2(\mu_3\text{-}1,1,3\text{-N}_3)_2(\text{MeOH})_2](\text{ClO}_4)_4$	-42.6; -24.0; +32.1	2.19	123
$[\text{Ni}_4(\text{L2f})_2(\mu\text{-}1,1\text{-N}_3)_2(\mu_4\text{-}1,1,3,3\text{-N}_3)(\text{O}_2\text{CMe})_2] \cdot \text{ClO}_4 \cdot \text{C}_3\text{H}_6\text{O}$	-110; +106; +2	2.15	125
$[\text{Ni}_4(\text{L2f})_2(\mu\text{-}1,1\text{-N}_3)_2(\mu_4\text{-}1,1,3,3\text{-N}_3)(\text{O}_2\text{CPh})_2] \cdot \text{ClO}_4 \cdot \text{NaClO}_4 \cdot 2\text{C}_3\text{H}_6\text{O} \cdot \text{H}_2\text{O}$	-111; +51; +9	2.15	125
$[\text{Ni}_4(\text{L2h})_2(\mu\text{-}1,1\text{-N}_3)_2(\mu_4\text{-}1,1,3,3\text{-N}_3)(\text{O}_2\text{CMe})_2] \cdot \text{ClO}_4$	-133; +129; +26	2.15	125
$[\text{Ni}_4(\text{L2h})_2(\mu\text{-}1,1\text{-N}_3)_2(\mu_4\text{-}1,1,3,3\text{-N}_3)(\text{O}_2\text{CAda})_2] \cdot \text{ClO}_4 \cdot \text{C}_3\text{H}_6\text{O}$	-111; +86; +5	2.15	125
$[\text{Ni}_4(\text{L2e})_2(\mu_4\text{-}1,1,3,3\text{-N}_3)(\text{O}_2\text{CAda})_4] \cdot \text{ClO}_4$	-39; +98; -12	2.15	125
$[\text{Ni}_4(\text{L2g})_2(\mu_4\text{-}1,1,3,3\text{-N}_3)(\text{O}_2\text{CAda})_4] \cdot \text{ClO}_4$	-50; +66; +7	2.15	125
$[\text{Ni}_4(\text{L2d})_2(\mu\text{-}1,1\text{-N}_3)_2(\mu\text{-}1,3\text{-N}_3)_2](\text{BPh}_4)_2 \cdot 2\text{C}_3\text{H}_6\text{O}$	-16.2; +2	2.01	126
$[\text{Ni}_2(\text{L2c})(\mu\text{-}1,1\text{-N}_3)(\mu_3\text{-}1,1,3\text{-N}_3)(\text{N}_3)]_2 \cdot 2\text{CH}_2\text{Cl}_2$	-19.7; +6	2.29	126
$[\text{Ni}_4(\text{L2g})_2(\mu\text{-}1,3\text{-N}_3)(\mu_3\text{-}1,1,3\text{-N}_3)_2(\text{O}_2\text{CMe})](\text{ClO}_4)_2$	+57; -51; -18; +6	2.29	127
$[\text{Ni}_4(\text{L2g})_2(\mu\text{-}1,3\text{-N}_3)(\mu_3\text{-}1,1,3\text{-N}_3)_2(\text{O}_2\text{CPh})](\text{ClO}_4)_2$	+25; -61; -12; +5	2.38	127
$[\text{Ni}_4(\text{L2h})_2(\mu\text{-}1,3\text{-N}_3)(\mu_3\text{-}1,1,3\text{-N}_3)_2(\text{O}_2\text{CPh})](\text{ClO}_4)_2$	+27; -53; -3; +6	2.30	127
$[\text{Ni}_4(\text{L2g})_2(\text{OCN}_2\text{H}_4)_2(\text{OCN}_2\text{H}_3)_2](\text{ClO}_4)_2$	+3.4	2.25	129

^a The azide's nomenclature does not follow the IUPAC's rules. Here $\mu\text{-}1,1\text{-N}_3$ and $\mu\text{-}1,3\text{-N}_3$ is used for the end-on and end-to-end bridge, respectively; ^b The J values describe the magnetic exchange interactions depending on the geometrical parameters of each compound. Ligand abbreviations are given in Figure 1.7.

All the compounds reported above contain thioether or amine arms in the amino substituents of the pyrazole ring. The incorporation of other functional groups, such as imidazole (HL2j ligand) has also been studied.¹³³ In this case, pH potentiometric studies in aqueous solution were performed in combination with the crystallographic characterization of the different polynuclear species formed in the presence of copper(II) ion.¹³³

Pyrazole ligands with N-donor substituents, pyridines

2-Pyridylpyrazole derivatives (Figure 1.9) have been proven to be good ligands to obtain different assemblies, such as metallohelicates^{135,136} or clusters.¹³⁷⁻¹⁴⁵ Together with the employ of another bridging ligand as phosphonate, they provide a good approach to obtain a decanuclear copper(II) cage with the formula $[\text{Cu}_5(\mu_3\text{-OH})_2(\text{tBuPO}_3)_3(\text{L3a})_2(\text{MeOH})]_2 \cdot 10\text{MeOH} \cdot 2\text{H}_2\text{O}$.¹⁴⁶ The reaction of an iron(II) salt with the 3-(2-pyridyl)-pyrazole ligand

formed by the decomposition of the ligand tris[3-(2-pyridyl)pyrazol-1-yl]hydroborate] (Tp^{Py}), leads to a tetranuclear compound, $[\text{Fe}_4(\text{HL3a})_2(\text{L3a})_6(\mu\text{-O})_2](\text{PF}_6)_2 \cdot 4\text{CH}_3\text{CN}$.¹⁴⁰

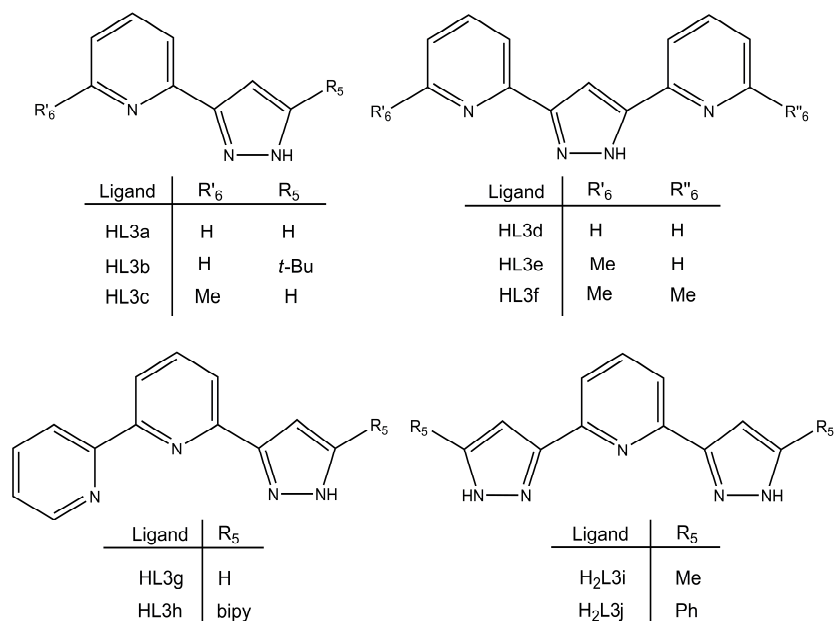


Figure 1.9. Pyrazole-based ligands with N-donor substituents, pyridines.

The coordination ability of the 3-(2-pyridyl)pyrazole ligand (HL3a) and its derivatives (HL3f, HL3g and HL3h) is also confirmed by the formation of copper(II) tetranuclear grids with the core $[\text{Cu}_4\text{L}_6]^{2+}$ or $[\text{Cu}_4\text{L}_4]^{4+}$ (Figure 1.10) in an isolated fashion or in 1-D chains.^{138,139,141,143,145} In such a type of grids, strong antiferromagnetic interactions are present between the copper(II) ions. The magnetic behaviour has been explained based on the number of pyrazole bridges and the distorted geometry of the pyrazole ligands.^{138,139,141,143,145} Other grid-types of structures are formed with cobalt(II) and manganese(II) ions.¹⁴⁵ However, different typologies and nuclearities can also be found with cobalt(II) ion and HL3f ligand¹⁴² and copper(I) and copper(II) ions with HL3c ligand, respectively.¹⁴⁴

5-*tert*-Butyl-3-(pyrid-2-yl)-1H-pyrazole (HL3b) is a very versatile ligand, leading to metallocycles (see section 1.3.4). However, in the case of copper(II) salts with non-coordination anions, a cubane-based structure is formed, $[\text{Cu}_4(\mu_3\text{-OH})_4(\text{L3b})_4](\text{ClO}_4)_4 \cdot x\text{CH}_2\text{Cl}_2$ ($x = 1-2$).¹⁴⁷ Small antiferromagnetic interactions between the copper(II) ions are present, as expected by Hatfield and Hodgson's correlation¹⁴⁸ depending on the Cu–O–Cu angle, because the angles found in this compound are within the range where both antiferromagnetic and ferromagnetic interactions can be present. The use of bispyrazole-pyridine ligands (H₂L3i and H₂L3j) affords octanuclear copper(I) compounds.¹⁴⁹

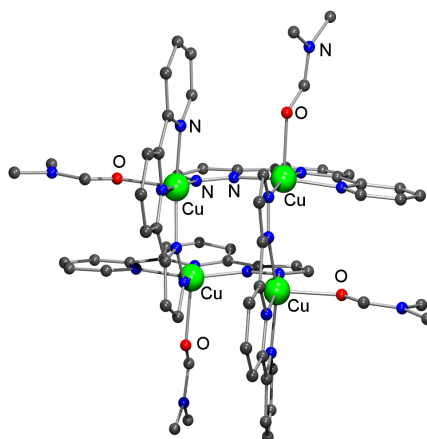


Figure 1.10. Molecular structure of the cation, $[\text{Cu}_4(\text{L3g})_4(\text{dmf})_4]^{2+}$.¹⁴¹

Pyrazole ligands with O-donor substituents, alcohols

The ligands described in this section, $\text{H}_2\text{L4a}$ – $\text{H}_2\text{L4d}$ (Figure 1.11), have been used by Winpenny and co-workers to explore the coordination chemistry of nickel(II) and manganese(II/III) ions. $[\text{Mn}_{14}\text{O}_2(\text{OH})_4(\text{L4c})_{18}(\text{HL4c})_4(\text{NO}_3)_4(\text{H}_2\text{O})_4]$ is a mixed-valent compound containing two manganese(III) and twelve manganese(II) ions. Strong antiferromagnetic interactions between the metal centres lead to a ground state of $S_T = 0$.¹⁵⁰ After the synthesis of this cluster and the wheel $[\text{Ni}_{24}(\text{OH})_8(\text{L4a})_{16}(\text{O}_2\text{CMe})_{24}(\text{HL4a})_{16}]$ that is described below as a metallocycle,¹⁵¹ derivatives of pyrazolinol-type of ligands (HL4b , HL4c , HL4d) were synthesized to study the reactivity towards nickel(II) ions in the presence of pivalate (piv^-) bridging ligands. As a result, different topologies have been obtained with nuclearities ranging from $[\text{Ni}_4\text{Na}_4]$, $[\text{Ni}_5\text{Na}_4]$, $[\text{Ni}_5\text{Li}_6]$, $[\text{Ni}_8\text{M}_2]$ ($\text{M} = \text{K}(\text{I})$, $\text{Rb}(\text{I})$, $\text{Cs}(\text{I})$) and $[\text{Ni}_8]$.¹⁵² Antiferromagnetic interactions between the nickel(II) ions are present leading to a zero spin or low-spin ground state in most of the cases, except for $[\text{Ni}_5\text{Li}_6]$ and $[\text{Ni}_8]$ in which ferromagnetic interactions are operative, yielding a ground state of $S_T \geq 1$ and $S_T = 6$, respectively.¹⁵² $[\text{Ni}_8\text{M}_2]$ and $[\text{Ni}_8]$ clusters are formed by two pseudo-cubanes linked by $\mu\text{-O}$ bridges.¹⁵² The differences in the magnetic behaviour of both types of clusters are explained in terms of the magneto-structural correlations within the $[\text{Ni}_4(\mu_3\text{-O})_4]$ core, in which Ni-O-Ni angles smaller than 99° favour ferromagnetic interactions, whereas larger angles promote antiferromagnetic interactions.¹⁵² The incorporation of alkaline metals in the final structure of some of the compounds led to an extension of the study with alkaline-earth metal ions.¹⁵³ In this case, the reactions were also performed with the dinuclear complex $[\text{Ni}_2(\text{H}_2\text{O})(\text{piv})_4(\text{Hpiv})_4]$ as a starting material and with HL4c , forming $[\text{Ni}_6\text{Mg}_2(\text{OH})_2(\text{L4c})_4(\text{piv})_{10}(\text{HL4c})_4(\text{MeOH})_2]$ and $[\text{Ni}_8\text{M}]$ ($\text{M} = \text{Sr}(\text{II})$, $\text{Ba}(\text{II})$) clusters.¹⁵³ The first compound is formed by two nickel(II) triangles bridged by magnesium(II) ions. Ferromagnetic exchange interactions are present between the nickel(II) ions forming the

triangle. The nonanuclear compounds, $[\text{Ni}_8\text{Sr}(\text{OH})_2(\text{L4c})_6(\text{piv})_{10}(\text{HL4c})_5(\text{Hpiv})_2(\text{CH}_3\text{CN})]$ and $[\text{Ni}_8\text{Ba}(\text{OH})_2(\text{L4c})_6(\text{piv})_{10}(\text{HL4c})_{5.3}(\text{Hpiv})_{0.7}(\text{CH}_3\text{CN})_2]$ are formed by two tetranuclear nickel(II) units bridged by strontium(II) and barium(II) ions, respectively. Dominant antiferromagnetic interactions are present between the nickel(II) ions leading to two independent ground states both with $S_T = 2$ corresponding to the two tetranuclear units. The use of silver(I) as a second metal ion resulted in the serendipitous formation of the large antiferromagnetic cluster $[\text{Ni}_{21}\text{Ag}(\mu_4\text{-OH})_4(\mu_3\text{-OH})_6(\text{L4d})_{13}(\text{piv})_{20}(\text{Hpiv})_4(\text{CH}_3\text{CN})_{3.5}(\text{H}_2\text{O})_{0.5}]$.¹⁵⁴ The exploration of new carboxylic acids, *i.e.* *t*-butylbenzoic acid and benzoic acid, and the introduction of azido ligands have demonstrated the unpredictability of the pyrazolinone ligands with three new compounds, $\text{Na}[\text{Ni}_8\text{Na}(\text{OH})_2\text{F}_8(\text{tBuPhCO}_2)_8(\text{HL4a})_8]$, $[\text{Ni}_8\text{Na}_2(\text{N}_3)_{12}(\text{tBuPhCO}_2)_2(\text{L4a})_4(\text{HL4a})_6(\text{EtOAc})_6]$ and $[\text{Ni}_8\text{Na}_2(\text{N}_3)_{12}(\text{PhCO}_2)_2(\text{L4a})_4(\text{HL4a})_6(\text{EtOAc})_6]$.¹⁵⁵ Figure 1.12 shows the molecular structure of $[\text{Ni}_8\text{Na}_2(\text{N}_3)_{12}(\text{PhCO}_2)_2(\text{L4a})_4(\text{HL4a})_6(\text{EtOAc})_6]$, in which ferromagnetic interactions between the nickel(II) ions are propagated through the azide groups; micro-Squid measurements indicate a single-molecule magnet behaviour.¹⁵⁵

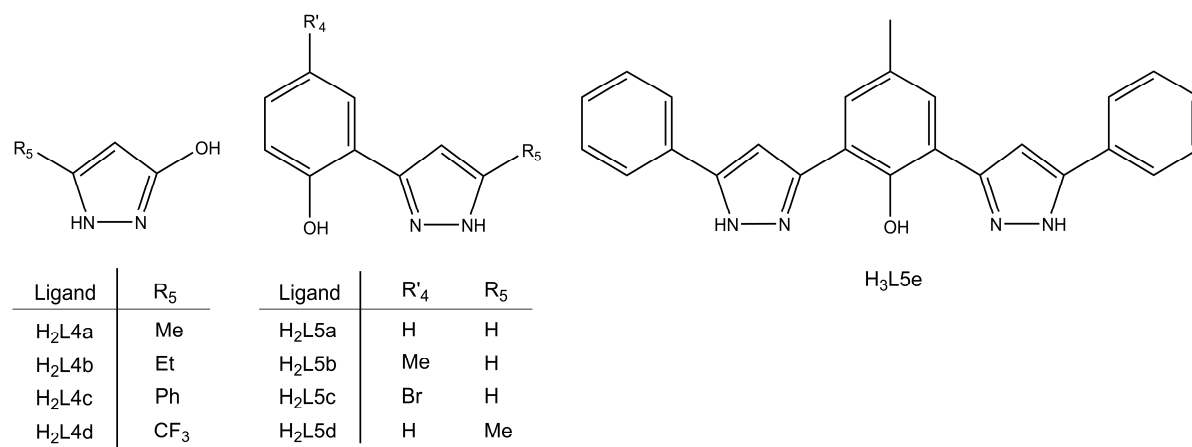


Figure 1.11. Pyrazole-based ligands with O-donor substituents, alcohols and phenols (H₂L5a and H₂L5d are called H₂pmpzH and H₂pmpzMe, respectively, in the following chapters).

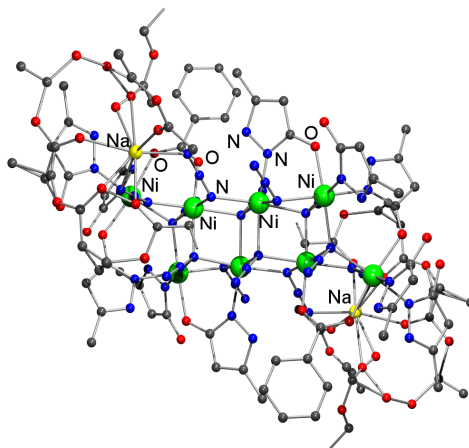


Figure 1.12. Molecular structure of $[\text{Ni}_8\text{Na}_2(\text{N}_3)_{12}(\text{PhCO}_2)_2(\text{L4a})_4(\text{HL4a})_6(\text{EtOAc})_6]$.¹⁵⁵

Pyrazole ligands with O-donor substituents, phenols

The phenol-pyrazole based ligands used for the compounds described in this section are shown in Figure 1.11. An octanuclear manganese(III) compound with the formula $[\text{Mn}_8(\mu_4\text{-O})_4(\text{L5d})_8(\text{thf})_4]$ has been reported by Reedijk and co-workers, in which strong antiferromagnetic interactions are operative between all the manganese(III) ions (Figure 1.13).³⁰ This compound resembles other octanuclear iron(III) compounds with a cubane core, described above.^{106,107} A tetranuclear nickel(II) compound with the formula $[\text{Ni}_4(\text{OH})(\text{OMe})_3(\text{HL5d})_4(\text{MeOH})_3]\cdot\text{MeOH}$ has also been reported with the same ligand, $\text{H}_2\text{L5d}$ (also called H_2phpzMe).²⁶ Ferromagnetic interactions are present leading to a ground state of $S_T = 4$. Trinuclear oxide-centred compounds are obtained with similar phenol-pyrazole ligands, $[\text{Mn}_3(\mu_3\text{-O})(\text{L})_3(\text{O}_2\text{CMe})(\text{MeOH})_x]$ ($\text{H}_2\text{L} = \text{H}_2\text{L5a}, \text{H}_2\text{L5b}$ and $x = 3, 4$) which form 1-D chains due to the acetate ligands that bridge the different trinuclear units.³¹ Long-range magnetic ordering was found in one of these compounds. If the methanol is replaced by ethanol, $[\text{Mn}_3(\mu_3\text{-O})(\text{L5b})_3(\text{O}_2\text{CMe})(\text{EtOH})_4]$ is formed. In this case, the chains are more isolated and the compound behaves as single-chain magnet below 4 K.²⁷ The influence of the solvent on the magnetic properties has also been observed in similar trinuclear manganese(III) units containing the ligand $\text{H}_2\text{L5c}$.^{156,157} Tao and co-workers extended the chemistry of these types of ligands with other transition-metal ions, such as the copper(II) ion.²⁸ The result is the formation of large cages with the formula $(\text{HNEt}_3)_2[\text{Cu}_{21}(\text{CH}_3\text{CN})_2(\text{H}_2\text{O})(\mu\text{-N}_3)_6(\mu_3\text{-N}_3)_2(\text{L5a})_{18}]\cdot 3\text{H}_2\text{O}\cdot 2\text{EtOH}$ and $[\text{Cu}_{16}(\text{EtOH})_2(\text{H}_2\text{O})_2(\text{L5b})_{16}]\cdot 9.5\text{H}_2\text{O}$.²⁸ Predominant antiferromagnetic interactions were found between the copper(II) ions in both compounds, although some ferromagnetic interactions are present between some of the copper(II) ions in $(\text{HNEt}_3)_2[\text{Cu}_{21}(\text{CH}_3\text{CN})_2(\text{H}_2\text{O})(\mu\text{-N}_3)_6(\mu_3\text{-N}_3)_2(\text{L5a})_{18}]\cdot 3\text{H}_2\text{O}\cdot 2\text{EtOH}$. Monte Carlo simulations were performed to evaluate the magnitude of the magnetic exchange interactions.²⁸ A phenol-bis(pyrazole) ligand was used to synthesize a mixed-valence manganese(II/III) linear trinuclear compound, $[\text{Mn}_3(\text{HL5e})_2(\text{O}_2\text{CMe})_3(\text{MeOH})_3]$.²⁹ Antiferromagnetic interactions between the manganese(II/III) ions are present in the molecule, leading to a ground state of $S_T = 3$.²⁹

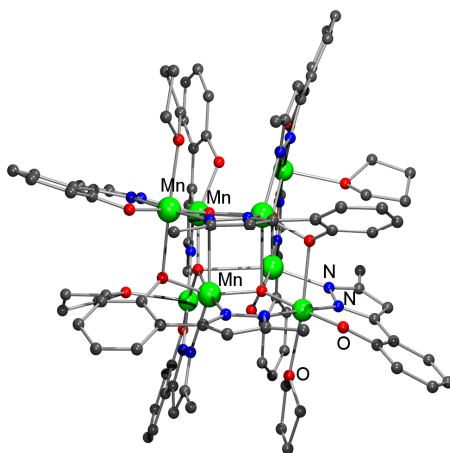


Figure 1.13. Molecular structure of $[\text{Mn}_8(\mu_4\text{-O})_4(\text{L5d})_8(\text{thf})_8]$.³⁰

Pyrazole ligands with other functional groups with N- and/or O-donor substituents

In this section, compounds with ligands that cannot be described under the previous classifications are presented (Figure 1.14).

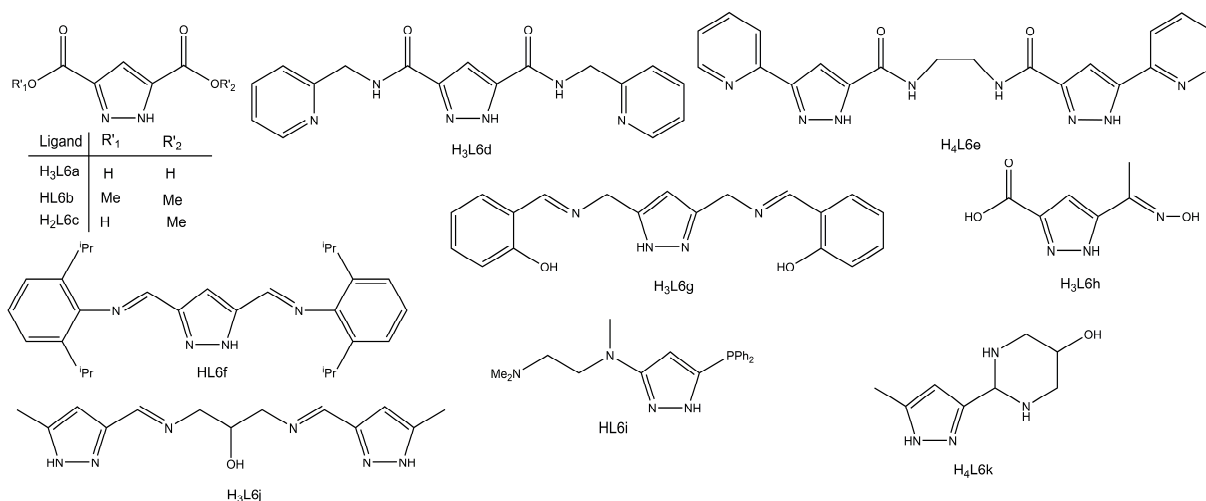


Figure 1.14. Pyrazole-based ligands with other functional groups with N- and/or O-donor substituents.

The functionalization of the pyrazole ligand with acid groups as substituents on the pyrazole ring, *i.e.* 3,5-pyrazoledicarboxylic acid (H₃L6a), introduces numerous coordination sites. Coordination polymers have been obtained by hydrothermal synthesis with a variety of transition metal ions¹⁵⁸⁻¹⁶⁰ and a combination of 3d and 4f metals ions, such as $\text{Cu}^{\text{II}}\text{Ln}^{\text{III}}_2$.¹⁶¹ An example with the 3,5-pyrazoledicarboxylic acid as a ligand, is a trinuclear copper(II) compound with formula $[\text{Cu}_3(\text{L6a})_2(\text{H}_2\text{O})_4]_n$.¹⁵⁸ Strong antiferromagnetic interactions between the copper(II) ions are mediated by the pyrazole ligand, and weaker ferromagnetic and antiferromagnetic interactions between the copper(II) ions are mediated by the carboxylate ligands in *syn-anti*-equatorial-equatorial and *syn-anti*-axial-equatorial type of bridge,

respectively.¹⁵⁸ Decomposition of an amide-pyrazole derivative ligand to L6a³⁻ ligand during the synthesis, resulted in the formation of trinuclear linear copper(II) compounds.¹⁶² Magnetic susceptibility studies revealed weak antiferromagnetic interactions, ascribed to the large separation between the copper(II) ions.¹⁶² The HL6b ligand has been used in the synthesis of a linear trinuclear copper(II) compound.¹⁶³ Hydrolysis of the HL6b ligand during the synthesis resulted in the formation of a tetranuclear copper(II) compound containing the HL6c ligand. Weak antiferromagnetic interactions between the copper(II) ions are observed.¹⁶⁴

Pyrazole-3,5-dicarboxamides are often used as intermediates in the synthesis of pyrazoles with chelating amine side arms. Therefore the coordination ability of this type of ligands has also been studied, because when the amide is deprotonated, the metal ion can coordinate through the N-atoms, whereas if it remains protonated the coordination would be through the oxygen. The ligand *N,N'*-bis(2-pyridylmethyl)pyrazole-3,5-dicarboxamide (H₃L6d) forms tetranuclear [2×2] grids with the general formula [M₄(HL6d)₄]·8H₂O (M = Cu(II), Ni(II)).¹⁶⁵ Magnetic susceptibility and EPR studies were performed only for the copper(II) compound.¹⁶⁵ The nickel(II) compound is diamagnetic, whilst antiferromagnetic interactions between the copper(II) ions are mediated by the pyrazole bridges. Other examples of tetranuclear nickel(II) and copper(II) compounds have been reported with amide-pyrazole ligands, *i.e.* with the H₄L6e ligand.^{166,167} These compounds have different topology depending on the metal ion, linear for nickel(II) ions and helical for copper(II) ions.¹⁶⁷ Weak and strong antiferromagnetic interactions have been found, respectively, between the metal ions.¹⁶⁷ Heterobimetallic compounds are also reported with the same ligand.¹⁶⁶

Diimine-pyrazole ligands are known to stabilize large clusters.¹⁶⁸⁻¹⁷⁰ Two hexanuclear nickel(II) compounds have been reported composed of three bimetallic units, [Ni₂(L6f)X₃] (X⁻ = Cl⁻, Br⁻) bridged by the halogen (Figure 1.15).^{168,169} Also, hexanuclear copper(II) compounds are obtained with the same ligand.¹⁷⁰ EPR and magnetic susceptibility studies revealed strong antiferromagnetic interactions between the copper(II) ions. A linear tetranuclear manganese(III) compound has been reported with H₃L6g, in which the salicylideneaminate moiety acts as chelating ligand and the pyrazole ligand bridges the manganese(III) ions.¹⁷¹ Weak antiferromagnetic interactions between the manganese(III) ions are observed.¹⁷¹

The coordination ability of ligands containing two different donor groups in the substituents of the pyrazole ligand has also been explored.^{172,173} As a result, a linear trinuclear copper(II) compound has been synthesized with the H₃L6h ligand that contains both an oxime and an acid substituent group. Strong antiferromagnetic interactions between the copper(II) ions are operative in this compound.¹⁷³ Another example is a tetranuclear nickel(II) compound with the HL6i ligand in which the nickel(II) ions are in low-spin electronic configuration.¹⁷² A

linear tetranuclear copper(II) compound was synthesized containing two different types of pyrazolate ligands, H₃L6j and H₃L6k.¹⁷⁴ Strong antiferromagnetic interaction between the copper(II) ions is present, as concluded from magnetic susceptibility and EPR studies.¹⁷⁴

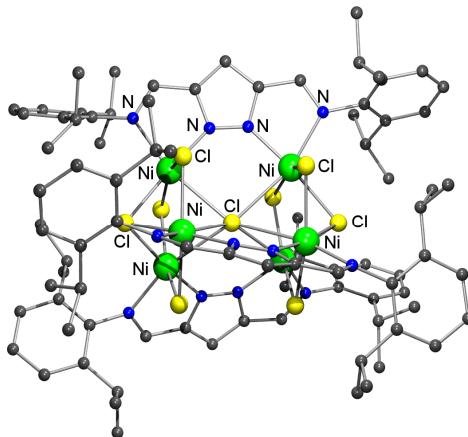


Figure 1.15. Molecular structure of [Ni₂(L6f)Cl₃].^{168,169}

1.3.4. Metalloclusters

Metal-directed self-assembly processes often form well-defined architectures.¹⁷⁵⁻¹⁷⁸ Cyclic metal-organic compounds with a central cavity or metalloclusters are one of these structural examples found in supramolecular chemistry.¹⁷⁵⁻¹⁷⁸ Some examples with pyrazole-based ligand have been reported in the literature.^{55,97,104,179-182} An octanuclear copper(II) wheel, [Cu₈(L1k)₈(OH)₈] (HL1k = 3,5-dimethylpyrazole), was formed by oxidation of [Cu(L1k)]_n, which is catalytically active in some oxidation reactions.⁵⁵ The reaction of the wheel with primary alcohols affords the octaalkoxido derivatives.⁵⁵ The removal of the chloride anion from [(Cu₃(μ₃-O)(L1a)₃Cl₃]²⁻ and [(Cu₃(μ₃-Cl)₂(L1a)₃Cl₃]²⁻ affords the rings [cis-Cu(μ-OH)(L1a)]_n (*n* = 6, 8, 9, 12 and 14), where the distorted square-planar copper(II) ions are connected by μ-pz ligands at the outside of the ring and μ-OH ligands at the inner side of the ring.¹⁸⁰ Two of these units encapsulate different ions (chloride, carbonate and sulfate) that are stabilized by the numerous weak hydrogen bonds. The ring size is not dependent of the encapsulated anion.¹⁸⁰ Copper(II) cages of smaller nuclearity have also been reported.^{97,179} An example is the compound [Cu₃(HL1i)₄(L1i)₂(μ-F)₂(μ₃-F)₂]₂F₂ (HL1i = 5-*tert*-butylpyrazole) in which antiferromagnetic interactions are present between the copper(II) ions, the stronger path being the one mediated by the [Cu(μ-F)₂]²⁺ bridges.¹⁰⁴ Another example is the hexanuclear copper(II) cage [Au(PPh₃)₂][Cu₆(μ-OH)₆(L11)₆Cl] (HL11 = 3,5-di(trifluoromethyl)-pyrazole), in which strong antiferromagnetic interactions are present between the copper(II) ions.¹⁸¹ The zinc(II) ion has also been found suitable for the formation

of a neutral macrocycle,¹⁸² in which the mercaptoethanol ligands are inside the ring and the pyrazole ligands are at the outside; a channel with a diameter of 4.7 Å is generated from this structure.

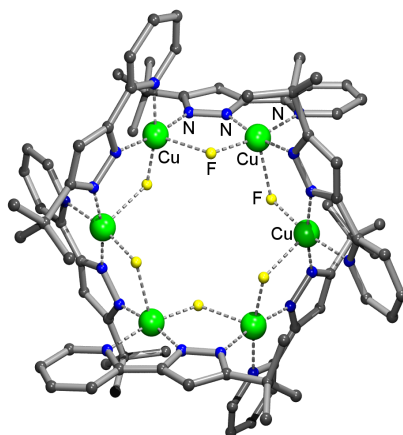


Figure 1.16. Molecular structure of the metallocycle $[\{\text{Cu}(\mu\text{-F})(\mu\text{-L3b})\}_6]$.¹⁸³

Pyrazole ligands bearing substituents with donor atoms are also capable of forming metallocycles.^{97,151,183-185} The 3(5)-pyrid-2-yl)-5-(3)-(tert-butyl)pyrazole ligand (HL3b) affords a metallocrown with the formula $[\{\text{Cu}(\mu\text{-F})(\mu\text{-L3b})\}_6(\text{H}_2\text{O})_2] \cdot 8\text{CH}_2\text{Cl}_2$ (Figure 1.17).¹⁸⁴ The study of guest molecules, such as Na^+ , K^+ , NH_4^+ , MeNH_3^+ and four amino acids has been carried out.¹⁸³ Larger guests cannot bind inside the cavity; therefore they bind exogenously to the two bowl-shaped cavities.¹⁸³ Strong hydrogen bonds stabilize all the structures.^{183,184} Magnetic susceptibility studies reveal antiferromagnetic interactions that are barely affected by the guest binding.¹⁸³ The use of less-coordinating anions of the copper(II) salt affords tetranuclear compounds.⁹⁷ Other metal ions such as cobalt(II) afford the mixed-valence Co(II/III) metallocrown, $[\text{Co}_6(\mu\text{-OH})_6(\mu\text{-L3b})_6]^{m+}$ ($m = 2$ or 3).¹⁸⁵ A large cage is formed by 24 high-spin nickel(II) ions in $[\text{Ni}_{24}(\text{OH})_8(\text{L4a})_{16}(\text{O}_2\text{CMe})_{24}(\text{HL4a})_{16}]$ (HL4a = 3-methyl-3-pyrazolin-5-one).¹⁵¹ It is described as an octamer of chemically trinuclear-based building blocks. Antiferromagnetic interactions between the nickel(II) ions are present and even at low temperature many excited states are populated.¹⁵¹

1.3.5. Metallohelicates

Another group of supramolecular architectures is formed by metallohelicates, based on not only coordinative bonds, but also on intermolecular noncovalent interactions, such as electrostatic interactions, hydrogen bonding and π - π stacking.^{186,187} Only a few examples have been reported so far involving pyrazole ligands.^{135,136} Actually, all of them contain the same ligand, 3,5-bis(2-pyridyl)pyrazole (HL3d). The compounds $[\{\text{M}(\mu\text{-L3d})_3\}_2\{\text{M}(\mu\text{-OH})\}](\text{SCN})_3 \cdot 6\text{H}_2\text{O}$ ($\text{M} = \text{Ni}(\text{II}), \text{Zn}(\text{II})$) were synthesized using solvothermal conditions.¹³⁵

In such compounds, the $[\text{Ni}_3(\mu\text{-OH})]^{5+}$ cluster core is wrapped by two terminal $[\text{Ni}(\mu\text{-L3d})_3]^-$ units with SCN^- as a counter anion.¹³⁵ These compounds were used in combination with CuSCN to obtain other compounds, $[\text{Cu}_{12}(\text{CN})_{11}(\text{SCN})_4][\{\text{M}(\mu\text{-L3d})_3\}_2\{\text{M}(\mu\text{-OH})\}]$ ($\text{M} = \text{Ni}(\text{II}), \text{Zn}(\text{II})$),¹³⁵ in which the double-helical strands are stabilized by the hydrogen bonding. Antiferromagnetic interactions between the nickel(II) ions were found in $[\{\text{Ni}(\mu\text{-L3d})_3\}_2\{\text{Ni}(\mu\text{-OH})\}](\text{SCN})_3 \cdot 6\text{H}_2\text{O}$ and $[\text{Cu}_{12}(\text{CN})_{11}(\text{SCN})_4][\{\text{Ni}(\mu\text{-L3d})_3\}_2\{\text{Ni}(\mu\text{-OH})\}]$.¹³⁵ Another example is the compound $[\{\text{Fe}(\mu\text{-L3d})_3\}_2\text{Fe}_3(\mu\text{-O})](\text{NCS})_2 \cdot 10\text{H}_2\text{O}$ (Figure 1.17), where the core $[\text{Fe}_3\text{O}]^{4+}$ with high-spin iron(II) ions is wrapped by two $[\text{Fe}(\text{L3d})_3]^-$ units with low-spin iron(II) ions.¹³⁶ Mössbauer spectroscopy confirmed the oxidation states of the iron(II) ions and antiferromagnetic interactions between high-spin iron(II) ions were found to be present in the core.¹³⁶

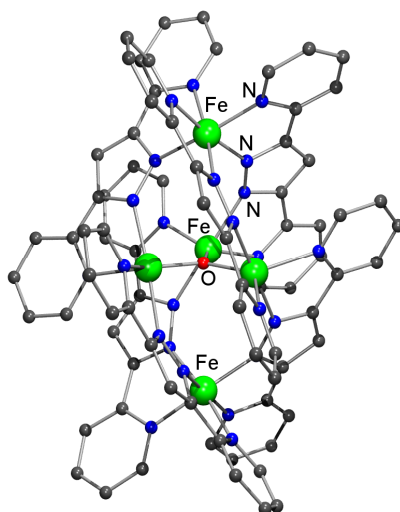


Figure 1.17. Molecular structure of $[\{\text{Fe}(\mu\text{-L3d})_3\}_2\text{Fe}_3(\mu\text{-O})](\text{NCS})_2 \cdot 10\text{H}_2\text{O}$.¹³⁶

To conclude, pyrazole-based ligands are very versatile ligands, since they are able to form different architectures, from polynuclear clusters to metallocycles or metallohelicates. The incorporation of other coordinating groups to the pyrazole ring increases the variety of polymetallic compounds that can be formed. In addition to the ability to bridge two or more metal ions, pyrazole ligands also provide an effective magnetic exchange pathway between them,

1.4. References

1. Rubahn, H.-G., *Basics on Nanotechnology*. Wiley VCH: Weinheim, 2008.
2. Martin, J. I.; Nogues, J.; Liu, K.; Vicent, J. L.; Schuller, I. K., *J. Magn. Magn. Mater.*, **2003**, 256, 449-501.
3. Gatteschi, D.; Sessoli, R.; Villain, J., *Molecular Nanomagnets*. Oxford University Press: Oxford, 2006.
4. Teo, B. K.; Sun, X. H., *J. Clust. Sci.*, **2006**, 17, 529-540.
5. *Molecular Magnetism: From Molecular Assemblies to the Devices*. Coronado, E.; Delhaès, P.; Gatteschi, D.; Miller, J. S., Eds. Kluwer Academic Publishers: Dordrecht, 1996.
6. *Magnetism: A Supramolecular Function*. Kahn, O., Ed. Kluwer Academic Publishers: Dordrecht, 1996.
7. Kahn, O., *Molecular Magnetism*. Wiley-VCH: New York, 1993.
8. Winpenny, R. E. P., *J. Chem. Soc.-Dalton Trans.*, **2002**, 1-10.
9. Aromí, G.; Aubin, S. M. J.; Bolcar, M. A.; Christou, G.; Eppley, H. J.; Folting, K.; Hendrickson, D. N.; Huffman, J. C.; Squire, R. C.; Tsai, H. L.; Wang, S.; Wemple, M. W., *Polyhedron*, **1998**, 17, 3005-3020.
10. Winpenny, R. E. P., *Adv. Inorg. Chem.*, **2001**, 52, 1-111.
11. Lescouëzec, R.; Toma, L. M.; Vaissermann, J.; Verdaguer, M.; Delgado, F. S.; Ruiz-Pérez, C.; Lloret, F.; Julve, M., *Coord. Chem. Rev.*, **2005**, 249, 2691-2729.
12. Thompson, L. K.; Waldmann, O.; Xu, Z. Q., *Coord. Chem. Rev.*, **2005**, 249, 2677-2690.
13. Fujita, M.; Umemoto, K.; Yoshizawa, M.; Fujita, N.; Kusukawa, T.; Biradha, K., *Chem. Commun.*, **2001**, 509-518.
14. Saalfrank, R. W.; Bernt, I.; Chowdhry, M. M.; Hampel, F.; Vaughan, G. B. M., *Chem.-Eur. J.*, **2001**, 7, 2765-2769.
15. Berlinguette, C. P.; Vaughn, D.; Cañada-Vilalta, C.; Galán-Mascarós, J. R.; Dunbar, K. R., *Angew. Chem.-Int. Edit.*, **2003**, 42, 1523-1526.
16. Marvaud, V.; Decroix, C.; Sculler, A.; Guyard-Duhayon, C.; Vaissermann, J.; Gonnet, F.; Verdaguer, M., *Chem.-Eur. J.*, **2003**, 9, 1677-1691.
17. Marvaud, V.; Decroix, C.; Sculler, A.; Tuyeras, F.; Guyard-Duhayon, C.; Vaissermann, J.; Marrot, M.; Gonnet, F.; Verdaguer, M., *Chem.-Eur. J.*, **2003**, 9, 1692-1705.
18. Miyasaka, H.; Saitoh, A.; Abe, S., *Coord. Chem. Rev.*, **2007**, 251, 2622-2664.
19. Ajò, D.; Bencini, A.; Mani, F., *Inorg. Chem.*, **1988**, 27, 2437-2444.
20. Matsushima, P.; Hamada, H.; Watanabe, K.; Koikawa, M.; Tokii, T., *J. Chem. Soc.-Dalton Trans.*, **1999**, 971-977.
21. Nishida, Y.; Kida, S., *Inorg. Chem.*, **1988**, 27, 447-452.
22. Tanase, S.; Koval, I. A.; Bouwman, E.; de Gelder, R.; Reedijk, J., *Inorg. Chem.*, **2005**, 44, 7860-7861.
23. Klingele, J.; Dechert, S.; Meyer, F., *Coord. Chem. Rev.*, **2009**, doi:10.16/j.ccr.2009.03.026.
24. LaMonica, G.; Ardizzoia, G. A., *Progr. Inorg. Chem.*, **1997**, 46, 151-238.
25. Halcrow, M. A., *Dalton Trans.*, **2009**, 2059-2073.
26. Aromí, G.; Bouwman, E.; Burzuri, E.; Carbonera, C.; Krzystek, J.; Luis, F.; Schlegel, C.; van Slageren, J.; Tanase, S.; Teat, S. J., *Chem.-Eur. J.*, **2008**, 14, 11158-11166.
27. Bai, Y. L.; Tao, J.; Wernsdorfer, W.; Sato, O.; Huang, R. B.; Zheng, L. S., *J. Am. Chem. Soc.*, **2006**, 128, 16428-16429.
28. Bai, Y. L.; V., T.; Huang, R. B.; Zheng, L. S.; Tao, J., *Chem.-Eur. J.*, **2009**, 15, 2377-2383.
29. Barrios, L. A.; Aromí, G.; Ribas, J.; Uber, J. S.; Roubeau, O.; Sakai, K.; Masaoka, S.; Gamez, P.; Reedijk, J., *Eur. J. Inorg. Chem.*, **2008**, 3871-3876.
30. Tanase, S.; Aromí, G.; Bouwman, E.; Kooijman, H.; Spek, A. L.; Reedijk, J., *Chem. Commun.*, **2005**, 3147-3149.
31. Tao, J.; Zhang, Y. Z.; Bai, Y. L.; Sato, O., *Inorg. Chem.*, **2006**, 45, 4877-4879.
32. Tanase, S.; Bouwman, E.; Long, G. J.; Shahin, A. M.; Mills, A. M.; Spek, A. L.; Reedijk, J., *Eur. J. Inorg. Chem.*, **2004**, 4572-4578.
33. Greenwood, N. N.; Earnshaw, A., *Chemistry of the elements*. Pergamon Press: London, 1984.

34. Carlin, R. L., *Magnetochemistry*. Springer Verlag: Berlin, 1986.
35. Viciano-Chumillas, M.; Marqués-Giménez, M.; Tanase, S.; Evangelisti, M.; Mutikainen, I.; Turpeinen, M.; Smits, J. M. M.; de Gelder, R.; de Jongh, L. J.; Reedijk, J., *J. Phys. Chem. C*, **2008**, 112, 20525–20534.
36. Viciano-Chumillas, M.; Tanase, S.; Mutikainen, I.; Turpeinen, M.; de Jongh, L. J.; Reedijk, J., *Inorg. Chem.*, **2008**, 47, 5919-5929.
37. Viciano-Chumillas, M.; Tanase, S.; Mutikainen, I.; Turpeinen, U.; de Jongh, L. J.; Reedijk, J., *Dalton Trans.*, **2009**, 7445-7453.
38. Viciano-Chumillas, M.; Tanase, S.; Aromí, G.; Smits, J. M. M.; de Gelder, R.; Solans, X.; Bouwman, E.; Reedijk, J., *Eur. J. Inorg. Chem.*, **2007**, 2635-2640.
39. Constable, E. C.; Steel, P. J., *Coord. Chem. Rev.*, **1989**, 93, 205-223.
40. Reedijk, J., in *Comprehensive Coordination Chemistry*, Wilkinson, G., Gillard, R.D., Mc Cleverty, J.A., Ed. Pergamon: Oxford, 1987; Vol. II, pp 73-98.
41. Fusco, R., in *Chemistry of Heterocyclic Compounds: A Series of Monographs*, Wiley, R. H. B., L. C.; Fusco, R., Jarboe, C.H., Ed. John Wiley & Sons, Ltd.: New York, 1967; Vol. 22, pp 1-174.
42. Büchner, E., *Chem. Ber.*, **1889**, 22, 842-847.
43. Trofimenko, S., *Chem. Rev.*, **1972**, 72, 497-509.
44. Trofimenko, S., *Adv. Chem.*, **1976**, 289-301.
45. Trofimenko, S., *Progr. Inorg. Chem.*, **1986**, 34, 115-210.
46. Trofimenko, S., *Chem. Rev.*, **1993**, 93, 943-980.
47. Halcrow, M. A., *Coord. Chem. Rev.*, **2005**, 249, 2880-2908.
48. Mukherjee, R., *Coord. Chem. Rev.*, **2000**, 203, 151-218.
49. Reedijk, J., *Recl. Trav. Chim. Pays-Bas*, **1970**, 89, 605-619.
50. Sadimenko, A. P.; Basson, S. S., *Coord. Chem. Rev.*, **1996**, 147, 247-297.
51. Maekawa, M.; Munakata, M.; Kuroda, T.; Nozaka, Y., *Inorg. Chim. Acta*, **1993**, 208, 243-244.
52. Rettig, S. J.; Storr, A.; Summers, D. A.; Thompson, R. C.; Trotter, J., *Can. J. Chem.-Rev. Can. Chim.*, **1997**, 75, 949-958.
53. Ehlert, M. K.; Rettig, S. J.; Storr, A.; Thompson, R. C.; Trotter, J., *Can. J. Chem.-Rev. Can. Chim.*, **1993**, 71, 1425-1436.
54. Miras, H. N.; Zhao, H.; Herchel, R.; Rinaldi, C.; Perez, S.; Raptis, R. G., *Eur. J. Inorg. Chem.*, **2008**, 4745-4755.
55. Ardizzoia, G. A.; Angaroni, M. A.; La Monica, G.; Cariati, F.; Cenini, S.; Moret, M.; Masciocchi, N., *Inorg. Chem.*, **1991**, 30, 4347-4353.
56. Ehlert, M. K.; Rettig, S. J.; Storr, A.; Thompson, R. C.; Trotter, J., *Can. J. Chem.-Rev. Can. Chim.*, **1992**, 70, 2161-2173.
57. Ehlert, M. K.; Storr, A.; Thompson, R. C., *Can. J. Chem.-Rev. Can. Chim.*, **1992**, 70, 1121-1128.
58. Masciocchi, N.; Galli, S.; Alberti, E.; Sironi, A.; Di Nicola, C.; Pettinari, C.; Pandolfo, L., *Inorg. Chem.*, **2006**, 45, 9064-9074.
59. Morawitz, T.; Lerner, H. W.; Bolte, M., *Acta Cryst. E*, **2006**, 62, M1474-M1476.
60. Murray, H. H.; Raptis, R. G.; Fackler, J. P., *Inorg. Chem.*, **1988**, 27, 26-33.
61. Omary, M. A.; Rawashdeh-Omary, M. A.; Gonser, M. W. A.; Elbjeirami, O.; Grimes, T.; Cundari, T. R., *Inorg. Chem.*, **2005**, 44, 8200-8210.
62. Raptis, R. G.; Fackler, J. P., *Inorg. Chem.*, **1988**, 27, 4179-4182.
63. Dias, H. V. R.; Diyabalanage, H. V. K., *Polyhedron*, **2006**, 25, 1655-1661.
64. Ehlert, M. K.; Rettig, S. J.; Storr, A.; Thompson, R. C.; Trotter, J., *Can. J. Chem.-Rev. Can. Chim.*, **1990**, 68, 1444-1449.
65. Masciocchi, N.; Moret, M.; Cairati, P.; Sironi, A.; Ardizzoia, G. A.; La Monica, G., *J. Am. Chem. Soc.*, **1994**, 116, 7668-7676.
66. Mohamed, A. A.; Pérez, L. M.; Fackler, J. P., *Inorg. Chim. Acta*, **2005**, 358, 1657-1662.
67. Dias, H. V. R.; Diyabalanage, H. V. K.; Eldabaja, M. G.; Elbjeirami, O.; Rawashdeh-Omary, M. A.; Omary, M. A., *J. Am. Chem. Soc.*, **2005**, 127, 7489-7501.
68. Mohamed, A. A.; Burini, A.; Fackler, J. P., *J. Am. Chem. Soc.*, **2005**, 127, 5012-5013.

69. Mohamed, A. A.; Galassi, R.; Papa, F.; Burini, A.; Fackler, J. P., *Inorg. Chem.*, **2006**, 45, 7770-7776.
70. Umakoshi, K.; Yamauchi, Y.; Nakamiya, K.; Kojima, T.; Yamasaki, M.; Kawano, H.; Onishi, M., *Inorg. Chem.*, **2003**, 42, 3907-3916.
71. Umakoshi, K.; Kojima, T.; Kim, Y. H.; Onishi, M.; Nakao, Y.; Sakaki, S., *Chem.-Eur. J.*, **2006**, 12, 6521-6527.
72. Piñero, D.; Baran, P.; Boča, R.; Herchel, R.; Klein, M.; Raptis, R. G.; Renz, F.; Sanakis, Y., *Inorg. Chem.*, **2007**, 46, 10981-10989.
73. Lukaszewicz, M.; Ciunik, Z.; Mazurek, J.; Sobczak, J.; Staron, A.; Wolowiec, S.; Ziolkowski, J. J., *Eur. J. Inorg. Chem.*, **2001**, 1575-1579.
74. Angaridis, P. A.; Baran, P.; Boča, R.; Cervantes-Lee, F.; Haase, W.; Mezei, G.; Raptis, R. G.; Werner, R., *Inorg. Chem.*, **2002**, 41, 2219-2228.
75. Boča, R.; Dihan, L.; Mezei, G.; Ortiz-Perez, T.; Raptis, R. G.; Telser, J., *Inorg. Chem.*, **2003**, 42, 5801-5803.
76. Mezei, G.; McGrady, J. E.; Raptis, R. G., *Inorg. Chem.*, **2005**, 44, 7271-7273.
77. Mezei, G.; Raptis, R. G., *Inorg. Chim. Acta*, **2004**, 357, 3279-3288.
78. Mezei, G.; Raptis, R. G.; Telser, J., *Inorg. Chem.*, **2006**, 45, 8841-8843.
79. Mezei, G.; Rivera-Carrillo, M.; Raptis, R. G., *Inorg. Chim. Acta*, **2004**, 357, 3721-3732.
80. Mezei, G.; Rivera-Carrillo, M.; Raptis, R. G., *Dalton Trans.*, **2007**, 37-40.
81. Casarin, M.; Cingolani, A.; Di Nicola, C.; Falcomer, D.; Monari, M.; Pandolfo, L.; Pettinari, C., *Cryst. Growth Des.*, **2007**, 7, 676-685.
82. Casarin, M.; Corvaja, C.; Di Nicola, C.; Falcomer, D.; Franco, L.; Monari, M.; Pandolfo, L.; Pettinari, C.; Piccinelli, F., *Inorg. Chem.*, **2005**, 44, 6265-6276.
83. Casarin, M.; Corvaja, C.; di Nicola, C.; Falcomer, D.; Franco, L.; Monari, M.; Pandolfo, L.; Pettinari, C.; Piccinelli, F.; Tagliatesta, P., *Inorg. Chem.*, **2004**, 43, 5865-5876.
84. Di Nicola, C.; Garau, F.; Karabach, Y. Y.; Martins, L.; Monari, M.; Pandolfo, L.; Pettinari, C.; Pombeiro, A. J. L., *Eur. J. Inorg. Chem.*, **2009**, 666-676.
85. Di Nicola, C.; Karabach, Y. Y.; Kirillov, A. M.; Monari, M.; Pandolfo, L.; Pettinari, C.; Pombeiro, A. J. L., *Inorg. Chem.*, **2007**, 46, 221-230.
86. Hulsbergen, F. B.; Tenhoedt, R. W. M.; Verschoor, G. C.; Reedijk, J.; Spek, A. L., *J. Chem. Soc.-Dalton Trans.*, **1983**, 539-545.
87. Liu, X. M.; de Miranda, M. P.; McInnes, E. J. L.; Kilner, C. A.; Halcrow, M. A., *Dalton Trans.*, **2004**, 59-64.
88. Rivera-Carrillo, M.; Chakraborty, I.; Mezei, G.; Webster, R. D.; Raptis, R. G., *Inorg. Chem.*, **2008**, 47, 7644-7650.
89. Zhou, J. H.; Liu, Z.; Li, Y. Z.; Song, Y.; Chen, X. T.; You, X. Z., *J. Coord. Chem.*, **2006**, 59, 147-156.
90. Angaroni, M.; Ardizzoia, G. A.; Beringhelli, T.; La Monica, G.; Gatteschi, D.; Masciocchi, N.; Moret, M., *J. Chem. Soc.-Dalton Trans.*, **1990**, 3305-3309.
91. Shen, W. Z.; Yi, L.; Cheng, P.; Yan, S. P.; Liao, D. Z.; Jiang, Z. H., *Inorg. Chem. Commun.*, **2004**, 7, 819-822.
92. Dias, H. V. R.; Diyabalanage, H. V. K.; Gamage, C. S. P., *Chem. Commun.*, **2005**, 1619-1621.
93. Sakai, K.; Yamada, Y.; Tsubomura, T.; Yabuki, M.; Yamaguchi, M., *Inorg. Chem.*, **1996**, 35, 542-544.
94. Kogane, T.; Yamamoto, T.; Hayashi, M.; Hirota, R.; Horiuchi, C. A., *Polyhedron*, **1995**, 14, 2475-2482.
95. Kavlakoglu, E.; Elmali, A.; Elerman, Y.; Svoboda, I., *Polyhedron*, **2002**, 21, 1539-1545.
96. Manzur, J.; García, A. M.; Garland, M. T.; Acuna, V.; González, O.; Peña, O.; Atria, A. M.; Spodine, E., *Polyhedron*, **1996**, 15, 821-827.
97. Mokuolu, Q. F.; Foguet-Albiol, D.; Jones, L. F.; Wolowska, J.; Kowalczyk, R. M.; Kilner, C. A.; Christou, G.; McGowan, P. C.; Halcrow, M. A., *Dalton Trans.*, **2007**, 1392-1399.
98. Sanz, M.; Mosquera, M. E. G.; Cuenca, T., *Dalton Trans.*, **2009**, 2616-2622.
99. Umakoshi, K.; Kojima, T.; Arikawa, Y.; Onishi, M., *Chem.-Eur. J.*, **2006**, 12, 5094-5104.
100. Ehlert, M. K.; Rettig, S. J.; Storr, A.; Thompson, R. C.; Trotter, J., *Acta Crystallogr. Sect. C-Cryst. Struct. Commun.*, **1994**, 50, 1023-1026.

101. Kruger, P. E.; Launay, F.; McKee, V., *Chem. Commun.*, **1999**, 639-640.
102. Liu, X. M.; McAllister, J. A.; de Miranda, M. P.; Whitaker, B. J.; Kilner, C. A.; Thornton-Pett, M.; Halcrow, M. A., *Angew. Chem.-Int. Edit.*, **2002**, 41, 756-758.
103. Liu, X. M.; McAllister, J. A.; de Miranda, M. P.; McInnes, E. J. L.; Kilner, C. A.; Halcrow, M. A., *Chem.-Eur. J.*, **2004**, 10, 1827-1837.
104. Liu, X. M.; McLaughlin, A. C.; de Miranda, M. P.; McInnes, E. J. L.; Kilner, C. A.; Halcrow, M. A., *Chem. Commun.*, **2002**, 2978-2979.
105. Merz, L.; Haase, W., *J. Chem. Soc.-Dalton Trans.*, **1980**, 875-879.
106. Raptis, R. G.; Georgakaki, I. P.; Hockless, D. C. R., *Angew. Chem.-Int. Edit.*, **1999**, 38, 1632-1634.
107. Baran, P.; Boča, R.; Chakraborty, I.; Giapintzakis, J.; Herchel, R.; Huang, Q.; McGrady, J. E.; Raptis, R. G.; Sanakis, Y.; Simopoulos, A., *Inorg. Chem.*, **2008**, 47, 645-655.
108. Capparelli, M. V.; Hodge, P.; Piggott, B., *Chem. Commun.*, **1997**, 937-938.
109. Ehlert, M. K.; Rettig, S. J.; Storr, A.; Thompson, R. C.; Trotter, J., *Inorg. Chem.*, **1993**, 32, 5176-5182.
110. Wu, H. Z.; Li, H. X.; Cheng, M. L.; Zhang, W. H.; Zhang, Y.; Lang, H. P., *Inorg. Chem. Commun.*, **2008**, 11, 8-10.
111. Xu, J. Y.; Qiao, X.; Song, H. B.; Yan, S. P.; Liao, D. Z.; Gao, S.; Journaux, Y.; Cano, J., *Chem. Commun.*, **2008**, 6414-6416.
112. Chandrasekhar, V.; Kingsley, S., *Angew. Chem.-Int. Edit.*, **2000**, 39, 2320-2322.
113. Kruger, P. E.; Moubaraki, B.; Fallon, G. D.; Murray, K. S., *J. Chem. Soc.-Dalton Trans.*, **2000**, 713-718.
114. He, J.; Yin, Y. G.; Wu, T.; Li, D.; Huang, X. C., *Chem. Commun.*, **2006**, 2845-2847.
115. Yu, S. Y.; Huang, H. P.; Li, S. H.; Jiao, Q.; Li, Y. Z.; Wu, B.; Sei, Y.; Yamaguchi, K.; Pan, Y. J.; Ma, H. W., *Inorg. Chem.*, **2005**, 44, 9471-9488.
116. Zhang, J. P.; Horike, S.; Kitagawa, S., *Angew. Chem.-Int. Edit.*, **2007**, 46, 889-892.
117. Zhang, J. P.; Kitagawa, S., *J. Am. Chem. Soc.*, **2008**, 130, 907-917.
118. La Monica, G.; Ardizzoia, G. A., *Progr. Inorg. Chem.*, **1997**, 46, 151-238.
119. Ackermann, J.; Meyer, F.; Pritzkow, H., *Z. Anorg. Allg. Chem.*, **2004**, 630, 2627-2631.
120. Bauer-Siebenlist, B.; Dechert, S.; Meyer, F., *Chem.-Eur. J.*, **2005**, 11, 5343-5352.
121. Bauer-Siebenlist, B.; Meyer, F.; Farkas, E.; Vidovic, D.; Cuesta-Seijo, J. A.; Herbst-Irmer, R.; Pritzkow, H., *Inorg. Chem.*, **2004**, 43, 4189-4202.
122. Bauer-Siebenlist, B.; Meyer, F.; Vidovic, D.; Pritzkow, H., *Z. Anorg. Allg. Chem.*, **2003**, 629, 2152-2156.
123. Demeshko, S.; Leibelng, G.; Dechert, S.; Fuchs, S.; Pruschke, T.; Meyer, F., *ChemPhysChem*, **2007**, 8, 405-417.
124. Demeshko, S.; Leibelng, G.; Dechert, S.; Meyer, F., *Dalton Trans.*, **2006**, 3458-3465.
125. Demeshko, S.; Leibelng, G.; Maringgele, W.; Meyer, F.; Mennerich, C.; Klauss, H. H.; Pritzkow, H., *Inorg. Chem.*, **2005**, 44, 519-528.
126. Leibelng, G.; Demeshko, S.; Bauer-Siebenlist, B.; Meyer, F.; Pritzkow, H., *Eur. J. Inorg. Chem.*, **2004**, 2413-2420.
127. Meyer, F.; Demeshko, S.; Leibelng, G.; Kersting, B.; Kaifer, E.; Pritzkow, H., *Chem.-Eur. J.*, **2005**, 11, 1518-1526.
128. Meyer, F.; Kircher, P.; Pritzkow, H., *Chem. Commun.*, **2003**, 774-775.
129. Meyer, F.; Konrad, M.; Kaifer, E., *Eur. J. Inorg. Chem.*, **1999**, 1851-1854.
130. Meyer, F.; Pritzkow, H., *Angew. Chem.-Int. Edit.*, **2000**, 39, 2112-2115.
131. Meyer, F.; Ruschewitz, U.; Schober, P.; Antelmann, B.; Zsolnai, L., *Dalton Trans.*, **1998**, 1181-1186.
132. Meyer, F.; Winter, R. F.; Kaifer, E., *Inorg. Chem.*, **2001**, 40, 4597-4603.
133. Prokofieva, A.; Prikhod'ko, A. I.; Enyedy, E. A.; Farkas, E.; Maringgele, W.; Demeshko, S.; Dechert, S.; Meyer, F., *Inorg. Chem.*, **2007**, 46, 4298-4307.
134. Stollenz, M.; Gross, C.; Meyer, F., *Chem. Commun.*, **2008**, 1744-1746.
135. Hou, J. Z.; Li, M.; Li, Z.; Zhan, S. Z.; Huang, X. C.; Li, D., *Angew. Chem.-Int. Edit.*, **2008**, 47, 1711-1714.

136. Yoneda, K.; Adachi, K.; Nishio, K.; Yamasaki, M.; Fuyuhiko, A.; Katada, M.; Kaizaki, S.; Kawata, S., *Angew. Chem.-Int. Edit.*, **2006**, 45, 5459-5461.
137. Chandrasekhar, V.; Kingsley, S.; Vij, A.; Lam, K. C.; Rheingold, A. L., *Inorg. Chem.*, **2000**, 39, 3238-3242.
138. Hu, T. L.; Li, J. R.; Liu, C. S.; Shi, X. S.; Zhou, J. N.; Bu, X. H.; Ribas, J., *Inorg. Chem.*, **2006**, 45, 162-173.
139. Jeffery, J. C.; Jones, P. L.; Mann, K. L. V.; Psillakis, E.; McCleverty, J. A.; Ward, M. D.; White, C. M., *Chem. Commun.*, **1997**, 175-176.
140. Jones, P. L.; Jeffery, J. C.; McCleverty, J. A.; Ward, M. D., *Polyhedron*, **1997**, 16, 1567-1571.
141. Mann, K. L. V.; Psillakis, E.; Jeffery, J. C.; Rees, L. H.; Harden, N. M.; McCleverty, J. A.; Ward, M. D.; Gatteschi, D.; Totti, F.; Mabbs, F. E.; McInnes, E. J. L.; Riedi, P. C.; Smith, G. M., *J. Chem. Soc.-Dalton Trans.*, **1999**, 339-348.
142. Picart, J. P.; Sánchez, F. J.; Casabó, J.; Rius, J.; Alvarez-Larena, A.; Ros, J., *Inorg. Chem. Commun.*, **2002**, 5, 130-133.
143. Pons, J.; Sanchez, F. J.; Casabó, J.; Alvarez-Larena, A.; Piniella, J. F.; Ros, J., *Inorg. Chem. Commun.*, **2003**, 6, 833-836.
144. Singh, K. J.; Long, J. R.; Stavropoulos, P., *Inorg. Chem.*, **1998**, 37, 1073-1079.
145. van der Vlugt, J. I.; Demeshko, S.; Dechert, S.; Meyer, F., *Inorg. Chem.*, **2008**, 47, 1576-1585.
146. Chandrasekhar, V.; Nagarajan, L.; Gopal, K.; Baskar, V.; Kogerler, P., *Dalton Trans.*, **2005**, 3143-3145.
147. Jones, L. F.; Kilner, C. A.; Halcrow, M. A., *Polyhedron*, **2007**, 26, 1977-1983.
148. Crawford, V. H.; Richardson, H. W.; Wasson, J. R.; Hodgson, D. J.; Hatfield, W. E., *Inorg. Chem.*, **1976**, 15, 2107-2110.
149. Zhou, Y.; Chen, W., *Dalton Trans.*, **2007**, 5123-5125.
150. Aromí, G.; Bell, A.; Teat, S. J.; Whittaker, A. G.; Winpenny, R. E. P., *Chem. Commun.*, **2002**, 1896-1897.
151. Dearden, A. L.; Parsons, S.; Winpenny, R. E. P., *Angew. Chem.-Int. Edit.*, **2001**, 40, 151-154.
152. Aromí, G.; Bell, A. R.; Helliwell, M.; Raftery, J.; Teat, S. J.; Timco, G. A.; Roubeau, O.; Winpenny, R. E. P., *Chem.-Eur. J.*, **2003**, 9, 3024-3032.
153. Aromí, G.; Roubeau, O.; Helliwell, M.; Teat, S. J.; Winpenny, R. E. P., *Dalton Trans.*, **2003**, 3436-3442.
154. Aromí, G.; Bell, A.; Teat, S. J.; Winpenny, R. E. P., *Chem. Commun.*, **2005**, 2927-2929.
155. Bell, A.; Aromí, G.; Teat, S. J.; Wernsdorfer, W.; Winpenny, R. E. P., *Chem. Commun.*, **2005**, 2808-2810.
156. Liu, C. M.; Zhang, D. Q.; Zhu, D. B., *Chem. Commun.*, **2008**, 368-370.
157. Liu, C. M.; Zhang, D. Q.; Zhu, D. B., *Inorg. Chem.*, **2009**.
158. King, P.; Clerac, R.; Anson, C. E.; Coulon, C.; Powell, A. K., *Inorg. Chem.*, **2003**, 42, 3492-3500.
159. King, P.; Clerac, R.; Anson, C. E.; Powell, A. K., *Dalton Trans.*, **2004**, 852-861.
160. Xing, Y. H.; Zhou, G. H.; An, Y.; Zeng, X. Q.; Ge, M. F., *Synth. React. Inorg. Met.-Org. Nano-Metal Chem.*, **2008**, 38, 514-517.
161. Zhou, X. H.; Peng, Y. H.; Du, X. D.; Wang, C. F.; Zuo, J. L.; You, X. Z., *Cryst. Growth Des.*, **2009**, 9, 1028-1035.
162. Driessen, W. L.; Chang, L.; Finazzo, C.; Gorter, S.; Rehorst, D.; Reedijk, J.; Lutz, M.; Spek, A. L., *Inorg. Chim. Acta*, **2003**, 350, 25-31.
163. Angaroni, M.; Ardizzoia, G. A.; La Monica, G.; Beccalli, E. M.; Masciocchi, N.; Moret, M., *J. Chem. Soc.-Dalton Trans.*, **1992**, 2715-2721.
164. Zhang, H.; Fu, D. G.; Ji, F.; Wang, G. X.; Yu, K. B.; Yao, T. Y., *J. Chem. Soc.-Dalton Trans.*, **1996**, 3799-3803.
165. Klingele, J.; Prikhod'ko, A. I.; Leibelng, G.; Demeshko, S.; Dechert, S.; Meyer, F., *Dalton Trans.*, **2007**, 2003-2013.
166. Kovbasyuk, L.; Pritzkow, H.; Kramer, R.; Fritsky, I. O., *Chem. Commun.*, **2004**, 880-881.
167. Kramer, R.; Fritsky, I. O.; Pritzkow, H.; Kovbasyuk, L. A., *J. Chem. Soc.-Dalton Trans.*, **2002**, 1307-1314.

168. Noel, G.; Roder, J. C.; Dechert, S.; Pritzckow, H.; Bolk, L.; Mecking, S.; Meyer, F., *Adv. Synth. Catal.*, **2006**, 348, 887-897.
169. Roder, J. C.; Meyer, F.; Pritzckow, H., *Chem. Commun.*, **2001**, 2176-2177.
170. Sachse, A.; Noël, G.; Dechert, S.; Demeshko, S.; Honecker, A.; Alfonsov, A.; Kataev, V.; Meyer, F., *Eur. J. Inorg. Chem.*, **2008**, 5390-5396.
171. Shindo, K.; Mori, Y.; Motoda, K.; Sakiyama, H.; Matsumoto, N.; Okawa, H., *Inorg. Chem.*, **1992**, 31, 4987-4990.
172. Konrad, M.; Wuthe, S.; Meyer, F.; Kaifer, E., *Eur. J. Inorg. Chem.*, **2001**, 2233-2240.
173. Penkova, L.; Demeshko, S.; Haukka, M.; Pavlenko, V. A.; Meyer, F.; Fritsky, I. O., *Z. Anorg. Allg. Chem.*, **2008**, 634, 2428-2436.
174. Pal, S.; Barik, A. K.; Gupta, S.; Hazra, A.; Kar, S. K.; Peng, S. M.; Lee, G. H.; Butcher, R. J.; El Fallah, M. S.; Ribas, J., *Inorg. Chem.*, **2005**, 44, 3880-3889.
175. Gale, P. A., *Coord. Chem. Rev.*, **2000**, 199, 181-233.
176. Schmidtchen, F. P.; Berger, M., *Chem. Rev.*, **1997**, 97, 1609-1646.
177. Pecoraro, V. L.; Stemmler, A. J.; Gibney, B. R.; Bodwin, J. J.; Wang, H.; Kampf, J. W.; Barwinski, A., *Prog. Inorg. Chem.*, **1997**, 45, 83-177.
178. Lehn, J. M., *Angew. Chem.-Int. Edit. Engl.*, **1988**, 27, 89-112.
179. Escartí, F.; Miranda, C.; Lamarque, L.; Latorre, J.; García-España, E.; Kumar, M.; Arán, V. J.; Navarro, P., *Chem. Commun.*, **2002**, 936-937.
180. Mezei, G.; Baran, P.; Raptis, R. G., *Angew. Chem.-Int. Edit.*, **2004**, 43, 574-577.
181. Mohamed, A. A.; Burini, A.; Galassi, R.; Paglialunga, D.; Galán-Mascarós, J. R.; Dunbar, K. R.; Fackler, J. P., *Inorg. Chem.*, **2007**, 46, 2348-2349.
182. Puerta, D. T.; Cohen, S. M., *Chem. Commun.*, **2003**, 1278-1279.
183. Jones, L. F.; Barrett, S. A.; Kilner, C. A.; Halcrow, M. A., *Chem.-Eur. J.*, **2008**, 14, 223-233.
184. Jones, L. F.; Kilner, C. A.; De Miranda, M. P.; Wolowska, J.; Halcrow, M. A., *Angew. Chem.-Int. Edit.*, **2007**, 46, 4073-4076.
185. Jones, L. F.; Kilner, C. A.; Halcrow, M. A., *Chem.-Eur. J.*, **2009**, 15, 4667-4675.
186. Albrecht, M., *Chem. Rev.*, **2001**, 101, 3457-3497.
187. Piguet, C.; Bernardinelli, G.; Hopfgartner, G., *Chem. Rev.*, **1997**, 97, 2005-2062.

Chapter 2

A family of mononuclear compounds:



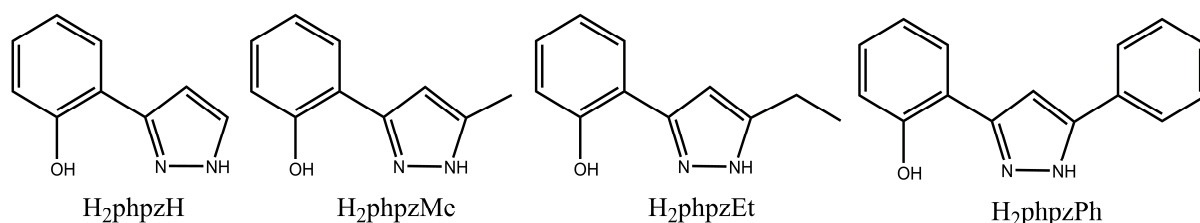
A series of mononuclear compounds was synthesized with the general formula of $[\text{Mn}(\text{HphpzR})_2\text{X}]$ ($\text{H}_2\text{phpzR} = 3(5)\text{-}(2\text{-hydroxyphenyl})\text{-}5(3)\text{-R-pyrazole}$, $\text{R} = \text{H, Me, Et, Ph}$; $\text{X}^- = \text{Cl}^-, \text{Br}^-$). All compounds are mononuclear manganese(III) coordination compounds in which the manganese(III) ion has a square-pyramidal geometry. The main difference arises from the crystal packing of the compounds which is caused by the ligand structure features. The influence of the ligand geometry is also reflected in the magnetic properties of the compounds.

* Part of this chapter has been published in the literature: Viciano-Chumillas M., Giménez-Marqués M., Tanase S., Evangelisti M., Mutikainen I., Turpeinen U., Smits J. M. M., de Gelder R., de Jongh L.J., Reedijk J., *J. Phys. Chem. C*, **2008**, 112, 20525–20534.

2.1. Introduction

Recently, polynuclear compounds have received considerable attention, since the field of molecular magnetism has greatly expanded due to the discovery of the single-molecule magnet (SMM) behaviour.¹⁻⁴ In synthetic respects, the search for novel SMM's with improved characteristic properties is rather complex and therefore the study of potential simple building blocks and their derivatives can be crucial for the design of SMM's. This can be illustrated by the studied manganese(III) salen complexes,⁵ in which slight changes in simple molecules can lead to a better understanding of how to tune the magnetic properties, especially when dealing with the design of higher nuclearity compounds.^{6,7}

Pyrazoles are very useful, functional bridging ligands, since they allow the connection of two metal ions by a variable superexchange pathway.^{8,9} Substitutions in the heterocyclic ring can render novel ligands, providing a variety of coordination compounds.¹⁰ In this respect, the ligand 3(5)-methyl-5(3)-(2-hydroxyphenyl)-pyrazole (H₂phpzMe) has exhibited a rich coordination chemistry with the introduction of a phenoxide moiety in the third position of the pyrazole ring providing another possible binding site with the metal ion.¹¹⁻¹³ Therefore, a library of phenol-pyrazole ligands, H₂phpzR (R = H, Me, Et, Ph) has now been synthesized with the purpose to study the structural effect of the substituent in the C5 position of the pyrazole ring (Scheme 2.1) on the magnetic properties of manganese(III) compounds. In this chapter, the synthesis, X-ray crystal structures, and magnetic and thermal properties are presented of a family of mononuclear manganese(III) compounds with the general formula [Mn(HphpzR)₂X] (R = H, Me, Et, Ph and X⁻ = Cl⁻, Br⁻). In these mononuclear compounds, the importance of the phenol-pyrazole derivatives is illustrated by the crystal packing and the magnetic properties. In addition, the influence of the different halogen on the magnetic properties has been studied.



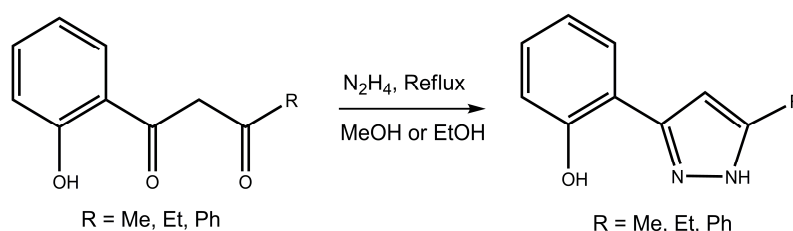
Scheme 2.1. Phenol-pyrazole based ligands (H₂phpzR; R = H, Me, Et, Ph) employed in this thesis.

2.2. Experimental Section

General remarks. Starting materials and the ligand 3(5)-(2-hydroxyphenyl)-pyrazole (H₂phpzH) were purchased from Aldrich and all manipulations were performed using materials as received.

Ligand synthesis

The ligands 3(5)-(2-hydroxyphenyl)-5(3)-methylpyrazole (H₂phpzMe), 3(5)-(2-hydroxyphenyl)-5(3)-ethylpyrazole (H₂phpzEt) and 3(5)-(2-hydroxyphenyl)-5(3)-phenylpyrazole (H₂phpzPh) have been synthesized according to reported procedures, by condensation of the 1,3-diketone derivatives¹⁴⁻¹⁶ with hydrazine in refluxing alcohol (methanol or ethanol) (Scheme 2.2).¹⁷



Scheme 2.2. H₂phpzR (R = Me, Et, Ph) ligand general synthesis.

General synthetic procedures for the coordination compounds

[Mn(HphpzR)₂Cl] (1, 3, 5, 7). MnCl₂·2H₂O (0.28 mmol) was dissolved in a mixture of acetonitrile/methanol in a ratio 1/1. The addition of a solution of H₂phpzH, H₂phpzMe, H₂phpzEt or H₂phpzPh (0.84 mmol) and triethylamine (0.14 mmol) in acetonitrile provided a green crystalline precipitate. The precipitate was collected by filtration, washed with diethyl ether and dried in vacuum. Green single crystals were obtained by slow evaporation of the filtrate in all four cases. Characterization details are given below.

[Mn(HphpzR)₂Br] (2, 4, 6, 8). The reaction of MnBr₂·4H₂O (0.28 mmol) in acetonitrile with a solution of H₂phpzH, H₂phpzMe, H₂phpzEt or H₂phpzPh (0.84 mmol) and triethylamine (0.14 mmol) in acetonitrile provided a green crystalline precipitate that was collected by filtration, washed with diethyl ether and dried in vacuum. The filtrate was allowed to slowly concentrate by evaporation, obtaining green single crystals in all four cases. Characterization details are given below.

[Mn(HphpzH)₂Cl] (1). Yield: 65% (77 mg). Anal. Calcd for **1** (C₁₈H₁₄ClMnN₄O₂): C, 52.90; H, 3.45; N, 13.71. Found: C, 52.35; H, 3.14; N, 13.68. IR (ν_{max}/cm⁻¹): 3260(m), 3055(w), 1602(s), 1563(m), 1520(s), 1505(s), 1469(m), 1442(s), 1436(s), 1362(m), 1314(m), 1294(s), 1248(s), 1173(s), 1143(s), 1115(vs), 1082(s), 1060(s), 1037(m), 974(m), 962(m),

924(m), 867(s), 852(s), 770(vs), 742(vs), 696(vs), 668(vs), 649(s), 586(vs), 572(vs), 533(vs), 468(vs), 448(s), 405(s), 369(s), 330(s), 313(s). ESI-MS (m/z): 405 $[\text{Mn}(\text{HphpzH})_2(\text{MeOH})]^+$, 373 $[\text{Mn}(\text{HphpzH})_2]^+$. UV/VIS/NIR in solid state (λ_{max} , nm): 268, 302, 454, 676.

[Mn(HphpzH)₂Br] (2). Yield: 45% (57 mg). Anal. Calcd for **2** (C₁₈H₁₄BrMnN₄O₂): C, 47.71; H, 3.11; N, 12.36. Found: C, 46.93; H, 3.11; N, 12.32. IR ($\nu_{\text{max}}/\text{cm}^{-1}$): 3287(m), 3054(w), 1602(s), 1563(m), 1520(s), 1505(s), 1496(s), 1468(m), 1443(s), 1436(s), 1361(w), 1313(m), 1297(s), 1246(vs), 1174(s), 1143(s), 1114(vs), 1082(s), 1058(s), 1036(m), 974(m), 964(m), 924(m), 868(s), 852(s), 772(vs), 745(vs), 689(vs), 674(vs), 649(s), 582(vs), 573(vs), 534(w), 449(s), 406(s), 370(m), 314(s). ESI-MS (m/z): 405 $[\text{Mn}(\text{HphpzH})_2(\text{MeOH})]^+$, 373 $[\text{Mn}(\text{HphpzH})_2]^+$. UV/VIS/NIR in solid state (λ_{max} , nm): 270, 377, 466, 674.

[Mn(HphpzMe)₂Cl] (3). Yield: 43% (53 mg). Anal. Calcd for **3** (C₂₀H₁₈ClMnN₄O₂): C, 55.00; H, 4.15; N, 12.83. Found: C, 55.12; H, 4.48; N, 12.98. IR ($\nu_{\text{max}}/\text{cm}^{-1}$): 3331(m), 3056(w), 1602(s), 1570(m), 1558(s), 1511(w), 1456(s), 1310(s), 1283(s), 1244(vs), 1194(w), 1170(m), 1120(vs), 1069(s), 1043(m), 1028(m), 988(m), 868(vs), 784(vs), 749(vs), 722(s), 667(s), 648(vs), 596(s), 571(vs), 468(s), 397(vs), 354(vs), 338(s). ESI-MS (m/z): 433 $[\text{Mn}(\text{HphpzMe})_2(\text{MeOH})]^+$, 401 $[\text{Mn}(\text{HphpzMe})_2]^+$. UV/VIS/NIR in solid state (λ_{max} , nm): 272, 378, 448, 678.

[Mn(HphpzMe)₂Br] (4). Yield: 50% (68 mg). Anal. Calcd for **4** (C₂₀H₁₈ClMnN₄O₂): C, 49.92; H, 3.77; N, 11.64. Found: C, 50.31; H, 4.09; N, 11.91. IR ($\nu_{\text{max}}/\text{cm}^{-1}$): 3345(m), 3053(w), 1601(s), 1570(m), 1558(s), 1511(m), 1456(s), 1312(s), 1283(s), 1246(vs), 1194(m), 1174(s), 1120(vs), 1070(s), 1043(s), 1028(m), 988(m), 970(w), 932(w), 871(s), 785(vs), 766(s), 758(m), 746(vs), 722(vs), 690(s), 678(m), 656(vs), 646(vs), 607(m), 570(vs), 535(m), 464(s), 398(s), 348(s). ESI-MS (m/z): 433 $[\text{Mn}(\text{HphpzMe})_2(\text{MeOH})]^+$, 401 $[\text{Mn}(\text{HphpzMe})_2]^+$. UV/VIS/NIR in solid state (λ_{max} , nm): 272, 381, 458, 694. During the crystallization process of **4**, a second minor product was characterized only crystallographically as $[\text{Mn}(\text{HphpzMe})_2(\text{H}_2\text{phpzMe})_2]\text{Br}$ (**9**).

[Mn(HphpzEt)₂Cl] (5). Yield: 34% (44 mg). Anal. Calcd for **5** (C₂₂H₂₂ClMnN₄O₂): C, 56.85; H, 4.77; N, 12.05. Found: C, 56.73; H, 5.49; N, 12.11. IR ($\nu_{\text{max}}/\text{cm}^{-1}$): 3308(m), 3054(w), 1601(s), 1568(m), 1558(s), 1554(s), 1540(m), 1506(m), 1476(s), 1448(vs), 1436(s), 1341(m), 1303(s), 1275(m), 1246(vs), 1172(m), 1117(vs), 1072(s), 1042(s), 1030(m), 993(m), 946(w), 861(vs), 804(vs), 758(vs), 714(m), 672(vs), 647(vs), 638(vs), 603(s), 570(vs), 541(m), 483(m), 469(w), 430(m), 391(m), 370(w), 336(s). ESI-MS (m/z): 461 $[\text{Mn}(\text{HphpzEt})_2(\text{MeOH})]^+$, 429 $[\text{Mn}(\text{HphpzEt})_2]^+$. UV/VIS/NIR in solid state (λ_{max} , nm): 271, 348, 446, 669.

[Mn(HphpzEt)₂Br] (6). Yield: 30% (43 mg). Anal. Calcd for **6** (C₂₂H₂₂BrMnN₄O₂): C, 51.88; H, 4.35; N, 11.00. Found: C, 51.79; H, 4.22; N, 11.20. IR ($\nu_{\max}/\text{cm}^{-1}$): 3324(m), 3054(w), 1601(s), 1568(m), 1558(s), 1554(s), 1540(w), 1506(w), 1472(s), 1447(vs), 1436(s), 1398(w), 1377(w), 1343(m), 1308(s), 1278(s), 1245(vs), 1174(s), 1116(vs), 1074(s), 1042(s), 1031(m), 992(m), 936(w), 860(vs), 802(vs), 748(vs), 710(m), 689(m), 651(vs), 586(s), 565(vs), 474(m), 426(s), 388(s), 336(s). ESI-MS (m/z): 461 [Mn(HphpzEt)₂(MeOH)]⁺, 429 [Mn(HphpzEt)₂]⁺. UV/VIS/NIR in solid state (λ_{\max} , nm): 272, 385, 446, 690.

[Mn(HphpzPh)₂Cl]·CH₃CN (7). Yield: 53% (90 mg). Anal. Calcd for **7** (C₃₂H₂₅ClMnN₅O₂): C, 63.85; H, 4.19; N, 11.63. Found: C, 63.41; H, 4.08; N, 11.51. IR ($\nu_{\max}/\text{cm}^{-1}$): 3367(m), 3040(vw), 1600(s), 1557(m), 1510(w), 1488(s), 1472(s), 1456(s), 1443(w), 1418(m), 1398(m), 1302(m), 1246(vs), 1198(m), 1126(vs), 1062(m), 1039(s), 994(s), 862(vs), 826(m), 804(m), 757(vs), 706(s), 690(vs), 676(m), 665(vs), 647(m), 618(w), 582(vs), 513(m), 466(m), 448(s), 403(w), 373(s), 334(vs). ESI-MS (m/z): 566 [Mn(HphpzPh)₂(CH₃CN)]⁺, 557 [Mn(HphpzPh)₂(MeOH)]⁺, 525 [Mn(HphpzPh)₂]⁺. UV/VIS/NIR in solid state (λ_{\max} , nm): 299, 392, 453, 695.

[Mn(HphpzPh)₂Br]·CH₃CN (8). Yield: 46% (83 mg). Anal. Calcd for **8** (C₃₂H₂₅BrMnN₅O₂): C, 59.46; H, 3.90; N, 10.83. Found: C, 59.95; H, 4.35; N, 10.97. IR ($\nu_{\max}/\text{cm}^{-1}$): 3367(m), 3040(vw), 1600(s), 1557(m), 1510(s), 1488(s), 1472(s), 1455(s), 1443(m), 1418(m), 1396(m), 1301(m), 1245(vs), 1198(m), 1152(w), 1126(vs), 1062(m), 1039(s), 994(s), 935(w), 920(w), 862(vs), 823(m), 805(m), 774(w), 756(vs), 708(s), 688(vs), 676(s), 666(vs), 648(s), 618(w), 582(vs), 512(m), 486(w), 466(m), 449(s), 410(w), 375(m), 334(vs), 314(w). ESI-MS (m/z): 566 [Mn(HphpzPh)₂(CH₃CN)]⁺, 557 [Mn(HphpzPh)₂(MeOH)]⁺, 525 [Mn(HphpzPh)₂]⁺. UV/VIS/NIR in solid state (λ_{\max} , nm): 298, 396, 458, 696.

Physical Measurements. Elemental analysis for C, H and N were performed on a Perkin-Elmer 2400 series II analyzer. Infrared spectra (4000–300 cm⁻¹) were recorded on a Perkin-Elmer Paragon 1000 FTIR spectrometer equipped with a Golden Gate ATR device, using the reflectance technique. Electronic absorption spectra were obtained on a Perkin-Elmer Lambda 900 spectrophotometer, using the diffuse reflectance technique, with MgO as a reference. Electrospray mass spectra (ESI-MS) in methanol solution were recorded on a Thermo Finnigan AQA apparatus. DC magnetic data were recorded using a Quantum Design MPMS-5 SQUID susceptometer. The magnetic susceptibilities were measured from 1.8 to 300 K on polycrystalline samples in a gelatine capsule with an applied field of 0.1 T. The magnetization was measured at 2, 4, 6 and 20 K in the 0–5(7) T range. Data were corrected for magnetization of the sample holder and for diamagnetic contributions, which were

estimated from Pascal's constants.¹⁸ Specific heat measurements in zero field were carried out in the range 0.3 K to 20 K with a commercial ³He set-up (PPMS), using the relaxation method. The investigated samples were in the form of microcrystalline powders.

X-ray Crystallography. Intensity data for single crystals of **2**, **3**, **7**, **8** and **9** were collected using MoK α radiation ($\lambda = 0.71073 \text{ \AA}$) on a Nonius KappaCCD diffractometer. Crystal and refinement data for **2**, **3**, **7** and **8** are collected in Table 2.1. The intensity data were corrected for Lorentz and polarization effects, and for absorption (multiscan absorption correction¹⁹). The structures were solved by Patterson methods.²⁰ The programs EvalCCD,^{21,22} DIRDIF96,²³ SHELXS-97²⁴ and SHELXL-97²⁵ were used for data reduction, structure solution and refinement respectively. All non-hydrogen atoms were refined with anisotropic displacement parameters. All hydrogen atoms were placed at calculated positions and were refined riding on their parent atoms.

2.3. Results and Discussion

Synthesis and General Characterization. The reaction between $\text{MnX}_2 \cdot n\text{H}_2\text{O}$ ($\text{X}^- = \text{Cl}^-, \text{Br}^-$) and H_2phpzR ($\text{R} = \text{H, Me, Et, Ph}$) in the presence of a small quantity of base in acetonitrile affords the compounds with the general formula $[\text{Mn}(\text{HphpzR})_2\text{X}]$. In the case of the manganese(II) chloride, methanol should be added to improve the solubility of the salt. This family of compounds contains the manganese(III) ion, formed by aerial oxidation upon stirring the manganese(II) salt. The reactions can also be performed in the stoichiometric ratio 1 to 2 (metal to ligand), but the yields do not change significantly compared with the described procedures. During the crystallization process of compound **4**, some secondary product was characterized crystallographically as $[\text{Mn}(\text{HphpzMe})_2(\text{H}_2\text{phpzMe})_2]\text{Br}$ (**9**). Probably the excess of the ligand in solution has rendered this new complex.

The infrared spectra of the compounds **1–8** display sharp bands in the range of $3260\text{--}3368 \text{ cm}^{-1}$ which belong to the $\nu_{\text{N-H}}$ stretching vibrations. Several weak bands are observed in the range of $2900\text{--}3100 \text{ cm}^{-1}$ due to the $\nu_{\text{C-H}}$ of the aromatic rings. The $\nu_{\text{C-O}}$ and $\nu_{\text{C=N}}$ stretching vibrations are shifted to lower energies, around 1602 and 1560 cm^{-1} , for compounds **1–8** as compared to the free ligand, indicating the coordination of the H_2phpzR ligand. This fact is also supported by the absence of any band in the range $3300\text{--}3600 \text{ cm}^{-1}$ from the protonated phenolic group.²⁶

In the electronic absorption spectra of compounds **1–8**, a broad band with the maximum in the range of $670\text{--}700 \text{ nm}$ is observed, which is ascribed to a d-d transition of the manganese(III) ion.²⁷ The band with shoulders in the range of $300\text{--}470 \text{ nm}$ is assigned to

LMCT transitions. The absorption bands around 265–300 nm belong to the π - π^* transitions within the ligand because of their high intensity.^{27,28}

The positive ESI-MS spectrum of a methanol solution of the compounds **1–8** exhibits two prominent signals that are assigned to the fragments $[\text{Mn}(\text{HphpzR})_2(\text{MeOH})]^+$ and $[\text{Mn}(\text{HphpzR})_2]^+$. Compounds **7** and **8** also show the fragment $[\text{Mn}(\text{HphpzPh})_2(\text{CH}_3\text{CN})]^+$. The good solubility of these compounds in methanol and the empty positions at the coordination sphere led to use these compounds as starting materials to obtain trinuclear manganese(III) clusters (see Chapter 3).²⁹ Compounds **1**, **4**, **5** and **6** were not characterized by X-ray crystallography. However, all the analyses performed on **1** and **4** indicate their isostructurality with the compounds **2** and **3**, respectively. In addition, the analysis of **5** and **6** also agrees with the formation of the mononuclear compounds, $[\text{Mn}(\text{HphpzEt})_2\text{X}]$ ($\text{X}^- = \text{Cl}^-$, Br^-).

Description of the Molecular Structures. Compounds **2**, **3**, **7** and **8** consist of a manganese(III) ion with a square-pyramidal $\text{N}_2\text{O}_2\text{X}$ chromophore ($\text{X}^- = \text{Cl}^-$, Br^-), where the two phenol-pyrazole ligands form the basal plane and the halogen is at the apical position. Figure 2.1 shows the molecular structure of compound **2**. In all compounds, the square-pyramidal geometry is thermodynamically favoured above the well known octahedral-based geometry for a manganese(III) ion, probably due to the formation of the neutral molecular compounds.³⁰ Nevertheless, a complex with octahedral geometry can also be formed in the presence of an excess of ligand as illustrated by the formation of compound **9** (Figure 2.2). In compounds **7** and **8**, the unit cell consists of two independent $[\text{Mn}(\text{HphpzPh})_2\text{X}]$ ($\text{X}^- = \text{Cl}^-$ (**7**), Br^- (**8**)) units and two molecules of acetonitrile as the Figure 2.3 shows for compound **7**.

All compounds crystallize in the triclinic space group P-1, except compound **9** which crystallizes in the monoclinic space group $\text{P}2_1/\text{c}$. The coordination geometry for compounds **2**, **3**, **7** and **8** is square-pyramidal with the value for τ in the range 0.02–0.16 ($\tau = 0$ for perfect square-pyramidal geometry and $\tau = 1$ for trigonal bipyramidal geometry).³¹ Compound **9** exhibits a distorted octahedral geometry with two mono deprotonated HphpzMe^- ligands in the equatorial plane ($\text{Mn}(1)\text{--O}(10) = 1.885(3)$ Å and $\text{Mn}(1)\text{--N}(21) = 2.012(4)$ Å). The axial positions are occupied by two nitrogen atoms of two neutral H_2phpzMe ligands, which display an elongated Jahn-Teller axis typical for manganese(III) ion ($\text{Mn}(1)\text{--N}(45) = 2.343(4)$ Å). The intramolecular hydrogen bonds involve the O(phenol)–H and N(pz)–H moieties. Intermolecular hydrogen bonds are present between the phenoxide moiety and the counterion, the bromide atom (Figure 2.2b and Table 2.4). The Mn–O average bond lengths are 1.85 Å, 1.85 Å, 1.86 Å and 1.87 Å for compounds **2**, **3**, **7** and **8**, respectively, while the Mn–N

average bond lengths are 1.97 Å, 2.02 Å, 1.99 Å and 1.99 Å for compounds **2**, **3**, **7** and **8**. The Mn–X bond is longer in the case of compounds **2** (2.60 Å) and **8** (av. 2.54 Å) than in the compounds **3** (2.41 Å) and **7** (av. 2.38 Å), which is ascribed to the smaller ionic radius and larger electronegativity of the Cl[−] anion as compared with Br[−]. This is also reflected in the distortion of the coordination geometry, where the distances of the manganese(III) ion from the plane formed by N₂O₂ are 0.272 Å and 0.312 Å for **2**, **3** respectively, and 0.337 Å for Mn(1) and 0.371 Å for Mn(2) in compound **7**, and 0.311 Å for Mn(1) and 0.343 Å for Mn(2) in compound **8**. Selected distances and angles are listed in Tables 2.2 and 2.3 for compounds **2**, **3**, **7** and **8**. The angles O–Mn–N are slightly smaller than 90° for all compounds. The dihedral angles between the phenol and the pyrazole ring are: 8.30° and 9.98° in compound **2**; 4.15° and 6.72° for Mn(1) and 5.05° and 7.42° for Mn(2) in compound **7**; and 3.92° and 7.93° for Mn(1) and 5.00° and 8.02° for Mn(2) in compound **8**. These values indicate nearly planar systems, as opposed to **3** for which values of 3.79° and 13.01° have been found as a result of the stronger distortion imposed by the ligand.

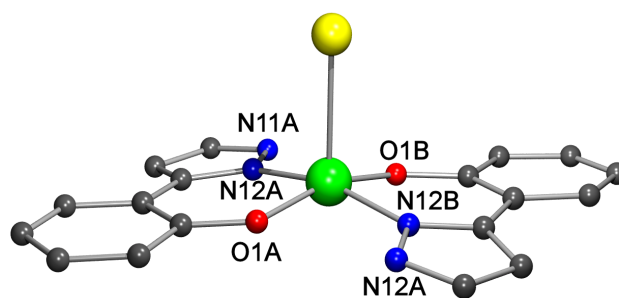


Figure 2.1. Pluton projection of the molecular structure of [Mn(HphpzH)₂Br] (**2**). Hydrogen atoms are omitted for clarity. Colour code: green, manganese; yellow, bromide; blue, nitrogen; red, oxygen; grey, carbon.

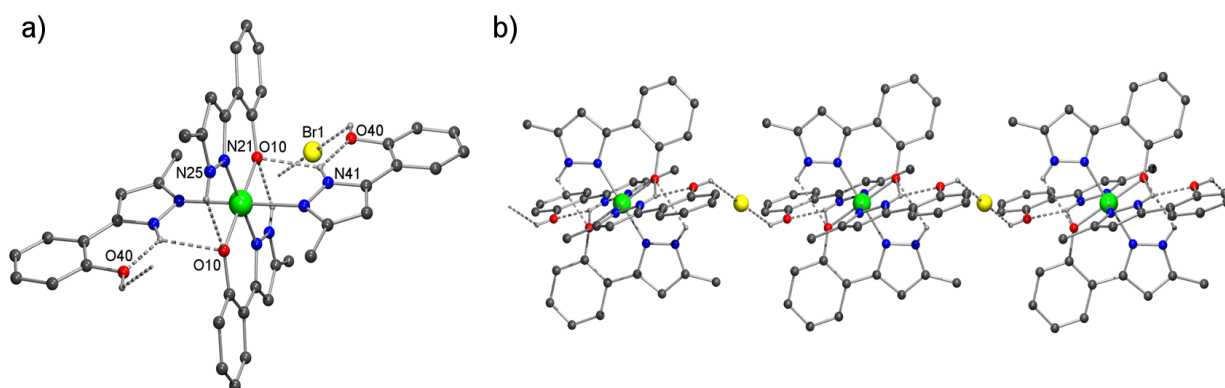


Figure 2.2. Pluton projection of the molecular structure of [Mn(HphpzMe)₂(H₂phpzMe)₂]Br (**9**) (a) showing the hydrogen bonding interactions (b). Hydrogen atoms that are not involved in hydrogen bonds are omitted for clarity. Colour code: green, manganese; yellow, bromide; blue, nitrogen; red, oxygen; grey, carbon.

Table 2.1. Crystal data and structure refinements for **2**, **3**, **7**, **8** and **9**.

	2	3	7	8	9
Formula	C ₁₈ H ₁₄ BrMnN ₄ O ₂	C ₂₀ H ₁₈ ClMnN ₄ O ₂	C ₃₂ H ₂₅ ClMnN ₅ O ₂	C ₃₂ H ₂₅ BrMnN ₅ O ₂	C ₄₀ H ₃₈ BrMnN ₈ O ₄
Formula weight [g mol ⁻¹]	453.17	436.77	601.96	646.41	829.62
Crystal system	Triclinic	Triclinic	Triclinic	Triclinic	Monoclinic
Space group	P-1	P-1	P-1	P-1	P2 ₁ /c
<i>a</i> [Å]	8.6761(10)	8.7790(18)	10.856(2)	10.812(2)	11.349(2)
<i>b</i> [Å]	9.3331(7)	10.361(2)	13.678(2)	13.893(3)	18.919(4)
<i>c</i> [Å]	11.2913(5)	11.622(2)	20.542(4)	20.995(4)	8.6560(17)
α [°]	91.992(5)	109.93(3)	88.93(3)	89.26(3)	90
β [°]	104.378(6)	90.73(3)	79.77(3)	79.51(3)	91.53(3)
γ [°]	105.636(6)	108.35(3)	70.75(3)	70.56(3)	90
V [Å ³]	847.82(13)	934.7(4)	2831.3(11)	2920.3(12)	1857.9(6)
Z	2	2	4	4	2
D _{calc} [g cm ⁻³]	1.7752	1.552	1.412	1.470	1.483
Crystal size	0.07×0.18×0.29	0.05×0.05×0.10	0.02×0.08×0.40	0.02×0.06×0.40	0.11×0.30×0.30
Number of collected reflections (unique)	26394(3889)	13915(4256)	34068(12486)	37936(12953)	22018(4214)
Number of observed reflections [I _o > 2σ(I _o)]	3078	2825	7391	6351	2018
Internal R factor	0.041	0.069	0.085	0.111	0.104
Number of parameters	235	253	741	741	247
Goodness-of-fit S on F ²	1.12	1.04	1.06	1.01	1.07
Largest peak and hole in final difference Fourier map [e Å ⁻³]	0.960 and -0.40	0.69 and -1.13	0.57 and -0.88	0.58 and -1.11	1.28 and -1.09
μ [mm ⁻¹]	3.156	0.874	0.600	1.858	1.483
R ₁ ^[a] [I > 2.0σ(I)]	0.0363	0.0588	0.0594	0.0631	0.0750
wR ₂ ^[b] [all data]	0.0834	0.1803	0.1612	0.1783	0.2467
T [°C]	208	173	173	173	173

^[a] $R_1 = \sum ||F_o| - |F_c|| / \sum |F_o|$. ^[b] $wR_2 = \{\sum [w(F_o^2 - F_c^2)^2] / \sum w(F_o^2)^2\}^{1/2}$.

The crystal packing of compounds **2** (Figure 2.4) and **3** is similar. The molecules align face-to-face to form ladder-like chains resulting from the intermolecular hydrogen bonds between the halogen ion from one molecule and the N–H group from the pyrazole ring of the next molecule. In case of the compound **3**, the hydrogen-bond interactions (N(45)–H(45A)⋯Cl(1) = 3.545(4) Å and N(25)–H(255A)⋯Cl(1) = 3.694(5) Å) are weaker than in the case of **2** (N(11A)–H(11A)⋯Br(1) = 3.289(3) Å and N(11B)–H(11B)⋯Br(1) = 3.304(3) Å), which is ascribed to the steric effect of the methyl moiety that increases the separation between mononuclear manganese(III) units. Hydrogen bond details are listed in Table 2.4 for compounds **2** and **3**. The “intrachain” Mn⋯Mn distances are 5.908 and 5.999 Å and the shortest “interchain” Mn⋯Mn distance is 5.179 Å for **2**. In the case of compound **3**, the “intrachain” Mn⋯Mn distances are 5.946 and 6.305 Å and the shortest “interchain” Mn⋯Mn distance is 5.832 Å.

Table 2.2. Selected bond lengths [Å] and angles [°] for [Mn(HphpzH)₂Br] (**2**) and [Mn(HphpzMe)₂Cl] (**3**).

Compound 2					
Bond Lengths					
Mn(1)–Br(1)	2.6025(6)	Mn(1)–O(1A)	1.8460(19)	Mn(1)–N(12B)	1.9628(26)
Mn(1)–O(1B)	1.8487(19)	Mn(1)–N(12A)	1.9692(25)		
Bond Angles					
Br(1)–Mn(1)–O(1A)	98.70(6)	Br(1)–Mn(1)–O(1B)	98.75(6)	Br(1)–Mn(1)–N(12B)	98.14(8)
O(1A)–Mn(1)–O(1B)	162.55(9)	O(1A)–Mn(1)–N(12A)	89.20(10)		
Compound 3					
Bond Lengths					
Mn(1)–Cl(1)	2.4129(13)	Mn(1)–O(10)	1.851(3)	Mn(1)–N(21)	2.022(3)
Mn(1)–O(30)	1.857(3)	Mn(1)–N(41)	2.026(3)		
Bond Angles					
Cl(1)–Mn(1)–O(10)	98.05(10)	Cl(1)–Mn(1)–O(30)	98.26(10)	Cl(1)–Mn(1)–N(21)	102.07(11)
Cl(1)–Mn(1)–N(41)	98.44(11)	O(10)–Mn(1)–O(30)	163.69(13)	O(10)–Mn(1)–N(21)	89.14(13)
O(10)–Mn(1)–N(41)	89.05(13)				

The packing diagram of compounds **7** and **8** differs from that of **2** and **3**, due to the presence of two crystallographically independent mononuclear units and two acetonitrile molecules in the unit cell. The two independent manganese(III) units have different orientations, where the angle between the N₂O₂ plane of the units is 56.94° and 56.39° for compounds **7** and **8**, respectively (Figure 2.3). One acetonitrile molecule forms an intermolecular hydrogen bond that involves its N(4) atom and N(25)–H function of one of the ligands coordinated to Mn(1) with a N–H⋯N distance of 3.040 Å and 3.069 Å for compounds **7** and **8**, respectively. In addition, intramolecular hydrogen bonds are present between the

N–H of the pyrazole ring and the O of the phenoxide moiety. In Figure 2.5, the packing of compound **8** is shown. The presence of the two units with different orientation derives in two layers, namely **I** (formed by the mononuclear entities containing Mn(1)) and **II** (formed by the mononuclear units containing Mn(2)). One acetonitrile molecule is found into the layer **I** and the other acetonitrile molecule lies between the layers **I** and **II**. Within the layers, the mononuclear entities align face-to-face although no direct interactions between the mononuclear units are observed. The shortest intermolecular face-to-face Mn \cdots Mn distances are 7.793 Å (Mn(1) \cdots Mn(1)) and 7.344 Å (Mn(2) \cdots Mn(2)) for compound **7**, and 7.905 Å (Mn(1) \cdots Mn(1)) and 7.433 Å (Mn(2) \cdots Mn(2)) for compound **8**, respectively. However, the closest distance between manganese(III) ions belongs to the manganese(III) ions that are opposite to each other, corresponding to 5.660 Å and 5.502 Å (Mn(2) \cdots Mn(2)) for compounds **7** and **8**, respectively.

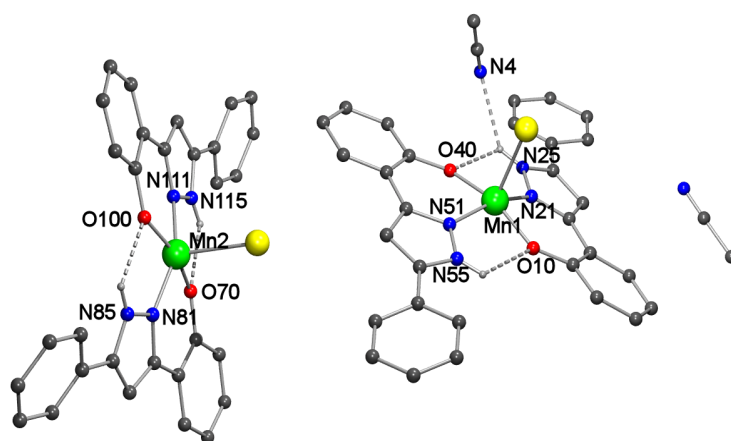


Figure 2.3. Pluton projection of the unit cell of the compound $[\text{Mn}(\text{HphpzPh})_2\text{Br}] \cdot \text{CH}_3\text{CN}$ (**8**) showing the two independent molecules and the hydrogen-bonding interactions. Hydrogen atoms that are not involved in hydrogen bonds are omitted for clarity. Colour code: green, manganese; yellow, bromide; blue, nitrogen; red, oxygen; grey, carbon.

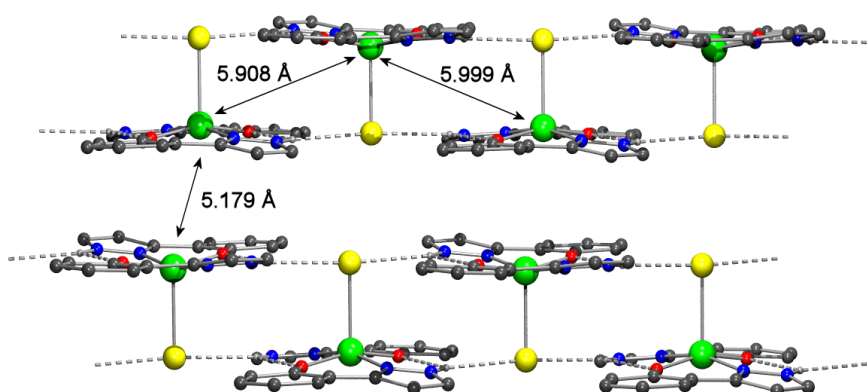


Figure 2.4. View of the ladder-like chain of $[\text{Mn}(\text{HphpzH})\text{Br}]$ (**2**) showing the intramolecular and intermolecular hydrogen bonds N–H \cdots Br \cdots N–H.

Table 2.3. Selected bond lengths [Å] and angles [°] for [Mn(HphpzPh)₂Cl]·CH₃CN (**7**) and [Mn(HphpzPh)₂Br]·CH₃CN (**8**).

Compound 7					
Bond Lengths					
Mn(1)–Cl(1)	2.3889(13)	Mn(1)–O(10)	1.864(3)	Mn(1)–N(21)	2.003(3)
Mn(1)–O(40)	1.857(3)	Mn(1)–N(51)	1.991(3)	Mn(2)–Cl(2)	2.3784(14)
Mn(2)–N(81)	1.983(3)	Mn(2)–O(70)	1.861(3)	Mn(2)–N(111)	1.991(3)
Mn(2)–O(100)	1.867(3)				
Bond Angles					
O(10)–Mn(1)–O(40)	161.55(13)	N(21)–Mn(1)–N(51)	158.28(13)	O(40)–Mn(1)–N(21)	88.35(12)
Cl(1)–Mn(1)–O(40)	100.17(10)	O(10)–Mn(1)–N(21)	89.18(13)	Cl(1)–Mn(1)–O(10)	98.25(10)
O(40)–Mn(1)–N(51)	88.17(13)	Cl(1)–Mn(1)–N(21)	101.09(10)	O(10)–Mn(1)–N(51)	87.39(12)
Cl(1)–Mn(1)–N(51)	100.63(10)	O(70)–Mn(2)–O(100)	162.91(13)	N(81)–Mn(2)–N(111)	152.97(13)
O(70)–Mn(2)–N(81)	88.69(13)	Cl(2)–Mn(2)–O(70)	99.22(10)	O(100)–Mn(2)–N(81)	87.37(12)
Cl(2)–Mn(2)–O(100)	97.85(10)	O(70)–Mn(2)–N(111)	87.96(13)	Cl(2)–Mn(2)–N(81)	106.35(10)
O(100)–Mn(2)–N(111)	88.01(13)	Cl(2)–Mn(2)–N(111)	100.66(10)		
Compound 8					
Bond Lengths					
Mn(1)–Br(1)	2.5441(12)	Mn(1)–O(10)	1.875(4)	Mn(1)–N(21)	1.994(4)
Mn(1)–O(40)	1.870(4)	Mn(1)–N(51)	2.001(4)	Mn(2)–Br(2)	2.5447(11)
Mn(2)–N(81)	1.986(4)	Mn(2)–O(70)	1.869(4)	Mn(2)–N(111)	1.999(4)
Mn(2)–O(100)	1.871(4)				
Bond Angles					
O(10)–Mn(1)–O(40)	162.22(18)	N(21)–Mn(1)–N(51)	160.71(18)	O(40)–Mn(1)–N(21)	88.61(18)
Br(1)–Mn(1)–O(40)	99.52(13)	O(10)–Mn(1)–N(21)	89.58(18)	Br(1)–Mn(1)–O(10)	98.22(12)
O(40)–Mn(1)–N(51)	88.74(17)	Br(1)–Mn(1)–N(21)	99.65(13)	O(10)–Mn(1)–N(51)	87.16(17)
Br(1)–Mn(1)–N(51)	99.63(13)	O(70)–Mn(2)–O(100)	163.33(16)	N(81)–Mn(2)–N(111)	155.94(18)
O(70)–Mn(2)–N(81)	89.18(17)	Br(2)–Mn(2)–O(70)	97.81(11)	O(100)–Mn(2)–N(81)	87.39(17)
Br(2)–Mn(2)–O(100)	98.83(11)	O(70)–Mn(2)–N(111)	88.37(17)	Br(2)–Mn(2)–N(81)	105.40(13)
O(100)–Mn(2)–N(111)	88.14(17)	Br(2)–Mn(2)–N(111)	98.65(12)		

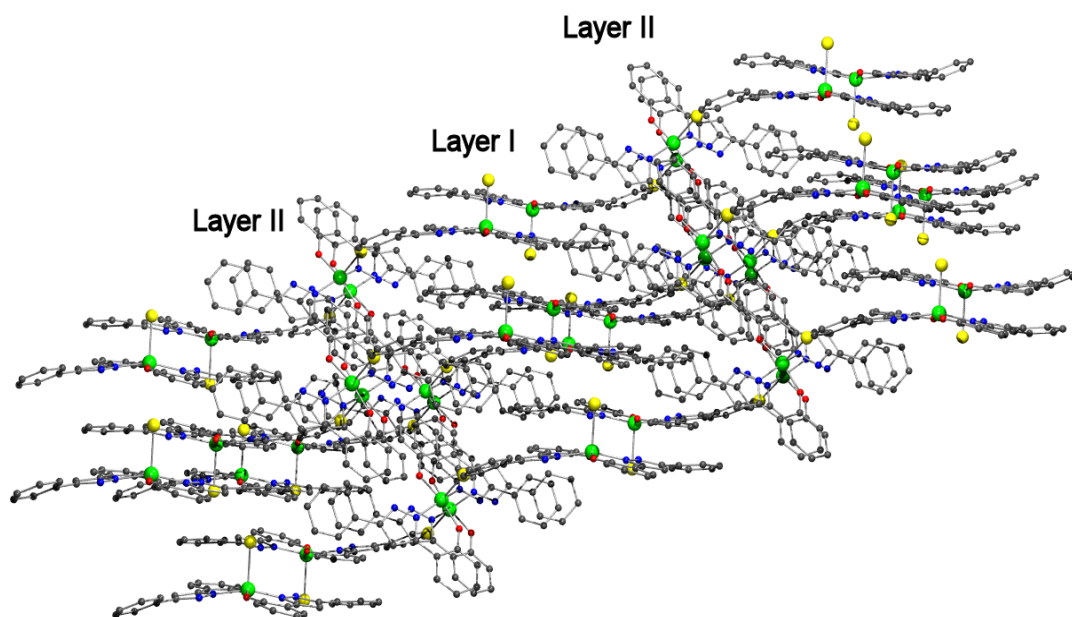


Figure 2.5. View of the 3-D network of $[\text{Mn}(\text{HphpzPh})_2\text{Br}] \cdot \text{CH}_3\text{CN}$ (**8**). Hydrogen atoms and acetonitrile molecules are omitted for clarity.

Table 2.4. Hydrogen bond details (lengths [\AA] and angles [$^\circ$]) for $[\text{Mn}(\text{HphpzH})_2\text{Br}]$ (**2**), $[\text{Mn}(\text{HphpzMe})_2\text{Cl}]$ (**3**) and $[\text{Mn}(\text{HphpzMe})_2(\text{H}_2\text{phpzMe})_2]\text{Br}$ (**9**).

Donor–H \cdots Acceptor	D–H	H \cdots A	D \cdots A	D–H \cdots A
Compound 2				
N(11A)–H(11A) \cdots O(1B)	0.8696	2.3695	2.774(3)	108.72
N(11A)–H(11A) \cdots Br(1)	0.8696	2.5931	3.289(3)	137.68
N(11B)–H(11B) \cdots O(1A)	0.8701	2.3631	2.774(3)	109.22
N(11B)–H(11B) \cdots Br(1)	0.8701	2.5974	3.304(3)	139.05
Compound 3				
N(25)–H(25A) \cdots O(30)	0.8797	2.4176	2.819(4)	108.20
N(45)–H(45A) \cdots O(10)	0.8801	2.4967	2.889(4)	107.70
N(45)–H(45A) \cdots Cl(1)	0.8801	2.7718	3.545(4)	147.44
N(25)–H(25A) \cdots Cl(1)	0.8797	2.9428	3.694(5)	144.50
Compound 9				
N(25)–H(25A) \cdots O(10)	0.8800	2.4927	2.906(6)	109.40
O(30)–H(301) \cdots Br(1)	0.8404	2.6172	3.151(4)	122.64
N(41)–H(41A) \cdots O(10)	0.8795	2.2809	2.842(5)	121.53
N(41)–H(41A) \cdots O(30)	0.8795	1.9676	2.589(6)	126.48

Magnetic Properties. Magnetic susceptibilities were measured under 0.1 T applied field in the 1.8–300 K temperature range for all compounds except **9**. The $\chi_M T$ values found at 300 K are seen to be in the range 2.7–2.9 cm³Kmol⁻¹, values which are slightly below the theoretical value (3.0 cm³Kmol⁻¹) expected for non-interacting manganese(III) ions with $S = 2$ and $g = 2$. Upon cooling to 2 K, the $\chi_M T$ values for all the compounds **1–8** decrease considerably, suggesting predominantly antiferromagnetic interactions between the manganese(III) ions along the structural chains (for compounds **1–4**) and between nearest neighbours (for compounds **7** and **8**). This conclusion is corroborated by magnetization measurements taken at low temperature (< 20 K). In all cases the field-dependent magnetization curves show substantial downward deviations from the calculated Brillouin curves for non-interacting spins, as will be further discussed below.

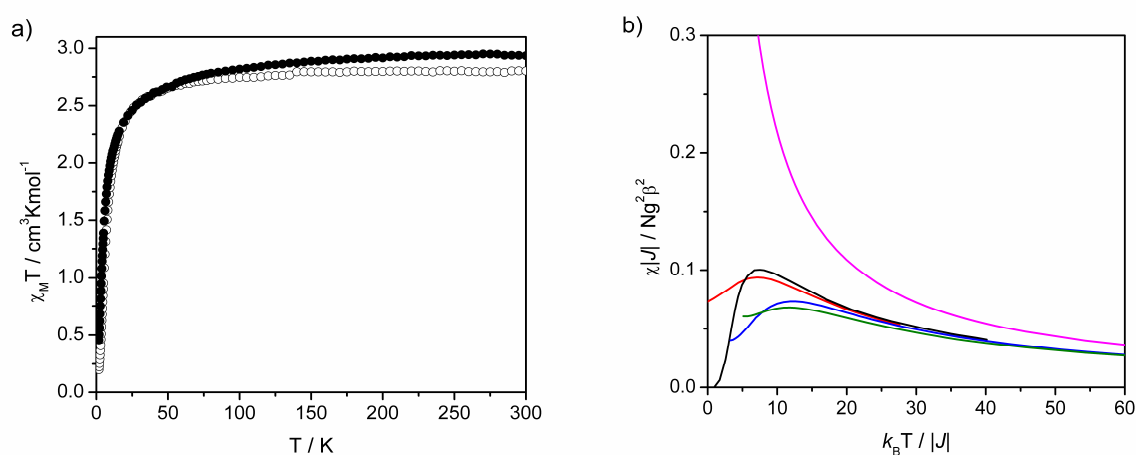


Figure 2.6. a) Plot of $\chi_M T$ vs T for **1** (\circ) and **2** (\bullet) in the range 1.8 to 300 K in 0.1 T applied field. b) Plot of $\chi_M |J| / N g^2 \beta^2$ vs $k_B T / |J|$ for **1** (blue) and **2** (green) together with the theoretical predictions for Heisenberg (red) and Ising (black) chains for $S = 2$ and the paramagnet behaviour (magenta).

Compounds 1 and 2. Interestingly, compounds **1** and **2** both exhibit a broad maximum in the susceptibility plot at 7 K and at 4 K, respectively (Figure 2.6b), which is a characteristic feature of antiferromagnetic linear chains.^{18,32} The increasing development of antiferromagnetic correlations along the chains as temperature is lowered is known to lead to broad maxima in the magnetic susceptibility and specific heat at temperatures of the order of the magnetic exchange constant.³³ These two compounds were therefore further investigated by specific heat measurements in the temperature range 0–20 K and in zero magnetic field (Figure 2.8). Since the measured specific heat is the sum of a magnetic (C_m) and a lattice (phonon) contribution (C_l), the latter has to be evaluated and subtracted from the raw data. At low temperature C_l can be well approximated by a temperature polynomial of the form:³⁴

$$C_l = aT^3 + bT^5 + cT^7 \quad (1)$$

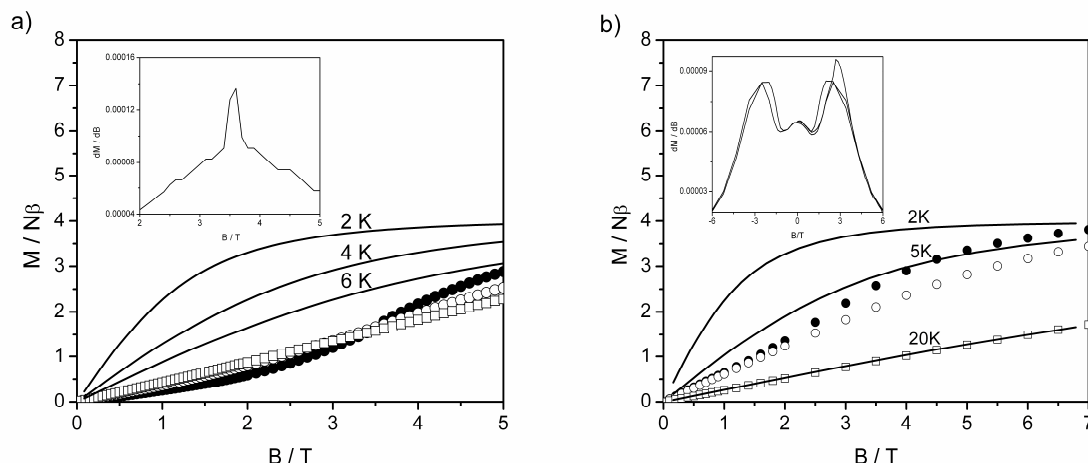


Figure 2.7. Plot of $M/N\beta$ vs magnetic field for **1** (a) and **2** (b) in the range 0 to 5 (7) T at 2 (●), 4 (5) (○) and 6 (20) (□) K and the theoretical curves calculated with the Brillouin function assuming non-interacting spins $S = 2$. Inset, dM/dB vs B for **1** and **2** at $T = 2$ K.

The experimental data in the range 12–20 K for **1** and 16–20 K for **2**, were least-square fitted with the equation (1) giving the parameters: $a = 0.0013 \text{ JK}^{-4} \text{ mol}^{-1}$, $b = -3.25 \times 10^{-6} \text{ JK}^{-6} \text{ mol}^{-1}$ and $c = 3.01 \times 10^{-9} \text{ JK}^{-8} \text{ mol}^{-1}$ and $a = 0.00168 \text{ JK}^{-4} \text{ mol}^{-1}$, $b = -5.04 \times 10^{-6} \text{ JK}^{-6} \text{ mol}^{-1}$ and $c = 5.32 \times 10^{-9} \text{ JK}^{-8} \text{ mol}^{-1}$ for compounds **1** and **2**, respectively. The T^3 term can be interpreted in terms of the Debye model:

$$\frac{C}{R} = \frac{12\pi^4}{5} \left(\frac{T}{\Theta_D} \right)^3 \quad (2)$$

from which a Debye temperature, $\theta_D = 56$ and 52 K is obtained for compounds **1** and **2**, respectively, which are typical values for this type of materials.³⁴ The magnetic heat capacities, C_m , obtained after subtracting the C_l as measured in zero applied field are displayed in Figure 2.8 for both compounds. The presence of broad maxima at temperatures 4.9 and 3.6 K for, respectively, compounds **1** and **2**, can be clearly distinguished by the heights of the maxima, amounting to about $C^{max}/R \approx 0.9$ for both. These maxima are interpreted as indicative of intrachain magnetic ordering. The much weaker anomalies observed around, *i.e.* 1.5 K and 1.4 K for compounds **1** and **2**, respectively, can be attributed to the establishment of long-range 3-D magnetic ordering between the chains, triggered by weak interchain magnetic coupling and likewise often observed in quasi-1-D magnetic materials.^{33,35} Furthermore, by integrating C_m/T with respect to the temperature the magnetic entropy S_m can be obtained as a function of temperature (see insets in Figures 2.8a,b) and thus the total entropy change (ΔS_m) associated with the magnetic degrees of freedom can be

deduced. For compounds **1** and **2**, the experimental ΔS_m values in zero field are found to be: $\Delta S_m/R = 1.32$ and 1.53 , respectively, close to the theoretical value $\Delta S_m/R = \ln(2S+1) = \ln 5 = 1.60 \text{ JK}^{-1} \text{ mol}^{-1}$ expected for a spin $S = 2$ system (per mol of substance).

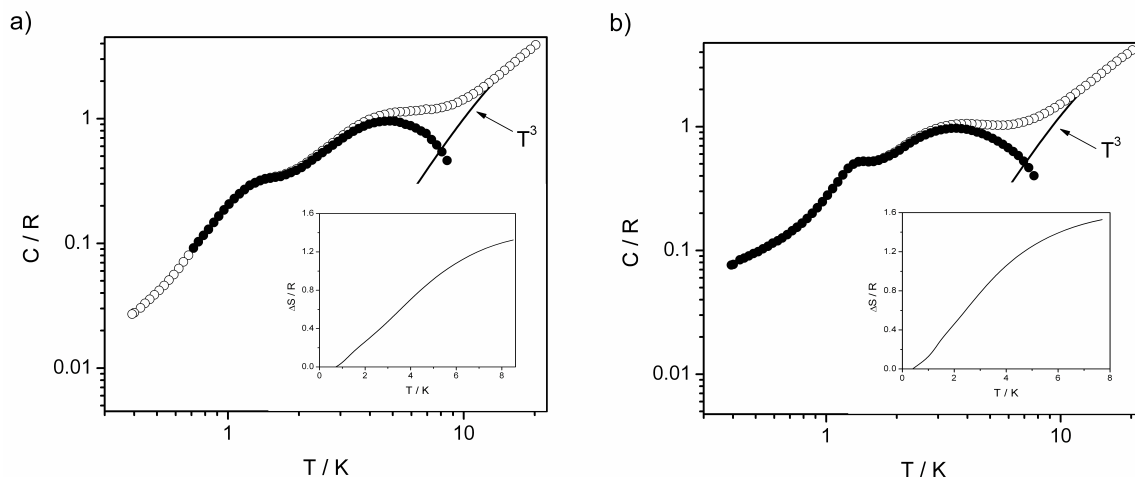


Figure 2.8. Total specific heat of compounds **1** (a) and **2** (b) measured in zero field. The estimated lattice contribution is shown by the solid curve. Dotted curves give the magnetic specific heat obtained after subtracting the phonon part. Inset, magnetic entropy curves obtained by integration of the data for compounds **1** and **2**.

From the positions of the maxima in the susceptibility (T_χ^{\max}) and specific heat (T_C^{\max}) a first rough estimate of the antiferromagnetic exchange constant J/k_B can be derived on basis of the predictions for the antiferromagnetic isotropic Heisenberg chain with $S = 2$.³³ With: $k_B T_\chi^{\max}/|J| = 7.1$ and $k_B T_C^{\max}/|J| = 4.25$, one obtains $J/k_B \approx 1 \text{ K}$ and 0.7 K for, respectively, compounds **1** and **2**. However, the observed height of the specific heat maximum is considerable larger than the value $C^{\max}/R \approx 0.67$ predicted for this model.³³ Indeed, since magnetic compounds of manganese(III) usually show sizable crystal field anisotropy, with D/k_B of order 1–10 K,³⁶ a comparison with predictions for the anisotropic (antiferromagnetic) Heisenberg chain with $S = 2$ should be more appropriate. In the simplest case of uniaxial anisotropy the corresponding Hamiltonian for the chain reads:

$$H = -2J \sum_{i=1}^{n-1} \{S_i \cdot S_{i+1}\} + D \sum_{i=1}^n S_{iz}^2 \quad (3)$$

Depending on the sign of D , the anisotropy can be either of the Ising-type, when $D < 0$, or of the XY (planar) type for $D > 0$. Numerical calculations of the specific heat anomalies predicted on basis of Hamiltonian (equation 3) with $S = 2$ have been published by Blöte for both signs of D .³⁷ Unfortunately, predictions for the susceptibility of this model are not available. Therefore the susceptibility data of **1** and **2** are compared in Figure 2.6b with

predictions for the isotropic ($D = 0$) $S = 2$ Heisenberg model³⁸ and for the parallel susceptibility of the $S = 2$ Ising model (for which the antiferromagnetic interaction is only present between the z-components of the spins).³³ As can be seen in Figure 2.6b, the predictions for the position and the height of the susceptibility maximum are not too different for the two models, and for temperatures $k_B T/|J| > 15$ the theoretical curves coincide. Fitting the experimental data in the 20–40 K range to theory yields the values $J/k_B \approx 1.1$ K and 0.7 K for, respectively, compounds **1** and **2**. The experimental susceptibility maxima lie below the isotropic case, as expected for the powder susceptibility of a Heisenberg antiferromagnet with crystal field anisotropy, since the latter lowers the susceptibility in the hard direction(s). Similar estimates of the exchange constants have been obtained from the analysis of the specific heat maxima. Using the temperatures 4.9 and 3.6 K of these maxima found for, respectively, compounds **1** and **2**, one obtains $k_B T_C^{\max}/|J| = 4.8$ and 4.0, respectively. The prediction by Blöte that comes closest to the experiments as regards position and height of the specific heat maximum is found to be the one with $|D/J| = 2$, with $D > 0$ (planar anisotropy) and $J < 0$ (antiferromagnetic). Although the prediction for $|D/J| = 2$ with $D < 0$ and $J < 0$ is not very different, it appears to decrease too fast in the temperature range below the maximum as compared to the experiment, see Figure 2.9 (the fast decrease is associated with the anisotropy gap in the energy spectrum induced by Ising-type anisotropy). In Figure 2.9 the data are compared to both these predictions, the fits yielding the same values as obtained from the susceptibility: $J/k_B \approx 1.1$ K and 0.7 K for compounds **1** and **2**, respectively. For comparison the predictions for the isotropic Heisenberg and the Ising chain models have been included. It can be clearly seen that the height of the specific heat maximum of the Ising model with $S = 2$ is much higher ($C^{\max}/R \approx 1.5$) than the experiment, whereas that of the pure Heisenberg case is too low ($C^{\max}/R \approx 0.67$). On basis of these results it is concluded that the magnetic anisotropy in **1** and **2** is not present in the magnetic exchange interaction, but arises instead from ligand field effects and is predominantly of planar symmetry. Obviously, on the basis of the present (powder) data it cannot be excluded that the symmetry is lower than uniaxial, for instance orthorhombic due to a substantial E -term. Therefore, HFEPN spectroscopic studies have been carried out to analyze the magnitude and symmetry of the zero-field splitting parameters (see Appendix A).

The behaviour of the field-dependent magnetization data, shown in Figure 2.7, confirms the above conclusions. Although ideally such measurements should be carried out on single crystals of the materials, powder data can still yield some valuable information. First, the comparison of the data with the Brillouin isotherms calculated for non-interacting spins $S = 2$, clearly confirms the presence of a substantial antiferromagnetic intrachain interaction, since the measured data fall much below the non-interacting limits. Second, for the anisotropic

Heisenberg antiferromagnet estimates of the antiferromagnetic exchange can be obtained from the saturation field, B_{sat} , measured at the lowest temperature. For the present purpose, the two comparisons can be approximately related by the equation $B_{\text{sat}} \approx 4z|J|S/g\beta$, bearing in mind that powder data are involved, *i.e.* the magnetization measured is an average over the different magnetic axes. Here z is the number of nearest magnetic neighbours ($z = 2$ for the chain). The magnetization curves taken at $T = 2$ K are seen to approach saturation for $B_{\text{sat}} \approx 7$ T for compound **2** (given that the saturation magnetization should correspond to $4 N\beta$). For compound **1** an (extrapolated) value of about 9–10 T appears to be indicated. With $B_{\text{sat}} \approx 9$ T and 7 T, it is estimated that $J/k_B \approx -1.2$ K and -0.9 K for compounds **1** and **2** respectively, in agreement with the values derived from susceptibility and specific heat.

Furthermore, for both materials a discontinuity in the slope of the M vs B curves as measured at $T = 2$ K may be noted at critical fields $B_c \approx 3.6$ T and 2.5 T for, respectively, compounds **1** and **2**. This discontinuity is seen more clearly in the plots of the slope dM/dB vs field given in the insets of Figure 2.7. At higher temperatures ($\gg z|J|/k_B$) the magnetization curve becomes linear, confirming that the discontinuity originates from the antiferromagnetic exchange. The effect could be due to a spin-flop phenomenon within the easy plane in case a weaker orthorhombic component E is present, imposing a preferential axis within this plane. However, more complicated field-induced transitions as may occur in more complex magnetic structures can of course not be excluded on basis of the present powder data.

As mentioned above, the small peaks observed in the specific heat of both compounds at approximately $T_c \approx 1.5$ K should correspond to the transition to 3-D long-range induced by the presence of weak interchain interactions, J'/k_B . The strength of these interchain couplings can be estimated from the ratio of T_c to the intrachain exchange J/k_B by a well known mean-field argument that runs as follows. In a system of weakly coupled chains, the 3-D ordering will occur at a temperature T_c at which the thermal energy, $k_B T_c$, equals the interaction energy between a given spin with a correlated chain segment in a neighbouring chain. Since the length of the correlated segment is proportional to the correlation length, the interchain ordering process is thus driven by the divergence of the intrachain correlation length $\xi(T)$ as $T \rightarrow 0$. Then the value of T_c will be given by the expression:

$$k_B T_c / |J| = \xi(T_c) R S(S+1) \quad (4)$$

where $R = |J'/J|$ is the ratio of inter- to intrachain exchange interactions. For the XY chain the temperature dependence of $\xi(T)$ is given by:

$$\xi(T) = 4|J|S(S+1)/k_B T_c \quad (5)$$

therefore:

$$k_B T_c / |J| = 2S(S+1)(R)^{1/2} \quad (6)$$

The obtained R values are equal to 0.013 and 0.028 for compounds **1** and **2**, corresponding to $|J|/k_B \approx 0.014$ K and 0.021 K, respectively. These values are of the order of the estimated magnetic dipolar interactions between neighbouring chains in these materials.

In summary, compounds **1** and **2** show antiferromagnetic behaviour as it is in fact expected for compounds in which superexchange is mediated through hydrogen bonds, since these are well known to mediate weak magnetic interactions.^{39,40} For compound **1**, the maxima in χ_M and C_m are found at higher temperatures than for compound **2**, indicating a larger value of the magnetic superexchange interaction. The analysis of the magnetic specific heat data shows that a fit for compounds **1** and **2** is not possible, neither with the pure isotropic Heisenberg model, nor with the pure Ising antiferromagnetic chain models. Reasonable agreement was found with predictions for the anisotropic Heisenberg model with planar anisotropy for the antiferromagnetic $S = 2$ chain, the anisotropy originating from ligand field effects on the manganese(III) ion. Further studies have been performed with HFEPN spectroscopy, to confirm the sign and the magnitude of the anisotropy (see Appendix A). The temperature dependence of the specific heat also revealed the presence of long-range 3-D magnetic ordering between the chains below about 1.5 K for both compounds, probably induced by the weak interchain dipolar interactions.

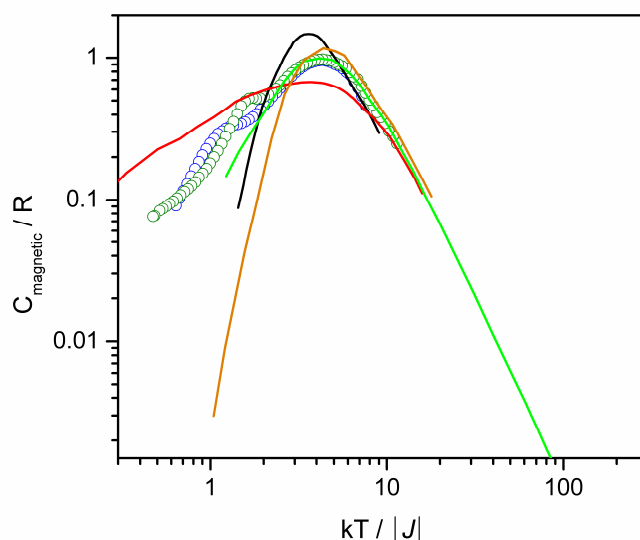


Figure 2.9. Comparison of the zero-field specific heat maximum for compounds **1** (blue circles) and **2** (green circles) with the predictions for the specific heat of the antiferromagnetic $S = 2$ chain for Heisenberg (red line), Ising (black line) and isotropic exchange interaction and positive D terms, $D/|J| = +2$ (light green line) and negative $D/|J| = -2$ (orange line), taken from Ref.37.

Compounds 3–6. Figure 2.10a shows no maximum in the χ_M vs T curve for both compounds **3** and **4**. Nevertheless, the magnetization data (Figure 2.11) taken at low temperature lie well below the calculated Brillouin curves for non-interacting spin $S = 2$ for both, indicating that antiferromagnetic intrachain interactions are likely to be present. In compound **3**, the $\chi_M T$ value stays almost constant down to about 20 K, where after it drops rather sharply. The deviations from the Brillouin curves are also smaller for this material than for **4**, suggesting that the antiferromagnetic intrachain interaction in **3** is quite weak and only becomes discernable below about 15 K. In compound **4**, the temperature dependence of χ_M and the behaviour of the magnetization suggest a stronger antiferromagnetic intrachain interaction. Compounds **3** and **4** form similar chain structures as compounds **1** and **2** where the N_2O_2 planes are parallel to each other in and between the chains. The most relevant structural difference is the increase of the distance between the manganese(III) ions along the chain imposed by the ligand $H_2phpzMe$. Consequently, antiferromagnetic interactions are weaker when compared with compounds **1** and **2**. Similar magnetic behaviour is observed for compounds **5** and **6**.

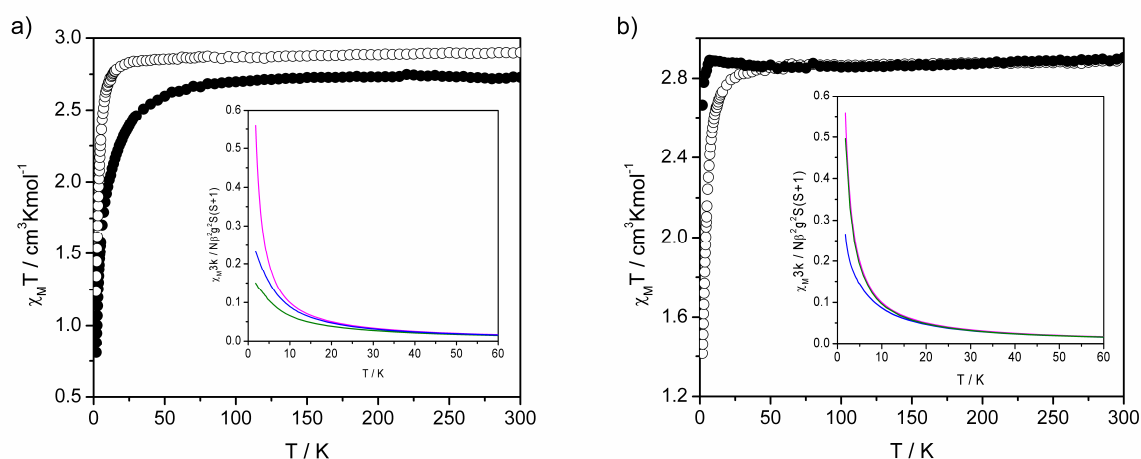


Figure 2.10. a) Plot of $\chi_M T$ vs T for **3** (\circ) and **4** (\bullet) in the range 1.8 to 300 K in 0.1 T applied field. Inset, plot of χ_M vs T for **3** (blue) and **4** (green) with the paramagnetic behaviour (magenta). b) Plot of $\chi_M T$ vs T for **7** (\circ) and **8** (\bullet) in the range 1.8 to 300 K in 0.1 T applied field. Inset, plot of χ_M vs T for **7** (blue) and **8** (green). The paramagnetic behaviour (magenta) just overlaps with the curve for **8** at all temperature range shown.

Compounds 7 and 8. The $\chi_M T$ value again remains almost constant down to about 30 K and 7 K for compounds **7** and **8**, respectively (Figure 2.10b). The temperature dependence of χ_M for compound **7** lies below the paramagnetic behaviour, while that of compound **8** overlaps with it. The low-temperature magnetization curves given in Figure 2.12, indicate the

presence of weak antiferromagnetic interactions in **7** (similar in strength as in **4**), whereas compound **8** basically behaves as a paramagnet.

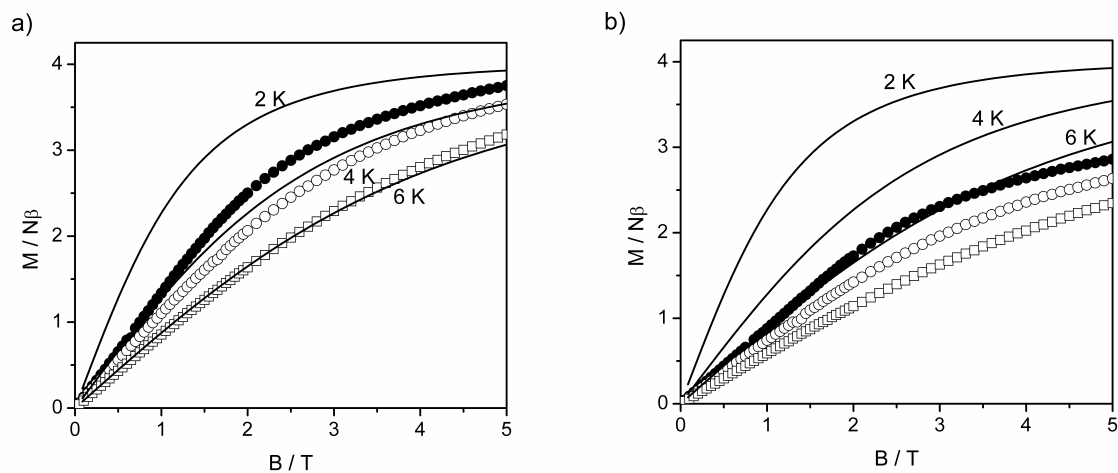


Figure 2.11. Plot of $M/N\beta$ vs magnetic field for **3** (a) and **4** (b) in the range 0 to 5 T at 2 (●), 4 (○) and 6 (□) K and the theoretical curves calculated with the Brillouin function assuming one non-interacting spin $S = 2$.

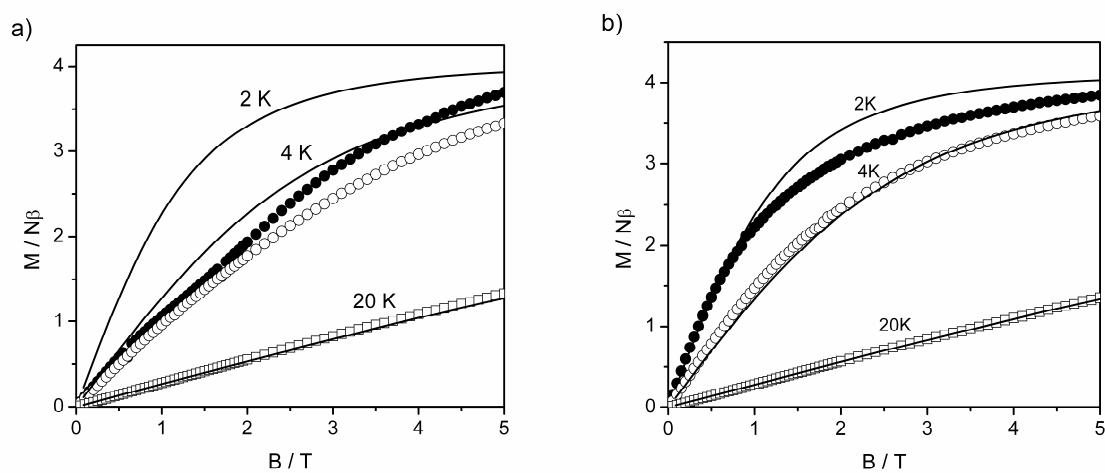


Figure 2.12. Plot of $M/N\beta$ vs magnetic field for **5** (a) and **6** (b) in the range 0 to 5 T at 2 (●), 4 (○) and 20 (□) K and the theoretical curves calculated with the Brillouin function assuming one non-interacting spin $S = 2$.

2.4. Conclusions

A family of five-coordinated manganese(III) compounds with the general formula $[\text{Mn}(\text{HphpzR})_2\text{X}]$ ($\text{R} = \text{H}, \text{Me}, \text{Et}, \text{Ph}$ and $\text{X}^- = \text{Cl}^-, \text{Br}^-$) (**1–8**), has been synthesized and characterized. In compounds **1–8**, the square-pyramidal geometry is thermodynamically favoured above the well known octahedral-based geometry for a manganese(III) ion, probably due to the formation of the neutral molecular compounds.³⁰ Nevertheless, a complex with octahedral geometry can also be formed in the presence of an excess of ligand as illustrated by the formation of compound **9** that was only characterized crystallographically. The type and the strength of magnetic interactions between manganese(III) ions have been studied by changing the ligand and the type of halogen coordinated to the manganese(III) ion. From the X-ray crystallographic studies, it can be seen that the presence of various substituents on the pyrazole ring of the ligand does neither significantly modify the coordination geometry of the metal ion, nor the coordination mode of the ligand. However, the steric effects of the ligand side groups result in a difference in the crystal packing of the compounds. Compounds **1–4** form ladder-like chains as a result of the intermolecular hydrogen bonding interactions, while compounds **7** and **8** are isolated mononuclear units arranged in a face-to-face manner that form hydrogen bonds only with the solvent molecules. The observed differences in the crystal packing, as well as the distance between the manganese(III) ions, appear to be essential in determining the type and the strength of the magnetic interactions. Compounds **1** and **2** show antiferromagnetic short-range interactions between the manganese(III) ions. Specific heat measurements confirm the presence of 1-D short-range correlations and long-range magnetic ordering below 1.5 K. Compounds **3–8** exhibit weaker antiferromagnetic interactions. In these cases, the strength of the magnetic interactions is smaller due to the steric hindrance of the ligand that separates the manganese(III) ions. This family of compounds proves that small structural differences can strongly influence the magnetic properties. Some of the compounds described here have been used as building blocks for the synthesis of higher nuclearity compounds that will be discussed in the following chapters (Chapter 3 and 5).

2.5. References

1. Aromí, G.; Brechin, E. K., *Struc. Bond.*, **2006**, 122, 1-67.
2. Christou, G.; Gatteschi, D.; Hendrickson, D. N.; Sessoli, R., *MRS Bull.*, **2000**, 25, 66-71.
3. Gatteschi, D.; Sessoli, R., *Angew. Chem.-Int. Edit.*, **2003**, 42, 268-297.
4. Wernsdorfer, W.; Aliaga-Alcalde, N.; Hendrickson, D. N.; Christou, G., *Nature*, **2002**, 416, 406-409.
5. Miyasaka, H.; Saitoh, A.; Abe, S., *Coord. Chem. Rev.*, **2007**, 251, 2622-2664.
6. Lecren, L.; Wernsdorfer, W.; Li, Y. G.; Vindigni, A.; Miyasaka, H.; Clérac, R., *J. Am. Chem. Soc.*, **2007**, 129, 5045-5051.
7. Kachi-Terajima, C.; Miyasaka, H.; Sugiura, K.; Clérac, R.; Nojiri, H., *Inorg. Chem.*, **2006**, 45, 4381-4390.

8. Ajò, D.; Bencini, A.; Mani, F., *Inorg. Chem.*, **1988**, 27, 2437-2444.
9. Tanase, S.; Koval, I. A.; Bouwman, E.; De Gelder, R.; Reedijk, J., *Inorg. Chem.*, **2005**, 44, 7860-7861.
10. Mukherjee, R., *Coord. Chem. Rev.*, **2000**, 203, 151-218.
11. Tanase, S.; Aromí, G.; Bouwman, E.; Kooijman, H.; Spek, A. L.; Reedijk, J., *Chem. Commun.*, **2005**, 3147-3149.
12. Tanase, S.; Bouwman, E.; Long, G. J.; Shahin, A. M.; Mills, A. M.; Spek, A. L.; Reedijk, J., *Eur. J. Inorg. Chem.*, **2004**, 4572-4578.
13. Viciano-Chumillas, M.; Tanase, S.; Aromí, G.; Smits, J. M. M.; de Gelder, R.; Solans, X.; Bouwman, E.; Reedijk, J., *Eur. J. Inorg. Chem.*, **2007**, 2635-2640.
14. Mozingo, R., *Org. Synth.*, **1941**, 21, 42-44.
15. Sequin, U., *Helv. Chim. Acta*, **1981**, 64, 2654-2664.
16. Wheeler, T. S., *Org. Synth.*, **1952**, 32, 72-76.
17. Addison, A. W.; Burke, P. J., *J. Heterocycl. Chem.*, **1981**, 18, 803-805.
18. Kahn, O., *Molecular Magnetism*. Wiley-VCH: New York, 1993.
19. Sheldrick, G. M. *Program for Empirical Absorption Correction*, University of Göttingen, Germany: 1996.
20. Beurskens, P. T.; Beurskens, G.; Strumpel, M.; Nordman, C. E., in *Patterson and Pattersons*. Glusker, J. P.; Patterson, B. K.; Rossi, M., Eds. Clarendon Press: Oxford: 1987.
21. Duisenberg, A. J. M.; Kroon-Batenburg, L. M. J.; Schreurs, A. M. M., *J. Appl. Crystallogr.*, **2003**, 220-229.
22. Duisenberg, A. J. M. Reflections on area detectors. PhD thesis, Utrecht, 1998.
23. Beurskens, P. T.; Beurskens, G.; Bosman, W. P.; De Gelder, R.; García-Granda, S.; Gould, R. O.; Israël, R.; Smits, J. M. M.; Smykalla, C. *The DIRDIF96. A computer program system for the crystal structure determination by Patterson methods and direct methods applied to difference structure factors*, Crystallography Laboratory, University of Nijmegen: Nijmegen, The Netherlands, 1996.
24. Sheldrick, G. M. *SHELXS-97: Program for Crystal Structures Determination*, University of Göttingen; Germany: Göttingen, 1997.
25. Sheldrick, G. M. *SHELXL-97: Program for the Refinement of Crystal Structures*, University of Göttingen; Germany: Göttingen, 1997.
26. Nakamoto, K., *Infrared and Raman Spectra of Inorganic and Coordination Compounds*. 4th ed ed.; John Wiley & Sons Inc 1997.
27. Lever, A. B. P., *Inorganic Electronic Spectroscopy*. Elsevier: Amsterdam, 1997.
28. Godbole, M. D.; Grigiotti, E.; Zanello, P.; Mills, A. M.; Spek, A. L.; Bouwman, E., *Inorg. Chim. Acta*, **2005**, 358, 233-238.
29. Viciano-Chumillas, M.; Tanase, S.; Mutikainen, I.; Turpeinen, M.; de Jongh, L. J.; Reedijk, J., *Inorg. Chem.*, **2008**, 47, 5919-5929.
30. Katsuki, T., *Coord. Chem. Rev.*, **1995**, 140, 189-214.
31. Addison, A. W.; Rao, T. N.; Reedijk, J.; Vanrijn, J.; Verschoor, G. C., *J. Chem. Soc.-Dalton Trans.*, **1984**, 1349-1356.
32. Carlin, R. L., *Magnetochemistry*. Springer-Verlag: Berlin, 1986.
33. de Jongh, L. J.; Miedema, A. R., *Adv. Phys.*, **2001**, 50, 947-1170.
34. Evangelisti, M.; Luis, F.; de Jongh, L. J.; Affronte, M., *J. Mater. Chem.*, **2006**, 16, 2534-2549.
35. Granroth, G. E.; Meisel, M. W.; Chaparala, M.; Jolicœur, T.; Ward, B. H.; Talham, D. R., *Phys. Rev. Lett.*, **1996**, 77, 1616-1619.
36. Boča, R., *Coord. Chem. Rev.*, **2004**, 248, 757-815.
37. Blote, H. W. J., **1975**, 79, 427-466.
38. Weng, C. H. PhD thesis, Carnegie-Mellon University, Pittsburg, PA, 1968.
39. Delgado, F. S.; Kerbellec, N.; Ruiz-Pérez, C.; Cano, J.; Lloret, F.; Julve, M., *Inorg. Chem.*, **2006**, 45, 1012-1020.
40. Desplanches, C.; Ruiz, E.; Rodríguez-Forteza, A.; Alvarez, S., *J. Am. Chem. Soc.*, **2002**, 124, 5197-5205.

Chapter 3

Mononuclear compounds as building blocks for the design of trinuclear manganese(III) compounds with a $[\text{Mn}_3(\mu_3\text{-O})(\text{phpzR})_3]^+$ core*

Mononuclear compounds with the general formula $[\text{Mn}(\text{HphpzR})_2\text{X}]$ have been used as building blocks for the synthesis of trinuclear oxide-centred manganese(III) compounds $[\text{Mn}_3(\mu_3\text{-O})(\text{phpzH})_3(\text{MeOH})_3(\text{OAc})]_n$ (**10**), $[\text{Mn}_3(\mu_3\text{-O})(\text{phpzMe})_3(\text{MeOH})_3(\text{OAc})] \cdot 1.5\text{MeOH}$ (**11**) and $[\text{Mn}_3(\mu_3\text{-O})(\text{phpzH})_3(\text{MeOH})_4(\text{N}_3)]_n \cdot n\text{MeOH}$ (**12**). The synthesis, crystal structure and magnetic properties of these three new manganese(III) compounds are reported. Temperature-dependent magnetic susceptibility studies indicate the presence of predominant antiferromagnetic intramolecular interactions between manganese(III) ions in **10** and **12**, while both antiferromagnetic and ferromagnetic intramolecular interactions are operative in **11**. A detailed discussion of magneto-structural correlations of oxide-centred trinuclear manganese(III) compounds is presented.

* This chapter has been published in the literature: Viciano-Chumillas M., Tanase S., Mutikainen I., Turpeinen U., de Jongh L.J., Reedijk J., *Inorg. Chem.*, **2008**, 47, 5919-5929.

3.1. Introduction

Polynuclear manganese clusters have been extensively studied for two main reasons. The first one is the biological relevance as models for the water oxidation centre of Photosystem II.¹ The second is the paramagnetic nature of the manganese ion in various oxidation states providing interesting magnetic properties.²⁻⁴ Synthetically, numerous efforts have been made in order to obtain a variety of manganese clusters.^{2,5} Two well known approaches have been developed in the literature. The first one, the designed synthesis of such clusters, is based upon the use of rigid ligands that allow the control of the geometry of the cluster.⁶ The second approach is based on the serendipitous assembly of flexible ligands with metal ions, where the use of different synthetic conditions can give rise to a rich chemistry.⁷ Whilst carboxylate ligands have been the most studied,⁸ considerable efforts have recently been applied to the design of various pyrazole-based ligands showing an interesting coordination chemistry.⁹⁻¹⁵

Synthetic strategies can also involve the use of preformed simple molecules, *i.e.* building blocks with tendency of self-assembly to form more complex molecules.^{8,16} In addition, new families of related compounds are very useful for the purpose of controlling the synthesis and investigating the structure/property relationships. To achieve this goal, in Chapter 2 a family of mononuclear manganese(III) compounds with general formula $[\text{Mn}(\text{HphpzR})_2\text{X}]$, has been synthesized, where H_2phpzR can be 3(5)-(2-hydroxyphenyl)-pyrazole ($\text{R} = \text{H}$) and 3(5)-(2-hydroxyphenyl)-5(3)-methylpyrazole ($\text{R} = \text{Me}$) and $\text{X}^- = \text{Cl}^-$, Br^- .¹⁷ These mononuclear manganese(III) compounds are five-coordinated. Therefore, the empty position in the coordination sphere of the manganese(III) ion and the lability of the halogen leads to use them as starting materials with different bridging ligands, *i.e.* acetate and azide. Moreover the structural differences on the phenol-pyrazole ligands can drive the formation of new compounds with several topologies. In this chapter, it is shown that these compounds are indeed promising building blocks to synthesize complexes of higher nuclearity containing the core $[\text{Mn}_3(\mu_3\text{-O})(\text{phpzR})_3]^+$ ($\text{R} = \text{H}, \text{Me}$). The synthesis, X-ray crystal structures and magnetic properties of the oxide-centred manganese(III) triangles $[\text{Mn}_3(\mu_3\text{-O})(\text{phpzH})_3(\text{MeOH})_3(\text{OAc})]_n$ (**10**), $[\text{Mn}_3(\mu_3\text{-O})(\text{phpzMe})_3(\text{MeOH})_3(\text{OAc})] \cdot 1.5\text{MeOH}$ (**11**) and $[\text{Mn}_3(\mu_3\text{-O})(\text{phpzH})_3(\text{MeOH})_4(\text{N}_3)]_n \cdot n\text{MeOH}$ (**12**) are described in detail. Most of the oxide-centred manganese(III) triangles described in the literature contain predominant antiferromagnetic interactions between the manganese(III) ions. Therefore, a detailed discussion of magneto-structural correlations of oxide-centred trinuclear manganese(III) compounds is described to understand the important factors for tuning the magnetic properties.

3.2. Experimental Section

Syntheses. All manipulations were performed using commercial materials as received. The compounds $[\text{Mn}(\text{HphpzR})_2\text{X}]$ ($\text{R} = \text{H}, \text{Me}$ and $\text{X}^- = \text{Cl}^-, \text{Br}^-$) have been synthesized according to the literature procedure.¹⁷ *Safety note:* Azide salts and perchlorate salts are potentially explosive. Such compounds should be used in small quantities and should be treated with utmost care at all times.

$[\text{Mn}_3(\mu_3\text{-O})(\text{phpzH})_3(\text{MeOH})_3(\text{OAc})]_n$ (10). $[\text{Mn}(\text{HphpzH})_2\text{Br}]$ (20 mg, 0.044 mmol) was dissolved in methanol, followed by the addition of a solution of sodium methoxide (7 mg, 0.13 mmol) and a solution of $\text{Mn}(\text{OAc})_2 \cdot 4\text{H}_2\text{O}$ (22 mg, 0.089 mmol) in methanol. Green single crystals (18 mg, 0.022 mmol) were obtained by slow evaporation of the reaction mixture. Yield: 75%. Anal. Calcd for **10** ($\text{C}_{32}\text{H}_{33}\text{Mn}_3\text{N}_6\text{O}_9$): C, 47.42; H, 4.10; N, 10.37. Found: C, 47.42; H, 4.37; N, 10.65. IR ($\nu_{\text{max}}/\text{cm}^{-1}$): 1599(m), 1541(m), 1515(w), 1481(vs), 1454(m), 1430(m), 1351(w), 1336(m), 1296(vs), 1250(s), 1142(s), 1132(s), 1078(s), 1028(m), 1014(s), 985(m), 860(s), 775(s), 749(vs), 674(vs), 645(vs), 600(vs), 577(m), 449(s), 394(s), 324(s). ESI-MS (m/z , %): 737 (100) $[\text{Mn}_3(\mu_3\text{-O})(\text{phpzH})_3(\text{CH}_3\text{CN})_2]^+$, 696 (77) $[\text{Mn}_3(\mu_3\text{-O})(\text{phpzH})_3(\text{CH}_3\text{CN})]^+$, 655 (16) $[\text{Mn}_3(\mu_3\text{-O})(\text{phpzH})_3]^+$.

$[\text{Mn}_3(\mu_3\text{-O})(\text{phpzMe})_3(\text{MeOH})_3(\text{OAc})] \cdot 1.5\text{MeOH}$ (11). A solution of sodium methoxide (8 mg, 0.14 mmol) in methanol was added to a methanolic solution of $[\text{Mn}(\text{HphpzMe})_2\text{Br}]$ (21 mg, 0.044 mmol), followed by a solution of $\text{Mn}(\text{OAc})_2 \cdot 4\text{H}_2\text{O}$ (22 mg, 0.090 mmol) in methanol. The slow evaporation of the reaction mixture affords green single crystals (16 mg, 0.018 mmol). Yield: 61%. Anal. Calcd for **11** ($\text{C}_{35}\text{H}_{39}\text{Mn}_3\text{N}_6\text{O}_9 \cdot 1.5(\text{CH}_4\text{O})$): C, 48.68; H, 5.04; N, 9.33. Found: C, 48.44; H, 4.16; N, 10.67. IR ($\nu_{\text{max}}/\text{cm}^{-1}$): 1599(m), 1558(m), 1532(m), 1496(m), 1456(s), 1405(m), 1297(vs), 1269(s), 1246(s), 1126(s), 1090(w), 1060(m), 1037(m), 864(s), 792(m), 748(vs), 725(vs), 668(vs), 648(vs), 604(vs), 580(s), 418(s), 412(s), 384(vs), 318(s). ESI-MS (m/z , %): 442 (100) $[\text{Mn}(\text{HphpzMe})_2(\text{CH}_3\text{CN})]^+$, 871 (34) $[\text{Mn}_3(\mu_3\text{-O})(\text{phpzMe})_3(\text{MeOH})_3(\text{OAc})(\text{H}_3\text{O})]^+$, 738 (22) $[\text{Mn}_3(\mu_3\text{-O})(\text{phpzMe})_3(\text{CH}_3\text{CN})]^+$.

$[\text{Mn}_3(\mu_3\text{-O})(\text{phpzH})_3(\text{MeOH})_4(\text{N}_3)]_n \cdot n\text{MeOH}$ (12). A solution of NaN_3 (17 mg, 0.26 mmol) was added to a solution of $[\text{Mn}(\text{HphpzH})_2\text{Cl}]$ (30 mg, 0.073 mmol) in MeOH. The solution was stirred for 5 minutes and filtered, and the green filtrate left undisturbed to concentrate slowly by evaporation. Green crystals (15 mg, 0.017 mmol) appeared within a few weeks. Yield: 70%. Anal. Calcd for **12** ($\text{C}_{32}\text{H}_{38}\text{Mn}_3\text{N}_9\text{O}_9$): C, 44.82; H, 4.47; N, 14.70. Found: C, 43.81; H, 3.84; N, 16.30. The discrepancy between calculated and obtained elemental percentages for compound **12** arises from analytical variations due to the incomplete combustion of the sample (the purity of the sample was checked by X-ray

crystallography). IR ($\nu_{\max}/\text{cm}^{-1}$): 3352(w), 2039(s), 1599(m), 1563(m), 1512(w), 1481(s), 1454(m), 1429(m), 1352(m), 1338(m), 1297(s), 1250(s), 1144(s), 1130(s), 1078(s), 1036(w), 1007(m), 986(m), 860(s), 782(m), 747(vs), 673(vs), 644(s), 598(vs), 448(s), 390(s), 353(w), 329(w). ESI-MS (m/z , %): 655 (29) $[\text{Mn}_3(\mu_3\text{-O})(\text{phpzH})_3]^+$, 696 (72) $[\text{Mn}_3(\mu_3\text{-O})(\text{phpzH})_3(\text{CH}_3\text{CN})]^+$, 736 (100) $[\text{Mn}_3(\mu_3\text{-O})(\text{phpzH})_3(\text{CH}_3\text{CN})_2]^+$.

Physical Measurements. Elemental analyses for C, H and N were performed on a Perkin-Elmer 2400 series II analyzer. Infrared spectra ($4000\text{--}300\text{ cm}^{-1}$) were recorded on a Perkin-Elmer Paragon 1000 FTIR spectrometer equipped with a Golden Gate ATR device, using the reflectance technique. Electrospray mass spectra (ESI-MS) in acetonitrile solution were obtained on a Thermo Finnigan AQA apparatus. DC magnetic data were recorded using a Quantum Design MPMS-5 SQUID susceptometer. The magnetic susceptibilities were measured from 1.8 to 300 K on polycrystalline samples in a gelatine capsule with applied field of 0.1 T. The magnetization was measured at 2, 4 and 6 K in the 0–5 T range. Data were corrected for magnetization of the sample holder and for diamagnetic contributions, which were estimated from Pascal's constants.¹⁸

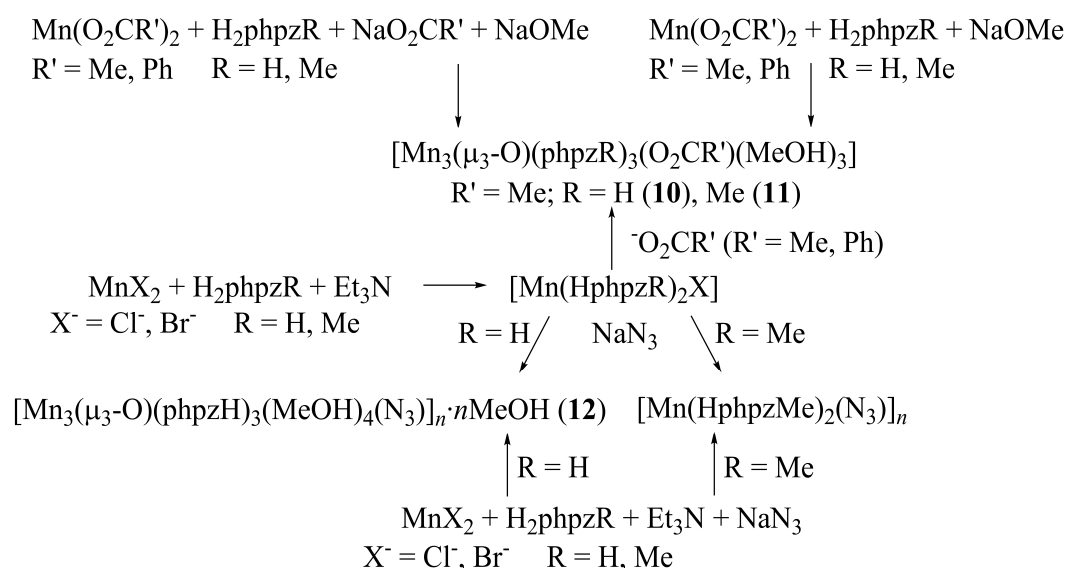
X-ray Crystallography. Intensity data for single crystals of **10**, **11** and **12** were collected using MoK α radiation ($\lambda = 0.71073\text{ \AA}$) on a Nonius KappaCCD diffractometer. Crystal and refinement data for **10**, **11** and **12** are collected in Table 3.1. The intensity data were corrected for Lorentz and polarization effects, and for absorption (multiscan absorption correction¹⁹). The structures were solved by Patterson methods.²⁰ The programs EvalCCD,²¹ DIRDIF96,²² SHELXS-97²³ and SHELXL-97^{24,25} were used for data reduction, structure solution and refinement, respectively. All non-hydrogen atoms were refined with anisotropic displacement parameters. Geometric calculations and molecular graphics were performed with the PLATON package.²⁶

3.3. Results and Discussion

Syntheses. Mononuclear complexes with the general formula $[\text{Mn}(\text{HphpzR})_2\text{X}]$ ($\text{R} = \text{H, Me}$; $\text{X}^- = \text{Cl}^-, \text{Br}^-$)¹⁷ prove to be excellent starting materials for high-nuclearity manganese(III) complexes as it is shown in the present chapter. Compounds **10** and **11** were synthesized with the addition of manganese(II) acetate to $[\text{Mn}(\text{HphpzR})_2\text{Br}]$ ($\text{R} = \text{H, Me}$) in the presence of sodium methoxide. An alternative route¹¹ was reported recently for compound **10**, using only the manganese(II) acetate salt. Following the same published procedure, with the ligand 3(5)-(2-hydroxyphenyl)-5(3)-methylpyrazole, H_2phpzMe , the compound **11** can

also be obtained in 82% yield. Additionally, both compounds can be synthesized using the reaction of the manganese(II) acetate salt with the ligand H₂phpzR (R = H, Me) in the presence of NaO₂CMe and NaOMe (Scheme 3.1). Some attempts to replace the acetate at the axial position by other carboxylates, such as benzoate were performed using the same described synthetic procedures (Scheme 3.1). The IR, EA and ESI-MS analyses revealed the formation of new complexes with the presence of the benzoate. However, single-crystals were not obtained to confirm the formula of the compounds as [Mn₃(μ₃-O)(phpzR)₃(MeOH)₃(O₂CPh)] (R = H, Me). Therefore new synthetic routes were explored (see Chapter 4).

Compound **12** was obtained by reaction of [Mn(HphpzH)₂Cl] and NaN₃ in methanol. The same compound can also be synthesized from manganese(II) chloride in the presence of H₂phpzH, sodium azide and triethylamine in methanol. The infrared spectrum reveals the presence of the azide exhibiting a sharp band at 2039 cm⁻¹. Following the same synthetic procedures of compound **12**, with the ligand H₂phpzMe, small green crystals were obtained. Unfortunately, the quality was not good enough for X-ray determination. However, IR, EA and ESI-MS analyses reveal the formation of the complex with formula [Mn(HphpzMe)₂N₃]_n. Probably a chain is formed, which may explain the poor solubility of the complex. Scheme 3.1 summarizes the synthetic procedures and complexes obtained that are discussed in this chapter. The ESI-MS studies for compounds **10–12** clearly show the stability of the core [Mn₃(μ₃-O)(phpzR)₃]⁺ (R = H, Me) in solution.



Scheme 3.1. Synthetic procedures for manganese(III) compounds discussed in this chapter.

Table 3.1. Crystal data and structure refinements for compounds **10**, **11** and **12**.

	10	11	12
Formula	C ₃₂ H ₃₃ Mn ₃ N ₆ O ₉	C ₃₅ H ₃₉ Mn ₃ N ₆ O ₉ , 1.5(CH ₄ O)	C ₃₂ H ₃₈ Mn ₃ N ₉ O ₉
Formula mass [g mol ⁻¹]	810.46	900.61	857.53
Crystal system	Monoclinic	Monoclinic	Monoclinic
Space group	P2 ₁ /c	C2/c	C2/c
<i>a</i> [Å]	20.364(4)	25.535(5)	45.999(9)
<i>b</i> [Å]	7.6580(15)	8.038(2)	7.512(2)
<i>c</i> [Å]	21.664(4)	39.853(9)	23.563(5)
α [°]	90	90	90
β [°]	91.41(3)	95.51(3)	116.35(3)
γ [°]	90	90	90
<i>V</i> [Å ³]	3377.4(11)	8142(3)	7296(3)
<i>Z</i>	4	8	8
<i>D</i> _{calc} [g cm ⁻³]	1.594	1.469	1.561
Crystal size	0.01×0.07×0.20	0.02×0.11×0.30	0.18×0.20×0.22
Crystal shape and colour	Needles and green	Needles and green	Blocks and green
Number of collected reflections (unique)	47972(7741)	39218(6877)	24373(6288)
Number of observed reflections [<i>I</i> _o > 2σ(<i>I</i> _o)]	5171	2862	4420
Internal R factor	0.097	0.185	0.043
Number of parameters	451	513	482
Goodness-of-fit <i>S</i> on <i>F</i> ²	1.02	1.04	1.04
μ [mm ⁻¹]	1.168	0.979	1.088
<i>R</i> ₁ ^[a] [<i>I</i> > 2.0σ(<i>I</i>)]	0.0464	0.0976	0.0381
<i>wR</i> ₂ ^[b] [all data]	0.1149	0.2456	0.0901
<i>T</i> [°C]	173	173	173
^[a] $R_1 = \sum F_o - F_c / \sum F_o $. ^[b] $wR_2 = \{\sum [w(F_o^2 - F_c^2)^2] / \sum w(F_o^2)^2\}^{1/2}$.			

Description of the Molecular Structures. The X-ray structure of compound **10** has been reported independently by others¹¹ during the progress of this work. As shown in Figure 3.1, it consists of an equilateral triangle formed by three manganese(III) ions that are bridged by a central oxygen. The three doubly deprotonated ligands, *phpzH*²⁻, are in a plane with their manganese(III) ions. Three methanol molecules and an acetate group are at the apical positions. As a result, all the three manganese(III) ions are hexacoordinated. The trinuclear units are linked by an acetate bridge. The Mn⋯Mn distances in the trinuclear unit are 3.306 Å, 3.313 Å and 3.307 Å for Mn(1)⋯Mn(2), Mn(1)⋯Mn(3) and Mn(2)⋯Mn(3), respectively. The μ₃-O²⁻ (O1) ion is 0.110 Å above the Mn₃ plane. The Mn–O(1) distances are 1.917(2) Å for Mn(1), 1.904(2) Å for Mn(2) and 1.919(2) Å for Mn(3). The Mn–O(1)–Mn angles are

Mn(1)–O(1)–Mn(2) = 119.78(12)°; Mn(1)–O(1)–Mn(3) = 119.47(11)° and Mn(2)–O(1)–Mn(3) = 119.77(11)°. Hydrogen bonding is present between the methanol molecules and the acetate ligand (Figure 3.1 and Table 3.4).

Table 3.2. Selected bonds lengths [Å] and angles [°] for compound **11**.

Bond Lengths					
Mn(1)–O(1)	1.900(6)	Mn(2)–O(6)	2.457(7)	Mn(3)–N(61)	1.958(10)
Mn(1)–O(5)	2.244(8)	Mn(2)–N(25)	2.008(8)	Mn(3)–O(3)	2.098(7)
Mn(1)–N(21)	1.957(9)	Mn(2)–O(2)	2.229(7)	Mn(3)–N(45)	2.035(8)
Mn(1)–O(4)	2.366(8)	Mn(2)–O(30)	1.860(8)	Mn(1)···Mn(2)	3.338
Mn(1)–O(10)	1.847(8)	Mn(2)–N(41)	1.934(8)	Mn(2)···Mn(3)	3.227
Mn(1)–N(65)	2.010(8)	Mn(3)–O(1)	1.859(7)	Mn(1)···Mn(3)	3.269
Mn(2)–O(1)	1.943(6)	Mn(3)–O(50)	1.810(8)		
Bond Angles					
O(1)–Mn(1)–O(4)	90.1(3)	O(1)–Mn(2)–O(6)	89.2(3)	O(1)–Mn(3)–O(3)	90.7(3)
O(1)–Mn(1)–O(5)	88.9(3)	O(1)–Mn(2)–N(25)	90.0(3)	O(1)–Mn(3)–N(45)	88.4(3)
O(1)–Mn(1)–O(10)	178.8(4)	O(2)–Mn(2)–O(6)	176.8(3)	O(3)–Mn(3)–O(50)	88.9(3)
O(1)–Mn(1)–N(21)	89.1(4)	O(2)–Mn(2)–N(25)	91.9(3)	O(3)–Mn(3)–N(61)	116.5(3)
O(1)–Mn(1)–N(65)	88.3(3)	O(6)–Mn(2)–O(30)	87.8(3)	O(50)–Mn(3)–N(61)	88.9(3)
O(4)–Mn(1)–O(5)	176.2(3)	O(6)–Mn(2)–N(41)	90.1(3)	O(1)–Mn(3)–O(50)	177.1(3)
O(4)–Mn(1)–O(10)	89.6(3)	O(30)–Mn(2)–N(41)	88.9(3)	O(1)–Mn(3)–N(61)	88.7(3)
O(4)–Mn(1)–N(65)	82.9(3)	O(1)–Mn(2)–O(2)	90.7(3)	O(3)–Mn(3)–N(45)	101.7(3)
O(5)–Mn(1)–N(21)	90.4(3)	O(1)–Mn(2)–O(30)	175.4(3)	O(50)–Mn(3)–N(45)	94.4(3)
O(10)–Mn(1)–N(21)	89.7(4)	O(1)–Mn(2)–N(41)	87.6(3)	N(45)–Mn(3)–N(61)	141.7(4)
N(21)–Mn(1)–N(65)	175.5(4)	O(2)–Mn(2)–O(30)	92.5(3)	Mn(1)–O(1)–Mn(2)	120.6(4)
O(4)–Mn(1)–N(21)	93.3(3)	O(2)–Mn(2)–N(41)	93.1(3)	Mn(1)–O(1)–Mn(3)	120.9(3)
O(5)–Mn(1)–O(10)	91.4(3)	O(6)–Mn(2)–N(25)	84.9(3)	Mn(2)–O(1)–Mn(3)	116.1(3)
O(5)–Mn(1)–N(65)	93.3(3)	O(30)–Mn(2)–N(25)	93.2(3)		
O(10)–Mn(1)–N(65)	92.8(3)	N(25)–Mn(2)–N(41)	174.4(3)		

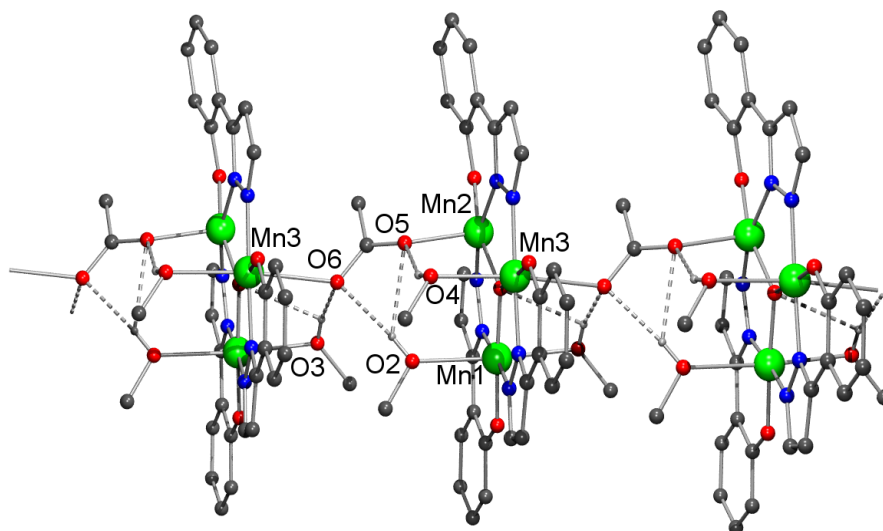


Figure 3.1. Pluton projection of the chain of $[\text{Mn}_3(\mu_3\text{-O})(\text{phpzH})_3(\text{MeOH})_3(\text{OAc})]_n$ (**10**) showing the hydrogen bonding interactions. Hydrogen atoms that are not involved in hydrogen bonds are omitted for clarity. Colour code: green, manganese; blue, nitrogen; red, oxygen; grey, carbon.

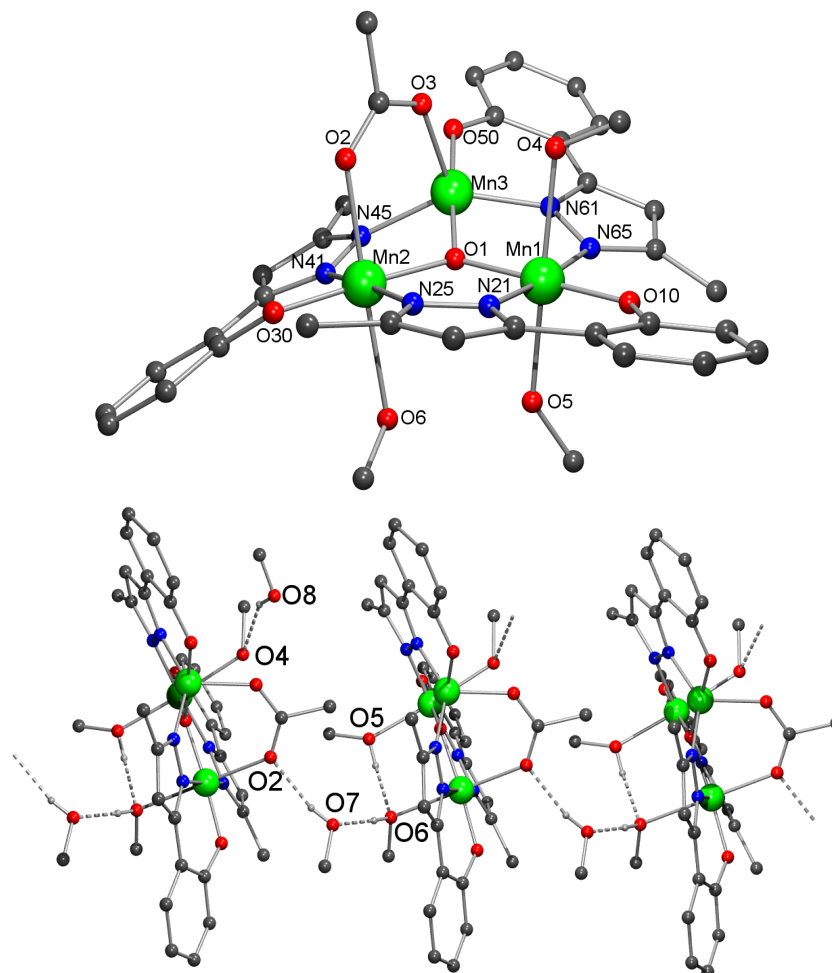


Figure 3.2. Pluton projection of the compound $[\text{Mn}_3(\mu_3\text{-O})(\text{phpzMe})_3(\text{MeOH})_3(\text{OAc})]$ (**11**) (top) and the hydrogen bonding interactions between the trinuclear units (bottom). Non-coordinated methanol molecules and hydrogen atoms that are not involved in hydrogen bonding interactions are omitted for clarity. Colour code: green, manganese; blue, nitrogen; red, oxygen; grey, carbon.

Compound **11** crystallizes in the monoclinic space group $C2/c$. The crystal structure is shown in Figure 3.2. The structure analysis reveals a trinuclear manganese(III) compound containing a μ_3 -oxide bridge. Each edge of the Mn_3 triangle is bridged by a $\eta^1\text{-}\eta^1,\mu$ -pyrazolato ligand with the phenolic oxygen and one pyrazole nitrogen atom chelating a manganese(III) ion. Selected bond lengths and angles are listed in Table 3.2. Intracluster $Mn\cdots Mn$ distances are 3.338 Å, 3.269 Å and 3.227 Å for $Mn(1)\cdots Mn(2)$, $Mn(1)\cdots Mn(3)$ and $Mn(2)\cdots Mn(3)$, respectively. The $\mu_3\text{-O}^{2-}$ (O1) ion is 0.171 Å above the Mn_3 plane. The $Mn\text{-O}(1)$ distances are 1.900(6) Å for $Mn(1)$, 1.943(6) Å for $Mn(2)$ and 1.859(7) Å for $Mn(3)$. The $Mn\text{-O}(1)\text{-Mn}$ angles are $Mn(1)\text{-O}(1)\text{-Mn}(2) = 120.6(4)^\circ$; $Mn(1)\text{-O}(1)\text{-Mn}(3) = 120.9(3)^\circ$ and $Mn(2)\text{-O}(1)\text{-Mn}(3) = 116.1(3)^\circ$. $Mn(1)$ and $Mn(2)$ are hexacoordinated; $Mn(1)$ contains two methanol molecules at the axial positions, whilst $Mn(2)$ is axially coordinated to a methanol molecule and an acetate ion. $Mn(3)$ is pentacoordinated with an acetate ion at the axial position. The main difference with compound **10** is that in this case the acetate ligand is bridging two manganese(III) ions from the same trinuclear unit, whereas in compound **10** it is binding two manganese(III) ions from different trinuclear units. Consequently, in compound **10** a chain is formed. Probably this difference arises from the steric effect of the methyl group from the pyrazole ring of the ligand. In compound **11**, one and a half methanol molecules are present in the asymmetric unit. Intra- and intermolecular hydrogen bonds are observed between the acetate group and coordinated methanol and the solvent present in the unit cell (Figure 3.2 and Table 3.4).

Compound **12** crystallizes in the monoclinic space group $C2/c$. As shown in Figure 3.3, **12** consists also of a trinuclear manganese(III) core in which the manganese(III) ions are bridged by a central oxide. These trinuclear units are bridged by a single azide ion in an end-to-end binding mode. The three doubly deprotonated $phpzH^{2-}$ ligands form a plane with the manganese(III) ions. The $\mu_3\text{-O}^{2-}$ (O1) ion lies 0.040 Å above the Mn_3 triangle. The manganese(III) ions are all hexacoordinated. $Mn(1)$ and $Mn(2)$ hold a methanol molecule and an azide molecule at the axial positions, whilst in $Mn(3)$ two methanol molecules occupy the axial positions. Selected bond lengths and angles are listed in Table 3.3. The $Mn\text{-O}(1)$ average distance is 1.913 Å. The $Mn\cdots Mn$ distances in the trinuclear unit are 3.329 Å, 3.326 Å and 3.299 Å for $Mn(1)\cdots Mn(2)$, $Mn(1)\cdots Mn(3)$ and $Mn(2)\cdots Mn(3)$, respectively. The $Mn\text{-O}(1)\text{-Mn}$ angles are $Mn(1)\text{-O}(1)\text{-Mn}(2) = 120.79(12)^\circ$, $Mn(1)\text{-O}(1)\text{-Mn}(3) = 120.11(14)^\circ$ and $Mn(2)\text{-O}(1)\text{-Mn}(3) = 118.96(12)^\circ$. The $Mn\text{-N}_{azido}$ distances are 2.327(3) Å and 2.339(4) Å. The shortest $Mn\cdots Mn$ distance between the trinuclear units is 6.483 Å through the azide bridge, which is slightly longer than the acetate-bridged distance in **10** (6.418 Å). The shortest interchain $Mn\cdots Mn$ distance is 8.153 Å between $Mn(1)$ atoms. A

methanol molecule in the lattice forms hydrogen bonds with a coordinated methanol (O(2)–H(2A)···O(10) 2.709(4) Å) and the phenoxido moiety of a phpzH^{2-} bridging ligand (O(10)–H(10D)···O(121) 2.932(4) Å) (Table 3.4 and Figure 3.3).

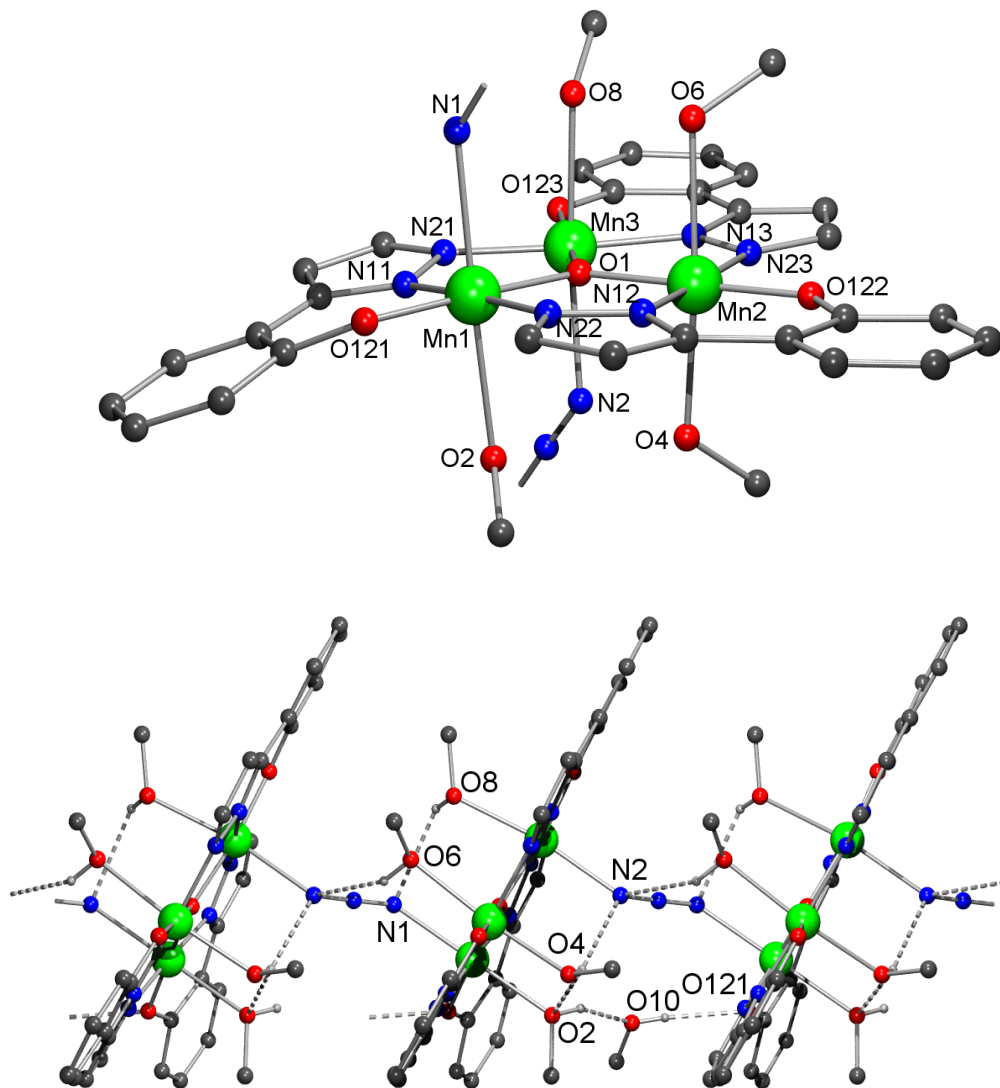


Figure 3.3. Pluton projection of $[\text{Mn}_3(\mu_3\text{-O})(\text{phpzH})_3(\text{MeOH})_4(\text{N}_3)]_n \cdot n\text{MeOH}$ (**12**) showing the detailed $\text{Mn}^{\text{III}}_3\text{O}$ unit (top) and the chain together with the hydrogen bonding interactions (bottom). Hydrogen atoms that are not involved in hydrogen bonding interactions are omitted for clarity. Colour code: green, manganese; blue, nitrogen; red, oxygen; grey, carbon.

Table 3.3. Selected bonds lengths [Å] and angles [°] for the compound **12**.

Bond Lengths			
Mn(1)–O(1)	1.900(6)	Mn(1)–O(4)	2.366(8)
Mn(1)–O(5)	2.244(8)	Mn(1)–O(10)	1.847(8)
Mn(1)–N(21)	1.957(9)	Mn(1)–N(65)	2.010(8)
Mn(2)–O(1)	1.943(6)	Mn(2)–O(2)	2.229(7)
Mn(2)–O(6)	2.457(7)	Mn(2)–O(30)	1.860(8)
Mn(2)–N(25)	2.008(8)	Mn(2)–N(41)	1.934(8)
Mn(3)–O(1)	1.859(7)	Mn(3)–O(3)	2.098(7)
Mn(3)–O(50)	1.810(8)	Mn(3)–N(45)	2.035(8)
Mn(3)–N(61)	1.958(10)	Mn(1)⋯Mn(2)	3.338
Mn(1)⋯Mn(3)	3.269	Mn(2)⋯Mn(3)	3.227
Bond Angles			
O(1)–Mn(1)–O(4)	90.1(3)	O(1)–Mn(1)–O(5)	88.9(3)
O(1)–Mn(1)–O(10)	178.8(4)	O(1)–Mn(1)–N(21)	89.1(4)
O(1)–Mn(1)–N(65)	88.3(3)	O(4)–Mn(1)–O(5)	176.2(3)
O(4)–Mn(1)–O(10)	89.6(3)	O(4)–Mn(1)–N(21)	93.3(3)
O(4)–Mn(1)–N(65)	82.9(3)	O(5)–Mn(1)–O(10)	91.4(3)
O(5)–Mn(1)–N(21)	90.4(3)	O(5)–Mn(1)–N(65)	93.3(3)
O(10)–Mn(1)–N(21)	89.7(4)	O(10)–Mn(1)–N(65)	92.8(3)
N(21)–Mn(1)–N(65)	175.5(4)	O(1)–Mn(2)–O(2)	90.7(3)
O(1)–Mn(2)–O(6)	89.2(3)	O(1)–Mn(2)–O(30)	175.4(3)
O(1)–Mn(2)–N(25)	90.0(3)	O(1)–Mn(2)–N(41)	87.6(3)
O(2)–Mn(2)–O(6)	176.8(3)	O(2)–Mn(2)–O(30)	92.5(3)
O(2)–Mn(2)–N(25)	91.9(3)	O(2)–Mn(2)–N(41)	93.1(3)
O(6)–Mn(2)–O(30)	87.8(3)	O(6)–Mn(2)–N(25)	84.9(3)
O(6)–Mn(2)–N(41)	90.1(3)	O(30)–Mn(2)–N(25)	93.2(3)
O(30)–Mn(2)–N(41)	88.9(3)	N(25)–Mn(2)–N(41)	174.4(3)
O(1)–Mn(3)–O(3)	90.7(3)	O(1)–Mn(3)–O(50)	177.1(3)
O(1)–Mn(3)–N(45)	88.4(3)	O(1)–Mn(3)–N(61)	88.7(3)
O(3)–Mn(3)–O(50)	88.9(3)	O(3)–Mn(3)–N(45)	101.7(3)
O(3)–Mn(3)–N(61)	116.5(3)	O(50)–Mn(3)–N(45)	94.4(3)
O(50)–Mn(3)–N(61)	88.9(3)	N(45)–Mn(3)–N(61)	141.7(4)
Mn(1)–O(1)–Mn(2)	120.6(4)	Mn(1)–O(1)–Mn(3)	120.9(3)
Mn(2)–O(1)–Mn(3)	116.1(3)		

Table 3.4. Hydrogen bond details (distances [Å] and angles [°]) for **10**, **11** and **12**.

Donor–H⋯Acceptor	D–H	H⋯A	D⋯A	D–H⋯A
Compound 10				
O(2)–H(2)⋯O(5)	0.8539	2.4177	3.035(4)	129.65
O(2)–H(2)⋯O(6)	0.8539	2.1552	3.000(3)	170.12
O(3)–H(3)⋯O(6)	0.8442	2.0542	2.859(4)	159.20
O(4)–H(5)⋯O(5)	0.8502	2.0591	2.857(3)	156.13
Compound 11				
O(5)–H(5D)⋯O(6)	0.8410	1.9865	2.760(11)	152.59
O(6)–H(6D)⋯O(7)	0.8438	1.7727	2.613(10)	173.63
O(7)–H(7)⋯O(2)	0.8398	1.9572	2.780(11)	166.42
O(8)–H(8)⋯O(4)	0.8406	2.2194	2.987(18)	151.76
Compound 12				
O(2)–H(2A)⋯O(10)	0.8407	1.9275	2.709(4)	154.04
O(4)–H(4A)⋯O(2)	0.8419	2.3718	2.951(4)	126.53
O(4)–H(4A)⋯N(2)	0.8419	2.3629	3.055(5)	139.90
O(6)–H(6A)⋯N(2)	0.8395	2.5857	3.290(4)	142.23
O(8)–H(8A)⋯N(1)	0.8408	2.4908	3.113(5)	131.56
O(10)–H(10D)⋯O(121)	0.8393	2.0974	2.932(4)	173.18

Magnetic Properties. Magnetic susceptibilities were measured under 0.1 T field in the 1.8–300 K temperature range for the compounds **10**–**12**. The temperature dependence of the $\chi_M T$ product for compound **10** is shown in Figure 3.4. The magnetic behaviour observed is identical to that reported independently, earlier.¹¹ Antiferromagnetic interactions are present between the manganese(III) ions in the trinuclear units. The increase of the magnetic susceptibility at low temperatures is attributed to ferromagnetic interactions between the trinuclear units along the chain. Compound **10** displays long-range magnetic ordering below at about 3.2 K.

As shown in Figure 3.5, the $\chi_M T$ values of **11** and **12** are 7.65 cm³Kmol⁻¹ and 7.40 cm³Kmol⁻¹ at 300 K, respectively, which is below the limiting spin-only value (9.0 cm³Kmol⁻¹) calculated for three non-interacting manganese(III) ions, assuming an isotropic g -value of 2.00.¹⁸ When lowering the temperature, the $\chi_M T$ product of **11** decreases gradually to 2.43 cm³Kmol⁻¹ at 15 K, and then more rapidly to 1.65 cm³Kmol⁻¹ at 1.8 K. As shown in Figure 3.5 b, the $\chi_M T$ product of **12** shows a similar decrease with temperature as for **11**, reaching an even lower value of 0.63 cm³Kmol⁻¹ at 1.8 K. The observed behaviour suggests the presence of (primarily) antiferromagnetic interactions between the manganese(III) ions within the trinuclear units.

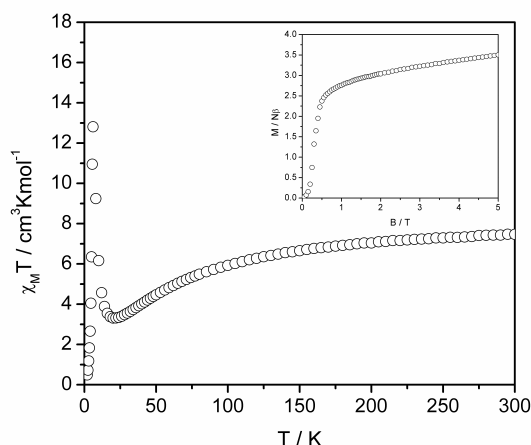


Figure 3.4. Plot of $\chi_M T$ vs T for **10** in the range 1.8 to 300 K in 0.1 T field. Inset, field dependence of the magnetization measured at 2 K.

In order to further characterize the low-temperature magnetic properties of **11** and **12**, magnetization measurements were carried out at $T = 2, 4$ and 6 K, in fields up to 5 T, as shown in the insets of Figure 3.5. At the lowest temperature of 2 K, the molar magnetization (M) of compounds **11** and **12** reaches a value of respectively $2.5 N\beta$ and $1.3 N\beta$ only (per trinuclear complex), even in 5 T. For non-interacting manganese(III) spins such a field/temperature combination would be sufficient to approach the saturation value of $M = 3gSN\beta = 12N\beta$ (per trinuclear complex). This is strong evidence for the presence of antiferromagnetic interactions J of the order of a few cm^{-1} in strength, the interaction in **12** being strongest. Furthermore, both compounds show an initially sharper increase of M in low fields, which points to incompletely compensated antiferromagnetic alignment of the spins within the trinuclear units (similar as in the well known weak ferromagnetic materials). Such an uncompensated component is indeed expected for a triangular spin arrangement on quite general grounds. Only for isotropic Heisenberg interactions between the three spins that are equal in sign (AF) and magnitude, complete compensation is possible, with the spins ordered under angles of 120° to one another, thus resulting in zero net moment for the trinuclear complex. As soon as the interactions become appreciably different, or when anisotropy is introduced, complete compensation will no longer occur. Such will be the situation for present compounds, since magnetic exchange interactions between the three spins on basis of the molecular structure cannot be expected. Weaker intermolecular interactions between the net moments of the trinuclear units will then become important at low temperature and reduce the total magnetization of the sample (in zero field) to zero. The initial steeper increase in the magnetization curves seen up to fields of about 1 T was interpreted in such terms, namely as the magnetization process whereby these small net moments per cluster become aligned by

the applied field. By extrapolating the quasi-linear high-field parts of the magnetization curves to zero field, the size of these net moments δM per cluster can be estimated, giving about $1 N\beta$ and $0.3 N\beta$ for compounds **11** and **12**, respectively. The fields B_{sat} of order 1 T where this initial process “saturates” give an estimate of the intercluster coupling via the (mean-field) formula: $zJ \approx g^2\beta^2 B_{\text{sat}}/\delta M$, yielding $zJ \approx 0.1\text{--}0.3 \text{ cm}^{-1}$.

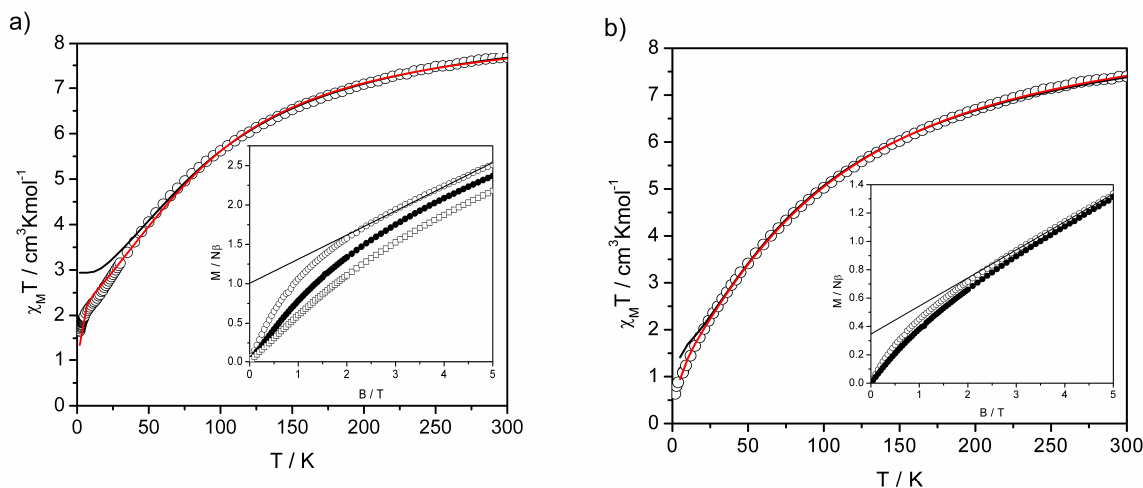


Figure 3.5. Plots of $\chi_M T$ vs T in the range 1.8 to 300 K in 0.1 T field and the experimental fit (black solid line for isosceles triangle and red solid line considering intermolecular interactions) for **11** (a) and **12** (b).

Insets, field dependence of the magnetization measured at 2 (○), 4 (●) and 6 K (□) and the linear extrapolation of the high-field parts at 2 K.

In view of the above results, the behaviour of the (low-field) susceptibility of **11** and **12** in the low-temperature (< 50 K) region is expected to be dominated by the presence of net moments per cluster, coupled by weak intermolecular interactions. In order to obtain quantitative estimates of the intracluster exchange interactions, the fits of the data to theoretical triangular cluster models are restricted to the temperature range above 50 K in a first step. In a second step a molecular field, $B_m = 2zJ^*S/g\beta$, representing the intermolecular coupling zJ^* is then added, the corrected magnetic susceptibility χ' being related to the uncorrected χ by the formula $\chi' = \chi/[1 + \lambda\chi]$ and the molecular field constant given by $\lambda = 2zJ^*/g^2\beta^2$ (z being the number of neighbouring clusters). In this latter procedure the data are fitted over the whole temperature range covered.

On basis of the non-equivalent exchange paths in the molecular structure, the data above 50 K were thus fitted to the susceptibility calculated from the magnetic energy level spectrum for three spins $S = 2$ coupled by isotropic Heisenberg interactions on the isosceles triangle:

$$\hat{H} = -2[J_1(\hat{S}_1\hat{S}_2) + J_1(\hat{S}_1\hat{S}_3) + J_2(\hat{S}_2\hat{S}_3)] \quad (1)$$

where J_1 represents the manganese(III)–manganese(III) magnetic exchange interaction parameter of the two exchange paths with similar distances and Mn–O_{oxide}–Mn angle, and J_2 refers to the path characterized by the unique Mn–O_{oxide}–Mn angle. In the case of compound **11**, J_2 is the Mn(2)–Mn(3) interaction (with angle Mn(2)–O(1)–Mn(3) = 116.10°), whereas in **12** it represents the Mn(2)–Mn(3) interaction (with angle Mn(2)–O(1)–Mn(3) = 118.96°). As is well known,²⁷ the energy levels for the isosceles triangle of spins S are given by:

$$E(S_T, S^*) = -J_1[S_T(S_T+1) - S^*(S^*+1) - S(S+1)] - J_2[S^*(S^*+1) - 2S(S+1)] \quad (2)$$

Here $S^* = S_2 + S_3$ and can take the values $S^* = 2S, 2S-1, \dots, 0$, whereas the total spin $S_T = (S^* + S), (S^* + S - 1), \dots, |S^* - S|$. Figure 3.6 shows the so-obtained energy spectrum as $E(S_T, S^*)/|J_1|$ versus the ratio $r = J_2/J_1$. For the lowest levels, the corresponding values for the total spin S_T of the trinuclear complex have been indicated. Note that the diagram shown is for antiferromagnetic (negative) values for J_1 ; for ferromagnetic J_1 the diagram has to be inverted. It can be seen that only in a small range around the equilateral limit ($J_2/J_1 = 1$) the ground state is indeed the fully compensated spin state with $S_T = 0$, confirming the qualitative discussion given in the above. For $r < 0.5$ and for all negative values of r the ground state is the $E(2,4)$ level, corresponding to net total spin $S_T = 2$ for the trinuclear complex. Furthermore, the total extent of the spectrum is of order 20 to 50 times $|J_1|$, so even for relatively weak exchange constants of a few cm^{-1} it may extend over a few 100 K, explaining why the $\chi_M T$ product is found still varying near room temperature and why the low temperature magnetization remains far from saturation even in 5 T (the ferromagnetic state $E(6,4)$ remains far above the ground state for all r).

For compound **12** the fits of the data above 50 K yielded $J_1 \approx -(6.2 \pm 0.4) \text{ cm}^{-1}$, $J_2 \approx -(3.7 \pm 1.0) \text{ cm}^{-1}$, with $g \approx 2.01 \pm 0.01$. The resulting ratio $r = 0.6$ is close enough to the equilateral limit $r = 1$ for the nonmagnetic $E(0,2)$ level to be still the ground state, see Figure 3.6. This explains why the $\chi_M T$ product becomes so low for $T = 0$. For the same reason it was found that inclusion of the data over the whole range 2–300 K did not change the values for J_1 and J_2 obtained from the fits. Adding nevertheless in the next step the intermolecular interaction zJ' , and fitting the data over the whole range, resulted in appreciably better fits, with somewhat different interaction constants $J_1 = -(7.0 \pm 0.1) \text{ cm}^{-1}$, $J_2 = -(5.0 \pm 0.1) \text{ cm}^{-1}$, and with $zJ' = +(0.8 \pm 0.2) \text{ cm}^{-1}$ and $g = 2.01 \pm 0.01$. The ratio J_2/J_1 thus remains almost the same at $r = 0.7$. The fits to the fully equilateral limit (and obviously without intermolecular interaction) were tried, but proven unsuccessful, with appreciable deviation appearing below 40 K.

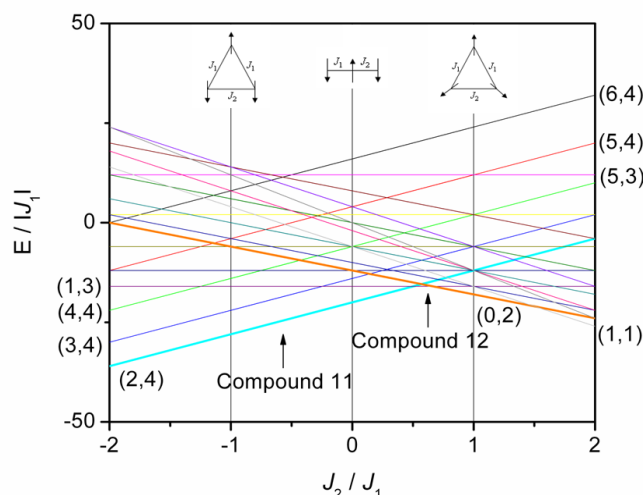


Figure 3.6. Energy levels for an isosceles triangle with $S_1 = S_2 = S_3 = 2$ calculated for $J_1 < 0$. States are labelled as (S_T, S^*) .

The best fits of the experimental data for **11** above 50 K gave $J_1 = -(7.1 \pm 0.1) \text{ cm}^{-1}$, $J_2 \approx + (4.4 \pm 1.3) \text{ cm}^{-1}$ and $g = 1.98 \pm 0.01$. Varying the g -value gave systematically higher positive values for J_2 the lower the used value of g , the value for J_1 remaining basically the same. Interestingly, J_2 was always found ferromagnetic, except for values of $g (\geq 2.01)$, where it approached zero. The reason for the wide range of possible J_2 values probably lies in the fact that the $E(2,4)$ level is the ground state for all negative r values, even up to positive $r = 0.5$, see Figure 3.6. Furthermore, the nearest excited state $E(3,4)$ runs in parallel at a distance of the order of 60 K. Indeed, forcing J_2 to be also negative, resulted in lesser fits $J_2 \approx 0 \text{ cm}^{-1}$, whereas $J_1 \approx -5.6 \text{ cm}^{-1}$. Adding in the next step the intercluster interaction zJ' as a molecular field, a best fit was obtained for $J_1 \approx -(6.8 \pm 0.1) \text{ cm}^{-1}$, $J_2 \approx + (7.2 \pm 1.3) \text{ cm}^{-1}$, $g = 1.96 \pm 0.2$ and $zJ' \approx -(0.35 \pm 0.03) \text{ cm}^{-1}$.

The values found for zJ' from the fitting of the susceptibility data are indeed similar to the rough estimate found above from the initial part of the magnetization curves. They are an order of magnitude larger than the estimated dipolar interaction between cluster moments, indicating the possible presence of superexchange between clusters.

Notwithstanding such shortcomings, it can be concluded that a ferromagnetic interaction J_2 in compound **11** is present, corresponding to the exchange path with the largest structural distortion of the Mn_3 triangle. For compound **12** the distortion is indeed much smaller and accordingly the J_2 parameter is still antiferromagnetic, although smaller in strength than J_1 . The change in sign is of special interest in view of the recent quests for molecular magnetic clusters with high-spin ground states. Indeed, in a number of related $[\text{Mn}^{\text{III}}_3(\mu_3\text{-O})]^{7+}$ compounds²⁸⁻³⁵ even a full ferromagnetic alignment within the molecule, *i.e.* both J_1 and $J_2 >$

0 and thus an $S = 6$ magnetic ground state at low temperatures, has been reported. Since it is of importance to single out the specific structural features responsible for the ferromagnetic exchange,³⁶ in the following section a systematic comparison of the magneto-structural parameters known from literature for this family of complexes is presented.

Magneto-structural Correlations. As mentioned above, the observation of a ferromagnetic interaction for the Mn(2)–O(1)–Mn(3) bond in compound **11**, which has the strongest distortion of the $[\text{Mn}_3(\mu_3\text{-O})]^{7+}$ core, is of special interest in view of the ferromagnetism observed recently in related, high-spin magnetic molecules containing these units, in particular since the great majority of the Mn_3 trinuclear complexes known in literature show (weak) antiferromagnetism. In this context, the fact that in all these materials the Mn–O_{oxide}–Mn angles are approximately 120° appears to be an important ingredient, since in previous theoretical and experimental studies it has been shown that around this value the net superexchange interaction can be expected to change from antiferromagnetic to ferromagnetic.³⁷ Whereas the 180° metal-ligand-metal bond is characterized by a relatively strong antiferromagnetic interaction, upon decreasing the bond angle the absolute value decreases and below 120° may become (weakly) ferromagnetic. This prediction appears to be common to the various existing models for superexchange (for a comparative discussion of these models, see ref.38). In all these models the net interaction J corresponding to the metal–ligand–metal bond arises from the competition of two contributions of opposite sign: $J = J_{\text{AF}} + J_{\text{F}}$. Evidently, in the experimental compounds such as the present, the situation can become much more complex than in the quoted theoretical treatments, for instance due to the simultaneous presence of several (different) superexchange paths linking the magnetic ions. In addition to the more simple parameters, such as the bridging angles between the metal ions, the metal···metal distances, the metal-ligand bond lengths, the overlap of the magnetic orbitals can then depend on the combination of complex structural factors, such as the spatial orientation of Jahn-Teller axes, and the dihedral angles between coordination planes.¹⁸ In a recent paper,³⁶ Cano *et al.* have made an attempt by means of DFT calculations to evaluate the various structural factors that may be at the origin of the occurrence of ferromagnetic intramolecular interactions in the $[\text{Mn}^{\text{III}}_3(\mu_3\text{-O})]^{7+}$ core in some of the Mn_3 triangular complexes. Indeed, since most of the related materials show antiferromagnetism it is of considerable interest to single out these features in view of the current quests for high-spin single molecule magnets. Although there appears to be an intimate relation with the structural distortion of the $[\text{Mn}^{\text{III}}_3(\mu_3\text{-O})]^{7+}$ triangle, Cano *et al.*³⁶ rightly point out that several other factors may play a role and that a systematic comparison of a series of these compounds would be welcome. In order to contribute to the discussion of these interesting questions, in

Tables 3.5–3.7 relevant magneto-structural data have been collected for a large number of related complexes of the family of trinuclear manganese(III) compounds. In order to facilitate the comparison, a subdivision in five groups has been made on basis of structural considerations and/or specific magnetic properties. In Figure 3.7 a schematic sketch is presented of the $[\text{Mn}_3(\mu_3\text{-O})]^{7+}$ core, showing the principal magneto-structural parameters that will be at stake here.

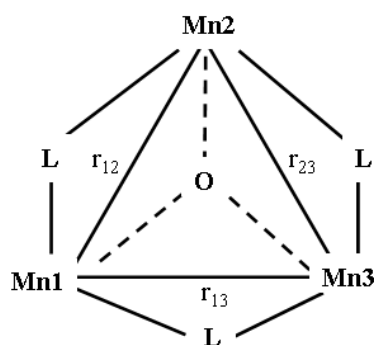


Figure 3.7. Schematic view of the $[\text{Mn}_3(\mu_3\text{-O})]^{7+}$ core with the possible magnetic pathways.

Group I: The first group is formed by the complexes with the general formula $[\text{Mn}^{\text{III}}_3\text{O}(\text{O}_2\text{CR})_6(\text{L})_3]^+$ ($\text{R} = \text{Me, Et, Pr, Ph}$ and $\text{L} = \text{py, 3-Mepy, Im, 4,4'-bipy}$) or commonly named basic carboxylates. These complexes have a $[\text{Mn}_3(\mu_3\text{-O})]^{7+}$ core, where the oxygen is (almost) within the plane formed by the three manganese(III) ions. Furthermore, the manganese(III) ions form an equilateral triangle, the distances between the manganese(III) ions and the $\text{Mn-O}_{\text{oxide}}\text{-Mn}$ angles being basically the same, the latter being close to or equal to 120° , see Table 3.5. The carboxylates bridge the manganese(III) ions and the pyridine or the imidazole ligands are at the terminal positions. All of the reported complexes give an antiferromagnetic behaviour with a J value around -12 cm^{-1} ($J = J_1 = J_2$).³⁹⁻⁴¹ It should be noted that the compound $[\text{Mn}_3(\mu_3\text{-O})(\text{O}_2\text{CCMe}_3)_6(\text{Im})_3]^{+42}$ is included in this group of complexes with an equilateral triangle, although it was analyzed as isosceles. Indeed, the reported values of J_1 and J_2 are nearly the same, probably because the deviations from 3-fold symmetry are very small. $[\text{Mn}_3(\mu_3\text{-O})(\text{PhCO}_2)_7(4,4'\text{-bpy})] \cdot 3\text{H}_2\text{O}$ is included as well in this group, because of the structural resemblance with the basic carboxylates.⁴³ However, in this case, the triangle is more distorted as it is reflected on the differences in the magnetic exchange interactions as compared with the trend of this group. The symmetric triangular coordination in these complexes apparently favours antiferromagnetic interactions between the manganese(III) ions. Furthermore, the ligands terminally coordinated to the metal ions do not appear to play an important role, as the J value does not change significantly when this ligand is varied (other parameters remaining the same). Thus the Mn–O–Mn superexchange

path should be the main responsible for the magnetic interaction, as concluded already by previous authors.⁴¹ Oxide ligands are indeed known to be good bridges for propagating the magnetic superexchange interaction between manganese ions.⁴⁴ At the same time this implies that the structural parameters involved in the Mn–O_{oxide}–Mn bond should be essential for determining the type and strength of the interaction. Since the bond-angle remains almost constant in this group, one expects the strength of the interaction to depend on the Mn–μ₃–O distances. This is indeed observed since with increasing Mn–μ₃–O distance (and thus less overlap of wave functions) the absolute value of J becomes systematically smaller through this series.

Group II: When three carboxylate ligands and the terminal ligands are replaced by the oximato-based bridging ligands mpko and ppko, an important distortion of the $[\text{Mn}_3(\mu_3\text{-O})]^{7+}$ core occurs.³²⁻³⁴ This structural distortion is reflected in a significant displacement of the central oxide bridge from the plane formed by the three manganese(III) ions (see Table 3.5), so that the angle Mn–O_{oxide}–Mn becomes appreciably smaller than 120°, the value appropriate for the ideal equilateral triangle. This category of complexes therefore forms an isosceles triangle with two different exchange interactions J_1 and J_2 between the manganese(III) ions that are found to be ferromagnetic, producing a high-spin $S = 6$ ground state for the molecule. In the recent literature several possible origins for this drastic switch from low-spin to high-spin configuration have been pointed out.⁴⁵ Firstly, the distortion from a perfect equilateral triangle will reduce the Mn_{dπ}–O_{pπ}–Mn_{dπ} orbital overlap, thereby weakening the antiferromagnetic contribution to the interaction. Since the magnetic superexchange interaction generally is the sum of two competing interactions ($J = J_{\text{AF}} + J_{\text{F}}$),⁴⁶ the ferromagnetic component along this pathway may then become predominant. Secondly, it has been pointed out on basis of DFT calculations that the replacement of the carboxylate bridge by the two-atom oximato bridge (non-planar with the Mn triangle), and the ensuing non-parallel spatial alignment of the manganese(III) Jahn-Teller axes, may have tipped the scales into the direction of ferromagnetism. From such considerations it is evident that as a consequence of the distortion the net value of the exchange will depend on many parameters, and it becomes difficult to distinguish systematic trends, such as a dependence on the Mn–O or the Mn···Mn distances.

Table 3.5. Selected magnetic and structural data for trinuclear manganese(III) compounds.

Compound ^a	J_1/cm^{-1}	J_2/cm^{-1}	g	Mn–O/Å ^b	Mn···Mn/Å ^c	Mn–O–Mn/ ^o ^d	O–Mn ₃ /Å ^e	Ref
Group I								
[Mn ₃ (μ ₃ -O)(MeCO ₂) ₆ (py) ₃](ClO ₄)	-10.2	-10.2	1.81	1.936	n.r.	120	n.r.	41
[Mn ₃ (μ ₃ -O)(PrCO ₂) ₆ (py) ₃](ClO ₄)	-12.36	-12.36	2.01	1.91; 1.84; 1.93	3.272; 3.283; 3.279	121.5; 121.1; 117.3	0.0330	40
[Mn ₃ (μ ₃ -O)(MeCO ₂) ₆ (3-Mepy) ₃](ClO ₄)	-12.87	-12.87	2.22	1.919; 1.910	1.881; 3.311; 3.2754; 3.3027	121.22; 119.56; 119.19	0.0085	39
[Mn ₃ (μ ₃ -O)(EtCO ₂) ₆ (3-Mepy) ₃](ClO ₄)	-12.31	-12.31	2.12	1.883; 1.897	1.887; 3.2662; 3.2800	3.2691; 120.1; 119.5; 120.4	0	39
[Mn ₃ (μ ₃ -O)(Me ₃ CCO ₂) ₆ (Im) ₃](Me ₃ CCO ₂)·0.5Me ₃ CCO ₂ H	-7.5	-5.2	2.1	A) 1.879; 1.890 B) 1.887; 1.880; 1.883	1.885; 3.260	A) 120.01; 119.79 B) 120.24; 120.06	A) 0.015 B) 0.019	42
[Mn ₃ (μ ₃ -O)(PhCO ₂) ₇ (4,4'-bpy)]·3H ₂ O	+2.8 -22.2	-22.5 +2.6	2.16 2.16	1.938; 1.874	1.871; 3.314; 3.241; 3.285	120.9; 119.85; 119.0	0.054	43
Group II								
[Mn ₃ (μ ₃ -O)(MeCO ₂) ₃ (mpko) ₃](ClO ₄)	+14.1	+3.8	1.92	1.865; 1.865	1.873; 3.188; 3.203; 3.192	117.08; 117.91; 117.68	0.295	32-34
[Mn ₃ (μ ₃ -O)(EtCO ₂) ₃ (mpko) ₃](ClO ₄)·H ₂ O	+12.1	+1.5	1.92	1.972; 2.105	1.874; 3.260; 3.346; 3.578	115.85; 114.35; 122.65	0.308	32, 34
[Mn ₃ (μ ₃ -O)(PhCO ₂) ₃ (mpko) ₃](ClO ₄)·2.5H ₂ O	+18.6	+6.7	1.92	1.880; 1.864	1.882; 3.212; 3.219; 3.200	117.24; 118.47; 117.42	0.286	32
[Mn ₃ (μ ₃ -O)(MeCO ₂) ₃ (ppko) ₃](ClO ₄)	+31.1	+6.7	1.91	A) 1.891; 1.872 B) 1.856; 1.890; 1.901	A) 3.209; 3.196 B) 3.216; 3.200; 3.207	A) 118.03; 118.27 B) 118.32; 115.21; 117.21	0.319	34

^a py = pyridine, 3-Mepy = 3-methylpyridine, Im = imidazole, mpkoH = methyl 2-pyridyl ketone oxime, ppkoH = phenyl 2-pyridyl ketone oxime, H₂sao = salicylaldoxime, ^bBusaoH₂ = 3,5-di-*tert*-butylsalicylaldoxime, Me-saoH₂ = methylsalicyloxime, Et-saoH₂ = ethylsalicyloxime, Ph-saoH₂ = phenylsalicyloxime, Me-H₂salox = 2-hydroxyphenylethanone oxime, H₂phpzH = H₂ppz = 5(3)-(2-hydroxyphenyl)-pyrazole, H₂Meppz = 3-(5-methyl-2-phenolate)-pyrazole, Brppz = 3-(5-bromo-2-phenolate)pyrazolate, H₂phpzMe = 3(5)-methyl-5(3)-(2-hydroxyphenyl)pyrazole, mpdpH₂ = *m*-phenylenedipropionic acid, H₂bamen = 1,2-bis(biacetylmonoximeimino)ethane, bta = anion of benzotriazole, 5-Br-H₂sap = 2-salicylidenamino-1-propanol, hmcH₃ = 2,6-bis(hydroxymethyl)-*p*-cresol. ^b Mn–μ₃-O²⁻ distance; ^c Mn···Mn distances, Mn(1)···Mn(2); Mn(2)···Mn(3); Mn(1)···Mn(3) respectively; ^d Mn–μ₃-O–Mn angle, Mn(1)–O–Mn(2); Mn(2)–O–Mn(3); Mn(1)–O–Mn(3) respectively; ^e distance of the μ₃-O²⁻ from the Mn₃ plane. A) and B) represent the different units at the asymmetric unit.; n.r. = not reported. Intermolecular interactions are not listed because they are irrelevant for the present discussion.

Table 3.6. Selected magnetic and structural data for trinuclear manganese(III) compounds.

Compound	J_1/cm^{-1}	J_2/cm^{-1}	g	Mn–O/Å ^b	Mn···Mn/Å ^c	Mn–O–Mn/ ^o ^d	O–Mn ₃ /Å ^e	Ref
Group III								
[Mn ₃ (μ ₃ -O)(sao) ₃ (MeCO ₂)(H ₂ O)(py) ₃]	+4	-10	2.07	n.r.	n.r.	n.r.	0	36
[Mn ₃ (μ ₃ -O)(sao) ₃ (PhCO ₂)(H ₂ O)(py) ₃]	+4	-10	1.99	n.r.	n.r.	n.r.	0	36
[Mn ₃ (μ ₃ -O)(^t Busao) ₃ (MeOH) ₅ Cl]·H ₂ O	-0.56	-1.97	1.99	1.895; 1.879; 1.876	3.268; 3.247; 3.265	120.00; 119.73; 119.98	0.059	47
[Mn ₃ (μ ₃ -O)(^t Busao) ₃ (Me ₃ OH) ₄ (HCO ₂)]·CH ₃ OH·0.5H ₂ O	-0.38	-1.37	2.03	1.882; 1.875; 1.879;	3.245; 3.261; 3.257	119.45; 120.58; 119.95	0.012	47
[Mn ₃ (μ ₃ -O)(^t Busao) ₃ (Me ₃ OH) ₄ (N ₃)]·0.5CH ₃ OH	-5.04	-9.51	2.07	1.878; 1.876; 1.885	3.250; 3.259; 3.258	119.90; 120.11; 119.98	0.009	47
[Mn ₃ (μ ₃ -O)(Me-sao) ₃ (MeCO ₂)(py) ₄]·2py	-1.06 (-1.58)	-2.82 (-0.10)	2.03 (2.07)	1.880; 1.899; 1.900	3.239; 3.178; 3.239	117.99; 113.57; 117.89;	0.359	29,4 8
[Mn ₃ (μ ₃ -O)(Me-sao) ₃ (Me ₄ PhCO ₂)(py) ₃]·EtOH	-	-	-	n.r.	n.r.	112.70; 118.2; 117.10	0.383; 0.382	29
(pyH·Na)[Mn ₃ (μ ₃ -O)(Me-sao) ₃ (anthraCO ₂)(py) ₃] ₂ (ClO ₄)·py	-1.20; -1.94; -0.40		2.02	n.r.	n.r.	110.80; 114.86; 116.99	0.464	29
[Mn ₃ (μ ₃ -O)(Et-sao) ₃ ((CF ₃) ₂ PhCO ₂)(EtOH)(H ₂ O) ₃]·EtOH·3H ₂ O	+1.52	+1.52	1.98	n.r.	n.r.	115.83; 119.96; 119.84	0.179	29
[Mn ₃ (μ ₃ -O)(Et-sao) ₃ ((Cl) ₂ PhCO ₂)(H ₂ O)(MeOH) ₃]	+1.84	+1.84	2.02	n.r.	n.r.	115.33; 120.10; 118.71	0.265	29
[Mn ₃ (μ ₃ -O)(Ph-sao) ₃ (anthraCO ₂)(MeOH) ₄]·Ph-saoH ₂	+0.85	+1.44	1.98	n.r.	n.r.	115.80; 121.54; 119.98	0.178	29
[Mn ₃ (μ ₃ -O)(Et-sao) ₃ (ClO ₄)(MeOH) ₃]	+2.8	+2.8	2.0	1.877	3.239	119.02; 119.13; 119.15	0.179	28
[Mn ₃ O(Me-salox) ₃ (2,4'-bpy) ₃ (ClO ₄)]0.5MeCN	+3.58	+3.58	1.95	1.899	3.255	118.04; 188.05; 177.99	0.28	35
Group IV								
[Mn ₃ (μ ₃ -O)(ppz) ₃ (MeOH) ₃ (MeCO ₂)]	-3.01	-3.01	1.88	1.901; 1.909; 1.908	3.297; 3.291; 3.298	119.88; 119.15; 119.98	0.109	11
[Mn ₃ (μ ₃ -O)(phpzH) ₃ (MeOH) ₃ (MeCO ₂)] (10)								This work
[Mn ₃ (μ ₃ -O)(Meppz) ₃ (MeOH) ₄ (MeCO ₂)]	-3.21	-3.21	1.93	1.909; 1.903; 1.915	3.308; 3.297; 3.314	120.42; 119.41; 120.14	0.015	11
[Mn ₃ (μ ₃ -O)(Meppz) ₃ (EtOH) ₄ (MeCO ₂)]	-1.87	-5.61	1.99	1.910; 1.902; 1.911	3.308; 3.276; 3.328	120.43; 118.44; 121.13	0.001	12
[Mn ₃ (μ ₃ -O)(Brppz) ₃ (MeOH) ₃ (N ₃)]·2MeOH	-3.87	-8.20	2.12	1.922; 1.915; 1.934	3.322; 3.319; 3.329	119.94; 119.17; 119.35	0.139	14
[Mn ₃ (μ ₃ -O)(Brppz) ₃ (MeOH) ₃ (N ₃)]	-4.66	-7.35	2.12	1.898; 1.903; 1.900	3.297; 3.273; 3.299	120.33; 118.75; 120.61	0.062	14
[Mn ₃ (μ ₃ -O)(Brppz) ₃ (MeOH) ₃ (MeCO ₂)]	-1.58	-5.50	2.04	1.906; 1.905; 1.908	3.302av	120.56; 118.18; 120.20	0.0279	15
[Mn ₃ (μ ₃ -O)(Brppz) ₃ (EtOH) ₃ (MeCO ₂)]	-1.02	-4.39	2.02	1.907; 1.917; 1.908	3.305av	120.3; 119.3; 120.4	0.0016	15
[Mn ₃ (μ ₃ -O)(Brppz) ₃ (EtOH) ₃ (MeCO ₂)]	-0.72	-3.13	2.02	1.911; 1.894; 1.903	3.295av	119.54; 120.15; 120.22	0.0240	15
[Mn ₃ (μ ₃ -O)(phpzMe) ₃ (MeOH) ₃ (MeCO ₂)] (11)	-7.1	+4.4	1.98	1.900; 1.943; 1.859	3.338; 3.227; 3.269	120.61; 116.10; 120.85	0.172	This work
[Mn ₃ (μ ₃ -O)(phpzH) ₃ (MeOH) ₄ (N ₃)] (12)	-6.2	-3.7	2.01	1.919; 1.910; 1.919	3.329; 3.299; 3.326	120.79; 118.96; 120.11	0.040	This work

Table 3.7. Selected magnetic and structural data for trinuclear manganese(III) compounds.

Compound	J_1/cm^{-1}	J_2/cm^{-1}	g	Mn–O/Å ^b	Mn···Mn/ Å ^c	Mn–O–Mn/ ° ^d	O–Mn ₃ /Å ^e	Ref
Group V								
[Mn ₃ (μ ₃ -O)(mpdp) ₃ (py) ₃] (ClO ₄)	–8.8 –6.0	–6.2 –10	n.r.	1.898; 1.888; 1.905	3.275; 3.273; 3.310	119.75; 119.27; 120.98	0.001	49
[Mn ₃ (μ ₃ -O)(μ ₃ -bamen) ₃] (ClO ₄)	+22.3	+22.3	2.06	1.908; 1.909; 1.898	3.300; 3.303; 3.295	119.67; 120.36; 119.96	0.015	31
(HNEt ₃) ₂ [Mn ₃ (μ ₃ -O)(bta) ₆ F ₃]	+5.01	+9.16	2	1.8741; 1.8635; 1.8894	3.226; 3.260; 3.260	119.33; 120.59; 120.06	0.013	50
[Mn ₃ (μ ₃ -O)(5-Br- sap) ₃ (H ₂ O) ₃] Cl·5.5H ₂ O	<0	<0	n.r.	1.934; 1.944; 1.931	3.012; 3.023; 3.024	102.4; 102.0; 102.9	0.843	51
[NEt ₃ (CH ₂ Cl ₂) ₂] [Mn ₃ O(hmcH) ₃ (hmcH ₂) ₃]	+8.7	+1.2	1.90	2.001; 1.860; 1.859	3.031; 3.006; 3.035	103.4; 107.9; 103.4	0.765	30

Group III: The third group is composed of complexes with salicylaldoxime derivative ligands (Table 3.6). Although for the first two members of this group complete crystallographic data are not yet available in the literature, they are included nonetheless, since they were the subject of the mentioned comparative DFT study by Cano *et al.*³⁶ The listed parameters have been taken from that publication. Most of the compounds possess an isosceles Mn₃ triangle with different distances between the manganese(III) ions. However, two main subgroups exist in this category. The first one is composed by [Mn₃(μ₃-O)(sao)₃(MeCO₂)(H₂O)(py)₃],³⁶ [Mn₃(μ₃-O)(sao)₃(PhCO₂)(H₂O)(py)₃],³⁶ [Mn₃(μ₃-O)(^tBusao)₃(MeOH)₅Cl],⁴⁷ [Mn₃(μ₃-O)(^tBusao)₃(Me₃OH)₄(HCO₂)],⁴⁷ and [Mn₃(μ₃-O)(^tBusao)₃(Me₃OH)₄(N₃)].⁴⁷ In this subgroup, the central oxygen atom is (almost) not displaced from the Mn₃ plane and the Mn–O_{oxide}–Mn angles are approximately 120°, similar as for Group I. Since also the Mn–O distances are similar to those for Group I, one would expect the antiferromagnetic contribution to the magnetic exchange from the Mn–O_{oxide}–Mn paths to be comparable. Furthermore, one may observe that the strengths of the magnetic exchange constants found in Groups I and III are roughly comparable, although in Group III one notices a tendency for smaller absolute values and for ferromagnetic interactions. This suggests that the contributions from the carboxylate paths and from the salicylaldoxime paths are comparable, both being weakly antiferromagnetic with a tendency for the latter to be ferromagnetic.

The other subgroup is formed by the rest of compounds listed on Table 3.6, in which a more distorted Mn₃ triangle is present. Therefore the Mn–O_{oxide}–Mn angles differ from the values for an equilateral triangle and a displacement of the central oxide occurs. In the compounds [Mn₃(μ₃-O)(Me-sao)₃(py)₄(MeCO₂)],^{29,48} [Mn₃(μ₃-O)(Me-

sao)₃(Me₄PhCO₂)(py)₃],²⁹ and (pyH)(Na)[Mn₃(μ₃-O)(Me-sao)₃(anthraCO₂)(py)₃]₂(ClO₄)·py²⁹ antiferromagnetic interactions are observed, whereas in the other compounds of the subgroup, ferromagnetic interactions are dominant.^{28,29,35} In fact, in complexes with salicylaldoxime ligands and higher nuclearity⁴⁵ the sign of the exchange has been reported to depend on the Mn–N–O–Mn torsion angle δ. For δ < 30.4° it was found to be antiferromagnetic, whereas both types of interactions could occur when δ ≈ 30.4–31.3°. In all reported antiferromagnetic trinuclear manganese(III) complexes with salicylaldoxime ligands the torsion angles are below 30.7°, corroborating the presence of antiferromagnetic interactions, whereas in the ferromagnetic triangles, the torsion angles are above 33°. In the mentioned DFT study it was found that indeed the oximate torsion angle plays a role due to the orbital countercomplementary.³⁶ This would imply that the distortion on its own is not a sufficient ingredient for the switch to ferromagnetism.

Group IV: This category is formed by trinuclear compounds with pyrazolate ligands where all of them have the same structural core, [Mn₃(μ-O₃)(phpzR)₃]⁺. The ligands phpzR²⁻ form a plane with the three manganese(III) ions. At the axial position, coordinated solvent molecules are present and other bridging ligands, as acetate and azide, depending on the complex. Two subcategories must be considered depending on whether the [Mn^{III}₃(μ₃-O)]⁷⁺ core involves an equilateral or an isosceles triangle (Table 3.6).

A model of equilateral triangle has been considered to evaluate the weak antiferromagnetic exchange interactions for compounds [Mn₃(μ₃-O)(Meppz)₃(MeOH)₄(MeCO₂)]¹¹ and [Mn₃(μ₃-O)(phpzH)₃(MeOH)₃(MeCO₂)] (**10**).¹¹ Both complexes differ only in the change of the phpzR²⁻ ligand and have Mn–O_{oxide}–Mn angles very close to 120° and nearly equal Mn–O and Mn···Mn distances. However, in the latter complex the central oxygen is appreciably displaced from the Mn₃ plane, implying that the overlap between the magnetic orbitals could be smaller. Nevertheless, the exchange constants are found to be almost equal.

The remaining complexes in Group IV, [Mn₃(μ₃-O)(Meppz)₃(EtOH)₄(MeCO₂)]¹², [Mn₃(μ₃-O)(Brppz)₃(MeOH)₃(N₃)]·2H₂O,¹⁴ [Mn₃(μ₃-O)(Brppz)₃(MeOH)₃(N₃)]¹⁴, [Mn₃(μ₃-O)(Brppz)₃(MeOH)₃(MeCO₂)]¹⁵ the polymorphs [Mn₃(μ₃-O)(Brppz)₃(EtOH)₃(MeCO₂)]¹⁵ and the compounds **11** and **12**, have been fitted with the isosceles triangle model. Here, isolated trinuclear manganese(III) units are present and 1-D chains comprised of trinuclear manganese(III) units linked by either carboxylates or azides bridges. Once more antiferromagnetic intramolecular interactions are found, except for compound **11** that possesses both ferromagnetic and antiferromagnetic interactions. With the exception of compound **11**, all complexes with pyrazole ligands have a planar [Mn₃(μ-O₃)]⁷⁺

core and angles Mn–O_{oxido}–Mn around 120°, which probably explains the occurrence of antiferromagnetic interactions. Compound **11** shows the most structurally distorted [Mn^{III}₃(μ₃-O)]⁷⁺ core, with one of the Mn–O_{oxido}–Mn angle of 116.10° and a deviation of the oxido bridge from the Mn₃ plane of 0.172 Å. In view of the arguments presented for Group II, the smaller Mn–O_{oxido}–Mn angle, corresponding with Mn(2)–O(1)–Mn(3), together with large dihedral angle ($\delta_{\text{MnNNMn-MnOMn}} = 40.11^\circ$) between the Mn–O–Mn plane and the Mn(2)–N_{pz}–N_{pz}–Mn(3) coordination plane, could be held responsible for the observed ferromagnetic interaction along this path. It should be pointed out, however, that strong effects of the bridging pyrazole ligands on the type of the magnetic interaction have been reported in other types of systems.^{52,53}

Group V: In this group are included the complexes that could not fit in any of the previous groups (Table 3.7). Similar as in the other undistorted complexes, weak antiferromagnetic interactions have been found for [Mn₃O(mpdp)₃(py)₃](ClO₄).⁴⁹ By contrast, the complex [Mn₃(μ₃-O)(μ₃-bamen)₃](ClO₄)³¹ in this group makes an interesting comparison, notably with Group II, since a fairly strong ferromagnetic intramolecular interaction is observed, in spite of the fact that the [Mn₃(μ₃-O)]⁷⁺ core geometry is not distorted. In this material the manganese(III) ions are pentagonal bipyramidally coordinated, instead of having the octahedral geometry as most commonly observed for trinuclear manganese(III) complexes. In the absence of a distortion, the origin of the ferromagnetic interactions has most probably to be attributed to the superexchange paths along the oximate groups. In the case of (HNEt₃)₂[Mn₃(μ₃-O)(bta)₆F₃],⁵⁰ some difficulties were reported in determining the strength of the interactions and the ground state, suggesting the presence of low-lying excited states, close in energy to the ground state. [Mn₃(μ₃-O)(5-Br-sap)₃(H₂O)₃]Cl·5.5H₂O is a very distorted triangle with antiferromagnetic interactions, although any exchange constant has been reported.⁵¹ Only recently, the compound [NEt₃(CH₂Cl)]₂[Mn₃(μ₃-O)(hmcH)₆(hmcH₂)₃]·3CH₂Cl₂ has been reported.³⁰ in which all the magnetic interactions are ferromagnetic. This is the first case in which ferromagnetic interactions are dominant without the existence of the oximate ligands. The authors³⁰ attribute it to the displacement of the μ₃-O²⁻ from the Mn₃ plane, confirming the made assumption in the observed compound **11**, in which the distortion of the [Mn₃(μ₃-O)]⁷⁺ core determines the sign of the magnetic exchange interaction.

3.4. Conclusions

The synthesis, crystal structure and magnetic studies of three new trinuclear manganese(III)-based compounds have been presented. Mononuclear complexes with the general formula, $[\text{Mn}(\text{HphpzR})_2\text{X}]$ ($\text{R} = \text{H}, \text{Me}, \text{X}^- = \text{Cl}^-, \text{Br}^-$) have been proven to be excellent starting materials for the synthesis of new manganese(III) clusters with a stable $[\text{Mn}_3(\mu_3\text{-O})(\text{phpzR})_3]^+$ core as it is shown in this chapter. Compounds **10–12** are composed of a triangle of manganese(III) ions with an oxide-centre bridge and the three doubly deprotonated ligands that are in a plane with the manganese(III) ions. Methanol molecules are at the terminal positions, and bridging ligands are acetate (Compounds **10** and **11**) or azide (Compound **12**). Compounds **10** and **12** form 1-D chain, in which the trinuclear units are bridged by acetate and azide anions, whereas in compound **11**, the trinuclear units are bridged by hydrogen bonding between the methanol and the acetate molecules.

Magnetic studies reveal antiferromagnetic intramolecular magnetic interactions for compounds **10** and **12**, whereas compound **11** presents both antiferromagnetic and ferromagnetic interactions between the manganese(III) centres. A magneto-structural study has been performed emphasizing the importance of the structural distortion of the $[\text{Mn}_3(\mu\text{-O}_3)]^{7+}$ core on the magnetic properties. Finally, the coordination geometry of the bridging pyrazole ligands can also tune the magnetic exchange interactions.

3.5. References

1. Mukhopadhyay, S.; Mandal, S. K.; Bhaduri, S.; Armstrong, W. H., *Chem. Rev.*, **2004**, 104, 3981-4026.
2. Aromí, G.; Brechin, E. K., *Struc. Bond.*, **2006**, 122, 1-67.
3. Christou, G.; Gatteschi, D.; Hendrickson, D. N.; Sessoli, R., *MRS Bull.*, **2000**, 25, 66-71.
4. Gatteschi, D.; Sessoli, R., *Angew. Chem.-Int. Edit.*, **2003**, 42, 268-297.
5. Christou, G., *Polyhedron*, **2005**, 24, 2065-2075.
6. Rebilly, J. N.; Mallah, T., *Struc. Bond.*, **2006**, 122, 103-131.
7. Winpenny, R. E. P., *J. Chem. Soc.-Dalton Trans.*, **2002**, 1-10.
8. Aromí, G.; Aubin, S. M. J.; Bolcar, M. A.; Christou, G.; Eppley, H. J.; Folting, K.; Hendrickson, D. N.; Huffman, J. C.; Squire, R. C.; Tsai, H. L.; Wang, S.; Wemple, M. W., *Polyhedron*, **1998**, 17, 3005-3020.
9. Tanase, S.; Bouwman, E.; Long, G. J.; Shahin, A. M.; Mills, A. M.; Spek, A. L.; Reedijk, J., *Eur. J. Inorg. Chem.*, **2004**, 4572-4578.
10. Tanase, S.; Aromí, G.; Bouwman, E.; Kooijman, H.; Spek, A. L.; Reedijk, J., *Chem. Commun.*, **2005**, 3147-3149.
11. Tao, J.; Zhang, Y. Z.; Bai, Y. L.; Sato, O., *Inorg. Chem.*, **2006**, 45, 4877-4879.
12. Bai, Y. L.; Tao, J.; Wernsdorfer, W.; Sato, O.; Huang, R. B.; Zheng, L. S., *J. Am. Chem. Soc.*, **2006**, 128, 16428-16429.
13. Viciano-Chumillas, M.; Tanase, S.; Aromí, G.; Smits, J. M. M.; de Gelder, R.; Solans, X.; Bouwman, E.; Reedijk, J., *Eur. J. Inorg. Chem.*, **2007**, 2635-2640.
14. Liu, C. M.; Zhang, D. Q.; Zhu, D. B., *Chem. Commun.*, **2008**, 368-370.
15. Liu, C. M.; Zhang, D. Q.; Zhu, D. B., *Inorg. Chem.*, **2009**, 48, 4980-4987.
16. Miyasaka, H.; Saitoh, A.; Abe, S., *Coord. Chem. Rev.*, **2007**, 251, 2622-2664.

17. Viciano-Chumillas, M.; Marqués-Giménez, M.; Tanase, S.; Evangelisti, M.; Mutikainen, I.; Turpeinen, M.; Smits, J. M. M.; de Gelder, R.; de Jongh, L. J.; Reedijk, J., *J. Phys. Chem. C*, **2008**, 112, 20525–20534.
18. Kahn, O., *Molecular Magnetism*. Wiley-VCH: New York, 1993.
19. Sheldrick, G. M. *Program for Empirical Absorption Correction*, University of Göttingen: Göttingen, Germany, 1996.
20. Beurskens, P. T.; Beurskens, G.; Strumpel, M.; Nordman, C. E., in *Patterson and Pattersons*. Glusker, J. P.; Patterson, B. K.; Rossi, M., Eds. Clarendon Press: Oxford: 1987.
21. Duisenberg, A. J. M.; Kroon-Batenburg, L. M. J.; Schreurs, A. M. M., *J. Appl. Crystallogr.*, **2003**, 220-229.
22. Beurskens, P. T.; Beurskens, G.; Bosman, W. P.; De Gelder, R.; García-Granda, S.; Gould, R. O.; Israël, R.; Smits, J. M. M.; Smykalla, C. *The DIRDIF96. A computer program system for the crystal structure determination by Patterson methods and direct methods applied to difference structure factors*, Crystallography Laboratory, University of Nijmegen: Nijmegen, The Netherlands, 1996.
23. Sheldrick, G. M. *SHELXS-97: Program for Crystal Structures Determination*, University of Göttingen: Göttingen, Germany, 1997.
24. Sheldrick, G. M. *SHELXL-97: Program for Crystal Structure Refinement*, University of Göttingen: Göttingen, Germany, 1997.
25. Duisenberg, A. J. M. Reflections on area detectors. PhD thesis, Utrecht University, Utrecht, The Netherlands 1998.
26. Spek, A. L. *PLATON, A Multipurpose Crystallographic Tool*, Utrecht University; The Netherlands, 2003.
27. Martin, R. L., in *New Pathways in Inorganic Chemistry*, Ebsworth, E. A. V.; Maddock, A. G.; Sharpe, A. G., Eds. Cambridge University Press: Cambridge, 1968; pp 175-231.
28. Inglis, R.; Jones, L. F.; Karotsis, G.; Parsons, S.; Perlepes, S. P.; Wernsdorfer, W.; Brechin, E. K., *Chem. Commun.*, **2008**, 5924-5926.
29. Inglis, R.; Jones, L. F.; Mason, K.; Collins, A.; Moggach, S. A.; Parsons, S.; Perlepes, S. P.; Wernsdorfer, W.; Brechin, E. K., *Chem.-Eur. J.*, **2008**, 14, 9117-9121.
30. Lampropoulos, C.; Abboud, K. A.; Stamatatos, T. C.; Christou, G., *Inorg. Chem.*, **2009**, 48, 813-815.
31. Sreerama, S. G.; Pal, S., *Inorg. Chem.*, **2002**, 41, 4843-4845.
32. Stamatatos, T. C.; Foguet-Albiol, D.; Lee, S. C.; Stoumpos, C. C.; Raptopoulou, C. P.; Terzis, A.; Wernsdorfer, W.; Hill, S. O.; Perlepes, S. P.; Christou, G., *J. Am. Chem. Soc.*, **2007**, 129, 9484-9499.
33. Stamatatos, T. C.; Foguet-Albiol, D.; Stoumpos, C. C.; Raptopoulou, C. P.; Terzis, A.; Wernsdorfer, W.; Perlepes, S. P.; Christou, G., *J. Am. Chem. Soc.*, **2005**, 127, 15380-15381.
34. Stamatatos, T. C.; Foguet-Albiol, D.; Stoumpos, C. C.; Raptopoulou, C. P.; Terzis, A.; Wernsdorfer, W.; Perlepes, S. P.; Christou, G., *Polyhedron*, **2007**, 26, 2165-2168.
35. Yang, C.-I.; Wernsdorfer, W.; Cheng, K.-H.; Nakano, M.; Lee, G.-H.; H.-L., T., *Inorg. Chem.*, **2008**, 47, 10184-10186.
36. Cano, J.; Cauchy, T.; Ruiz, E.; Milios, C. J.; Stoumpos, C. C.; Stamatatos, T. C.; Perlepes, S. P.; Christou, G.; Brechin, E. K., *J. Chem. Soc.-Dalton Trans.*, **2008**, 234-240.
37. Crawford, V. H.; Richardson, H. W.; Wasson, J. R.; Hodgson, D. J.; Hatfield, W. E., *Inorg. Chem.*, **1976**, 15, 2107-2110.
38. Vankalkeren, G.; Schmidt, W. W.; Block, R., *Physica B & C*, **1979**, 97, 315-337.
39. An, J.; Chen, Z. D.; Bian, J. A.; Jin, X. L.; Wang, S. X.; Xu, G. X., *Inorg. Chim. Acta*, **1999**, 287, 82-88.
40. Li, J.; Yang, S. M.; Zhang, F. X.; Tang, Z. X.; Ma, S. L.; Shi, Q. Z.; Wu, Q. J.; Huang, Z. X., *Inorg. Chim. Acta*, **1999**, 294, 109-113.
41. Vincent, J. B.; Chang, H. R.; Folting, K.; Huffman, J. C.; Christou, G.; Hendrickson, D. N., *J. Am. Chem. Soc.*, **1987**, 109, 5703-5711.
42. Baca, S. G.; Stoeckli-Evans, H.; Ambrus, C.; Malinovskii, S. T.; Malaestean, I.; Gerbeleu, N.; Decurtins, S., *Polyhedron*, **2006**, 25, 3617-3627.

43. Zartilas, S.; Moushi, E. E.; Nastopoulos, V.; Boudalis, A. K.; Tasiopoulos, A. J., *Inorg. Chim. Acta*, **2008**, 361, 4100-4106.
44. Baldwin, M. J.; Stemmler, T. L.; Riggsgelasco, P. J.; Kirk, M. L.; Pennerhahn, J. E.; Pecoraro, V. L., *J. Am. Chem. Soc.*, **1994**, 116, 11349-11356.
45. Milios, C. J.; Inglis, R.; Vinslava, A.; Bagai, R.; Wernsdorfer, W.; Parsons, S.; Perlepes, S. P.; Christou, G.; Brechin, E. K., *J. Am. Chem. Soc.*, **2007**, 129, 12505-12511.
46. Hotzelmann, R.; Wieghardt, K.; Florke, U.; Haupt, H. J.; Weatherburn, D. C.; Bonvoisin, J.; Blondin, G.; Girerd, J. J., *J. Am. Chem. Soc.*, **1992**, 114, 1681-1696.
47. Xu, H.-B.; Wang, B.-W.; Pan, F.; Wang, Z.-M.; Gao, S., *Angew. Chem.-Int. Edit.*, **2007**, 46, 7388-7393.
48. Milios, C. J.; Wood, P. A.; Parsons, S.; Foguet-Albiol, D.; Lampropoulos, C.; Christou, G.; Perlepes, S. P.; Brechin, E. K., *Inorg. Chim. Acta*, **2007**, 360, 3932-3940.
49. Cañada-Vilalta, C.; Huffman, J. C.; Streib, W. E.; Davidson, E. R.; Christou, G., *Polyhedron*, **2001**, 20, 1375-1380.
50. Jones, L. F.; Rajaraman, G.; Brockman, J.; Murugesu, M.; Sañudo, E. C.; Raftery, J.; Teat, S. J.; Wernsdorfer, W.; Christou, G.; Brechin, E. K.; Collison, D., *Chem.-Eur. J.*, **2004**, 10, 5180-5194.
51. Nihei, M.; Hoshino, N.; Ito, T.; Oshio, H., *Chem. Lett.*, **2002**, 1016-1017.
52. Tanase, S.; Koval, I. A.; Bouwman, E.; de Gelder, R.; Reedijk, J., *Inorg. Chem.*, **2005**, 44, 7860-7861.
53. Ajò, D.; Bencini, A.; Mani, F., *Inorg. Chem.*, **1988**, 27, 2437-2444.

Chapter 4

From 1-D to isolated trinuclear compounds: impact of the co-ligand and the carboxylate on the core $[\text{Mn}_3(\mu_3\text{-O})(\text{phpzR})_3]^{+*}$

The effects of the co-ligand and the carboxylate on the trinuclear core $[\text{Mn}_3(\mu_3\text{-O})(\text{phpzR})_3]^+$ have been studied with the synthesis of three new compounds, $[\text{Mn}_3(\mu_3\text{-O})(\text{phpzMe})_3(\text{O}_2\text{CMe})(\text{EtOH})]\cdot\text{EtOH}$ (**13**), ${}^n\text{Bu}_4\text{N}[\text{Mn}_3(\mu_3\text{-O})(\text{phpzMe})_3(\text{O}_2\text{CPh})_2]$ (**14**) and ${}^n\text{Bu}_4\text{N}[\text{Mn}_3(\mu_3\text{-O})(\text{phpzPh})_3(\text{O}_2\text{CPh})_2]$ (**15**). Hydrogen bonding interactions between the trinuclear units of **13** result in a 1-D chain structure. Compounds **14** and **15** are isolated trinuclear units. Magnetic susceptibility studies indicate the presence of both antiferromagnetic and ferromagnetic interactions in compound **13**, while only antiferromagnetic interactions are found in compounds **14** and **15**. The ferromagnetic interactions in the trinuclear unit have been ascribed mainly to the distortion of the Mn–O–Mn angle of the core $[\text{Mn}_3(\mu_3\text{-O})(\text{phpzR})_3]^+$.

* Part of this chapter has been published in the literature: Viciano-Chumillas M., Tanase S., Mutikainen I., Turpeinen U., de Jongh L.J., Reedijk J., *Dalton Trans.*, **2009**, 7445-7453.

4.1. Introduction

Oxide-centred trinuclear manganese(III) compounds are well known for several years in the literature.¹ The first reported compounds were commonly named basic carboxylates and they have the general formula $[\text{Mn}_3(\mu_3\text{-O})(\text{O}_2\text{CR})_6\text{L}_3]^+$ (R = Me, Et, Pr, Piv, Ph, and L = py, 3-Mepy, Im, H₂O).¹⁻⁶ Lately, the carboxylate ligands and solvent molecules have been replaced by other types of ligands, such as salicylaldoxime,⁷⁻¹¹ or pyrazole derivatives,¹²⁻¹⁶ thereby extending the group of trinuclear manganese(III) compounds. All these compounds show predominant antiferromagnetic interactions between the manganese(III) ions, with the exception of those containing oximato-based ligands^{7,8,11,17-19} and the compound $[\text{NEt}_3(\text{CH}_2\text{Cl})_2][\text{Mn}_3(\mu_3\text{-O})(\text{Hhmc})_3(\text{H}_2\text{hmc})_3]$ (H₃hmc = 2,6-bis(hydroxymethyl)-*p*-cresol)²⁰, in which ferromagnetic interactions are operative. Due to the complexity of the magnetic exchange paths, several factors have been proposed as the origins of the observed ferromagnetic behaviour.^{16,17,20,21} An important cause appears to be the distortion of the $[\text{Mn}_3(\mu_3\text{-O})]^{7+}$ core, where the Mn–O–Mn angle is smaller than 120° (value for an equilateral triangle);^{16,17,21} a switch from antiferromagnetic to ferromagnetic exchange is observed at angles below approximately 120°.²² The displacement of the $\mu_3\text{-O}^{2-}$ ion from the plane formed by all manganese(III) ions seems also to be an important factor for the presence of ferromagnetic interactions.²⁰ It has been shown that the ligand distortion, *i.e.* the Mn–N–O–Mn torsion angle in oximate ligands, plays an important role as well; a larger torsion angle giving rise to a stronger ferromagnetic coupling.^{7,8,17,21}

In Chapter 3,¹⁶ some trinuclear manganese(III) compounds obtained with mononuclear manganese(III) building blocks containing phenol-pyrazole ligands were described. Temperature-dependent magnetic susceptibility studies have revealed that the antiferromagnetic intramolecular interactions are dominant in most of the cases, with the exception of one compound that displays both antiferromagnetic and ferromagnetic interactions between the manganese(III) ions.¹⁶ In the later case, the ferromagnetic exchange interaction was found to correspond to the major distortion of the Mn–O–Mn angle of the $[\text{Mn}_3(\mu_3\text{-O})]^{7+}$ core. In the present chapter, a new approach is reported within the strategy of modifying known complexes, *i.e.* the controlled distortion of the $[\text{Mn}_3(\mu_3\text{-O})]^{7+}$ core to elucidate the crucial magnetic exchange paths. In this respect, the effect of different carboxylate ligands and co-ligands on the geometry of the $[\text{Mn}_3(\mu_3\text{-O})]^{7+}$ core has been studied. Three new trinuclear manganese(III) compounds, $[\text{Mn}_3(\mu_3\text{-O})(\text{phpzMe})_3(\text{O}_2\text{CMe})(\text{EtOH})]\cdot\text{EtOH}$ (**13**), ${}^n\text{Bu}_4\text{N}[\text{Mn}_3(\mu_3\text{-O})(\text{phpzMe})_3(\text{O}_2\text{CPh})_2]$ (**14**) and ${}^n\text{Bu}_4\text{N}[\text{Mn}_3(\mu_3\text{-O})(\text{phpzPh})_3(\text{O}_2\text{CPh})_2]$ (**15**) are presented and their synthesis, X-ray crystal structures and magnetic properties are described in detail.

4.2. Experimental Section

General remarks. Starting materials were purchased from Aldrich. All manipulations were performed using materials as received. $\text{Mn}(\text{O}_2\text{CPh})_2 \cdot 2\text{H}_2\text{O}$,²³ ${}^n\text{Bu}_4\text{NMnO}_4$ ⁵ and the ligands 3(5)-(2-hydroxyphenyl)-5(3)-methylpyrazole (H_2phpzMe) and 3(5)-(2-hydroxyphenyl)-5(3)-phenylpyrazole (H_2phpzPh) have been synthesized according to reported procedures.²⁴

General synthetic procedure

Solid ${}^n\text{Bu}_4\text{NMnO}_4$ (0.07 mmol) was added to a solution of $\text{Mn}(\text{O}_2\text{CR}')_2 \cdot n\text{H}_2\text{O}$ ($\text{R}' = \text{Me}, \text{Ph}$) (0.28 mmol) in ethanol. The resulting solution was stirred for a few minutes, followed by the addition of H_2phpzR ($\text{R} = \text{Me}, \text{Ph}$) (0.21 mmol) in ethanol. The solution mixture resulted in the formation of a brown precipitate, which was filtered off and discarded. The filtrate was allowed to evaporate slowly, affording brown crystals within a few days in all cases. The crystals were collected by filtration, washed with Et_2O and dried in vacuum.

$[\text{Mn}_3(\mu_3\text{-O})(\text{phpzMe})_3(\text{O}_2\text{CMe})(\text{EtOH})] \cdot \text{EtOH}$ (13). Yield: 17% (30 mg). Anal. Calcd for **13** ($\text{C}_{36}\text{H}_{39}\text{Mn}_3\text{N}_6\text{O}_8$): C, 50.96; H, 4.63; N, 9.90. Found: C, 50.53; H, 5.05; N, 9.90. IR ($\nu_{\text{max}}/\text{cm}^{-1}$): 3070(w), 1597(m), 1560(m), 1550(m), 1530(s), 1496(m), 1458(s), 1322(m), 1296(vs), 1268(vs), 1249(vs), 1144(w), 1127(s), 1090(m), 1062(m), 1036(s), 982(w), 864(s), 792(s), 784(m), 752(s), 742(s), 725(s), 668(vs), 647(vs), 601(vs), 484(m), 418(s), 381(s), 312(s).

${}^n\text{Bu}_4\text{N}[\text{Mn}_3(\mu_3\text{-O})(\text{phpzMe})_3(\text{O}_2\text{CPh})_2]$ (14). Yield: 11% (28 mg). Anal. Calcd for **14** ($\text{C}_{60}\text{H}_{70}\text{Mn}_3\text{N}_7\text{O}_8$): C, 60.97; H, 5.97; N, 8.29. Found: C, 60.47; H, 6.78; N, 8.36. IR ($\nu_{\text{max}}/\text{cm}^{-1}$): 2964(m), 2875(w), 1594(s), 1563(s), 1558(vs), 1540(m), 1531(m), 1494(s), 1456(vs), 1374(vs), 1330(m), 1296(vs), 1268(vs), 1254(vs), 1152(m), 1127(s), 1088(m), 1064(s), 1056(s), 1034(s), 988(m), 938(m), 866(s), 834(m), 782(m), 766(s), 760(s), 752(vs), 720(vs), 680(vs), 668(vs), 642(vs), 612(s), 580(s), 542(m), 442(s), 422(s), 417(s), 379(vs), 350(s), 334(s).

${}^n\text{Bu}_4\text{N}[\text{Mn}_3(\mu_3\text{-O})(\text{phpzPh})_3(\text{O}_2\text{CPh})_2]$ (15). Yield: 13% (37 mg). Anal. Calcd for **15** ($\text{C}_{75}\text{H}_{76}\text{Mn}_3\text{N}_7\text{O}_8$): C, 65.84; H, 5.60; N, 7.17. Found: C, 65.21; H, 6.37; N, 7.21. IR ($\nu_{\text{max}}/\text{cm}^{-1}$): 2962(m), 2880(w), 1595(s), 1564(m), 1558(vs), 1539(m), 1532(m), 1506(m), 1476(vs), 1456(s), 1448(s), 1428(m), 1378(vs), 1297(s), 1266(s), 1249(s), 1175(w), 1122(s), 1098(s), 1026(m), 995(m), 935(w), 864(s), 836(w), 797(m), 752(s), 719(vs), 710(s), 696(vs), 686(s), 668(vs), 662(s), 646(s), 610(m), 588(m), 534(m), 492(w), 456(m), 448(m), 435(m), 421(s), 378(m), 374(m), 333(s).

Physical Measurements. Elemental analyses for C, H and N were performed on a Perkin-Elmer 2400 series II analyzer. Infrared spectra ($4000\text{--}300\text{ cm}^{-1}$) were recorded on a Perkin-Elmer Paragon 1000 FTIR spectrometer equipped with a Golden Gate ATR device, using the reflectance technique. DC and AC magnetic data were recorded using a Quantum Design MPMS-5 SQUID susceptometer. The magnetic susceptibilities were measured from 1.8 to 300 K on powdered single-crystal samples in a gelatine capsule with an applied field of 0.1 T. The magnetization was measured from 2 up to 20 K in the 0–5 T range. Data were corrected for magnetization of the sample holder and for diamagnetic contributions, which were estimated from Pascal's constants.²⁵

X-ray Crystallography. Intensity data for single crystals of **13**, **14** and **15** were collected using MoK α radiation ($\lambda = 0.71073\text{ \AA}$) on a Nonius KappaCCD diffractometer. Crystal and refinement data for **13**, **14** and **15** are collected in Table 4.1. The intensity data were corrected for Lorentz and polarization effects, and for absorption (multiscan absorption correction²⁶). The structures were solved by Patterson methods.²⁷ The programs EvalCCD,^{28,29} DIRDIF96,³⁰ SHELXS-97³¹ and SHELXL-97³² were used for data reduction, structure solution and refinement, respectively. All non-hydrogen atoms were refined with anisotropic displacement parameters. Geometric calculations and molecular graphics were performed with the PLATON package.³³

4.3. Results and Discussion

Synthesis. μ_3 -oxide bridged trinuclear manganese(III) compounds have been previously obtained by reacting mononuclear manganese(III) building blocks, containing phenol-pyrazole ligands, with manganese(II) acetate or with sodium azide (see Chapter 3).¹⁶ These compounds contain the same core with the general formula $[\text{Mn}_3(\mu_3\text{-O})(\text{phpzR})_3]^+$; methanol molecules, and acetate or azide bridging ligands have been found at the terminal positions. In the present chapter, the influence of a different carboxylate ligand, namely benzoate and a different starting solvent, namely ethanol, in these type of trinuclear manganese(III) compounds is presented. In addition, new synthetic routes have been explored by starting from manganese(II) carboxylate salts, ${}^n\text{Bu}_4\text{NMnO}_4$ and phenol-pyrazole ligands in the same reaction. Manganese(II) salts together with ${}^n\text{Bu}_4\text{NMnO}_4$ are an excellent and well known starting source to generate manganese(III) and/or manganese(IV) ions; depending on the used ratio, complexes of different nuclearities can be obtained.^{5,23} The manganese(II)/manganese(VII) ratio employed can be either 4/1 or 3/1. The presence of ${}^n\text{Bu}_4\text{N}^+$ in the final product is necessary to balance the charges in the compounds

${}^n\text{Bu}_4\text{N}[\text{Mn}_3(\mu_3\text{-O})(\text{phpzMe})_3(\text{O}_2\text{CPh})_2]$ (**14**) and ${}^n\text{Bu}_4\text{N}[\text{Mn}_3(\mu_3\text{-O})(\text{phpzPh})_3(\text{O}_2\text{CPh})_2]$ (**15**), because there are two benzoate groups present. The use of the other ${}^n\text{Bu}_4\text{N}^+$ salts, *i.e.* ${}^n\text{Bu}_4\text{NBr}$ instead of ${}^n\text{Bu}_4\text{NMnO}_4$, did result in a decrease of the reaction yields. Compound $[\text{Mn}_3(\mu_3\text{-O})(\text{phpzMe})_3(\text{O}_2\text{CMe})(\text{EtOH})]\cdot\text{EtOH}$ (**13**) contains one acetate group only, therefore the ${}^n\text{Bu}_4\text{N}^+$ is absent. The infrared spectra of complexes **13–15** are very similar. The main difference is that compounds **14** and **15** exhibit the bands expected for the ${}^n\text{Bu}_4\text{N}^+$ at 2964, 2875 and 1374 cm^{-1} that are absent in compound **13**, in agreement with the X-ray crystallographic studies.

Table 4.1. Crystal data and structure refinements for $[\text{Mn}_3(\mu_3\text{-O})(\text{phpzMe})_3(\text{O}_2\text{CMe})(\text{EtOH})]\cdot\text{EtOH}$ (**13**), ${}^n\text{Bu}_4\text{N}[\text{Mn}_3(\mu_3\text{-O})(\text{phpzMe})_3(\text{O}_2\text{CPh})_2]$ (**14**), ${}^n\text{Bu}_4\text{N}[\text{Mn}_3(\mu_3\text{-O})(\text{phpzPh})_3(\text{O}_2\text{CPh})_2]$ (**15**).

	13	14	15
Formula	$\text{C}_{34}\text{H}_{33}\text{Mn}_3\text{N}_6\text{O}_7, \text{C}_2\text{H}_6\text{O}$	$\text{C}_{44}\text{H}_{34}\text{Mn}_3\text{N}_6\text{O}_8, \text{C}_{16}\text{H}_{36}\text{N}$	$\text{C}_{59}\text{H}_{40}\text{Mn}_3\text{N}_6\text{O}_8, \text{C}_{16}\text{H}_{36}\text{N}$
FW [g mol^{-1}]	848.55	1182.05	1368.24
Crystal system	Triclinic	Monoclinic	Triclinic
Space group	P-1	P2 ₁ /c	P-1
<i>a</i> [Å]	8.4040(13)	12.4030(10)	13.805(2)
<i>b</i> [Å]	11.5702(15)	21.1640(10)	16.257(2)
<i>c</i> [Å]	18.427(2)	24.603(2)	16.495(2)
α [°]	98.205(10)	90	101.53(2)
β [°]	91.345(7)	120.27(1)	100.39(2)
γ [°]	93.355(11)	90	109.06(2)
V [Å ³]	1769.5(4)	5577.7 (9)	3305.6(10)
Z	2	4	2
D _{calc} [g cm^{-3}]	1.593	1.408	1.374
Crystal size	0.15×0.20×0.20	0.10×0.20×0.20	0.12×0.25×0.28
Number of collected reflections (unique)	28899(7338)	52922(12736)	58112(12942)
Number of observed reflections [$I_o > 2\sigma(I_o)$]	6261	8686	10168
Internal R factor	0.0280	0.048	0.055
Number of parameters	488	710	889
Goodness-of-fit S on F ²	1.05	1.05	1.08
μ [mm^{-1}]	1.118	0.731	0.627
R ₁ ^[a] [$I > 2.0\sigma(I)$]	0.0280	0.0383	0.0408
wR ₂ ^[b] [all data]	0.0696	0.0887	0.0979
T [°C]	173	173	173

^[a] $R_1 = \sum||F_o| - |F_c|| / \sum|F_o|$. ^[b] $wR_2 = \{\sum[w(F_o^2 - F_c^2)^2] / \sum w(F_o^2)^2\}^{1/2}$.

Description of the Molecular Structures. Compound **13** crystallizes in the triclinic space group $P\bar{1}$. As shown in Figure 4.1, the crystal structure reveals a trinuclear manganese(III) compound in which the three manganese(III) ions are bridged by a central oxide. Selected bond lengths and angles are listed in Table 4.2. Intracluster Mn \cdots Mn distances are 3.153 Å, 3.330 Å and 3.300 Å for Mn(1) \cdots Mn(2), Mn(1) \cdots Mn(3) and Mn(2) \cdots Mn(3), respectively. The $\mu_3\text{-O}^{2-}$ (O1) is located 0.064 Å above the Mn₃ plane. The Mn–O(1)–Mn angles are 112.65(6)°, 124.28(6)° and 122.73(7)° for Mn(1)–O(1)–Mn(2), Mn(1)–O(1)–Mn(3) and Mn(2)–O(1)–Mn(3), respectively. All the manganese(III) ions are pentacoordinated square-pyramidal based. An acetate molecule is bridging the Mn(1) and the Mn(2) ions, whereas Mn(3) contains an ethanol molecule at the axial position. In the lattice, another ethanol molecule is present, forming intermolecular hydrogen bonds with the coordinated ethanol of one trinuclear unit and also with the acetate group of a neighbouring trinuclear unit (O(5)–H(5) \cdots O(7) = 2.591(2) Å and O(7)–H(7) \cdots O(3) = 2.783(2) Å), thus forming a chain structure along the *a* direction (Figure 4.1). The shortest distance between the manganese(III) ions from the trinuclear units bridged by hydrogen bonding is Mn(1) \cdots Mn(3), equal to 7.404 Å. The shortest interchain Mn \cdots Mn distance is 6.386 Å, along the *c* direction and it belongs to a Mn(2) \cdots Mn(2) distance.

Table 4.2. Selected bonds lengths [Å] and angles [°] for compound **13**.

Bond Lengths					
Mn(1)–O(1)	1.8979(13)	Mn(1)–O(3)	2.1026(13)	Mn(1)–O(112)	1.8377(14)
Mn(1)–N(11)	1.9375(15)	Mn(1)–N(32)	2.0175(15)	Mn(2)–O(1)	1.8911(12)
Mn(2)–O(2)	2.0794(13)	Mn(2)–O(212)	1.8257(14)	Mn(2)–N(12)	2.0195(16)
Mn(2)–N(21)	1.9518(15)	Mn(3)–O(1)	1.8689(12)	Mn(3)–O(5)	2.1458(15)
Mn(3)–O(312)	1.8247(14)	Mn(3)–N(22)	2.0385(16)	Mn(3)–N(31)	1.9679(16)
Mn(1) \cdots Mn(2)	3.153	Mn(1) \cdots Mn(3)	3.330	Mn(2) \cdots Mn(3)	3.300
Bond Angles					
O(1)–Mn(1)–O(3)	94.17(5)	O(1)–Mn(1)–O(112)	174.50(6)	O(1)–Mn(1)–N(11)	87.87(6)
O(1)–Mn(1)–N(32)	88.27(6)	O(3)–Mn(1)–O(112)	90.60(6)	O(3)–Mn(1)–N(11)	102.02(6)
O(3)–Mn(1)–N(32)	102.87(6)	O(112)–Mn(1)–N(11)	88.45(6)	O(112)–Mn(1)–N(32)	93.35(6)
N(11)–Mn(1)–N(32)	155.02(7)	O(1)–Mn(2)–O(2)	90.97(5)	O(1)–Mn(2)–O(212)	178.90(6)
O(1)–Mn(2)–N(12)	87.07(6)	O(1)–Mn(2)–N(21)	89.51(6)	O(2)–Mn(2)–O(212)	89.19(6)
O(2)–Mn(2)–N(12)	106.01(6)	O(2)–Mn(2)–N(21)	117.60(6)	O(212)–Mn(2)–N(12)	93.92(6)
O(212)–Mn(2)–N(21)	89.46(6)	N(12)–Mn(2)–N(21)	136.30(6)	O(1)–Mn(3)–O(5)	93.65(6)
O(1)–Mn(3)–O(312)	173.12(6)	O(1)–Mn(3)–N(22)	89.61(6)	O(1)–Mn(3)–N(31)	87.84(6)
O(5)–Mn(3)–O(312)	92.98(6)	O(5)–Mn(3)–N(22)	94.27(6)	O(5)–Mn(3)–N(31)	96.77(6)
O(312)–Mn(3)–N(22)	91.76(6)	O(312)–Mn(3)–N(31)	89.53(6)	N(22)–Mn(3)–N(31)	168.80(6)
Mn(1)–O(1)–Mn(2)	112.65(6)	Mn(1)–O(1)–Mn(3)	124.28(6)	Mn(2)–O(1)–Mn(3)	122.73(7)

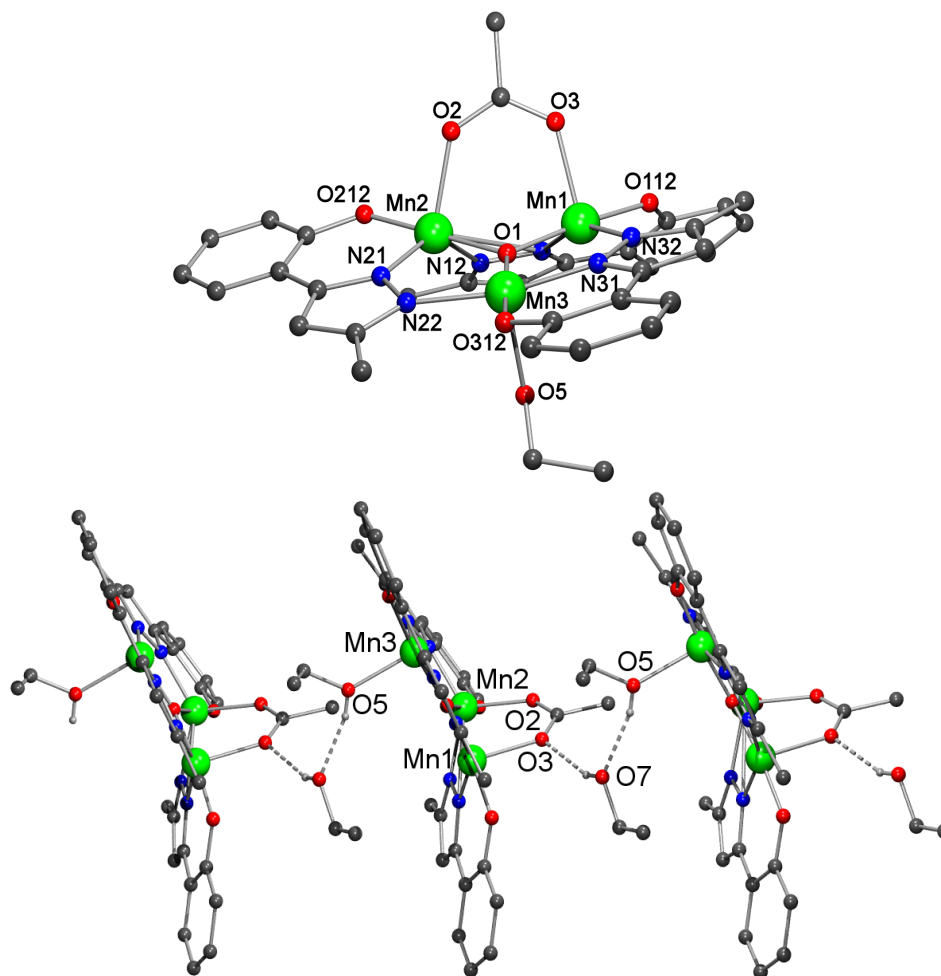


Figure 4.1. Pluton projection of the molecular structure of $[\text{Mn}_3(\mu_3\text{-O})(\text{phpzMe})_3(\text{O}_2\text{CMe})(\text{EtOH})] \cdot \text{EtOH}(\mathbf{13})$ showing the detailed $\text{Mn}^{\text{III}}_3\text{O}$ unit (top) and the crystal packing (bottom) showing the hydrogen bonding interactions and the non-coordinated ethanol molecule. Hydrogen atoms that are not involved in hydrogen bonds are omitted for clarity. Colour code: green, manganese; blue, nitrogen; red, oxygen; grey, carbon.

Compounds **14** and **15** crystallize in the monoclinic space group $P2_1/c$ and in the triclinic space group $P\bar{1}$, respectively. Their molecular structures are shown in Figures 4.2 and 4.3. For both compounds, the crystallographic analyses reveal a trinuclear manganese(III) unit containing a μ_3 -oxide bridge. Each edge of the Mn_3 triangle is bridged by a η^1, η^1, μ -pyrazolato ligand with the phenolic oxygen and one pyrazole nitrogen atom chelating a manganese(III) ion. Selected bond lengths and angles are listed in Table 4.3 and Table 4.4 for both compounds **14** and **15**, respectively. For compound **14**, intracuster $\text{Mn} \cdots \text{Mn}$ distances are 3.299 Å, 3.214 Å and 3.224 Å for $\text{Mn}(1) \cdots \text{Mn}(2)$, $\text{Mn}(1) \cdots \text{Mn}(3)$ and $\text{Mn}(2) \cdots \text{Mn}(3)$, respectively. For compound **15**, intracuster $\text{Mn} \cdots \text{Mn}$ distances are 3.350 Å, 3.209 Å and 3.250 Å for $\text{Mn}(1) \cdots \text{Mn}(2)$, $\text{Mn}(1) \cdots \text{Mn}(3)$ and $\text{Mn}(2) \cdots \text{Mn}(3)$, respectively. The $\mu_3\text{-O}^{2-}$ (O1) ion lies 0.029 Å above the Mn_3 plane for compound **14** and 0.001 Å for compound **15**,

respectively. In compound **14**, the Mn–O(1)–Mn angles are Mn(1)–O(1)–Mn(2) = 124.67(9)°, Mn(1)–O(1)–Mn(3) = 117.35(8)° and Mn(2)–O(1)–Mn(3) = 117.91(10)°; whereas in compound **15**, the Mn–O(1)–Mn angles are Mn(1)–O(1)–Mn(2) = 125.59(9)°, Mn(1)–O(1)–Mn(3) = 116.66(8)° and Mn(2)–O(1)–Mn(3) = 117.75(9)°. For both compounds, one manganese(III) ion is hexacoordinated and the other two manganese(III) ions are pentacoordinated. The shortest intermolecular Mn⋯Mn distance is 8.816 Å and 7.228 Å for compounds **14** and **15**, respectively. Therefore in the case of **15**, π – π stacking interactions (3.717 Å) are present between the pyrazole ring of one trinuclear unit and the phenol ring of the closest trinuclear unit, with a dihedral angle between the rings of 6.92°. The main difference with compound **13** is the presence of two bridging benzoate ligands in **14** and **15**, and the ${}^n\text{Bu}_4\text{N}^+$ as a counter ion, whereas in compound **13** only one bridging acetate is present. As consequence, the coordination sphere of the manganese(III) ions in **13** is completed with solvent molecules. In **13** the solvent present in the lattice is involved in hydrogen bonding that links the trinuclear units, thus forming a chain. Compounds **14** and **15** are isolated trinuclear units.

Table 4.3. Selected bonds lengths [Å] and angles [°] for ${}^n\text{Bu}_4\text{N}[\text{Mn}_3(\mu_3\text{-O})(\text{phpzMe})_3(\text{O}_2\text{CPh})_2]$ (**14**).

Bond Lengths					
Mn(1)–O(1)	1.8615(18)	Mn(1)–O(58)	2.0648(16)	Mn(1)–O(112)	1.835(2)
Mn(1)–N(11)	1.9704(19)	Mn(1)–N(22)	2.0354(19)	Mn(2)–O(1)	1.8629(17)
Mn(2)–O(48)	2.0035(17)	Mn(2)–O(212)	1.8515(18)	Mn(2)–N(21)	1.953(2)
Mn(2)–N(32)	2.0740(18)	Mn(3)–O(1)	1.9006(16)	Mn(3)–O(49)	2.2987(18)
Mn(3)–O(59)	2.274(2)	Mn(3)–O(312)	1.8627(16)	Mn(3)–N(12)	2.011(2)
Mn(3)–N(31)	1.9515(19)	Mn(1)⋯Mn(2)	3.299	Mn(1)⋯Mn(3)	3.214
Mn(2)⋯Mn(3)	3.224				
Bond Angles					
O(1)–Mn(1)–O(58)	96.47(7)	O(1)–Mn(1)–O(112)	164.51(8)	O(1)–Mn(1)–N(11)	88.07(8)
O(1)–Mn(1)–N(22)	87.09(8)	O(58)–Mn(1)–O(112)	98.89(8)	O(58)–Mn(1)–N(11)	95.66(7)
O(58)–Mn(1)–N(22)	101.22(7)	O(112)–Mn(1)–N(11)	88.43(8)	O(112)–Mn(1)–N(22)	91.87(8)
N(11)–Mn(1)–N(22)	162.85(8)	O(1)–Mn(2)–O(48)	91.18(7)	O(1)–Mn(2)–O(212)	175.57(8)
O(1)–Mn(2)–N(21)	87.31(8)	O(1)–Mn(2)–N(32)	87.64(7)	O(48)–Mn(2)–O(212)	89.82(7)
O(48)–Mn(2)–N(21)	124.13(8)	O(48)–Mn(2)–N(32)	105.91(8)	O(212)–Mn(2)–N(21)	88.55(8)
O(212)–Mn(2)–N(32)	96.23(8)	N(21)–Mn(2)–N(32)	129.77(8)	O(1)–Mn(3)–O(49)	85.75(7)
O(1)–Mn(3)–O(59)	89.42(7)	O(1)–Mn(3)–O(312)	177.29(7)	O(1)–Mn(3)–N(12)	87.83(8)
O(1)–Mn(3)–N(31)	88.43(7)	O(49)–Mn(3)–O(59)	168.38(7)	O(49)–Mn(3)–O(312)	94.61(7)
O(49)–Mn(3)–N(12)	81.22(8)	O(49)–Mn(3)–N(31)	94.51(7)	O(59)–Mn(3)–O(312)	90.70(7)
O(59)–Mn(3)–N(12)	88.05(8)	O(59)–Mn(3)–O(31)	95.91(7)	O(312)–Mn(3)–N(12)	94.88(8)
O(312)–Mn(3)–N(31)	88.87(8)	N(12)–Mn(3)–N(31)	174.52(8)	Mn(1)–O(1)–Mn(2)	124.67(9)
Mn(1)–O(1)–Mn(3)	117.35(8)	Mn(2)–O(1)–Mn(3)	117.91(10)		

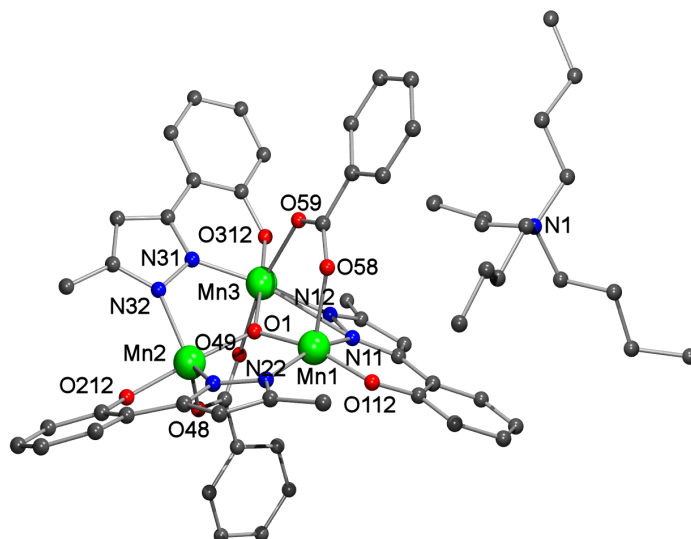


Figure 4.2. Pluton projection of the compound ${}^n\text{Bu}_4\text{N}[\text{Mn}_3(\mu_3\text{-O})(\text{phpzMe})_3(\text{O}_2\text{CPh})_2]$ (**14**). Hydrogen atoms are omitted for clarity. Colour code: green, manganese; blue, nitrogen; red, oxygen; grey, carbon.

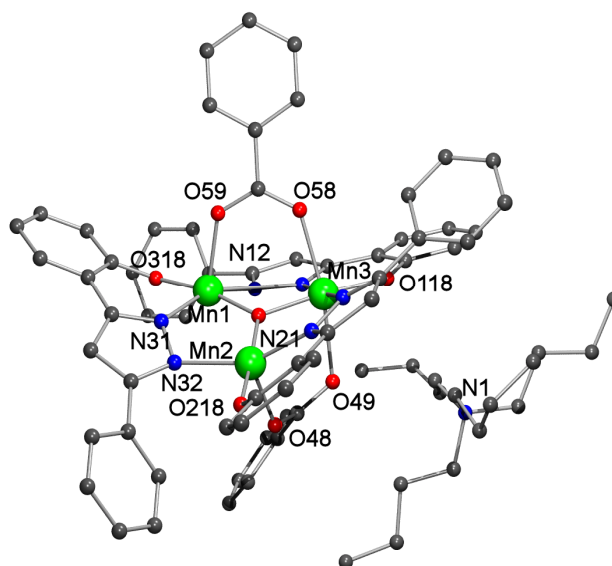


Figure 4.3. Pluton projection of the compound ${}^n\text{Bu}_4\text{N}[\text{Mn}_3(\mu_3\text{-O})(\text{phpzPh})_3(\text{O}_2\text{CPh})_2]$ (**15**). Hydrogen atoms are omitted for clarity. Colour code: green, manganese; blue, nitrogen; red, oxygen; grey, carbon.

Some structural differences are observed between the trinuclear manganese(III) compounds reported here and those described previously,¹²⁻¹⁶ all containing phenol-pyrazole ligands. The introduction of a substituent on the fifth position of the pyrazole ring, as methyl or phenyl, drives the carboxylate to bind to two manganese(III) ions from the same trinuclear unit, instead of bridging the trinuclear manganese(III) units, as was observed previously.^{12,14-16} If the carboxylate ligand is small, *i.e.* acetate, these trinuclear units can form chains, because of the hydrogen bonds established between the carboxylate and the solvent molecules (*e.g.* compound **13** and $[\text{Mn}_3(\mu_3\text{-O})(\text{phpzMe})_3(\text{O}_2\text{CMe})(\text{MeOH})_3]\cdot 1.5\text{MeOH}$ (**11**)¹⁶). However, if the carboxylate is bulkier, such as benzoate, the trinuclear units become isolated

and no intermolecular hydrogen bonding interactions are observed. It appears that the size of the co-ligand or the solvent molecule is also an important driving force in stabilizing the type of structure as the replacement of methanol¹⁶ by ethanol (*e.g.* compounds **14** and **15**) induces the coordination of two bridging carboxylate ligands in the same $[\text{Mn}_3(\mu_3\text{-O})]^{7+}$ core.

Table 4.4. Selected bonds lengths [\AA] and angles [$^\circ$] for ${}^n\text{Bu}_4\text{N}[\text{Mn}_3(\mu_3\text{-O})(\text{phpzPh})_3(\text{O}_2\text{CPh})_2]$ (**15**).

Bond Lengths					
Mn(1)–O(1)	1.8700(17)	Mn(1)–O(59)	2.0404(18)	Mn(1)–O(318)	1.8402(18)
Mn(1)–N(12)	2.051(2)	Mn(1)–N(31)	1.988(2)	Mn(2)–O(1)	1.8970(16)
Mn(2)–O(48)	2.036(2)	Mn(2)–O(218)	1.8402(18)	Mn(2)–N(21)	1.957(2)
Mn(2)–N(32)	2.053(2)	Mn(3)–O(1)	1.8999(17)	Mn(3)–O(49)	2.296(2)
Mn(3)–O(58)	2.2245(19)	Mn(3)–O(118)	1.8576(19)	Mn(3)–N(11)	1.972(2)
Mn(3)–N(22)	2.041(2)	Mn(1)⋯Mn(2)	3.350	Mn(1)⋯Mn(3)	3.209
Mn(2)⋯Mn(3)	3.250				
Bond Angles					
O(1)–Mn(1)–O(59)	95.25(7)	O(1)–Mn(1)–O(318)	169.72(8)	O(1)–Mn(1)–N(12)	90.00(8)
O(1)–Mn(1)–N(31)	85.93(8)	O(59)–Mn(1)–O(318)	94.47(8)	O(59)–Mn(1)–N(12)	94.81(8)
O(59)–Mn(1)–N(31)	107.59(8)	O(318)–Mn(1)–N(12)	92.55(9)	O(318)–Mn(1)–N(31)	87.93(9)
N(12)–Mn(1)–N(31)	157.50(9)	O(1)–Mn(2)–O(48)	90.01(8)	O(1)–Mn(2)–O(218)	174.03(9)
O(1)–Mn(2)–N(21)	88.46(8)	O(1)–Mn(2)–N(32)	88.18(8)	O(48)–Mn(2)–O(218)	95.91(9)
O(48)–Mn(2)–N(21)	105.74(9)	O(48)–Mn(2)–N(32)	102.85(8)	O(218)–Mn(2)–N(21)	89.20(8)
O(218)–Mn(2)–N(32)	91.24(8)	N(21)–Mn(2)–N(32)	151.21(9)	O(1)–Mn(3)–O(49)	81.99(7)
O(1)–Mn(3)–O(58)	89.54(7)	O(1)–Mn(3)–O(118)	174.95(8)	O(1)–Mn(3)–N(11)	89.96(8)
O(1)–Mn(3)–N(22)	88.65(8)	O(49)–Mn(3)–O(58)	168.40(7)	O(49)–Mn(3)–O(118)	92.97(8)
O(49)–Mn(3)–N(11)	88.65(8)	O(49)–Mn(3)–N(22)	96.10(8)	O(58)–Mn(3)–O(118)	95.41(8)
O(58)–Mn(3)–N(11)	83.51(8)	O(58)–Mn(3)–N(22)	91.60(8)	O(118)–Mn(3)–N(11)	89.60(9)
O(118)–Mn(3)–N(22)	92.22(8)	N(11)–Mn(3)–N(22)	174.92(9)	Mn(1)–O(1)–Mn(2)	125.59(9)
Mn(1)–O(1)–Mn(3)	116.66(8)	Mn(2)–O(1)–Mn(3)	117.75(9)		

Magnetic Properties. Magnetic susceptibilities were measured as a function of temperature under a 0.1 T applied field in the range 1.8–300 K. In Figures 4.4a and 4.5 the results as plots of $\chi_{\text{M}}T$ vs T are shown for, respectively, the compounds **13–15**. Similar as observed for other trinuclear manganese(III) compounds,^{2-5,12,13,15,16,34} the $\chi_{\text{M}}T$ product is still increasing with temperature near room temperature and the measured $\chi_{\text{M}}T$ values at 300 K are therefore below the high-temperature limit of $9.00 \text{ cm}^3\text{Kmol}^{-1}$ expected for three non-interacting manganese(III) ions. For compounds **13**, **14** and **15**, the $\chi_{\text{M}}T$ values measured at room temperature are $6.68 \text{ cm}^3\text{Kmol}^{-1}$, $6.18 \text{ cm}^3\text{Kmol}^{-1}$, and $6.52 \text{ cm}^3\text{Kmol}^{-1}$, respectively. With decreasing temperatures the $\chi_{\text{M}}T$ value is seen to decrease drastically in all cases. This

behaviour can be attributed to the presence of predominant intramolecular antiferromagnetic interactions (J) between the three manganese(III) ions composing the trinuclear units.³⁵ As a result, the magnetic energy level spectrum of the triangular units spans a wide energy range of the order of 40–70 times the magnetic exchange interaction constants (see Figure 4.6), *i.e.* amounting to a few hundreds Kelvin in thermal energy, even for J/k_B values of a few Kelvin only. As compared to the other two compounds, **13** is exceptional in that the product $\chi_M T$ passes through a minimum of $2.87 \text{ cm}^3 \text{Kmol}^{-1}$ at 30 K, increases up to about $5.26 \text{ cm}^3 \text{Kmol}^{-1}$ at 2.6 K and finally decreases again to $5.05 \text{ cm}^3 \text{Kmol}^{-1}$ at 1.8 K (Figure 4.4a). For compound **14** the $\chi_M T$ product shows a continuous gradual decrease with temperature, reaching a value of $0.67 \text{ cm}^3 \text{Kmol}^{-1}$ at 1.8 K (Figure 4.5a). For compound **15** upon cooling the $\chi_M T$ value likewise decreases continuously down to a value of $1.53 \text{ cm}^3 \text{Kmol}^{-1}$ at 15 K, and then more steeply to $0.41 \text{ cm}^3 \text{Kmol}^{-1}$ at 1.8 K (Figure 4.5b).

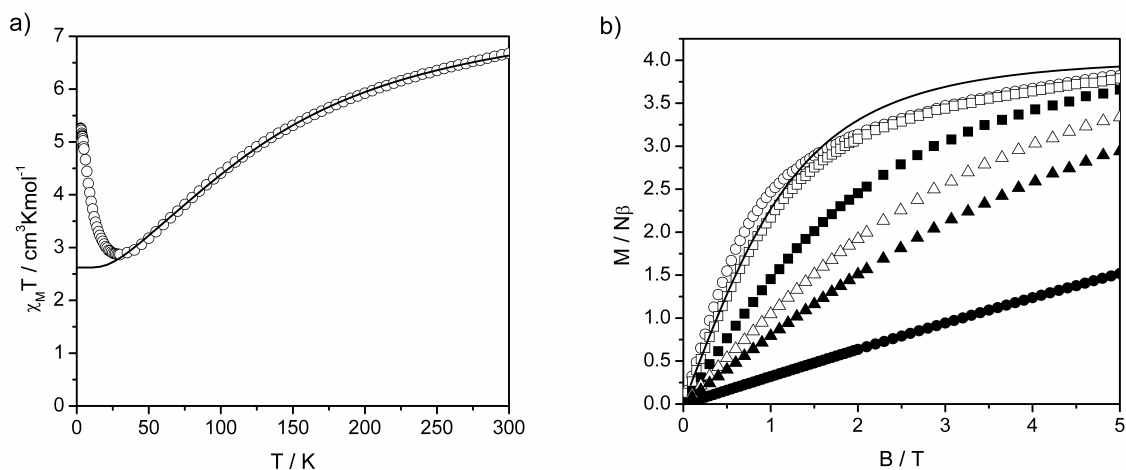


Figure 4.4. a) Plot of $\chi_M T$ vs T for **13** in the range 1.8 to 300 K in 0.1 T applied field with the experimental fit from 50 to 300 K (solid line). b) Field dependence of the magnetization measured at 2 (\circ), 4 (\square), 6 (\blacksquare), 8 (\triangle), 10 (\blacktriangle) and 20 (\bullet) K. The Brillouin function (solid line) is included for one $S = 2$ and $g = 2$ at 2 K.

As will become clear from the theoretical analysis presented below, the upturn of the $\chi_M T$ product in **13** below 30 K is due to a partial ferromagnetic coupling between the manganese(III) moments within the triangular cluster, in combination with a ferromagnetic intermolecular interaction between the trinuclear units along the chains. The latter interaction will be propagated through the hydrogen bonds present between the acetate and the ethanol molecules within the 1-D chain (see Figure 4.2). For compounds **14** and **15** all intracluster interactions turn out to be antiferromagnetic.

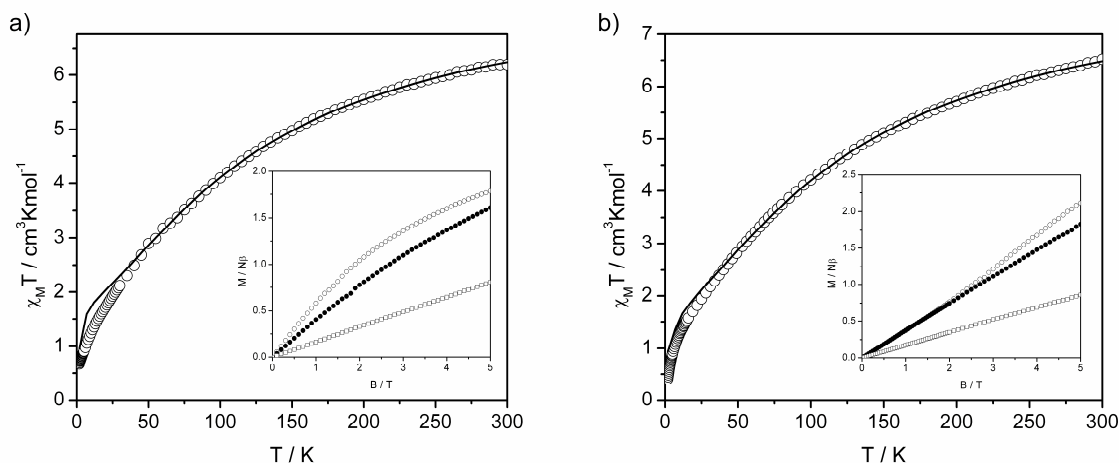


Figure 4.5. Plot of $\chi_M T$ vs T for **14** (a) and **15** (b) in the range 1.8 to 300 K in 0.1 T applied field with the experimental fit (solid line). Inset, field dependence of the magnetization measured at 2 (\circ), 4 (\bullet) and 20 (\square) K.

Field-dependent magnetization studies were carried out at low temperatures for all three materials and are shown in Figure 4.4b and as inserts in Figure 4.5. As can be noted, even at the maximum field of 5 T the values measured for the molar magnetization fall far below the saturation limit of $12 N\beta$, which is appropriate for three non-interacting manganese(III) ions. This observation confirms the above-mentioned large extent in energy of the magnetic energy level spectrum for the trinuclear cluster, compared to which the Zeeman energy of the applied field is very small. Compound **13** is again exceptional in that its $M(B)$ measured at the lowest temperatures shows a fast initial increase, reaching a value of $\approx 3 N\beta$ at about 1 T already, not far below the $4 N\beta$ corresponding to one manganese(III) ion or one third of the saturated moment of the trinuclear unit. This feature again strongly suggests a partial ferromagnetic coupling within the triangle, which should result in a ground state of $S_T = 2$ for the triangular unit, as found previously also for $[\text{Mn}_3(\mu_3\text{-O})(\text{phpzMe})_3(\text{MeOH})_3(\text{O}_2\text{CMe})] \cdot 1.5\text{MeOH}$ (**11**).¹⁶ Indeed, the experimental $M(B)$ curve for **13** at 2 K is very close to the Brillouin function for a single spin $S = 2$ calculated for that temperature, included in Figure 4.4b. At 2 K, the experimental data at lower fields (< 1 T) are slightly above this Brillouin function, indicating the presence of additional ferromagnetic intermolecular interactions, as also mentioned above in connection with the observed upturn in the magnetic susceptibility below 30 K. The behaviour of the magnetization for compounds **14** and **15**, on the other hand, indicate a low-spin magnetic ground state for the triangular units, *i.e.* all intramolecular interactions are apparently antiferromagnetic in these materials.

For a more quantitative analysis of the exchange interactions, the susceptibility data were fitted with the Hamiltonian for an isosceles triangle:

$$\hat{H} = -2[J_2(\hat{S}_1\hat{S}_2) + J_1(\hat{S}_1\hat{S}_3) + J_1(\hat{S}_2\hat{S}_3)] \quad (1)$$

where J_1 represents the Mn(III)–Mn(III) exchange interaction parameter of the two exchange paths with similar Mn···Mn distances and Mn–O_{oxide}–Mn angles, and J_2 refers to the path characterized by the unique Mn–O_{oxide}–Mn angle (Mn(1)–O(1)–Mn(2)). Briefly, the energy levels for the isosceles triangle of spins S are given by:

$$E(S_T, S^*) = -J_1[S_T(S_T+1) - S^*(S^*+1) - S(S+1)] - J_2[S^*(S^*+1) - 2S(S+1)] \quad (2)$$

Here $S^* = S_2 + S_3$ and can take the values $S^* = 2S, 2S-1, \dots, 0$, whereas the total spin $S_T = (S^* + S), (S^* + S - 1), \dots, |S^* - S|$. In Figure 4.6, the so-obtained energy spectrum is plotted as $E(S_T, S^*)/|J_1|$ versus the ratio $r = J_2/J_1$. For some levels the corresponding values for the total spin S_T of the trinuclear compound have been indicated. Note that the diagram shown is for antiferromagnetic (negative) values for J_1 , for ferromagnetic J_1 the diagram has to be inverted.

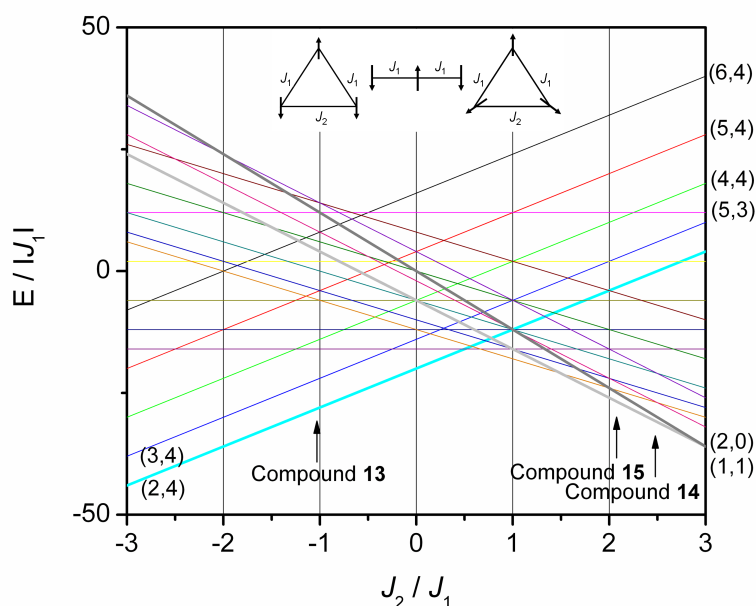


Figure 4.6. Energy levels for an isosceles triangle with $S_1 = S_2 = S_3 = 2$ calculated for $J_1 < 0$. States are labelled as (S_T, S^*) .

When fitting the experimental data to these predictions one should restrict preferably to the temperature range above 50 K, to avoid the complications of intercluster interactions and zero-field manganese(III) splitting (crystal field anisotropy), which may influence the data at lower temperatures and are obviously not taken into account in the model of equation (1). On the basis of the data above 50 K, the best fitting parameters for compound **13** gave $g = 1.87 \pm$

0.03, $J_1 = -(10.3 \pm 0.3) \text{ cm}^{-1}$ and $J_2 = +(10.9 \pm 2.4) \text{ cm}^{-1}$. Furthermore, the best fits of the experimental data above 50 K were $g = 1.88 \pm 0.02$, $J_1 = -(4.2 \pm 0.1) \text{ cm}^{-1}$ and $J_2 = -(10.3 \pm 1.2) \text{ cm}^{-1}$ for compound **14**, and $g = 1.93 \pm 0.02$, $J_1 = -(4.8 \pm 0.1) \text{ cm}^{-1}$ and $J_2 = -(10.2 \pm 1.2) \text{ cm}^{-1}$ for compound **15**. Referring to the magnetic energy level diagram calculated for the isosceles triangle as presented in Figure 4.7, one may note that the ratio $r = J_2/J_1$ equals to about -1.0 for compound **13**. This ratio corresponds indeed with an $S_T = 2$ ground state for the triangle, the nearest excited magnetic level being at a distance of $\approx 6 \text{ cm}^{-1}$ in this case.

For compounds **14** and **15** $r = +2.5$ and $+2.1$ are found, respectively, corresponding to an antiferromagnetic ($S_T = 1$) ground state, as already anticipated above. The solid curves drawn in Figures 4.4a and 4.5 represent the predictions based on the above mentioned intramolecular magnetic exchange constants. For the purely antiferromagnetic compounds **14** and **15** the downward trend with lowering temperature of the predicted $\chi_M T$ curve is closely followed by the experiments over the whole range; the somewhat more rapid decrease of the experimental data at the lowest temperatures ($\leq 15 \text{ K}$) can be attributed to the effects of antiferromagnetic intercluster couplings and zero-field splitting of the manganese(III) levels not considered in the Hamiltonian of equation (1). For compound **13**, on the other hand, the upturn of the experimental data below 30 K from the calculated solid curve (representing purely paramagnetic behaviour for the net spins $S_T = 2$ per cluster), should be ascribed to ferromagnetic intercluster couplings between the spins along the crystallographic chains. AC-susceptibility measurements were carried out on compound **13** in the range 1.8–10 K in zero DC field and at frequencies up to 997 Hz. Although no maximum in the susceptibility is yet in sight, the data do show slight frequency dependence with the appearance of an out-of-phase signal at highest frequencies. This could be interpreted either as signalling the advent of single-chain magnet behaviour or as the approach of a transition to long-range 3-D magnetic order induced by weak inter-chain interactions *e.g.* of dipolar origin. Further studies at lower temperatures ($< 2 \text{ K}$) would be needed to clarify this behaviour.

To summarize, it has been shown that compound **13** presents both ferromagnetic and antiferromagnetic intracluster interactions, whilst only antiferromagnetic intracluster interactions are present in compounds **14** and **15**. As described in Chapter 3,¹⁶ the occurrence of the ferromagnetic interaction in **13** can be attributed to the major distortion of the Mn–O–Mn angle of the $[\text{Mn}_3\text{O}]^{7+}$ triangle, *i.e.* $\text{Mn}(1)\text{–O}(1)\text{–Mn}(2) = 112.65^\circ$. Previous theoretical and experimental studies have shown that the superexchange interaction can change from antiferromagnetic to ferromagnetic when the metal ion–ligand–metal ion angle decreases, with a the critical angle value of around 120° .^{22,36} In compound **13**, the ferromagnetic interaction is stronger than observed previously¹⁶ for

$[\text{Mn}_3(\mu_3\text{-O})(\text{phpzMe})_3(\text{MeOH})_3(\text{O}_2\text{CMe})]\cdot 1.5\text{MeOH}$ (**11**), due to the appreciably shorter Mn–O distances observed in **13** as compared to those in $[\text{Mn}_3(\mu_3\text{-O})(\text{phpzMe})_3(\text{MeOH})_3(\text{O}_2\text{CMe})]\cdot 1.5\text{MeOH}$ (**11**).¹⁶ For compounds **14** and **15**, the deviation of the Mn–O–Mn angle from the value of 120° (corresponding to an equilateral triangle) towards lower values is less pronounced. As a consequence, all intracluster magnetic interactions are antiferromagnetic. Similar behaviour has also been reported previously in related compounds.^{12,13,15,16} However, in the compounds with phenol-pyrazole ligands, the magnetic exchange interaction could be expected to also depend on the geometry of the pyrazolato bridge, as it has been shown that the dihedral angle ($\delta_{\text{pz-bend}}$) of the least-squares plane of the pyrazole ring relative to the M–N(pz)–N(pz)–M plane is also an important factor affecting the magnetic interaction.³⁷ Therefore Table 4.5 contains the structural and magnetic data of the $[\text{Mn}_3\text{O}]^{7+}$ compounds containing phenol-pyrazole derivatives. From this compilation it can be concluded that it is difficult to correlate the magnetic exchange parameters with this structural parameter.

As discussed above, the overall intracluster magnetic interactions are antiferromagnetic in μ_3 -oxide trinuclear manganese(III) compounds with phenol-pyrazole ligands.¹²⁻¹⁶ When the trinuclear units are linked by carboxylate bridges, ferromagnetic interactions emerge between the trinuclear units within the chain,¹⁴⁻¹⁶ whilst antiferromagnetic or ferromagnetic interactions are observed when the trinuclear units are linked by end-to-end azido bridges.^{13,16} In the case of the compound $[\text{Mn}_3(\mu_3\text{-O})(\text{Meppz})_3(\text{EtOH})_4(\text{O}_2\text{CMe})]^{12}$ in which the trinuclear units are bridged by acetate ligands, antiferromagnetic interactions are present. For the one-dimensional chains formed through hydrogen bonds established between the trinuclear units, ferromagnetic intrachain interactions are operative if the separation between the manganese(III) ions that bridge the clusters is smaller than *ca.* 7.4 Å, as it is the case for compound **13**. The intrachain interactions become antiferromagnetic for larger separation between the trinuclear units of *ca.* 8.04 Å, as observed¹⁶ for the compound $[\text{Mn}_3(\mu_3\text{-O})(\text{phpzMe})_3(\text{MeOH})_3(\text{O}_2\text{CMe})]\cdot 1.5\text{MeOH}$ (**11**).

Table 4.5. Selected magnetic and structural data for trinuclear oxide-bridged manganese(III) compounds containing phenol-pyrazole ligands.

Compound	J_1/cm^{-1}	J_2/cm^{-1}	zJ'/cm^{-1}	g	r^b	Mn–O–Mn ^c	$\delta_{\text{pz-bend}}^d$	$\delta_{(\text{MnNNMn})-(\text{MnOMn})}^e$	Ref
[Mn ₃ (μ_3 -O)(ppz) ₃ (MeOH) ₃ (O ₂ CMe)]	-3.01	-3.01	+0.32	1.88	1.0	119.88; 119.15;	2.87; 2.50; 6.98	14.87; 2.07; 13.47	15,16
[Mn ₃ (μ_3 -O)(phpzH) ₃ (MeOH) ₃ (O ₂ CMe)] (10)						119.98			
[Mn ₃ (μ_3 -O)(Meppz) ₃ (MeOH) ₄ (O ₂ CMe)]	-3.21	-3.21	+0.68	1.93	1.0	120.42; 119.41;	3; 3.37; 7.63	2.63; 7.91, 9.96	15
						120.14			
[Mn ₃ (μ_3 -O)(Meppz) ₃ (EtOH) ₄ (O ₂ CMe)]	-1.87	-5.61	-0.014	1.99	3.0	120.43; 118.44;	1.47; 3.60; 3.69	0.86; 6.84; 7.46	12
						121.13			
[Mn ₃ (μ_3 -O)(Brppz) ₃ (MeOH) ₃ (N ₃)]·2MeOH	-3.87	-8.20	-0.07	2.12	2.1	119.91; 119.17;	5.89; 2.30; 4.91	6.82; 18.43; 2.35	13
						119.35			
[Mn ₃ (μ_3 -O)(Brppz) ₃ (MeOH) ₃ (N ₃)]	-4.66	-7.35	-0.30	2.12	1.6	120.33; 118.75;	4.93; 1.47; 4.71	13.02; 14.57; 8.48	13
						120.61			
[Mn ₃ (μ_3 -O)(Brppz) ₃ (MeOH) ₃ (O ₂ CMe)]	-1.58	-5.50	-0.27	2.04	3.5	120.56; 119.18;	8.82; 2.55; 3.66	6.34; 12.50; 9.33	14
						120.20			
[Mn ₃ (μ_3 -O)(Brppz) ₃ (EtOH) ₃ (O ₂ CMe)]	-1.02	-4.39	-0.31	2.02	4.3	120.3; 119.3;	5.25; 6.37; 0.00	5.09; 2.73; 3.73	14
						120.4			
[Mn ₃ (μ_3 -O)(Brppz) ₃ (EtOH) ₃ (O ₂ CMe)]	-0.72	-3.13	-0.18	2.02	4.3	119.54; 120.15;	4.05; 2.76; 3.87	0.37; 7.71; 3.10	14
						120.22			
[Mn ₃ (μ_3 -O)(phpzMe) ₃ (O ₂ CMe)(MeOH) ₃]·1.5MeOH (11)	-7.1	+4.4	-	1.98	-0.6	120.61; 116.10;	11.97; 2.44;	12.57; 40.11;	16
						120.85	24.86	26.02	
[Mn ₃ (μ_3 -O)(phpzH) ₃ (MeOH) ₄ (N ₃)]·MeOH (12)	-6.2	-3.7	-	2.01	0.6	120.79; 118.96;	4.69; 3.59; 7.12	4.51; 4.22; 1.29	16
						120.11			
[Mn ₃ (μ_3 -O)(phpzMe) ₃ (O ₂ CMe)(EtOH)]·EtOH (13)	-10.3	+10.9	-	1.87	-1.0	112.65; 122.73;	6.21; 2.89; 3.90	48.09; 7.31; 10.38	This work
						124.28			
ⁿ Bu ₄ N[Mn ₃ (μ_3 -O)(phpzMe) ₃ (O ₂ CPh) ₂] (14)	-4.2	-10.3	-	1.88	2.5	124.67; 117.91;	2.04; 4.12; 4.57	21.41; 38.51;	This work
						117.35		37.96	
ⁿ Bu ₄ N[Mn ₃ (μ_3 -O)(phpzPh) ₃ (O ₂ CPh) ₂] (15)	-4.8	-10.2	-	1.93	2.1	117.75; 125.58;	3.82; 3.36; 17.00	34.66; 5.13; 33.17	This work
						116.66			

^a H₂phpzH = H₂ppz = 5(3)-(2-hydroxyphenyl)-pyrazole, H₂Meppz = 3-(5-methyl-2-phenolate)-pyrazole, H₂Brppz = 4-bromo-2-(1-H-pyrazol-3-yl)phenol, H₂phpzMe = 3(5)-methyl-5(3)-(2-hydroxyphenyl)pyrazole. ^b $r = J_2/J_1$; ^c Mn– μ_3 –O–Mn angle, Mn(1)–O–Mn(2); Mn(2)–O–Mn(3); Mn(1)–O–Mn(3) respectively; ^d dihedral angle between the pz ring plane and Mn–N(pz)–N(pz)–Mn plane; ^e dihedral angle between the Mn–N(pz)–N(pz)–Mn plane and Mn–O–Mn plane.

4.4. Conclusions

The synthesis, crystal structure and magnetic studies of three new manganese(III) compounds are reported. Compounds **13–15** are trinuclear μ_3 -oxide-bridged manganese(III) compounds containing phenol-pyrazole ligands. Following previous results (Chapter 3),¹⁶ the effect of the solvent or co-ligand and the type of carboxylate ligand were studied in the present work. Compound **13** forms 1-D chains due to the intermolecular hydrogen bonding between the non-coordinated ethanol molecule with the coordinated ethanol and the bridging acetate group, whereas **14** and **15** behave as isolated trinuclear manganese(III) compounds with two bridging benzoate ligands and ${}^n\text{Bu}_4\text{N}^+$ as a counter ion. Compounds **13–15** present overall intramolecular antiferromagnetic interactions between the three manganese(III) ions composing the trinuclear unit. In addition, compound **13** shows a ferromagnetic interaction between two manganese(III) ions in the trinuclear unit that can be ascribed to the most distorted structural path, resulting in a $S_T = 2$. Moreover, ferromagnetic intermolecular interactions along the chain are propagated through the hydrogen bonds.

4.5. References

1. Cannon, R. D.; White, R. P., *Prog. Inorg. Chem.*, **1988**, 36, 195-298.
2. An, J.; Chen, Z. D.; Bian, J. A.; Jin, X. L.; Wang, S. X.; Xu, G. X., *Inorg. Chim. Acta*, **1999**, 287, 82-88.
3. Baca, S. G.; Stoeckli-Evans, H.; Ambrus, C.; Malinovskii, S. T.; Malaestean, I.; Gerbeleu, N.; Decurtins, S., *Polyhedron*, **2006**, 25, 3617-3627.
4. Li, J.; Yang, S. M.; Zhang, F. X.; Tang, Z. X.; Ma, S. L.; Shi, Q. Z.; Wu, Q. J.; Huang, Z. X., *Inorg. Chim. Acta*, **1999**, 294, 109-113.
5. Vincent, J. B.; Chang, H. R.; Folting, K.; Huffman, J. C.; Christou, G.; Hendrickson, D. N., *J. Am. Chem. Soc.*, **1987**, 109, 5703-5711.
6. Wu, R. W.; Poyraz, M.; Sowrey, F. E.; Anson, C. E.; Wocadlo, S.; Powell, A. K.; Jayasooriya, U. A.; Cannon, R. D.; Nakamoto, T.; Katada, M.; Sano, H., *Inorg. Chem.*, **1998**, 37, 1913-1921.
7. Inglis, R.; Jones, L. F.; Karotsis, G.; Parsons, S.; Perlepes, S. P.; Wernsdorfer, W.; Brechin, E. K., *Chem. Commun.*, **2008**, 5924-5926.
8. Inglis, R.; Jones, L. F.; Mason, K.; Collins, A.; Moggach, S. A.; Parsons, S.; Perlepes, S. P.; Wernsdorfer, W.; Brechin, E. K., *Chem.-Eur. J.*, **2008**, 14, 9117-9121.
9. Milios, C. J.; Wood, P. A.; Parsons, S.; Foguet-Albiol, D.; Lampropoulos, C.; Christou, G.; Perlepes, S. P.; Brechin, E. K., *Inorg. Chim. Acta*, **2007**, 360, 3932-3940.
10. Xu, H.-B.; Wang, B.-W.; Pan, F.; Wang, Z.-M.; Gao, S., *Angew. Chem.-Int. Edit.*, **2007**, 46, 7388-7393.
11. Yang, C.-I.; Wernsdorfer, W.; Cheng, K.-H.; Nakano, M.; Lee, G.-H.; H.-L., T., *Inorg. Chem.*, **2008**, 47, 10184-10186.
12. Bai, Y. L.; Tao, J.; Wernsdorfer, W.; Sato, O.; Huang, R. B.; Zheng, L. S., *J. Am. Chem. Soc.*, **2006**, 128, 16428-16429.
13. Liu, C. M.; Zhang, D. Q.; Zhu, D. B., *Chem. Commun.*, **2008**, 368-370.
14. Liu, C. M.; Zhang, D. Q.; Zhu, D. B., *Inorg. Chem.*, **2009**, 48, 4980-4987.
15. Tao, J.; Zhang, Y. Z.; Bai, Y. L.; Sato, O., *Inorg. Chem.*, **2006**, 45, 4877-4879.
16. Viciano-Chumillas, M.; Tanase, S.; Mutikainen, I.; Turpeinen, U.; de Jongh, L. J.; Reedijk, J., *Inorg. Chem.*, **2008**, 47, 5919-5929.

17. Stamatatos, T. C.; Foguet-Albiol, D.; Lee, S. C.; Stoumpos, C. C.; Raptopoulou, C. P.; Terzis, A.; Wernsdorfer, W.; Hill, S. O.; Perlepes, S. P.; Christou, G., *J. Am. Chem. Soc.*, **2007**, 129, 9484-9499.
18. Stamatatos, T. C.; Foguet-Albiol, D.; Stoumpos, C. C.; Raptopoulou, C. P.; Terzis, A.; Wernsdorfer, W.; Perlepes, S. P.; Christou, G., *J. Am. Chem. Soc.*, **2005**, 127, 15380-15381.
19. Stamatatos, T. C.; Foguet-Albiol, D.; Stoumpos, C. C.; Raptopoulou, C. P.; Terzis, A.; Wernsdorfer, W.; Perlepes, S. P.; Christou, G., *Polyhedron*, **2007**, 26, 2165-2168.
20. Lampropoulos, C.; Abboud, K. A.; Stamatatos, T. C.; Christou, G., *Inorg. Chem.*, **2009**, 48, 813-815.
21. Cano, J.; Cauchy, T.; Ruiz, E.; Milios, C. J.; Stoumpos, C. C.; Stamatatos, T. C.; Perlepes, S. P.; Christou, G.; Brechin, E. K., *J. Chem. Soc.-Dalton Trans.*, **2008**, 234-240.
22. Vankalkeren, G.; Schmidt, W. W.; Block, R., *Physica B & C*, **1979**, 97, 315-337.
23. Wemple, M. W.; Tsai, H. L.; Wang, S. Y.; Claude, J. P.; Streib, W. E.; Huffman, J. C.; Hendrickson, D. N.; Christou, G., *Inorg. Chem.*, **1996**, 35, 6437-6449.
24. Addison, A. W.; Burke, P. J., *J. Heterocycl. Chem.*, **1981**, 18, 803-805.
25. Kahn, O., *Molecular Magnetism*. Wiley-VCH: New York, 1993.
26. Sheldrick, G. M. *Program for Empirical Absorption Correction*, University of Göttingen: Göttingen, Germany, 1996.
27. Beurskens, P. T.; Beurskens, G.; Strumpel, M.; Nordman, C. E., in *Patterson and Pattersons*. Glusker, J. P.; Patterson, B. K.; Rossi, M., Eds. Clarendon Press: Oxford: 1987.
28. Duisenberg, A. J. M.; Kroon-Batenburg, L. M. J.; Schreurs, A. M. M., *J. Appl. Crystallogr.*, **2003**, 220-229.
29. Duisenberg, A. J. M. Reflections on area detectors. PhD thesis, Utrecht University, Utrecht, The Netherlands 1998.
30. Beurskens, P. T.; Beurskens, G.; Bosman, W. P.; De Gelder, R.; García-Granda, S.; Gould, R. O.; Israël, R.; Smits, J. M. M.; Smykalla, C. *The DIRDIF96. A computer program system for the crystal structure determination by Patterson methods and direct methods applied to difference structure factors*, Crystallography Laboratory, University of Nijmegen: Nijmegen, The Netherlands, 1996.
31. Sheldrick, G. M. *SHELXS-97: Program for Crystal Structures Determination*, University of Göttingen: Göttingen, Germany, 1997.
32. Sheldrick, G. M. *SHELXL-97: Program for Crystal Structure Refinement*, University of Göttingen: Göttingen, Germany, 1997.
33. Spek, A. L. *PLATON, A Multipurpose Crystallographic Tool*, Utrecht University; The Netherlands, 2003.
34. Zartilas, S.; Moushi, E. E.; Nastopoulos, V.; Boudalis, A. K.; Tasiopoulos, A. J., *Inorg. Chim. Acta*, **2008**, 361, 4100-4106.
35. Martin, R. L., in *New Pathways in Inorganic Chemistry*, Ebsworth, E. A. V.; Maddock, A. G.; Sharpe, A. G., Eds. Cambridge University Press: Cambridge, 1968; pp 175-231.
36. Crawford, V. H.; Richardson, H. W.; Wasson, J. R.; Hodgson, D. J.; Hatfield, W. E., *Inorg. Chem.*, **1976**, 15, 2107-2110.
37. Tanase, S.; Koval, I. A.; Bouwman, E.; de Gelder, R.; Reedijk, J., *Inorg. Chem.*, **2005**, 44, 7860-7861.

Chapter 5

Manganese(III) compounds of high nuclearity*

Three high-nuclearity manganese(III) clusters have been synthesized and characterized: $[\text{Mn}_8(\mu_4\text{-O})_4(\text{phpzH})_8(\text{thf})_4]$ (**16**), $[\text{Mn}_8(\mu_4\text{-O})_4(\text{phpzH})_4(\text{EtOH})_4]\cdot 2\text{EtOH}$ (**17**), and $[\text{Mn}_6(\mu_3\text{-O})_4(\mu_3\text{-Br})_2(\text{HphpzEt})_6(\text{phpzEt})]$ (**18**). Compounds **16** and **17** contain a $[\text{Mn}_8(\mu_4\text{-O}_4)(\text{phpzH})_8]$ core in which antiferromagnetic interactions between the manganese(III) ions are found present. Compound **18** is a hexanuclear manganese(III) cluster in which weak ferromagnetic interactions appear to be operative. The formation and the stability of the cluster cores in relation to the type of phenol-pyrazole ligand and the reaction conditions are discussed.

* Part of this chapter will be submitted for publication.

5.1. Introduction

Polynuclear paramagnetic transition-metal compounds have attracted much attention in the last decades, because of their relevance to bioinorganic chemistry as functional models for the active sites of many metalloproteins¹ and also because of their magnetic properties.^{2,3} The interest in the magnetic properties of these polynuclear compounds derives from their ability to act as molecule-based magnets, exhibiting a remanent magnetic moment below a critical magnetic ordering temperature. Besides the more familiar long-range magnetic ordering into a 3-D magnetic lattice, the magnetic remanence can also appear in the form of a 0-D phenomenon,⁴ with the so-called single-molecule magnet behaviour (SMM),^{2,3} in which the origin of the remanent moment is purely molecular and interesting quantum properties are associated with this type of behaviour. In the search of novel SMM's, numerous polynuclear cluster compounds have been synthesized. Most of them are formed by manganese ions in various oxidation states stabilized by carboxylate and oxime ligands.^{2,5} However, the use of pyrazole ligands to obtain large polymetallic clusters is still under research and the number of polynuclear compounds containing these type of ligands, especially of high-nuclearity remains still low.^{6,7} For most of the polymetallic clusters containing pyrazole ligands reported so far, antiferromagnetic interactions between the metal ions are present.⁶ Only in a few cases, predominant ferromagnetic interactions between the metal ions are found operative.⁸⁻¹² As a result, more efforts should be performed in this direction, not only to obtain novel polymetallic compounds containing new pyrazole-based ligands, but also to obtain molecular-based material with the desired magnetic properties.

A common synthetic approach to obtain new polymetallic clusters is the modification of known molecules by introducing subtle variations, such as suitable bridging ligands, addition of solvents, *etc.* In this way, it is also easier to establish magneto-structural correlations and to modify further the molecule to achieve desired magnetic properties. In our group, an octanuclear manganese(III) compound with the formula $[\text{Mn}_8(\mu_4\text{-O}_4)(\text{phpzMe})_8(\text{thf})_4]$ was reported with the ligand 5(3)-(2-hydroxyphenyl)-3(5)-methylpyrazole, H_2phpzMe .¹³ This octanuclear cluster contains solvent molecules at the periphery. Therefore, the study of the stability of the $[\text{Mn}_8(\mu_4\text{-O}_4)(\text{phpzR})_8]$ core is presented in this chapter with the aim to investigate the effect of different solvents. Furthermore, the replacement of the phenol-pyrazole ligand H_2phpzMe by other derivatives such as H_2phpzH and H_2phpzEt , under similar synthetic conditions was carried out to check whether the metal-core motif remains unperturbed. In this chapter, two new octanuclear manganese(III) compounds with the general formula $[\text{Mn}_8(\mu_4\text{-O})_4(\text{phpzH})_8(\text{S})_4]$ ($\text{S} = \text{thf}$ (**16**) and EtOH (**17**)) and one hexanuclear manganese(III) compound, $[\text{Mn}_6(\mu_3\text{-O})_4(\mu_3\text{-Br})_2(\text{HphpzEt})_6(\text{phpzEt})]$ (**18**) are reported. Temperature dependent magnetic susceptibility studies indicate strong antiferromagnetic

interactions in the octanuclear compounds **16** and **17**, whereas weak ferromagnetic interactions are found operative in the compound **18**.

5.2. Experimental Section

General remarks. Starting materials and the ligand 3(5)-(2-hydroxyphenyl)pyrazole ($H_2\text{phpzH}$) were purchased from Aldrich. All manipulations were performed using materials as received. The ligand 3(5)-(2-hydroxyphenyl)-5(3)-ethylpyrazole ($H_2\text{phpzEt}$) has been synthesized according to the reported procedure.¹⁴

Synthesis

[Mn₈(μ_4 -O)₄(phpzH)₈(thf)₄] (16). The reaction of $\text{Mn}(\text{ClO}_4)_2 \cdot 6\text{H}_2\text{O}$ (102 mg, 0.28 mmol) in tetrahydrofuran (THF) with $H_2\text{phpzH}$ (91 mg, 0.56 mmol) in THF in the presence of triethylamine (1.12 mmol) affords a dark brown solid (53 mg, 0.026 mmol). Yield: 74%. Slow evaporation of the reaction mixture affords brown crystals (**16a**). The poor quality of the crystal (**16a**) reveals a missing tetrahydrofuran molecule being the formula $[\text{Mn}_8(\mu_4\text{-O})_4(\text{phpzH})_8(\text{thf})_3]$. Anal. Calcd for **16** ($\text{C}_{88}\text{H}_{80}\text{Mn}_8\text{N}_{16}\text{O}_{16}$): C, 51.38; H, 3.92; N, 10.89. Found: C, 51.92; H, 4.51; N, 10.60. IR ($\nu_{\text{max}}/\text{cm}^{-1}$): 1600(m), 1564(m), 1477(vs), 1456(s), 1436(m), 1340(m), 1295(s), 1234(s), 1136(s), 1080(s), 1036(m), 980(m), 860(s), 845(s), 753(vs), 668(vs), 648(s), 623(vs), 584(vs), 563(vs), 443(vs).

[Mn₈(μ_4 -O)₄(phpzH)₄(EtOH)₄]·2EtOH (17). The reaction of $\text{Mn}(\text{ClO}_4)_2 \cdot 4\text{H}_2\text{O}$ (102 mg, 0.28 mmol) in ethanol with a solution of $H_2\text{phpzH}$ (90 mg, 0.56 mmol) and triethylamine (1.12 mmol) in ethanol provides brown crystals (28 mg, 0.015 mmol) that were collected by filtration, washed with Et_2O and dried in vacuum. Compound **17** was found to exchange the ethanol terminal ligands by water molecules upon air exposure to form $[\text{Mn}_8(\mu_4\text{-O})_4(\text{phpzH})_4(\text{H}_2\text{O})_4] \cdot \text{H}_2\text{O}$ (**17a**). Yield: 43%. Anal. Calcd for **17a** ($\text{C}_{72}\text{H}_{58}\text{Mn}_8\text{N}_{16}\text{O}_{17}$): C, 46.52; H, 3.12; N, 12.06. Found: C, 46.79; H, 2.85; N, 11.98. IR ($\nu_{\text{max}}/\text{cm}^{-1}$): 3054(vw), 2988(vw), 1600(s), 1564(m), 1558(m), 1516(m), 1480(vs), 1456(s), 1436(s), 1338(s), 1293(s), 1249(s), 1232(vs), 1216(s), 1133(vs), 1079(s), 1036(m), 980(m), 943(w), 862(s), 844(s), 782(m), 747(vs), 677(vs), 668(vs), 650(s), 618(vs), 586(vs), 561(vs), 436(s), 384(s), 358(s), 328(s), 306(s).

[Mn₆(μ_3 -O)₄(μ_3 -Br)₂(HphpzEt)₆(phpzEt)] (18). The reaction of $\text{MnBr}_2 \cdot 4\text{H}_2\text{O}$ (86 mg, 0.3 mmol) with $H_2\text{phpzEt}$ (56 mg, 0.3 mmol) in the presence of triethylamine (0.6 mmol) in CH_3CN , resulted in the formation of a dark brown crystalline precipitate (49 mg, 0.026 mmol). Yield: 53%. Crystals suitable for X-ray crystallography were obtained by diffusion of hexane into a dichloromethane solution of **18**. Anal. Calcd for $[\text{Mn}_6(\mu_3\text{-O})_4(\mu_3\text{-}$

$\text{Br}_2(\text{HphpzEt})_6(\text{phpzEt})$ (**18**) ($\text{C}_{77}\text{H}_{76}\text{Br}_2\text{Mn}_6\text{N}_{14}\text{O}_{11}$): C 49.64, H 4.11, N 10.53. Found: C 49.29, H 4.27, N 10.7. IR ($\nu_{\text{max}}/\text{cm}^{-1}$): 3242(w), 2972(w), 1600(s), 1568(m), 1558(s), 1532(w), 1506(w), 1480(s), 1464(s), 1448(vs), 1409(w), 1337(m), 1306(s), 1282(s), 1268(s), 1250(vs), 1194(w), 1120(vs), 1053(w), 1036(m), 990(m), 934(w), 860(s), 805(m), 748(vs), 712(s), 668(vs), 614(s), 586(s), 565(s), 442(w), 424(w), 415(w), 384(w), 366(m), 352(w), 311(w).

Physical Measurements. Elemental analyses for C, H and N were performed on a Perkin-Elmer 2400 series II analyzer. Infrared spectra ($4000\text{--}300\text{ cm}^{-1}$) were recorded on a Perkin-Elmer Paragon 1000 FTIR spectrometer equipped with a Golden Gate ATR device, using the reflectance technique. Thermogravimetric analysis was carried out on a Mettler Toledo TGS/SDTA851e in the temperature range 25 to 250 °C. DC and AC magnetic data were recorded using a Quantum Design MPMS-5 SQUID susceptometer. The magnetic susceptibilities were measured from 1.8 to 300 K on polycrystalline samples in a gelatine capsule with an applied field of 0.1 T. The magnetization was measured from 2 up to 20 K in the 0–5 T range. Data were corrected for magnetization of the sample holder and for diamagnetic contributions, which were estimated from Pascal's constants.⁴

X-ray Crystallography. Intensity data for single crystals of **16a**, **17** and **18** were collected using MoK α radiation ($\lambda = 0.71073\text{ \AA}$) on a Nonius KappaCCD diffractometer. Crystal and refinement data for **16** is collected in Appendix B, whereas for **17** and **18** are collected in Table 5.1. The intensity data were corrected for Lorentz and polarization effects, and for absorption (multiscan absorption correction¹⁵). The structures were solved by Patterson methods.¹⁶ The programs EvalCCD,^{17,18} DIRDIF96,¹⁹ SHELXS-97²⁰ and SHELXL-97²¹ were used for data reduction, structure solution and refinement, respectively. All non-hydrogen atoms were refined with anisotropic displacement parameters. Compound **18** contains disordered solvent molecules, being three CH_2Cl_2 each with population 0.5 and eight water molecules with population parameters from 0.5 to 0.3333. Geometric calculations and molecular graphics were performed with the PLATON package.²²

Table 5.1. Crystal data and structure refinements for $[\text{Mn}_8(\mu_4\text{-O})_4(\text{phpzH})_4(\text{EtOH})_4]\cdot 2\text{EtOH}$ (**17**), $[\text{Mn}_6(\mu_3\text{-O})_4(\mu_3\text{-Br})_2(\text{HphpzEt})_6(\text{phpzEt})]$ (**18**).

	17	18
Formula	$\text{C}_{80}\text{H}_{72}\text{Mn}_8\text{N}_{16}\text{O}_{16},$ $2(\text{C}_2\text{H}_6\text{O})$	$\text{C}_{77}\text{H}_{76}\text{Br}_2\text{Mn}_6\text{N}_{14}\text{O}_{11},$ $0.5(\text{CH}_2\text{Cl}_2\text{O}), \text{CH}_2\text{Cl}_2\text{O}_3$
Formula weight [g mol^{-1}]	2045.20	2046.19
Crystal system	Triclinic	Monoclinic
Space group	P-1	P2 ₁ /c
<i>a</i> [Å]	15.284(3)	14.589(2)
<i>b</i> [Å]	15.918(3)	28.014(4)
<i>c</i> [Å]	18.924(3)	24.429(4)
α [°]	82.82(3)	90
β [°]	69.50(3)	103.478(16)
γ [°]	84.94(3)	90
<i>V</i> [Å ³]	4273.8(16)	9709(3)
<i>Z</i>	2	4
<i>D</i> _{calc} [g cm^{-3}]	1.589	1.400
Crystal size	0.04×0.08×0.20	0.05×0.15×0.18
Number of collected reflections (unique)	60496 (16578)	133876(19030)
Number of observed reflections [$I_0 > 2\sigma(I_0)$]	11208	13305
Internal R factor	0.068	0.065
Number of parameters	1173	1120
Goodness-of-fit <i>S</i> on <i>F</i> ²	1.06	1.09
Largest peak and hole in final difference Fourier map [e Å^{-3}]	0.67 and -0.75	1.26 and -0.50
μ [mm^{-1}]	1.220	1.724
R_1 ^[a] [$I > 2.0\sigma(I)$]	0.0463	0.0580
wR_2 ^[b] [all data]	0.1011	0.1595
<i>T</i> [°C]	173	173

^[a] $R_1 = \sum ||F_o| - |F_c|| / \sum |F_o|$. ^[b] $wR_2 = \{ \sum [w(F_o^2 - F_c^2)^2] / \sum w(F_o^2)^2 \}^{1/2}$.

5.3. Results and Discussion

Syntheses. The reaction of $\text{Mn}(\text{ClO}_4)_2 \cdot 6\text{H}_2\text{O}$ with H_2phpzH in tetrahydrofuran in the ratio 1 to 2 or 1 to 1 and in the presence of triethylamine as base yielded the compound **16**, which is of similar geometry as the cluster $[\text{Mn}_8(\mu_4\text{-O})_4(\text{phpzMe})_8(\text{thf})_4]$ reported previously.¹³ The same reaction in ethanol affords compound **17**. As is shown in this chapter, these octanuclear manganese(III) compounds contain a stable core, where the main difference arises from the different solvent used in the reaction. The addition of an excess of triethylamine to a solution of mononuclear compounds with the general formula $[\text{Mn}(\text{HphpzR})_2\text{X}]$ ($\text{R} = \text{H}, \text{Me}, \text{X}^- = \text{Cl}^-, \text{Br}^-$) (Chapter 2) affords also complexes containing

the core $[\text{Mn}_8(\mu_4\text{-O})_4(\text{phpzR})_8]$. The formation of the octanuclear compounds $[\text{Mn}_8(\mu_4\text{-O})_4(\text{phpzR})_8]$ ($\text{R} = \text{H}, \text{Me}$) can be avoided with the use of more hindered ligands such as H_2phpzEt . For example the hexanuclear compound **18** is formed in the presence of triethylamine as base and acetonitrile as solvent. The amount of base is paramount, since it leads to the formation of mononuclear manganese(III) complexes (see Chapter 2),²³ or higher nuclearity manganese(III) complexes, such compounds **16–18**, presented in this chapter.

Repeated elemental analyses of compound **17** show that the solvent molecules are substituted by water molecules upon air exposure to form $[\text{Mn}_8(\mu_4\text{-O})_4(\text{phpzH})_8(\text{H}_2\text{O})_4]\cdot\text{H}_2\text{O}$ (**17a**). Thermogravimetric analysis (TGA) of **17a** was performed by heating up the sample to 250 °C; a mass loss of *ca.* 5% has been observed, in agreement with the presence of five water molecules.

Description of the Molecular Structures. Crystal and refinement data are shown in Table 5.1 for compounds **17** and **18** and in Table B.1 (Appendix B) for compound **16a**. Compounds **16a** and **17** crystallize in the triclinic space group P-1. Both structures comprise eight manganese(III) ions, four of them are bound through oxide ligand bridges in a distorted cubane geometry, as shown in Figure 5.1 for compound **17**. The other four manganese(III) ions are at the periphery with eight doubly deprotonated phpzH^{2-} ligands and solvent molecules, tetrahydrofuran and ethanol for compound **16a** and **17**, respectively. Compound **16a** contains only three tetrahydrofuran molecules, as shown in Appendix B. The relatively poor quality of the crystal of compound **16** reveals a missing tetrahydrofuran molecule, considering the elemental analysis performed and the analogy with the related cluster $[\text{Mn}_8(\mu_4\text{-O})_4(\text{phpzMe})_8(\text{thf})_4]$, reported previously.¹³ More detailed crystallographic details for compounds **16a–18** are given in Appendix B. Compound **17**, $[\text{Mn}_8(\mu_4\text{-O})_4(\text{phpzH})_8(\text{EtOH})_4]\cdot 2\text{EtOH}$, contains four coordinated ethanol molecules and two ethanol molecules of crystallization, stabilized by hydrogen bonding interactions (Figure 5.1a). The $\text{Mn}-\text{O}_{\text{solvent}}$ distances are larger in **17** (av. 2.33 Å) than in **16a** (av. 2.28 Å). As a result of the weak $\text{Mn}-\text{O}_{\text{solvent}}$ bonds in **17**, the crystallinity is partially lost, upon removing the crystals from the mother liquid, as confirmed by the elemental analysis and the TGA analysis. The closest $\text{Mn}\cdots\text{Mn}$ bond distances are in the range of 3.175–3.434 Å and 3.221–3.463 Å for compounds **16a** and **17**, respectively. Selected angles for the compound $[\text{Mn}_8(\mu_4\text{-O})_4(\text{phpzH})_8(\text{EtOH})_4]\cdot 2\text{EtOH}$ (**17**) are shown in Table 5.2. The Jahn-Teller axes involve the solvent molecules (tetrahydrofuran or ethanol) coordinated to the peripheral manganese(III) ions. Considering the distortion of compounds **16a** and **17**, the Jahn-Teller axes are arranged in two main directions that are “perpendicular” to each other, with the same

number of Jahn-Teller axes in the “same direction” for the manganese(III) ions that are at the periphery and in the cubane core (Figure 5.1b (**17**) and Figure B.1b (**16a**)). In compound **17**, hydrogen bonding is present between the lattice ethanol molecules and the coordinated ethanol molecules (Table B.4 in Appendix B).

Table 5.2. Selected angles ($^{\circ}$) for the compound $[\text{Mn}_8(\mu_4\text{-O})_4(\text{phpzH})_8(\text{EtOH})_4]\cdot 2\text{EtOH}$ (**17**).

Bond Angles					
Mn(1)–O(1)–Mn(2)	125.19(14)	Mn(1)–O(1)–Mn(3)	119.49(15)	Mn(1)–O(1)–Mn(4)	96.89(10)
Mn(2)–O(1)–Mn(3)	115.21(13)	Mn(2)–O(1)–Mn(4)	87.64(10)	Mn(3)–O(1)–Mn(4)	88.32(10)
Mn(2)–O(2)–Mn(4)	86.29(10)	Mn(2)–O(2)–Mn(7)	95.61(11)	Mn(2)–O(2)–Mn(8)	86.71(10)
Mn(4)–O(2)–Mn(7)	123.32(14)	Mn(4)–O(2)–Mn(8)	115.33(14)	Mn(7)–O(2)–Mn(8)	121.33(14)
Mn(3)–O(3)–Mn(4)	115.51(13)	Mn(3)–O(3)–Mn(5)	123.62(14)	Mn(3)–O(3)–Mn(8)	87.78(10)
Mn(4)–O(3)–Mn(5)	120.74(14)	Mn(4)–O(3)–Mn(8)	89.36(11)	Mn(5)–O(3)–Mn(8)	95.99(10)
Mn(2)–O(4)–Mn(3)	87.49(10)	Mn(2)–O(4)–Mn(6)	120.41(13)	Mn(2)–O(4)–Mn(8)	115.27(12)
Mn(3)–O(4)–Mn(6)	93.92(11)	Mn(3)–O(4)–Mn(8)	87.08(10)	Mn(6)–O(4)–Mn(8)	124.30(13)

Table 5.3. Selected bond lengths (\AA) and angles ($^{\circ}$) for the complex $[\text{Mn}_6(\mu_3\text{-O})_4(\mu_3\text{-Br})_2(\text{HphpzEt})_6(\text{phpzEt})]$ (**18**).

Bond Lengths					
Mn(1)–O(2)	1.876(3)	Mn(1)–O(1)	1.901(3)	Mn(1)–Br(1)	2.7488(10)
Mn(1)–Br(2)	3.0076(10)	Mn(2)–O(3)	1.878(3)	Mn(2)–O(1)	1.924(3)
Mn(2)–Br(2)	2.814(4)	Mn(3)–O(3)	1.863(3)	Mn(3)–O(2)	1.905(3)
Mn(3)–Br(2)	2.7353(11)	Mn(3)–O(612)	2.577(3)	Mn(4)–O(1)	1.898(3)
Mn(4)–O(4)	1.903(3)	Mn(4)–N(52)	2.260(4)	Mn(4)–Br(1)	2.9014(11)
Mn(5)–O(4)	1.901(3)	Mn(5)–O(612)	1.994(3)	Mn(5)–O(3)	2.158(3)
Mn(5)–N(61)	2.221(4)	Mn(6)–O(2)	1.910(3)	Mn(6)–O(4)	1.916(3)
Mn(6)–Br(1)	2.8517(11)	Mn(6)–O(612)	2.294(3)	Mn(1)⋯Mn(2)	3.250
Mn(1)⋯Mn(4)	3.239	Mn(1)⋯Mn(6)	3.228	Mn(2)⋯Mn(3)	3.171
Mn(2)⋯Mn(4)	3.225	Mn(2)⋯Mn(5)	3.470	Mn(3)⋯Mn(5)	3.288
Mn(3)⋯Mn(6)	3.221	Mn(5)⋯Mn(6)	3.057		
Bond Angles					
Mn(1)–Br(1)–Mn(4)	69.90(3)	Mn(1)–Br(1)–Mn(6)	70.37(3)	Mn(4)–Br(1)–Mn(6)	70.13(3)
Mn(2)–Br(2)–Mn(3)	70.92(3)	Mn(1)–O(1)–Mn(2)	116.37(16)	Mn(1)–O(1)–Mn(4)	117.01(16)
Mn(2)–O(1)–Mn(4)	115.07(17)	Mn(1)–O(2)–Mn(3)	118.19(17)	Mn(1)–O(2)–Mn(6)	117.01(16)
Mn(3)–O(2)–Mn(6)	115.21(17)	Mn(2)–O(3)–Mn(3)	115.89(18)	Mn(2)–O(3)–Mn(5)	118.40(16)
Mn(3)–O(3)–Mn(5)	109.49(15)	Mn(4)–O(4)–Mn(5)	122.04(17)	Mn(4)–O(4)–Mn(6)	119.87(18)
Mn(5)–O(4)–Mn(6)	106.46(15)				

Compound **18** crystallizes in the monoclinic space group $P2_1/c$. As shown in Figure 5.2, **18** consists of a hexanuclear manganese(III) compound with a $[\text{Mn}_6(\mu_3\text{-O})_4(\mu_3\text{-Br})_2]^{8+}$ core. At the periphery, six HphpzEt^- ligands are present in a bidentate chelating mode and one phpzEt^{2-} ligand is bridging two manganese(III) ions, Mn(4) and Mn(5). The $[\text{Mn}_6(\mu_3\text{-O})_4(\mu_3\text{-Br})_2]^{8+}$ core can be described as an octahedron in which the manganese(III) ions are in the vertices (Figure 5.2b). Mn(2), Mn(3), Mn(4) and Mn(6) form the equatorial plane of the octahedron, whereas Mn(1) and Mn(5) are at the axial positions. Another possible description for **18** is as an inverted adamantane, $[\text{Mn}_6\text{O}_4]$, since the Mn/O ratio is inverted with regard to the commonly observed value for the adamantane subunit, $[\text{Mn}_4\text{O}_6]$.²⁴ The octahedron is comprised of four faces in which the manganese(III) ions are bridged by μ_3 -oxide ligands, two faces are bridged by the μ_3 -bromide ligand, one face is bridged by a μ -phenolato oxygen of one of the HphpzEt^- ligand and one face contains a phpzEt^{2-} ligand, in which the pyrazolato ligand bridges Mn(4) and Mn(5). Selected bond distances and angles are listed in Table 5.3 and more detailed crystallographic information is provided in Appendix B. The Mn–Br bond lengths are in the range of 2.731–3.008 Å. The manganese(III) ions are in an very distorted octahedral geometry. The Jahn-Teller distortion involves the bromide ions, except for Mn(5), which is formed by O(3)–Mn(5)–N(61), where O(3) is a μ_3 -oxide ligand and N(61) is a nitrogen from the pyrazole ring of the HphpzEt^- ligand. The angles spanned by the atoms that form the Jahn-Teller axes have values ranging between 154.42–167.87° (Figure 5.2b). The Mn–O_{eq} distances are in the range of 1.863 to 1.994 Å, whereas the Mn–N_{eq} distances are between 1.975–2.035 Å. The smallest intercluster distance is 8.182 Å. Disordered dichloromethane and water molecules are present in the crystal lattice as a result of the recrystallization process of compound **18**.

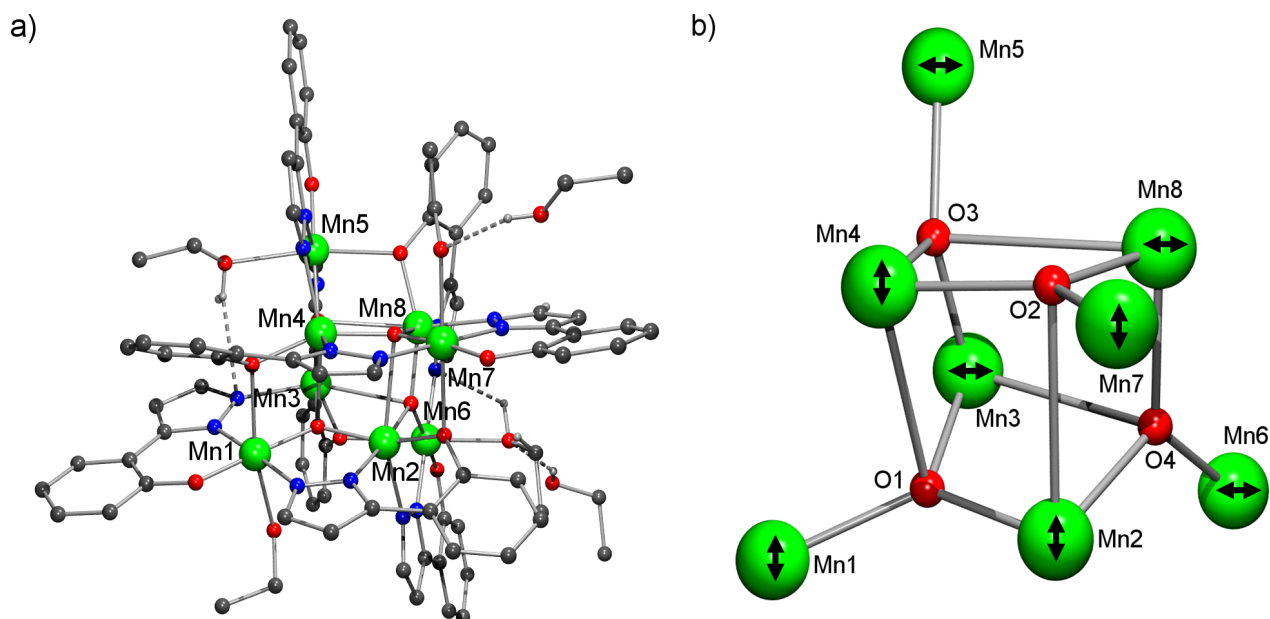


Figure 5.1. a) Pluton projection of the compound $[\text{Mn}_8(\mu_4\text{-O})_4(\text{phpzH})_8(\text{EtOH})_4]\cdot 2\text{EtOH}$ (**17**). b) The $[\text{Mn}_8(\mu_4\text{-O})_4]^{16+}$ core of **17** showing the Jahn-Teller axes (\leftrightarrow). Hydrogen atoms that are not involved in hydrogen bonding interactions are omitted for clarity. Colour code: green, manganese; blue, nitrogen; red, oxygen; grey, carbon.

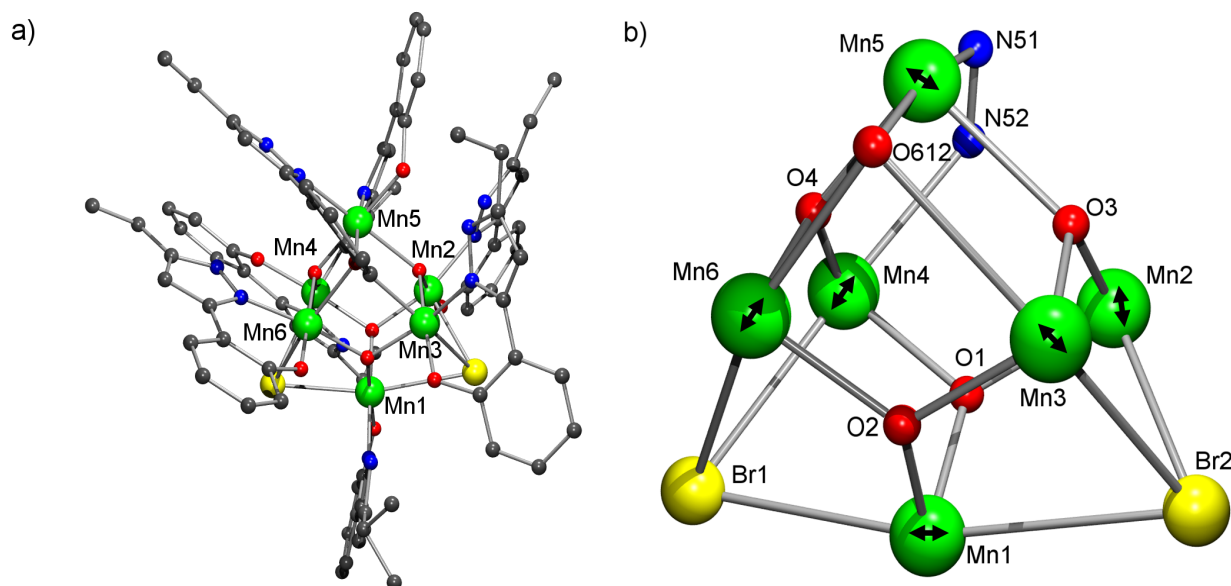


Figure 5.2. a) Pluton projection of the compound $[\text{Mn}_6(\mu_3\text{-O})_4(\mu_3\text{-Br})_2(\text{HphpzEt})_6(\text{phpzEt})]$ (**18**). b) The $[\text{Mn}_6(\mu_3\text{-O})_4(\mu_3\text{-O}(\text{phpzEt}))(\mu_3\text{-Br})_2]^{8+}$ core of **18**, showing the Mn_6 octahedral geometry and the Jahn-Teller axes (\leftrightarrow). Hydrogen atoms are omitted for clarity. Colour code: green, manganese; yellow, bromide; blue, nitrogen; red, oxygen; grey, carbon.

Magnetic properties. Magnetic susceptibilities were measured for compounds **16–18** as a function of temperature under a 0.1 T applied field in the range 1.8–300 K. The $\chi_M T$ product at 300 K amounts to 19.49 cm³mol⁻¹K and 19.45 cm³mol⁻¹K for compounds **16** and **17a**, respectively (as shown in Figure 5.3a). These values are substantially lower than as expected for eight non-interacting manganese(III) ions with $g = 2.00$ (24 cm³mol⁻¹K), which indicates the presence of strong antiferromagnetic interactions between the eight manganese(III) ions even at room temperature. Indeed, the $\chi_M T$ value gradually decreases to 0.37 cm³mol⁻¹K at 2 K and 1.04 cm³mol⁻¹K at 4.3 K for compounds **16** and **17a**, respectively, suggesting a ground state $S_T = 0$ with low-lying excited levels. In fact, the χ_M curve presents a maximum at *ca.* 29 K for both compounds. Field dependence of the magnetization was measured at 2 K (Figure 5.3b). The values at 5 T are 1.82 and 2.08 N β for compounds **16** and **17a**, respectively. In both cases, the values are far below the saturation limit of 32 N β for eight non-interacting manganese(III) ions, confirming the presence of strong antiferromagnetic interactions between the manganese(III) ions. Compounds **16a** and **17** contain four manganese(III) ions in a distorted cubane core, [Mn₄O₄] and four manganese(III) ions in the periphery. Because of the low symmetry of the cluster geometry, it is not possible to apply the Kambe vector-coupling method to evaluate the magnetic exchange interactions. Although several other octanuclear manganese(III) compounds have been reported in the literature,^{24,34} none of them contains the same structural topology. One type of octanuclear manganese(III) compounds consists of two linked tetranuclear subunits,^{27,28,30,31,34} in which antiferromagnetic interactions between the manganese(III) ions in the subunits are observed and rather weak antiferromagnetic interactions between these subunits are found.^{27,28,31,34} In other compounds with different topologies, antiferromagnetic interactions resulting in a high-spin ground state,²⁵ or even ferromagnetic interactions are seen between the manganese(III) ions.^{24,26,32,33} In most of these reported compounds, the magnetic exchange interactions can be modelled on the basis of the alignment of the Jahn-Teller axes and the spin frustration present in the [Mn₄O₂]⁸⁺ butterfly core.^{24-29,31-34} On the other hand, an iron(III) compound has been reported with the same core structure as observed here for compounds **16a** and **17**, in which strong antiferromagnetic interactions are found present between the iron(III) ions in the cubane core with those in the periphery.³⁵ In compounds **16a** and **17**, the Jahn-Teller axes are in two main directions that are nearly perpendicular to each other, considering the distortion of the cubane core (Figures 5.1b and B.1b in Appendix B). From this point of view, the number of Jahn-Teller axes in the same direction is equal for the manganese(III) ions in the cubane core and for those at the periphery. In addition, the manganese(III) ions in the periphery form two large Mn–O–Mn angles of values in the range of 119–125° and one

Mn–O–Mn angle around 96° with the manganese(III) ions in the core (see Table 5.2). The strength and the sign of the magnetic exchange interaction is known to be dependent on the metal–ligand–metal angle, with strongest antiferromagnetic interactions when the metal–ligand–metal angle has a value of about 180° and weak ferromagnetic interactions at angles around 90° .³⁶ In compounds **16a** and **17**, the values of the Mn–O–Mn angles are appreciable larger than 90° , therefore a strong antiferromagnetic interactions are expected between the manganese(III) ions. Also, the directions of the Jahn-Teller axes favours the antiferromagnetic interactions, since the spins can cancel each other and no spin canting is involved.⁴

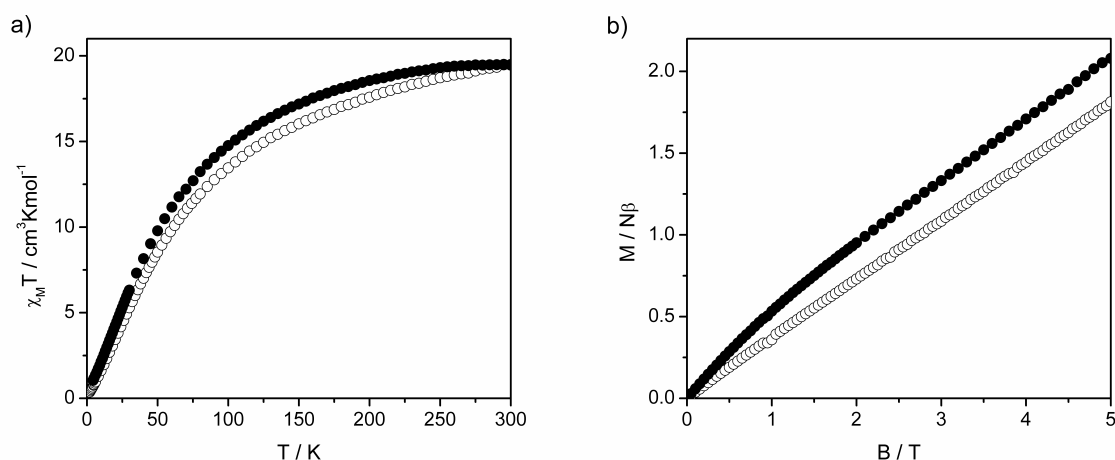


Figure 5.3. Magnetic data for $[\text{Mn}_8(\mu_4\text{-O})_4(\text{phpzH})_4(\text{thf})_4]$ (**16**) (○) and $[\text{Mn}_8(\mu_4\text{-O})_4(\text{phpzH})_4]\cdot 5\text{H}_2\text{O}$ (**17a**) (●). a) Plot of $\chi_{\text{M}}T$ vs T in the range 4 to 300 K in 0.1 T applied field. b) Field dependence of the magnetization at 2 K.

For compound **18**, the $\chi_{\text{M}}T$ value of approximately $20.13 \text{ cm}^3\text{Kmol}^{-1}$ at 300 K is higher than $18 \text{ cm}^3\text{Kmol}^{-1}$, the value expected for six non-interacting manganese(III) ions (Figure 5.4a). When lowering the temperature, the $\chi_{\text{M}}T$ value increases gradually to about $27 \text{ cm}^3\text{Kmol}^{-1}$ at 16 K, then raises more steeply to about $30 \text{ cm}^3\text{Kmol}^{-1}$ at 2.7 K, followed by a final decrease that can be attributed to zero-field splitting and/or weak intermolecular interactions. The initial increase of the $\chi_{\text{M}}T$ curve is attributed to the presence of predominant ferromagnetic interactions between the manganese(III) ions. The values reached by $\chi_{\text{M}}T$ below 20 K are close to the value of $28 \text{ cm}^3\text{Kmol}^{-1}$ corresponding to a ground state of $S_{\text{T}} = 7$ with $g = 2$. The magnetic susceptibility data above 100 K were fitted to the Curie-Weiss law, with $C = 18.85 \text{ cm}^3\text{Kmol}^{-1}$ and $\theta = +18.65 \text{ K}$. The Curie constant C is in agreement with six paramagnetic manganese(III) ions with $S = 2$ and $g = 2.04$, while the positive value of the Curie-Weiss temperature θ indicates dominant albeit weak ferromagnetic interactions. From

the mean-field equation, $\theta = 2zJ_{\text{eff}}S(S+1)/3$, the effective intracuster magnetic interaction is estimated at $J_{\text{eff}} \approx 1.16$ K, assuming a number $z = 4$ of nearest neighbours in view of the molecular structure described above.

Field dependent magnetization studies were carried out below 20 K. The molar magnetization of compound **18** reaches a value of about $12 N\beta$ at 5 T at 2 K as shown in Figure 5.4b. For six non-interacting manganese(III) ions the saturation value should be $24 N\beta$. The magnetization at 2 K shows an initial fast increase, reaching a value of $10 N\beta$ at 1 T, not far below the $14 N\beta$ corresponding to $S_T = 7$, *i.e.* to the net cluster spin indicated by the χ_{MT} product at lowest temperature. This value of $14 N\beta$ is also obviously still far below the saturation limit of $24 N\beta$. These results can be understood in terms of the weakness of the exchange interactions in combination with the strong crystal field anisotropy of the manganese(III) ions. When the intramolecular magnetic interactions are weak, the direction of the moments of the manganese(III) ions in the cluster will be dictated by their local site symmetry rather than by the magnetic exchange, *i.e.* the direction of each moment will be (at least to large extent) along its individual local Jahn-Teller axis. Since the Jahn-Teller axes for the different sites are at large angles to one another, this results in a canted magnetic structure for this cluster yielding an apparent effective net moment of about $S_T = 7 N\beta$. Since the interactions are ferromagnetic; this net moment is relatively easily saturated in a field of few Tesla, where after the remaining magnetic response in higher fields will be due to the sum of the magnetic responses of the individual manganese(III) ions. For higher fields therefore, the Zeeman energy of the applied field is just competing with the single-ion anisotropy energy of the individual ions. Unfortunately, the field range needed to align the moments completely parallel to the field is not attained in the experiment. Indeed, as shown in Figure 5.4b, in the range 10–20 K the experimental $M(B)$ curves are rather close to the predictions from the Brillouin function for a single spin $S_T = 7$ at the same temperatures (solid lines). Below about 12 K the experiments fall increasingly below these predictions, which can be attributed to the single-ion anisotropy. To substantiate these assumptions, a very rough estimation of the (average) anisotropy can be obtained by adding an anisotropic field ($g\beta B_A = 2DS$) to the applied field in the argument of the Brillouin function resulting in the dashed line for $T = 2$ K. This clearly gives a closer fit to the experiment and yields an estimated D value of -4 cm^{-1} , which is in the range commonly observed for other manganese(III) ions in low site symmetry.³⁷ The corresponding anisotropy is obtained as $B_A \approx 12$ T, far above our experimental limit. Obviously, since powder data are involved, this result can only be interpreted as a qualitative explanation of the experiment.

AC magnetic susceptibility measurements were carried out in the range 2–10 K in zero DC field at different frequencies (1–10³ Hz) and in varying DC fields (0–0.1 T) at a frequency of 99 Hz. No maximum in the susceptibility was detected down to 2 K, the susceptibility keeps increasing continuously down to the lowest temperature with no clear indication of a dependence on frequency or applied DC field. Apparently, the magnetic interactions are too weak to lead to single-molecule magnetic behaviour above 2 K.

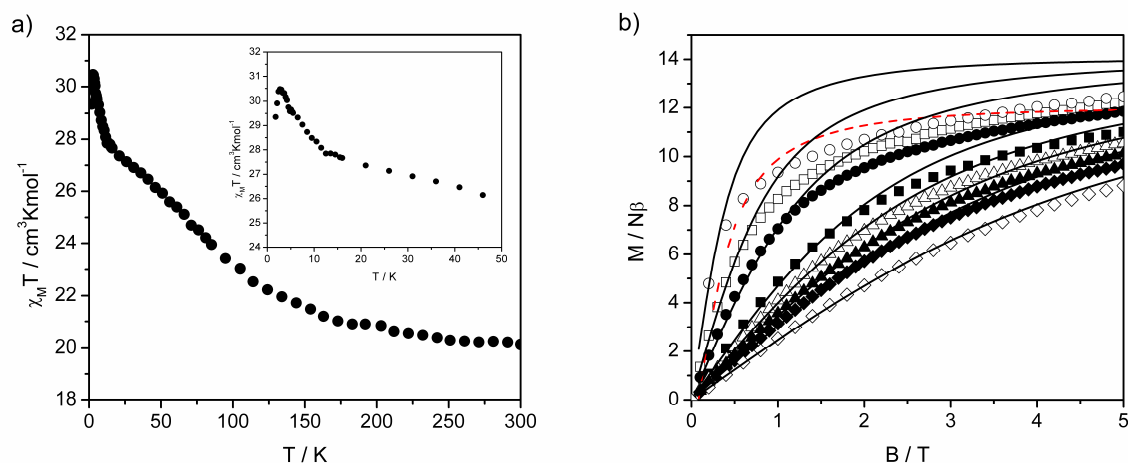


Figure 5.4. a) Plot of $\chi_M T$ vs T for **18** in the range 2 to 300 K in 0.1 T applied field. Inset, plot of $\chi_M T$ vs T in the range 2 to 50 K. b) Field dependence of the magnetization measured at 2 (○), 4 (□), 6 (●), 10 (■), 12 (△), 14 (▲), 16 (◆) and 20 (◇) K. Solid curves are the Brillouin functions calculated for $S = 2$ and $g = 2$ at the same temperatures. Dashed curve is the prediction at $T = 2$ K with an anisotropy field incorporated in the argument.

As mentioned before, compound **18** can be described as an octahedron with the manganese(III) ions at the vertices. The Hamiltonian developed for such system³⁸ considering only two types of magnetic interactions depending on the distances between the manganese(III) ions in the octahedron, cannot be applied to this compound due to the lower symmetry of this cluster in which several magnetic paths should be considered. However, some considerations based on the literature can be of interest to understand better the magnetic behaviour of compound **18**. Only few hexanuclear manganese(III) clusters are known in the literature,^{24,38-41} except for the extended family of compounds with the general formula, $[\text{Mn}_6\text{O}_2(\text{R-sao})_6(\text{X})_2(\text{solvent})_{4-6}]$ with salicyladoxime derivative ligands (R-sao), synthesized mainly by Brechin *et al.*^{5,42-45} Some of the hexanuclear manganese(III) compounds reported in the literature show dominant antiferromagnetic interactions between the manganese(III) ions, resulting in a zero or low-spin magnetic ground state.^{24,28,40,41} The compounds $[\text{Mn}_6\text{O}_4\text{X}_4(\text{Rdbm})_6]$ ($\text{X}^- = \text{Cl}^-, \text{Br}^-$, $\text{dbm}^- = \text{dibenzoylmethane anion}$ and $\text{R} = \text{Me}$,

Et) present dominant ferromagnetic interactions with a total ground state of $S_T = 12$.^{38,39} In the group of compounds with salicylaldoxamine ligands, antiferromagnetic and ferromagnetic interactions can be observed between the manganese(III) ions, leading to different total ground states between $4 < S_T \leq 12$. The type of magnetic exchange interactions has been ascribed mainly to the angle of the oxime ligand. Thus, a large distortion of the Mn–N–O–Mn angle ($\alpha > 31.3^\circ$) can result in ferromagnetic interactions between the manganese(III) ions. As previously pointed out for other compounds, two main parameters should be considered to analyze the ferromagnetic interactions present between the manganese(III) ions, the Jahn-Teller axes that are the single-ion manganese(III) anisotropy axes and the Mn–O–Mn angles. In compound **18**, five of the Jahn-Teller axes intersect at bromide ions. Mn(2), Mn(3), Mn(4) and Mn(6) are similar with a bromide donor atom and a N or O donor atom defining the Jahn-Teller axes, whilst in Mn(1) such axes are defined by the two bromide atoms. The Mn–Br bond distances are long, so the magnetic interaction through them must be weak. Then, the dominant superexchange magnetic path must be through the oxido bridges. Previously, it has been observed in oxide-centred manganese(III) triangles that a distortion of the Mn–O–Mn angle towards lower values from the value of 120° for an equilateral triangle gives rise to a ferromagnetic interaction.⁴⁶⁻⁴⁸ In compound **18** four faces of the octahedron contain such triangles, in which O(1), O(2), O(3) and O(4) are the oxido centres that bridge the three manganese(III) ions. The Mn–O–Mn angles vary from 106° to 122° and might be responsible for some ferromagnetic interactions between the manganese(III) ions. In addition, because of the low symmetry of the compound resulting in Jahn-Teller axes with different directions, substantial spin-canting could be present. In view of all these interviewing factors, it is difficult to arrive at a reliable prediction for the precise molecular magnetic structure.

5.4. Conclusions

High-nuclearity manganese(III) compounds have been synthesized and characterized, *i.e.* two octanuclear manganese(III) compounds with the general formula $[\text{Mn}_8(\mu_4\text{-O}_4)(\text{phpzH})_8(\text{S})_4]$ ($\text{S} = \text{thf}$ (**16**) and EtOH (**17**)) and one hexanuclear, $[\text{Mn}_6(\mu_3\text{-O})_4(\mu_3\text{-Br})_2(\text{HphpzEt})_6(\text{phpzEt})]$ (**18**). The influence of different solvents has been studied on the stability of the $[\text{Mn}_8(\mu_4\text{-O}_4)(\text{phpzR})_8]$ core. Strong antiferromagnetic interactions between the manganese(III) ions are present, leading to a ground state $S_T = 0$ for compounds **16** and **17a**. The variation of the substituents in the 5-position of the pyrazole ring, from proton and methyl to an ethyl group, indicate that the $[\text{Mn}_8(\mu_4\text{-O}_4)(\text{phpzR})_8]$ core is not retained, probably due to the steric hindrance imposed by the ethyl group. Instead, a hexanuclear compound is obtained, *i.e.* compound **18**. In this compound, weak ferromagnetic

interactions are found operative between the manganese(III) ions, leading to an effective net moment of $S_T = 7$ for the cluster. Compound **18** is one of the few examples of transition-metal ion clusters containing pyrazole ligands with dominant ferromagnetic interactions.

5.5. References

1. Mullins, C. S.; Pecoraro, V. L., *Coord. Chem. Rev.*, **2008**, 252, 416-443.
2. Aromí, G.; Brechin, E. K., *Struc. Bond.*, **2006**, 122, 1-67.
3. Gatteschi, D.; Sessoli, R.; Villain, J., *Molecular Nanomagnets*. Oxford University Press: Oxford, UK, 2006.
4. Kahn, O., *Molecular Magnetism*. Wiley-VCH: New York, 1993.
5. Milios, C. J.; Inglis, R.; Vinslava, A.; Bagai, R.; Wernsdorfer, W.; Parsons, S.; Perlepes, S. P.; Christou, G.; Brechin, E. K., *J. Am. Chem. Soc.*, **2007**, 129, 12505-12511.
6. Halcrow, M. A., *Dalton Trans.*, **2009**, 2059-2073.
7. Klingele, J.; Dechert, S.; Meyer, F., *Coord. Chem. Rev.*, **2009**, doi:10.16/j.ccr.2009.03.026.
8. Aromí, G.; Bouwman, E.; Burzuri, E.; Carbonera, C.; Krzystek, J.; Luis, F.; Schlegel, C.; van Slageren, J.; Tanase, S.; Teat, S. J., *Chem.-Eur. J.*, **2008**, 14, 11158-11166.
9. Aromí, G.; Roubeau, O.; Helliwell, M.; Teat, S. J.; Winpenny, R. E. P., *Dalton Trans.*, **2003**, 3436-3442.
10. Bell, A.; Aromí, G.; Teat, S. J.; Wernsdorfer, W.; Winpenny, R. E. P., *Chem. Commun.*, **2005**, 2808-2810.
11. Boča, R.; Dihan, L.; Mezei, G.; Ortiz-Pérez, T.; Raptis, R. G.; Telsler, J., *Inorg. Chem.*, **2003**, 42, 5801-5803.
12. Demeshko, S.; Leibel, G.; Dechert, S.; Meyer, F., *Dalton Trans.*, **2006**, 3458-3465.
13. Tanase, S.; Aromí, G.; Bouwman, E.; Kooijman, H.; Spek, A. L.; Reedijk, J., *Chem. Commun.*, **2005**, 3147-3149.
14. Addison, A. W.; Burke, P. J., *J. Heterocycl. Chem.*, **1981**, 18, 803-805.
15. Sheldrick, G. M. *Program for Empirical Absorption Correction*, University of Göttingen, Germany: 1996.
16. Beurskens, P. T.; Beurskens, G.; Strumpel, M.; Nordman, C. E., in *Patterson and Pattersons*. Glusker, J. P.; Patterson, B. K.; Rossi, M., Eds. Clarendon Press: Oxford: 1987.
17. Duisenberg, A. J. M. Reflections on area detectors. PhD thesis, Utrecht, 1998.
18. Duisenberg, A. J. M.; Kroon-Batenburg, L. M. J.; Schreurs, A. M. M., *J. Appl. Crystallogr.*, **2003**, 220-229.
19. Beurskens, P. T.; Beurskens, G.; Bosman, W. P.; De Gelder, R.; García-Granda, S.; Gould, R. O.; Israël, R.; Smits, J. M. M.; Smykalla, C. *The DIRDIF96. A computer program system for the crystal structure determination by Patterson methods and direct methods applied to difference structure factors*, Crystallography Laboratory, University of Nijmegen: Nijmegen, The Netherlands, 1996.
20. Sheldrick, G. M. *SHELXS-97: Program for Crystal Structures Determination*, University of Göttingen; Germany: Göttingen, 1997.
21. Sheldrick, G. M. *SHELXL-97: Program for Crystal Structure Refinement*, University of Göttingen; Germany: Göttingen, 1997.
22. Spek, A. L. *PLATON, A Multipurpose Crystallographic Tool*, Utrecht University; The Netherlands, 2003.
23. Viciano-Chumillas, M.; Marqués-Giménez, M.; Tanase, S.; Evangelisti, M.; Mutikainen, I.; Turpeinen, M.; Smits, J. M. M.; de Gelder, R.; de Jongh, L. J.; Reedijk, J., *J. Phys. Chem. C*, **2008**, 112, 20525-20534.
24. Godbole, M. D.; Roubeau, O.; Mills, A. M.; Kooijman, H.; Spek, A. L.; Bouwman, E., *Inorg. Chem.*, **2006**, 45, 6713-6722.
25. Brechin, E. K.; Soler, M.; Christou, G.; Helliwell, M.; Teat, S. J.; Wernsdorfer, W., *Chem. Commun.*, **2003**, 1276-1277.
26. Godbole, M. D.; Roubeau, O.; Clérac, R.; Kooijman, H.; Spek, A. L.; Bouwman, E., *Chem. Commun.*, **2005**, 3715-3717.

27. Grillo, V. A.; Knapp, M. J.; Bollinger, J. C.; Hendrickson, D. N.; Christou, G., *Angew. Chem.-Int. Edit. Engl.*, **1996**, 35, 1818-1820.
28. Hoshino, N.; Ito, T.; Nihei, M.; Oshio, H., *Inorg. Chem. Commun.*, **2003**, 6, 377-380.
29. Jones, L. F.; Brechin, E. K.; Collison, D.; Raftery, J.; Teat, S. J., *Inorg. Chem.*, **2003**, 42, 6971-6973.
30. Libby, E.; Folting, K.; Huffman, C. J.; Huffman, J. C.; Christou, G., *Inorg. Chem.*, **1993**, 32, 2549-2556.
31. Sañudo, E. C.; Cauchy, T.; Ruiz, E.; Laye, R. H.; Roubeau, O.; Teat, S. J.; Aromí, G., *Inorg. Chem.*, **2007**, 46, 9045-9047.
32. Tasiopoulos, A. J.; Wernsdorfer, W.; Moulton, B.; Zaworotko, M. J.; Christou, G., *J. Am. Chem. Soc.*, **2003**, 125, 15274-15275.
33. Tsai, H. L.; Wang, S. Y.; Folting, K.; Streib, W. E.; Hendrickson, D. N.; Christou, G., *J. Am. Chem. Soc.*, **1995**, 117, 2503-2514.
34. Wang, S.; Tsai, H. L.; Folting, K.; Martin, J. D.; Hendrickson, D. N.; Christou, G., *J. Chem. Soc.-Chem. Commun.*, **1994**, 671-673.
35. Baran, P.; Boča, R.; Chakraborty, I.; Giapintzakis, J.; Herchel, R.; Huang, Q.; McGrady, J. E.; Raptis, R. G.; Sanakis, Y.; Simopoulos, A., *Inorg. Chem.*, **2008**, 47, 645-655.
36. Vankalkeren, G.; Schmidt, W. W.; Block, R., *Physica B & C*, **1979**, 97, 315-337.
37. Krzystek, J.; Ozarowski, A.; Telser, J., *Coord. Chem. Rev.*, **2006**, 250, 2308-2324.
38. Aromí, G.; Knapp, M. J.; Claude, J. P.; Huffman, J. C.; Hendrickson, D. N.; Christou, G., *J. Am. Chem. Soc.*, **1999**, 121, 5489-5499.
39. Aromí, G.; Claude, J. P.; Knapp, M. J.; Huffman, J. C.; Hendrickson, D. N.; Christou, G., *J. Am. Chem. Soc.*, **1998**, 120, 2977-2978.
40. Chakov, N. E.; Zakharov, L. N.; Rheingold, A. L.; Abboud, K. A.; Christou, G., *Inorg. Chem.*, **2005**, 44, 4555-4567.
41. Xia, X. P.; Verelst, M.; Daran, J. C.; Tuchagues, J. P., *J. Chem. Soc.-Chem. Commun.*, **1995**, 2155-2157.
42. Miliós, C. J.; Manoli, M.; Rajaraman, G.; Mishra, A.; Budd, L. E.; White, F.; Parsons, S.; Wernsdorfer, W.; Christou, G.; Brechin, E. K., *Inorg. Chem.*, **2006**, 45, 6782-6793.
43. Miliós, C. J.; Raptopoulou, C. P.; Terzis, A.; Lloret, F.; Vicente, R.; Perlepes, S. P.; Escuer, A., *Angew. Chem.-Int. Edit.*, **2004**, 43, 210-212.
44. Miliós, C. J.; Vinslava, A.; Wernsdorfer, W.; Prescimone, A.; Wood, P. A.; Parsons, S.; Perlepes, S. P.; Christou, G.; Brechin, E. K., *J. Am. Chem. Soc.*, **2007**, 129, 6547-6561.
45. Raptopoulou, C. P.; Boudalis, A. K.; Lazarou, K. N.; Psycharis, V.; Panopoulos, N.; Fardis, M.; Diamantopoulos, G.; Tuchagues, J. P.; Mari, A.; Papavassiliou, G., *Polyhedron*, **2008**, 27, 3575-3586.
46. Lampropoulos, C.; Abboud, K. A.; Stamatatos, T. C.; Christou, G., *Inorg. Chem.*, **2009**, 48, 813-815.
47. Viciano-Chumillas, M.; Tanase, S.; Mutikainen, I.; Turpeinen, M.; de Jongh, L. J.; Reedijk, J., *Inorg. Chem.*, **2008**, 47, 5919-5929.
48. Viciano-Chumillas, M.; Tanase, S.; Mutikainen, I.; Turpeinen, U.; de Jongh, L. J.; Reedijk, J., *Dalton Trans.*, **2009**, 7445-7453.

Chapter 6

Coordination versatility of 3(5)-methyl-5(3)-(2-hydroxyphenyl)-pyrazole with Co(III), Ni(II) and Cu(II) ions*

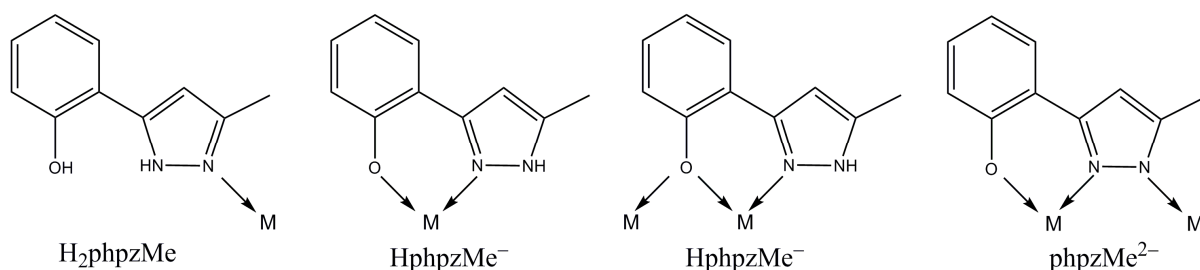
New compounds with the ligand 3(5)-methyl-5(3)-(2-hydroxyphenyl)-pyrazole, H₂phpzMe, [Co₂(H₂phpzMe)(HphpzMe)₂(phpzMe)₂·3CH₃CN (**19**), [Ni(HphpzMe)₂] (**20**) and [Cu(HphpzMe)₂] (**21**) have been synthesized and structurally characterized. Compound **19** is a dinuclear cobalt(III) compound, in which the ligand H₂phpzMe shows four different coordination modes with the metal ion. Compounds **20** and **21** are mononuclear compounds with a distorted square-planar geometry.

* This chapter has been published in the literature: Viciano-Chumillas, M.; Tanase, S.; Aromí, G.; Smits, J. M. M.; de Gelder, R.; Solans, X.; Bouwman, E.; Reedijk, J., *Eur. J. Inorg. Chem.*, **2007**, 2635-2640.

6.1. Introduction

Pyrazole-based ligands have received a great deal of attention over the last decades, as detailed in Chapter 1, due to their interesting coordination chemistry, unusual structural features, and remarkable physical and chemical properties.¹⁻³ The incorporation of pyrazole groups in the design of new ligands allows studying their structural properties to serve specific stereochemical requirements for a particular metal-binding site. Although a significant number of coordination compounds containing pyrazole ligands have been obtained to date, the design and synthesis of novel pyrazole-containing complexes by employing more versatile ligands or by varying the nature of the reactants and synthetic conditions are still under active investigation.^{4,5} An important factor to be considered is the nature of the metal ion for the synthesis of new complexes. The ligand preferences and the kinetics of the metal ion can drive the formation of different compounds. In the previous chapters the coordination chemistry of phenol-pyrazole based ligands with the manganese(III) ion has been explored.⁶⁻⁸ It has been shown that the amount of base and the type of solvents are paramount in controlling the different coordination modes, thereby providing a rich binding versatility to the ligands and affording a variety of manganese(III) compounds.

In this chapter, different transition-metal ions, *i.e.* cobalt(III), nickel(II) and copper(II) ions are investigated for the formation of new coordination compounds with the ligand H₂phpzMe. As a result, the synthesis, characterization, and crystal structure of three new compounds are reported; a quite unusual dinuclear cobalt(III) compound [Co₂(H₂phpzMe)(HphpzMe)₂(phpzMe)₂] \cdot 3CH₃CN (**19**), triply-bridged by one phenoxide and two pyrazolate groups, as well as two new isomorphous mononuclear compounds [Ni(HphpzMe)₂] (**20**) and [Cu(HphpzMe)₂] (**21**). It appears that **19** is the first example of a dinuclear cobalt(III) compound bridged by both pyrazolate and phenoxide groups. A remarkable feature of this compound is the observed binding versatility of the ligand H₂phpzMe, which is coordinated in four different modes to the two cobalt(III) ions (Scheme 6.1).



Scheme 6.1. Four different coordination modes of the ligand H₂phpzMe in compound **19**.

6.2. Experimental Section

General Remarks. Starting materials were purchased from Aldrich and all manipulations were performed using the materials as received. The ligand 3(5)-methyl-5(3)-(2-hydroxyphenyl)-pyrazole (H₂phpzMe) has been synthesized according to the reported procedure.⁹

Synthesis

[Co₂(H₂phpzMe)(HphpzMe)₂(phpzMe)₂]₃CH₃CN (19). A solution of H₂phpzMe (61 mg, 0.35 mmol) and triethylamine (67 mg, 0.66 mmol) in 7 ml of acetonitrile was slowly added to a solution of Co(ClO₄)₂·6H₂O (66 mg, 0.18 mmol) in 2 ml of acetonitrile. The resulting purple solution was stirred for five minutes to give a purple precipitate. The purple solid was collected by filtration, washed with acetonitrile and diethyl ether and dried in air. Yield: 34% (26.03 mg). Crystals suitable for X-ray diffraction were obtained by slow evaporation of the filtrate. Anal. Calcd for **19** (C₅₆H₅₃Co₂N₁₃O₅): C, 60.82; H, 4.83; N, 16.46. Found: C, 58.13; H, 5.00; N, 15.08. Loss of some lattice acetonitrile may result in lower C, N, H analyses, as the acetonitrile molecules are weakly held in the lattice, replacement of one acetonitrile by three molecules of water would generate a more accurate C, H, N analysis (Calcd. for compound **19**·2CH₃CN·3H₂O: C, 57.96; H, 5.04; N, 15.02). IR (ν_{max}/cm⁻¹): 3425(w), 3280(w), 1596(m), 1558(s), 1463(s), 1456(s), 1299(m), 1229(s), 1188(w), 1116(m), 1038(w), 986(s), 850(s), 772(m), 752(m), 744(m), 641(m), 602(m), 584(s), 436(m), 418(s). UV/VIS/NIR in solid state (λ_{max}/nm): 576, 335, 271.

[Ni(HphpzMe)₂] (20). The ligand H₂phpzMe (161 mg, 0.92 mmol) and 1 M methanolic Bu₄NOH (2ml, 2 mmol) were dissolved in methanol (10 ml). To this solution was added a solution of Ni(ClO₄)₂·6H₂O (367 mg, 1 mmol) in methanol (10 ml) and the mixture was then stirred. A green microcrystalline precipitate formed immediately. After a few minutes, the solid (230 mg) was collected by filtration and dissolved in CH₂Cl₂ (20 ml). The dark green solution was layered with Et₂O in various sealed tubes. After a few days, dark large green crystals suitable for X-ray crystallography were collected. Yield: 15% (27.53 mg). Anal. Calcd for **20** (C₂₀H₁₈N₄NiO₂): C, 53.16; H, 4.19; N, 11.95. The calculated EA given here are for the compound **20**·0.75CH₂Cl₂. The presence of CH₂Cl₂ is not unexpected as the complex was crystallized from this solvent. Found: C, 53.87; H, 4.36; N, 12.42. IR (ν_{max}/cm⁻¹): 3299(s), 1600(s), 1553(s), 1471(s), 1412(s), 1314(s), 1249(s), 1197(m), 1121(m), 1039(m), 1117(m), 864(s), 788(s), 738(m), 668(m), 645(m), 587(s), 475(m), 384(s). UV/VIS/NIR in solid state (λ_{max}/nm): 622, 490, 415, 360, 268. The reaction of two equivalents of H₂phpzMe with one equivalent of Ni(OAc)₂·4H₂O in acetonitrile and in the absence of base afforded **20**

as polycrystalline sample with yield of 76%. The copper(II) doped nickel(II) compound was prepared using this method, but using a ratio Ni/Cu of 100:2.

[Cu(HphpzMe)₂] (21). A solution of H₂phpzMe (35 mg, 0.20 mmol) and sodium methoxide (22 mg, 0.40 mmol) in 5 ml of methanol was slowly added to a solution of Cu(ClO₄)₂·6H₂O (76 mg, 0.20 mmol) in 2 ml of methanol. The resulting green solution was stirred for five minutes to give a green precipitate. The solid was removed by filtration and the slow evaporation of the filtrate gives large green needles suitable for X-ray crystallography. Yield: 58% (23.78 mg). Anal. Calcd for **21** (C₂₀H₁₈CuN₄O₂): C, 58.60; H, 4.43; N, 13.67. Found: C, 58.43; H, 4.30; N, 13.76. IR ($\nu_{\max}/\text{cm}^{-1}$): 3311(s), 1599(m), 1548(s), 1464(s), 1316(s), 1247(m), 1196(w), 1121(m), 1065(m), 1039(w), 1018(m), 857(s), 791(m), 739(m), 668(m), 641(m), 618(m), 593(s), 575(s), 470(m), 371(s). UV/VIS/NIR in solid state (λ_{\max}/nm): 660, 455, 380, 350, 263. The reaction of two equivalents of H₂phpzMe with one equivalent of Cu(OAc)₂·H₂O in acetonitrile and in the absence of base, afforded **21** as polycrystalline sample with yield of 72%.

Physical Measurements. Elemental analysis for C, H and N were performed on a Perkin-Elmer 2400 series II analyzer. Infrared spectra (4000–300 cm⁻¹) were recorded on a Perkin-Elmer Paragon 1000 FTIR spectrometer equipped with a Golden Gate ATR device, using the reflectance technique. Solid electronic absorption spectra were obtained on a Perkin-Elmer Lambda 900 spectrophotometer using the diffuse reflectance technique, with MgO as a reference. The electrochemical measurements were performed with an Autolab PGstat10 potentiostat controlled by GPES4 software. A three-electrode system was used, consisting of a platinum working electrode, a platinum auxiliary electrode, and an Ag/AgCl reference electrode. The experiments were carried out at room temperature under argon with tetrabutylammonium hexafluoridophosphate as supporting electrolyte. All potentials are reported relative to Ag/AgCl. Electrospray mass spectra in acetonitrile/water (80:20) were recorded on a Thermo Finnigan AQA apparatus. The ¹H NMR spectra were recorded on a DPX300 Bruker spectrometer. All chemical shifts were reported with respect to the residual solvent peak. X-band powder EPR spectra were obtained on a JEOL RE2x electron-spin resonance spectrometer using DPPH ($g = 2.0036$) as a standard. Magnetic susceptibility measurements (2–300 K) were carried out at 0.1 T using a Quantum Design MPMS-5 5T SQUID magnetometer.

X-ray Crystallography. Intensity data for single crystals were collected using MoK α radiation ($\lambda = 0.71073 \text{ \AA}$) on a Nonius KappaCCD diffractometer. Crystal and refinement data are collected in Table 6.1 for **19**, **20** and **21**. The intensity data were corrected for Lorentz

and polarization effects, and for absorption (multiscan absorption correction¹⁰). The structures were solved by Patterson methods.¹¹ The programs EvalCCD, DIRDIF96 and SHELXL-97 were used for data reduction, structure solution, refinement, and evaluation respectively.¹²⁻¹⁵ All non-hydrogen atoms were refined with anisotropic displacement parameters. All hydrogens were placed at calculated positions and were refined riding on the parent atoms. Geometric calculations and molecular graphics were performed with the PLATON package.¹⁶

Table 6.1. Crystal data and structure refinements for [Co₂(H₂phpzMe)(HphpzMe)₂(phpzMe)₂] \cdot 3CH₃CN (**19**), [Ni(HphpzMe)₂] (**20**) and [Cu(HphpzMe)₂] (**21**).

	19	20	21
Formula	C ₅₆ H ₅₃ Co ₂ N ₁₃ O ₅	C ₂₀ H ₁₈ N ₄ NiO ₂	C ₂₀ H ₁₈ CuN ₄ O ₂
Formula mass [g mol ⁻¹]	1105.97	405.09	409.93
Crystal system	Monoclinic	Monoclinic	Monoclinic
Space group	P2 ₁ /c	P2 ₁ /n	P2 ₁ /n
<i>a</i> [Å]	10.6796(14)	12.637(8)	12.5018(13)
<i>b</i> [Å]	26.103(3)	5.735(3)	5.6636(6)
<i>c</i> [Å]	18.3933(12)	12.736(4)	12.785(4)
β [°]	92.492(8)	110.64(2)	110.420(11)
<i>V</i> [Å ³]	5122.6(10)	863.8(8)	848.4(3)
<i>Z</i>	4	2	2
<i>D</i> _{calc} [g cm ⁻³]	1.434	1.557	1.605
Crystal size [mm ³]	0.22×0.12×0.04	0.11×0.13×0.18	0.38×0.07×0.04
Number of collected reflections (unique)	76586(9012)	6786(2121)	9188(1494)
Number of observed reflections [<i>I</i> _o > 2σ(<i>I</i> _o)]	6636	1883	1089
Internal R factor	0.0953	0.058	0.052
Number of parameters	694	124	125
Goodness-of-fit <i>S</i> on <i>F</i> ²	1.247	1.11	1.08
μ [mm ⁻¹]	0.712	1.147	1.312
<i>R</i> ₁ ^[a] [<i>I</i> > 2σ(<i>I</i>)]	0.0861	0.0547	0.0458
<i>wR</i> ₂ ^[b] [all data]	0.1780	0.1495	0.0870
<i>T</i> [°C]	208	293	208

^[a] $R_1 = \sum ||F_o| - |F_c|| / \sum |F_o|$. ^[b] $wR_2 = \{ \sum [w(F_o^2 - F_c^2)^2] / \sum w(F_o^2)^2 \}^{1/2}$.

6.3. Results and Discussion

Synthesis and Spectroscopic Properties. The reaction of 3(5)-methyl-5(3)-(2-hydroxyphenyl)-pyrazole (H₂phpzMe) with Co(ClO₄)₂·6H₂O in the ratio 2 to 1 in the presence of two equivalents of triethylamine yields the diamagnetic cobalt(III) compound

[Co₂(H₂phpzMe)(HphpzMe)₂(phpzMe)₂]₂·3CH₃CN (**19**) as a purple solid. After filtration, slow evaporation of the solution affords purple crystals suitable for X-ray crystallography. The presence of base, as well as the aerial conditions are responsible for the oxidation of cobalt(II) to cobalt(III). The infrared spectrum of **19** suggests the coordination of the ligand to the cobalt(III) ion as indicated by the shift of the ν_{C-O} stretching vibration from 1636 cm⁻¹ in the free ligand to 1596 cm⁻¹ in the complex and the $\nu_{C=N}$ stretching vibration from 1576 cm⁻¹ in the free ligand to 1558 cm⁻¹ in the complex. The peak observed at 3425 cm⁻¹ can be assigned to the phenolic hydrogen of the H₂phpzMe ligand that remains neutral by coordination to cobalt(III) ion. The band due to ν_{N-H} stretching vibration is observed at 3280 cm⁻¹ and is less broad as compared to the free ligand due to the coordination of the ligands in the complex.¹⁷ The electronic absorption spectrum of **19** in the solid state exhibits a broad absorption band at 576 nm that is characteristic for octahedral cobalt(III) complexes. The band at 335 nm can be assigned based on its intensity to a $p_{\pi} \rightarrow d_{\sigma}^*$ transition, whilst the band at 271 nm arises from a $\pi \rightarrow \pi^*$ ligand transition.¹⁸

The reaction of Ni(ClO₄)₂·6H₂O, H₂phpzMe and Bu₄NOH in a 1/1/2 ratio in methanol yields a green compound¹⁹ that upon dissolution in dichloromethane followed by slow diffusion of diethyl ether afforded compound **20** as dark green crystals. Compound **20** is thermodynamically very stable, since it can be obtained from numerous synthetic procedures, such as in the reaction of Ni(OAc)₂·4H₂O in acetonitrile and in the absence of base that afforded **20** as polycrystalline samples with yields up to 76% for **20**. The infrared spectrum of **20** displays a strong band assigned to the ν_{N-H} stretching vibration at 3299 cm⁻¹. Several sharp weak bands observed in the range 2900–3150 cm⁻¹ are likely to be due to the ν_{C-H} stretches of the methyl group. As the free H₂phpzMe ligand displays the ν_{C-O} stretching vibration at 1636 cm⁻¹, the shift of this band to 1600 cm⁻¹ in compound **20** suggests the coordination of the phenolic oxygen. The electronic absorption spectrum of **20** in the solid state displays two broad bands at 490 nm and 622 nm assigned to d–d transitions for the low-spin nickel(II) compound; the absorption band at 622 nm is assigned to a $d_{x^2-y^2} \rightarrow d_{zy}$ transition, whilst the absorption band at 490 nm is attributed to the $d_z^2 \rightarrow d_{zy}$ transition.²⁰ The absorptions observed in the range 420 to 270 nm are likely due to the metal-to-ligand and inter- or intra-ligand charge transfer transitions. The solid compound turned out to be diamagnetic, as expected for square-planar nickel(II), thereby allowing the study of a solid solution (dope) of the isomorphous copper(II) compound.

Compound **21** can be obtained by reaction of Cu(ClO₄)₂·6H₂O and H₂phpzMe in a 1 to 1 or 1 to 2 ratio and in the presence of two equivalents of sodium methoxide or tetramethylammonium hydroxide as base. The reaction of H₂phpzMe with Cu(OAc)₂·H₂O in

acetonitrile and in the absence of base afforded **21** as polycrystalline samples with yields up to 72% for **21**. The infrared spectrum of compound **21** is very similar to that of compound **21** and it exhibits the bands expected for the monoanionic ligand HphpzMe⁻. Notably, the shift of the stretching vibrations $\nu_{\text{C-O}}$ at 1599 cm⁻¹ and $\nu_{\text{C=N}}$ at 1548 cm⁻¹ is observed to lower energies comparing with the IR spectrum of the pure ligand. The electronic absorption spectrum shows a broad asymmetric band at 660 nm attributed to d–d transitions of copper(II) complexes with square-planar geometry; the absorption bands in the range 455–350 nm are due to Cu–O and Cu–N charge transfer transitions.

Description of the Molecular Structures. A single-crystal X-ray analysis of **19** revealed the identity of the product as [Co₂(H₂phpzMe)(HphpzMe)₂(phpzMe)₂] \cdot 3CH₃CN. As shown in Figure 6.1, the molecular structure of **19** consists of a highly asymmetric dinuclear unit with two cobalt(III) ions bridged by two pyrazolate groups and one phenoxide group with a Co \cdots Co separation of 3.154 Å. This distance is slightly longer than those observed for other triply-bridged dinuclear cobalt(III) compounds.²¹ Most remarkably, the ligand H₂phpzMe shows four different coordination modes in the molecular structure of **19**: (i) quite unusual, the H₂phpzMe ligand remains neutral and it is N-monodentate bound to Co(2), with the ligand present in the 3-methyl-5-(2-hydroxyphenyl)-pyrazole mode; (ii) a uninegative HphpzMe⁻ ligand is NO-chelating to Co(1); (iii) a second uninegative HphpzMe⁻ molecule act as a NO-bidentate chelating ligand and it links the two cobalt(III) ions through a phenoxido bridge; (iv) two ligand molecules are doubly deprotonated and these phpzMe²⁻ ligands coordinate in a N₂O-tridentate manner to link the two cobalt(III) ions by a double pyrazolato bridge. In the last three binding modes the ligand is present in the 3-(2-hydroxyphenyl)-5-methyl-pyrazole conformation. As a result, both cobalt(III) ions have a distorted octahedral geometry and are in quite different coordination environments. The Co(1) ion has a CoN₄O₂ donor set in a *trans* octahedral geometry, whilst the Co(2) ion has a CoN₃O₃ donor set in a *mer* octahedral geometry. The Co–O and Co–N bond distances are in the range of 1.865–2.001 Å and 1.875–1.971 Å, respectively, as expected for low-spin cobalt(III) complexes.²² Selected bond lengths and angles for **1** are listed in Table 6.2. The largest deviation from the octahedral geometry is observed for the *trans* angle which is O(81)–Co(2)–O(41) = 174.90(17)°. The Co(1)–O(81)–Co(2) angle is 107.09° and it is slightly smaller than the angle normally observed for phenoxido-bridged dinuclear cobalt(III) complexes.^{23,24} The least-squares plane of the aromatic ring of the N₂O-tridentate ligand phpzMe²⁻ and the plane defined by Co(1), Co(2) and O(81) have a dihedral angle of 38.11°. The bending angle of the bridging pyrazole least-squares planes to the Co(1)–N(11)–N(12)–Co(2) and Co(1)–N(32)–N(31)–Co(2)

coordination planes is 5.36° and 5.64° , respectively. The dihedral angle between the planes of the two bridging pyrazole rings is 79.91° , whilst the dihedral angle between the $\text{CoN}_{\text{pz}}\text{N}_{\text{pz}}\text{Co}$ planes is 75.98° .

The ligands adopt conformations that vary from nearly planar to considerably twisted with the dihedral angle between the phenyl and pyrazole ring planes ranging from 1.34° to 23.37° . These conformations are determined by the presence of strong intramolecular and intermolecular hydrogen bonds involving the O(phenol)–H and N(pz)–H functions, as well as acetonitrile lattice molecules. The strongest intramolecular hydrogen bond involves the N–H function of the N-monodentate ligand bound to Co(1) ($\text{N}(92)\text{--H}(92)\cdots\text{O}(101) = 2.624 \text{ \AA}$); the distance $\text{N}(72)\text{--H}(71)\cdots\text{O}(21)$ of 2.756 \AA would also suggest hydrogen bonding, but the angle of 107.9° is rather small. In addition, the O–H function of O(101) participates in an intermolecular donor hydrogen-bonding interaction with a lattice acetonitrile molecule ($\text{O}(101)\text{--H}(101)\cdots\text{N}(3) = 2.962 \text{ \AA}$). The other two acetonitrile lattice molecules are at longer hydrogen bond distances (from N(51) and N(71)). The acetonitrile molecules are kept rather weakly bound in the lattice, as is also indicated by the elemental analyses (C, N, H) and some acetonitrile molecule might be replaced by atmospheric water. Table 6.3 gives some details of the hydrogen-bonding patterns.

Table 6.2. Selected bonds lengths [\AA] and angles [$^\circ$] for the compound $[\text{Co}_2(\text{H}_2\text{phpzMe})(\text{HphpzMe})_2(\text{phpzMe})_2]\cdot 3\text{CH}_3\text{CN}$ (**19**).

Bond Lengths					
Co(1)–O(21)	1.865(4)	Co(1)–N(72)	1.914(5)	Co(2)–N(32)	1.875(6)
Co(1)–N(12)	1.875(5)	Co(1)–N(91)	1.969(6)	Co(2)–O(61)	1.916(4)
Co(1)–N(31)	1.925(6)	Co(2)–N(11)	1.929(5)	Co(2)–N(52)	1.893(5)
Co(1)–O(81)	1.919(4)	Co(2)–O(41)	1.879(4)	Co(2)–O(81)	2.002(4)
Co(1)⋯Co(2)	3.154				
Bond Angles					
N(91)–Co(1)–O(81)	88.0(2)	N(31)–Co(1)–O(21)	92.5(2)	N(72)–Co(1)–N(91)	90.4(2)
O(21)–Co(1)–N(91)	88.0(2)	O(21)–Co(1)–N(12)	91.6(2)	O(21)–Co(1)–N(72)	88.4(2)
O(21)–Co(1)–O(81)	179.31(18)	O(81)–Co(1)–N(12)	88.0(2)	O(81)–Co(1)–N(72)	92.0(2)
N(32)–Co(2)–N(11)	88.8(2)	N(32)–Co(2)–O(81)	84.8(2)	N(11)–Co(2)–O(81)	84.9(2)
N(52)–Co(2)–N(32)	92.0(2)	N(52)–Co(2)–O(61)	89.9(2)	N(52)–Co(2)–O(81)	91.0(2)
N(52)–Co(2)–O(41)	90.7(2)	O(41)–Co(2)–N(11)	93.6(2)	O(41)–Co(2)–N(32)	90.3(2)
O(61)–Co(2)–N(11)	89.5(2)	O(61)–Co(2)–O(41)	87.76(17)	O(81)–Co(2)–O(61)	97.07(17)
Co(1)–O(81)–Co(2)	107.1(2)				

Table 6.3. Hydrogen bond details (distances [Å] and angles [°]) for [Co₂(H₂phpzMe)(HphpzMe)₂(phpzMe)₂] \cdot 3CH₃CN (**19**).

Donor–H \cdots Acceptor	D–H	H \cdots A	D \cdots A	D–H \cdots A
N(71)–H(71) \cdots O(21)	0.87	2.36	2.756(8)	107.9
N(92)–H(92) \cdots O(101)	0.87	2.03	2.624(8)	124.6
O(101)–H(101) \cdots N(3)	0.83	2.01	2.800(9)	159.8
N(51)–H(51) \cdots N(6)	0.87	2.17	2.996(9)	157.9
N(71)–H(71) \cdots N(9)	0.87	2.49	3.271(12)	149.8

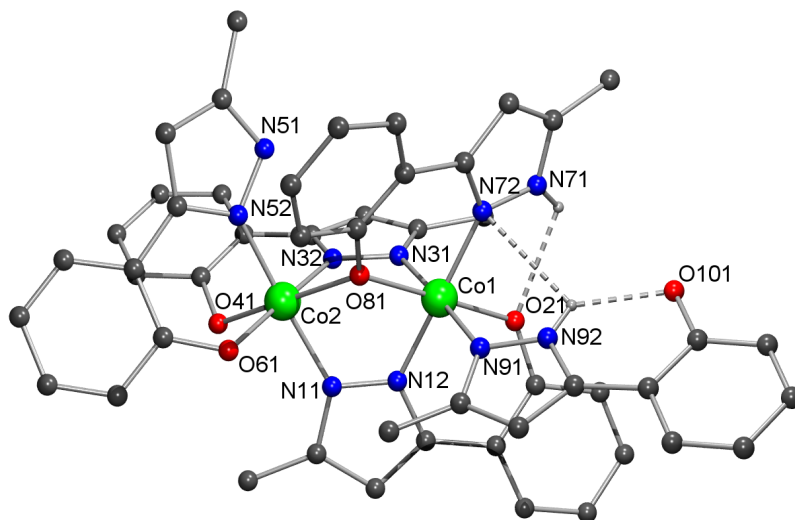


Figure 6.1. Pluton projection of the neutral compound [Co₂(H₂phpzMe)(HphpzMe)₂(phpzMe)₂] \cdot 3CH₃CN (**19**) showing the intramolecular hydrogen bonding interactions. Hydrogen atoms that are not involved in hydrogen bonds and the acetonitrile molecules are omitted for clarity.

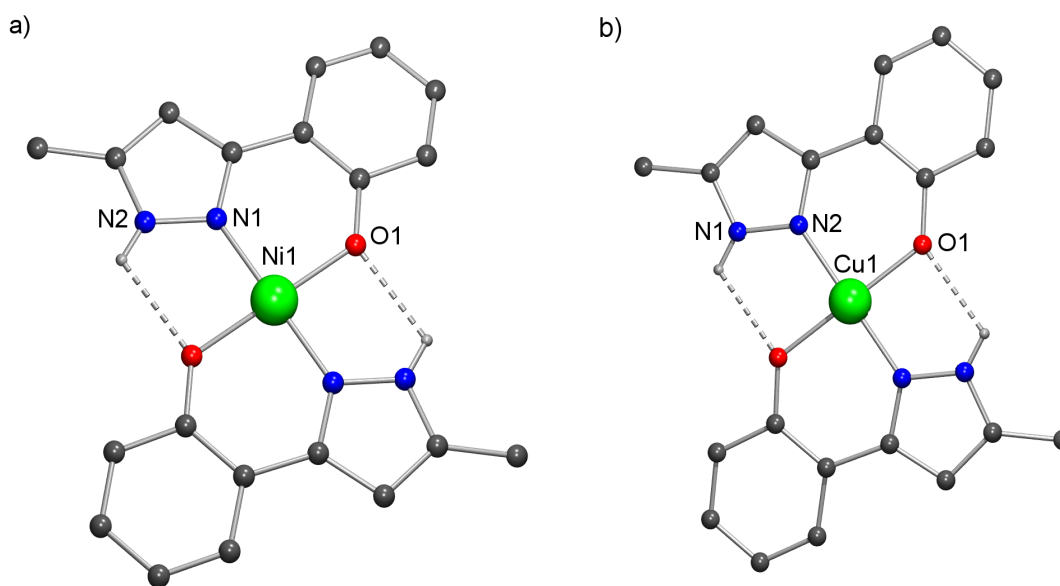


Figure 6.2. Pluton projection of the molecular structure of [Ni(HphpzMe)₂] (**20**) (a) [Cu(HphpzMe)₂] (**21**) (b), showing the intramolecular hydrogen bonding interactions. Hydrogen atoms that are not involved in hydrogen bonds are omitted for clarity.

Compounds **20** and **21** are isostructural and they crystallize in the space group $P2_1/n$. In both cases the asymmetric unit contains half of a centrosymmetric mononuclear unit. The metal ion has a *trans*- MN_2O_2 environment formed by two $HphzMe^-$ ligands that bind in a NO-bidentate chelating manner in the 3-(2-hydroxyphenyl)-5-methyl-pyrazole mode. The molecular structures of **20** and **21** are shown in Figure 6.2, respectively. The coordination geometry of the NiN_2O_2 chromophore is slightly distorted square-planar ($N(1)-Ni-O(1) = 91.90^\circ$; $O(1)-Ni-N(1a) = 88.10(8)^\circ$). The $Ni-N$ (1.862(2) Å) and $Ni-O$ (1.868(2) Å) bond distances agree well with the values expected for a low-spin nickel(II) ion in a square-planar environment.²⁵ The dihedral angle between the phenyl and pyrazole ring planes within the ligand is 4.62° . In compound **21**, the copper(II) ion is in a slightly distorted square-planar geometry, with the bond angle values of $89.36(4)^\circ$ ($O(1)-Cu(1)-N(2)$) and $90.64(14)^\circ$ ($O(1)-Cu(1)-N(2)a$). The $Cu-N$ and $Cu-O$ bond lengths are 1.9007(36) and 1.9261(26) Å, respectively. As shown in Figure 6.2, there are two strong intramolecular hydrogen bonds with the acid N-H group as donor and the phenoxide group as acceptor ($N(2)\cdots O(1a) = 2.612(3)$ Å; $N(2)-H(2)\cdots O(1a) = 111^\circ$ and $N(1)\cdots O(1) = 2.693(5)$ Å; $N(1)-H(1)\cdots O(1) = 113^\circ$ for compounds **20** and **21**, respectively). For compounds **20** and **21**, the crystal lattice is further stabilized by very weak $\pi-\pi$ interactions involving the pyrazole rings; the shortest distance between the pyrazole planes is 3.919 Å and 3.861 Å respectively. The closest $M\cdots M$ separation is 5.735 Å and 5.664 Å for compounds **20** and **21**, respectively.

EPR and Magnetic susceptibility. Compounds **19** and **20** display no EPR signal, neither in the solid state, nor in CH_2Cl_2 solution, not at room temperature (RT) and not at 77 K. These results strongly indicates that **19** and **20** are diamagnetic ($S = 0$), as expected for low-spin cobalt(III) octahedral d^6 complexes and low-spin d^8 square-planar nickel(II) complexes.

The polycrystalline powder EPR spectrum of **21** recorded at RT and 77 K shows a broad spectrum ($g = 2.06$) and no resolved hyperfine splitting is observed (Figure 6.3). When copper(II) ions are separated by dilution as a 2% dope in the diamagnetic host lattice of **20**, both hyperfine and superhyperfine splitting were observed (Figure 6.3). The superhyperfine structure is observed in the perpendicular region of the spectrum, arising from the interaction of the copper(II) unpaired electron with the two nitrogen donor atoms of two ligand molecules that results in a five line splitting ($A_N = 10$ G). The magnitude of $g_{||}$ and $A_{||}$ (2.25, 200 G) and the five superhyperfine lines indicate that copper(II) ion has an axial coordination geometry with two nitrogen donors in the equatorial plane²⁶, in agreement with the X-ray crystal structure. The spectrum shows an unusual transition in the equatorial region. This transition is

caused by so-called overshoot features, which result in overlap of the equatorial and the axial transitions.²⁷

The temperature-dependent magnetic susceptibility of **21** in the range 2–300 K shows paramagnetic behaviour, which results from the absence of effective exchange magnetic interactions between the mononuclear units. At 300 K, the $\chi_M T$ value is equal to 0.35 cm³Kmol⁻¹ that is close to the theoretical value of 0.375 cm³Kmol⁻¹ expected for a single non-coupled copper(II) ions ($S = 1/2$).

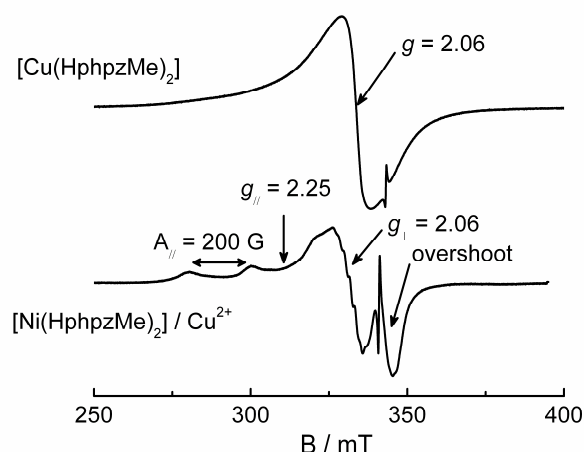


Figure 6.3. EPR spectra recorded at room temperature of [Ni(HphpzMe)₂] (**20**)/Cu²⁺ (bottom) and [Cu(HphpzMe)₂] (**21**) (top), with radical DPPH marker at $g = 2.00$.

Solution chemistry. The positive ion mass spectrum of a solution of **19** in methanol exhibits prominent signals at $m/z = 983$ and 810 that can be assigned to the molecular ion $\{[\text{Co}_2(\text{H}_2\text{phpzMe})(\text{HphpzMe})_2(\text{phpzMe})_2] + \text{H}^+\}^+$, and the fragment $\{[\text{Co}_2(\text{HphpzMe})_2(\text{phpzMe})_2] + \text{H}^+\}^+$. These results suggest that compound **19** retains its dinuclear structure in solution. Therefore, the redox behaviour of **19** has been studied in acetonitrile solution within the potential range -1.8 to 1.5 V *versus* an Ag/AgCl electrode at ambient temperature (300 K). The cyclic voltammogram of compound **1** shows one irreversible wave at $+1.2$ V that could be assigned to the oxidation of the ligand on the electrode surface. No cathodic peak could be observed in agreement with the high stability of the dinuclear cobalt(III) core in solution.

The NMR analysis of **19** shows a complicated spectrum due to the low symmetry of the compound. The peaks could not be assigned due to the splitting of multiple peaks in the aromatic region of the coordination compound as compared with the five peaks of the free ligand. Nevertheless the integration of the aromatic peaks is in agreement with the different coordination modes of the ligand in the coordination compound.

The study of the electrochemical behaviour of the copper(II) and nickel(II) compounds was carried out in CH₂Cl₂ solution in the range +1.2 to -1 V. For both **20** and **21**, a quasi-reversible ligand oxidation at 0.9 V has been observed in the positive range. No other redox processes were observed for **20**. For **21**, the additional anodic process observed at 0.62 V can be assigned to a quasi-reversible one electron oxidation of copper(II) to copper(III) ion and no cathodic process was observed. This result is not surprising given the preference of copper(I) ion for non-planar coordination geometry.

6.4. Conclusions

The synthesis, crystal structure and spectroscopic characterization of an unusual dinuclear cobalt(III) compound and two new mononuclear nickel(II) and copper(II) compounds have been presented. The reaction of the ligand 3(5)-methyl-5(3)-(2-hydroxyphenyl)-pyrazole with cobalt has provided access to a new dinuclear compound, in which the versatility of the ligand, showing four different coordination modes, is beautifully illustrated. This dinuclear cobalt compound is unique, as it is triply bridged by two pyrazolate and one phenoxide moieties with a Co...Co distance of 3.154 Å. This compound is stabilized through N-H...O intramolecular hydrogen interactions. Additionally N-H...N intermolecular hydrogen interactions are present with acetonitrile lattice molecules. ESI-MS and cyclic voltammetry studies have shown that the dinuclear compound is highly stable in solution. Additionally, the reaction of the H₂phpzMe ligand with nickel(II) and copper(II) ions readily affords stable mononuclear species of type [M(HphpzMe)₂] with square-planar geometry. In compound **20**, the ligand appears to be strong enough to generate the low-spin nickel(II) cation. The EPR of the copper(II) dope in this lattice has confirmed the geometry and chromophore.

6.5. References

1. Constable, E. C.; Steel, P. J., *Coord. Chem. Rev.*, **1989**, 93, 205-223.
2. LaMonica, G.; Ardizzoia, G. A., *Progr. Inorg. Chem.*, **1997**, 46, 151-238.
3. Mukherjee, R., *Coord. Chem. Rev.*, **2000**, 203, 151-218.
4. Halcrow, M. A., *Dalton Trans.*, **2009**, 2059-2073.
5. Klingele, J.; Dechert, S.; Meyer, F., *Coord. Chem. Rev.*, **2009**.
6. Tanase, S.; Aromí, G.; Bouwman, E.; Kooijman, H.; Spek, A. L.; Reedijk, J., *Chem. Commun.*, **2005**, 3147-3149.
7. Viciano-Chumillas, M.; Marqués-Giménez, M.; Tanase, S.; Evangelisti, M.; Mutikainen, I.; Turpeinen, M.; Smits, J. M. M.; de Gelder, R.; de Jongh, L. J.; Reedijk, J., *J. Phys. Chem. C*, **2008**, 112, 20525-20534.
8. Viciano-Chumillas, M.; Tanase, S.; Mutikainen, I.; Turpeinen, M.; de Jongh, L. J.; Reedijk, J., *Inorg. Chem.*, **2008**, 47, 5919-5929.

9. Addison, A. W.; Burke, P. J., *J. Heterocycl. Chem.*, **1981**, 18, 803-805.
10. Sheldrick, G. M. *Program for Empirical Absorption Correction*, University of Göttingen, Germany: 1996.
11. Beurskens, P. T.; Beurskens, G.; Strumpel, M.; Nordman, C. E., *In Patterson and Pattersons*. Glusker, J. P.; Patterson, B. K.; Rossi, M., Eds. Clarendon Press: Oxford: 1987.
12. Beurskens, P. T.; Beurskens, G.; Bosman, W. P.; De Gelder, R.; García-Granda, S.; Gould, R. O.; Israël, R.; Smits, J. M. M.; Smykalla, C. *The DIRDIF96. A computer program system for the crystal structure determination by Patterson methods and direct methods applied to difference structure factors*, Crystallography Laboratory, University of Nijmegen: Nijmegen, The Netherlands, 1996.
13. Sheldrick, G. M. *SHELXL-97: Program for the refinement of crystal structures*, University of Göttingen; Germany: Göttingen, 1997.
14. Duisenberg, A. J. M. Reflections on area detectors. PhD thesis, Utrecht, 1998.
15. *COLLECT, data collection software*, Nonius, B.V.: 1999.
16. Spek, A. L. *PLATON, A Multipurpose Crystallographic Tool*, Utrecht University; The Netherlands, 2003.
17. Nakamoto, K., *Infrared and Raman Spectra of Inorganic and Coordination Compounds*. 4th ed.; John Wiley & Sons Inc New York, 1986.
18. Lever, A. B. P., *Inorganic Electronic Spectroscopy*. Elsevier: Amsterdam, 1997.
19. Aromí, G.; Bouwman, E.; Burzuri, E.; Carbonera, C.; Krzystek, J.; Luis, F.; Schlegel, C.; van Slageren, J.; Tanase, S.; Teat, S. J., *Chem.-Eur. J.*, **2008**, 14, 11158-11166.
20. Dingle, R., *Inorg. Chem.*, **1971**, 10, 1141-1144.
21. Dreos, R.; Tazher, G.; Trendafilova, D. H.; Nardin, G.; Randaccio, L., *Inorg. Chem.*, **1996**, 35, 2715-2716.
22. Chattopadhyay, S.; Bocelli, G.; Musatti, A.; Ghosh, A., *Inorg.Chem.Comm.*, **2006**, 9, 1053-1057.
23. Campbell, V. D.; Parsons, E. J.; Pennington, W. T., *Inorg. Chem.*, **1993**, 32, 1773-1778.
24. Seo, J. S.; Hynes, R. C.; Williams, D.; Chin, J.; Sung, N. D., *J. Am. Chem. Soc.*, **1998**, 120, 9943-9944.
25. Benisvy, L.; Kannappan, R.; Song, Y. F.; Milikisyants, S.; Huber, M.; Mutikainen, U.; Turpeinen, P.; Gamez, P.; Bernasconi, L.; Baerends, E. J.; Hartl, F.; Reedijk, J., *Eur. J. Inorg. Chem.*, **2007**, 637-642.
26. Hathaway, B. J., *Comprehensive Coordination Chemistry*. Wilkinson, G.; Gillard, R. D.; McCleverty, J. A., Eds. Pergamon Press: Oxford, 1987.
27. Mabbs, F. E.; Collison, D., *Electronic Paramagnetic Resonance of d Transition Metal Compounds*. Elsevier: Amsterdam, 1992.

Chapter 7

Summary, conclusions and perspectives

7.1. Summary, conclusions and future perspectives

This last chapter deals with a brief overview and evaluation of all the herein described work and it provides some conclusions and suggestions for further research.

Numerous efforts have been undertaken to develop new molecular magnetic materials.¹ To achieve such a task, it is necessary to understand the magnetic properties at the nanoscopic level. In coordination chemistry, the origin of the magnetic moments stems from the unpaired electrons of transition-metal ions or rare-earth ions. Nevertheless, the presence of organic ligands is required to bridge the metal ions and to stabilize the whole molecule. Therefore, the magnetic properties generally depend on the nature of the paramagnetic metal ion, on the ability of the ligand to propagate magnetic exchange interactions between the metal ions and on the different structural topologies imposed by the metal-ligand interactions.

In this thesis, the manganese(III) ion has been selected to study its coordination chemistry with a variety of new phenol-pyrazole ligands, because of its paramagnetic behaviour. The manganese(III) ion displays negative Ising-type of anisotropy, which often leads to interesting magnetic properties.¹ Carboxylates and Schiff-base ligands are well known bridging ligands, able to stabilize the manganese ion in various oxidation states in polymetallic clusters.^{2,3} Therefore, efforts have been undertaken in the search for new types of ligands, which would preferentially give novel polymetallic systems with peculiar magnetic properties. The selection of the bridging ligand is crucial for the synthesis of novel molecules with the desired topology and magnetic properties; therefore in Chapter 1 a detailed bibliographic survey has been presented to understand the ability of the pyrazole to act as a bridging ligand capable to propagate the magnetic exchange interactions in polymetallic compounds. In this thesis project, a phenol group has been introduced as substituent on the pyrazole ring, to enhance the number of possible binding sites for the metal ions due to the oxygen-donor site. Therefore, a series of phenol-pyrazole ligands has been synthesized with variations in the 5-position of the pyrazole ring, *i.e.* hydrogen, methyl, ethyl and phenyl, to investigate the role of the ligand in the formation of new complexes. Consequently, the aim of this PhD research work has been to explore the coordination chemistry of these new phenol-pyrazole based ligands towards mainly the manganese(III) ion and to study the formation of new complexes and their magnetic properties.

In Chapter 2, a family of mononuclear manganese(III) compounds is presented with the general formula $[\text{Mn}(\text{HphpzR})_2\text{X}]$ ($\text{R} = \text{H}, \text{Me}, \text{Et}, \text{Ph}$ and $\text{X}^- = \text{Cl}^-, \text{Br}^-$). All these compounds contain a square-pyramidal geometry for manganese(III). It is shown how the nature of the ligand determines the crystal packing, since the presence of small substituents in the 5-position of the pyrazole ring allows the formation of 1-D chains stabilized by hydrogen bonding, whereas bulky substituents in the 5-position of the pyrazole ring, *i.e.* phenyl,

preclude the formation of such chains. Magnetic and thermal properties were studied, showing the importance of the crystal packing on the magnetic properties. The effect on the magnetic exchange interaction by the exchange of the halogen from chloride to bromide was also analyzed in this type of compounds. Compounds of formula $[\text{Mn}(\text{HphpzH})_2\text{X}]$ ($\text{X}^- = \text{Cl}^-$, Br^-) form chains, which are stabilized by strong hydrogen bonding and the distances between the manganese(III) ions are small enough to form magnetic chains. The analysis of the magnetic data and the thermal studies, as reported in Chapter 2, indicated Heisenberg type of chains with XY (planar) anisotropy (positive sign of D). The presence of long-range ordering was observed at *ca.* 1.5 K with specific heat studies. The finding of a planar type of anisotropy was a bit surprising, since the manganese(III) ion in most cases displays an Ising-type of anisotropy (negative D).⁴ As described in Appendix A, HFEP spectroscopy was therefore performed to determine more reliably the sign and magnitude of the zero-field splitting parameters, D and E of these two compounds. The HFEP spectra of the compounds in their powder form are reported, revealing indeed a negative sign of D and in addition a large E parameter for both compounds. Probably the absence of the E term in the theoretical models available for the analysis of the specific heat data is at the origin of the discrepancy in the sign of the D term found in the two experiments. The additional HFEP spectra, taken in solution, revealed drastic changes in the zero-field splitting parameters, indicating the low stability of these compounds in solution. In Appendix A a discussion of the sign and magnitude of the zero-field splitting parameters for other mononuclear manganese(III) compounds reported in the literature in relation to their crystal structure is also presented. The sign and the magnitude of the zero-field splitting parameter, D , is found to depend mainly on the type of ligands at the axial positions. Therefore, the study of different monodentate ligands at the axial position can be of interest, especially the iodide ligand which might lead to a positive sign of D . The replacement of the monodentate ligand X^- in compounds $[\text{Mn}(\text{HphpzH})_2\text{X}]$ can be interesting not only for the study of the zero-field splitting parameters, but also for the possible effect on the strength of the magnetic exchange interaction. For instance, the introduction of a smaller ligand, such as the fluoride ion, can be expected to increase the strength of the magnetic exchange interaction, similar as observed when bromide is replaced by chloride. The compounds $[\text{Mn}(\text{HphpzMe})_2\text{X}]$ ($\text{X}^- = \text{Cl}^-$, Br^-) also form 1-D chains and an increase of the distance between the manganese(III) ions along the chain is imposed by the ligand H_2phpzMe . As a consequence, weaker antiferromagnetic interactions are observed in comparison with the compounds $[\text{Mn}(\text{HphpzH})_2\text{X}]$ ($\text{X}^- = \text{Cl}^-$, Br^-) and 1-D magnetic ordering is not observed above 2 K. The introduction of a bulky substituent in the pyrazole ring, such as a phenyl group, precludes the formation of 1-D chains, as observed in the compounds $[\text{Mn}(\text{HphpzPh})_2\text{X}]$ ($\text{X}^- = \text{Cl}^-$, Br^-). Since the distances

between the manganese(III) ions are large, almost a paramagnetic behaviour is observed. A bulky phenol-pyrazole ligand induces weaker magnetic exchange interactions between the manganese(III) ions. To overcome this, the substitution of the halogen could be performed by other functional groups, such as azide, acetate or dicyanamide. Thus, 1-D chains oriented along the perpendicular direction of the plane formed by the phenol-pyrazole ligands and the manganese(III) would be formed. In such compounds, the new structural effects on the magnetic exchange interaction could be studied. In addition, the compounds $[\text{Mn}(\text{HphpzR})_2\text{X}]$ can also be used for the synthesis of high nuclearity compounds, as shown in Chapter 3; the lability of the halogen, the empty position in the coordination sphere of the manganese(III) ion and the still empty coordination bonding site of the N–H group of the pyrazole ring allow the formation of interesting clusters. The investigation of these compounds as building blocks could be further explored with various other bridging ligands, such as cyanide, azide, dicyanamide, *etc.*, or with preformed complexes to form new compounds with different topologies.³

Chapters 3 and 4 deal with oxide-centred trinuclear manganese(III) complexes.^{5,6} All of them contain the trinuclear core $[\text{Mn}_3(\mu_3\text{-O})(\text{phpzR})_3]^+$, in which the three phenol-pyrazole ligands are in the plane formed by three manganese(III) ions and the axial positions are occupied by solvent molecules (methanol or ethanol) and bridging ligands (carboxylate and azide). As a result, in these chapters the influence of the type of phenol-pyrazole ligand and of the co-ligands on the structural symmetry of the $[\text{Mn}_3(\mu_3\text{-O})(\text{phpzR})_3]^+$ and consequently, on its magnetic properties, have been carefully investigated. Apparently the role of the phenol-pyrazole ligand is to determine the type of structure that is formed, *i.e.* either an isolated trinuclear unit or a 1-D chain.⁵⁻¹⁰ In these 1-D chains, the trinuclear units can be linked by a bridging ligand, *i.e.* acetate and azide or by hydrogen bonding interactions. Substituents in the 4-position of the phenol ring allow the formation of 1-D chains.⁷⁻¹⁰ The introduction of these substituents do not create a distortion of the $[\text{Mn}_3(\mu_3\text{-O})]^{7+}$ core and might control the separation between the 1-D chains. However, the substituents in the 5-position of the pyrazole ring,^{5,6} such as methyl or phenyl can generate a difference in the $[\text{Mn}_3(\mu_3\text{-O})]^{7+}$ core and the dimensionality of the complex depending on the type of ligands at the axial positions of the three manganese(III) ions. The presence of substituents in the 5-position of the pyrazole ring, such as methyl or phenyl, drives the carboxylate to bind to two manganese(III) ions from the same trinuclear manganese(III) unit, instead of bridging the trinuclear units (Chapter 3 and 4). If the carboxylate ligand is small, *i.e.* acetate, these trinuclear units can form chains because of the hydrogen bonds established between the carboxylate and solvent molecules (compounds **11** and **13**). If the carboxylate ligand is bulkier, such as benzoate, two carboxylates are binding to the two manganese(III) ions of the same trinuclear unit

(compounds **14** and **15**) and they become isolated. Consequently, in all these cases with carboxylate ligands, the Mn–O–Mn angle(s) in which the carboxylate ligand binds the manganese(III) ions from the same trinuclear unit is (are) found to deviate strongly from the value of 120° towards smaller values; whereas the remaining angle(s) is (are) distorted toward higher values. The coordinated solvent molecules are also found to be important. The number of solvent molecules bound to manganese(III) ions can vary. For example in compound **13** only one solvent molecule is coordinated (ethanol), instead of three methanol molecules in compound **11**, thereby forcing the trinuclear units in the 1-D chain to be closer than when methanol is present. In all trinuclear manganese(III) compounds containing phenol-pyrazole ligands, predominant antiferromagnetic interactions are found between the manganese(III) ions in the trinuclear unit. For an equilateral triangle, the Mn–O–Mn angles are 120° and the oxide bridge lie in the plane formed by the three manganese(III) ions. In this geometry, antiferromagnetic interactions are indeed to be expected. However, when a distortion in the $[\text{Mn}_3(\mu_3\text{-O})]^{7+}$ core is present, notably when the Mn–O–Mn angles become smaller than 120° and a concomitant displacement of the $\mu_3\text{-O}^{2-}$ from the plane formed by the three manganese(III) ions occurs, the type of magnetic interactions between the manganese(III) ions may change drastically. In the present project such examples were encountered with the compounds $[\text{Mn}_3(\mu_3\text{-O})(\text{phpzMe})_3(\text{MeOH})_3(\text{OAc})] \cdot 1.5\text{MeOH}$ (**11**) and $[\text{Mn}_3(\mu_3\text{-O})(\text{phpzMe})_3(\text{O}_2\text{CMe})(\text{EtOH})] \cdot \text{EtOH}$ (**13**), in which a ferromagnetic interaction was deduced in relation to the uniquely distorted pathway. Since the most important structural parameter in the magnetic exchange path has been found to be the Mn–O–Mn angle, the distortion in the three angles should be responsible for the occurrence of predominant ferromagnetic interactions. Therefore, to achieve overall ferromagnetic behaviour in the triangle, the introduction of a suitable ligand able to distort the three Mn–O–Mn angles toward smaller values is needed. The introduction of a third carboxylate ligand might induce such distortion, since the presence of two carboxylate ligands induces the distortion in two Mn–O–Mn angles (Chapter 4). Another possible bridging ligand could be a group able to bind all the three manganese(III) ions together, *i.e.* a triol-based ligand, $(\text{HO})_3\text{CR}'$ ($\text{R}' = \text{CF}_3$, *etc.*). However, in both cases, the compound will need two positive counter ions to balance the total charge of the complex. Another option is the addition of a counter ion, *i.e.* perchlorate or tetraphenylborate in which the distortion of the $[\text{Mn}_3(\mu_3\text{-O})]^{7+}$ core can be caused by electronic effects. The overall magnetic behaviour that have been found in the trinuclear manganese(III) units with phenol-pyrazole ligands are all antiferromagnetic so far.⁵⁻¹⁰ However, the dimensionality of the compounds and the packing of these trinuclear units is important to observe different magnetic exchange interactions between the trinuclear

manganese(III) units. The majority of the trinuclear compounds composed by phenol-pyrazole ligands forms 1-D chains, in which the trinuclear units are bridged by acetate, or azide ligands.^{5,7-10} In case of the introduction of a substituent in the 5-position of the pyrazole ring, such as methyl, the acetate ligand binds to two manganese(III) ions from the same trinuclear units (compound **11** and **13**).^{5,6} As a consequence, the trinuclear units are forming 1-D chains stabilized by the hydrogen bonding established between the solvent molecules and the acetate ligand. In the case of a bulkier carboxylate ligands, such as benzoate, two carboxylate ligands are at the axial positions of the manganese(III) ions of the trinuclear units. Therefore, these trinuclear units become isolated (compounds **14** and **15**). In most of the 1-D chains, ferromagnetic interactions are observed between the trinuclear units that form the chain.⁶⁻¹⁰ Therefore, different magnetic behaviours are observed, varying from single-chain magnet behaviour to long-range magnetic ordering.⁵⁻¹⁰ To elucidate the factors that determine the type of magnetic exchange interactions and the dimensionality of the magnetic ordering in trinuclear manganese(III) units, the synthesis of new 1-D chains formed by trinuclear complexes is needed. Variations in the bridging ligands, such as using formate, terephthalate or even nitrogen-donor ligands, like pyrazine can be applied to bridge the trinuclear manganese(III) units. Moreover, reactions with non-alcoholic solvents, like pyridine, could be tried to check if the $[\text{Mn}_3(\mu_3\text{-O})(\text{phpzR})_3]^+$ core is retained. In addition, the trinuclear units can also be used as building blocks to obtain clusters of even higher nuclearities or other topologies as it has been performed with the basic carboxylates, $[\text{Mn}_3(\mu_3\text{-O})(\text{O}_2\text{CR})_6\text{L}_3]^+$.¹¹

Chapter 5 deals with the synthesis and characterization of high-nuclearity manganese(III) compounds. Additionally, Appendix B contains some crystallographic information of these compounds. Previously, the compound $[\text{Mn}_8(\mu_4\text{-O}_4)(\text{phpzMe})_8(\text{thf})_4]$ has been reported in our group.¹² Therefore, in the present study the influence of different solvents on the stability of the $[\text{Mn}_8(\mu_4\text{-O}_4)(\text{phpzR})_8]$ core has been investigated. The $[\text{Mn}_8(\mu_4\text{-O}_4)(\text{phpzR})_8]$ core is preserved when the H_2phpzH or the H_2phpzMe ligands are employed even when using solvents, such as ethanol or acetonitrile. However, the use of a bulkier ligand such as H_2phpzEt under suitable synthetic conditions induces the formation of a new type of core, probably due to the steric effects imposed by the ethyl group. Instead, a hexanuclear compound is obtained, $[\text{Mn}_6(\mu_3\text{-O})_4(\mu_3\text{-Br})_2(\text{HphpzEt})_6(\text{phpzEt})]$ (**18**). In the octanuclear manganese(III) compounds $[\text{Mn}_8(\mu_4\text{-O}_4)(\text{phpzR})_8(\text{s})]$ ($\text{R} = \text{H}, \text{Me}$; $\text{s} = \text{solvent}$), strong antiferromagnetic interactions between the manganese(III) ions are present (Chapter 5 and ref. 12) leading to a ground state of $S_T = 0$. The solvent does not neither modify the type of structure, nor the magnetic properties, since the strong antiferromagnetism is due principally to the magnetic exchange interaction between the manganese(III) ions in the core and in the periphery and weak antiferromagnetic interactions are expected to be present between the

manganese(III) ions in the core. However, in the hexanuclear compound **18**, weak ferromagnetic interactions are observed. Apparently, this new core favours the existence of weak ferromagnetic interactions. Due to the low symmetry of the cluster it is very difficult to quantify the magnetic exchange interaction. DFT studies would be appealing to determine the main magnetic paths to further modify the molecule and increase the strength of the magnetic exchange interactions. In addition, studies at lower temperatures (< 2 K) could be performed to check the type of magnetic ordering. Although non-coordinated solvents are present in the cluster, the synthesis in other solvents might lead to the same cluster or new complexes. Although the bromide atoms are weakly bonded to the manganese(III) ions and are not expected to provide a strong magnetic exchange path, it would be of interest to replace them by chloride or azide ligands.

Chapter 6 presents the coordination chemistry of the ligand H₂phpzMe towards other transition metal ions, such as cobalt(III), copper(II) and nickel(II). The choice of the transition-metal ion can lead to different products. In the case of cobalt, a dinuclear cobalt(III) compound is formed by aerial oxidation of the cobalt(II) ion. This compound is diamagnetic and the four different binding modes of the ligand to cobalt(III) ion highlight the coordination versatility of the phenol-pyrazole ligands. In the case of nickel(II) and copper(II) ions, isostructural mononuclear compounds are formed. These compounds have been prepared by numerous synthetic routes, indicating their high stability. However, under specific conditions, clusters can also be formed.^{13,14} So, suitable synthetic conditions could lead to the formation of other new compounds. In the case of copper(II) ion, an excess of base would be enough to doubly deprotonate the H₂phpzMe ligand and the copper(II) ions could be coordinated to the three possible binding sites since an octahedral geometry is also favoured by copper(II) ions. By contrast, in the case of nickel(II) ions this might be more difficult, since the nickel(II) ion, being diamagnetic, has a strong preference for the square-planar geometry.

7.2. References

1. Gatteschi, D.; Sessoli, R.; Villain, J., *Molecular Nanomagnets*. Oxford University Press: UK, 2006.
2. Christou, G., *Polyhedron*, **2005**, 24, 2065-2075.
3. Miyasaka, H.; Saitoh, A.; Abe, S., *Coord. Chem. Rev.*, **2007**, 251, 2622-2664.
4. Krzystek, J.; Ozarowski, A.; Telser, J., *Coord. Chem. Rev.*, **2006**, 250, 2308-2324.
5. Viciano-Chumillas, M.; Tanase, S.; Mutikainen, I.; Turpeinen, M.; de Jongh, L. J.; Reedijk, J., *Inorg.Chem.*, **2008**, 47, 5919-5929.
6. Viciano-Chumillas, M.; Tanase, S.; Mutikainen, I.; Turpeinen, U.; de Jongh, L. J.; Reedijk, J., *Dalton Trans.*, **2009**, 7445-7453.
7. Bai, Y. L.; Tao, J.; Wernsdorfer, W.; Sato, O.; Huang, R. B.; Zheng, L. S., *J. Am. Chem. Soc.*, **2006**, 128, 16428-16429.
8. Liu, C. M.; Zhang, D. Q.; Zhu, D. B., *Chem. Commun.*, **2008**, 368-370.
9. Liu, C. M.; Zhang, D. Q.; Zhu, D. B., *Inorg.Chem.*, **2009**, 48, 4980-4987.

10. Tao, J.; Zhang, Y. Z.; Bai, Y. L.; Sato, O., *Inorg. Chem.*, **2006**, 45, 4877-4879.
11. Christou, G., *Accounts Chem. Res.*, **1989**, 22, 328-335.
12. Tanase, S.; Aromí, G.; Bouwman, E.; Kooijman, H.; Spek, A. L.; Reedijk, J., *Chem. Commun.*, **2005**, 3147-3149.
13. Aromí, G.; Bouwman, E.; Burzuri, E.; Carbonera, C.; Krzystek, J.; Luis, F.; Schlegel, C.; van Slageren, J.; Tanase, S.; Teat, S. J., *Chem.-Eur. J.*, **2008**, 14, 11158-11166.
14. Bai, Y. L.; V., T.; Huang, R. B.; Zheng, L. S.; Tao, J., *Chem.-Eur. J.*, **2009**, 15, 2377-2383.

Appendix A

HFEPR spectroscopic studies for $[\text{Mn}(\text{HphpzH})_2\text{X}]$ ($\text{X}^- = \text{Cl}^-$, Br^-) as complementary tool of magnetic susceptibility and specific heat techniques

HFEPR spectroscopy have been used to determine the magnetic anisotropy as represented by the zero-field splitting parameters, D and E , for the compounds $[\text{Mn}(\text{HphpzH})_2\text{X}]$ ($\text{X}^- = \text{Cl}^-$ (1), Br^- (2)) presented in Chapter 2. A discussion of the sign and magnitude of the zero-field splitting parameters obtained by the different techniques is given in relation to the crystal structure of mononuclear manganese(III) compounds reported in the literature.

A.1. Introduction

Electron paramagnetic resonance (EPR) spectroscopy is a well known technique for determining the spin Hamiltonian parameters, in particular the zero-field splitting, since it measures the magnetic field at which radiation of the appropriate frequency is absorbed by molecules with unpaired spins. The corresponding splittings between the different energy states arise from the interaction of the unpaired electrons with the magnetic field (Zeeman Effect), which is given by the formula:

$$\Delta E = h\nu = m_s g \beta B \quad (1)$$

For more information on general EPR spectroscopy, see ref.1,2. In recent years, the EPR technique has been extended to the so-called HFEPR with the possibility of measuring at very high fields (25 T and above) and frequencies (900 GHz and above), *i.e.* far above the conventional W-band frequency (95 GHz) and field (3.4 T).^{3,4} Thus, some important advantages are achieved such as the increase of the spectral resolution for quasi-isotropic ($g \sim 2$) system and particularly that the ‘EPR-silent’ species at X-band become EPR detectable. The latter situation occurs for non-Kramers or integer spin systems with large zero-field splitting. These include complexes with such transition-metal ions as chromium(II), iron(II), nickel(II), vanadium(III), and particularly manganese(III).⁵⁻⁷ In these cases, (HF)EPR can determine the zero-field splitting parameters with a great accuracy. Therefore it can be used as a complementary technique together with the magnetic susceptibility studies to determine properly the magnetic and electronic properties of the studied systems.

In Chapter 2 of this thesis, mononuclear manganese(III) compounds with the general formula $[\text{Mn}(\text{HphpzH})_2\text{X}]$ ($\text{H}_2\text{phpzH} = 3(5)\text{-}(2\text{-hydroxyphenyl})\text{pyrazole}$, $\text{X}^- = \text{Cl}^-$ (**1**), Br^- (**2**)) are described. In both compounds, the manganese(III) ion has a square-pyramidal geometry. Intermolecular hydrogen bonds are present, thereby forming ladder-like chains. Temperature-dependent susceptibility and magnetic specific heat measurements on **1** and **2** have indicated the presence of antiferromagnetic $S = 2$ chains, the magnetic interaction being described by the anisotropic Heisenberg model with predominantly planar (XY) type of crystal field anisotropy.⁸ On the other hand, the manganese(III) ion usually displays an Ising-type of anisotropy, due to the presence of an elongated Jahn-Teller axis. Accordingly, HFEPR spectroscopy has been used to determine more accurately the magnetic anisotropy of the above compounds as represented by the zero-field splitting parameters, D and E . In this appendix, the spectra in both powder samples and in solution are reported for the mononuclear compounds, which have been used as building blocks to synthesize compounds of higher nuclearities (Chapter 3).⁹ A discussion of the sign and magnitude of the zero-field splitting parameters obtained by the different techniques is given in relation to the crystal structure of these mononuclear manganese(III) compounds.

A.2. Experimental Section

Materials and Samples. [Mn(HphpzH)₂X] (H₂phpzH = 3(5)-(2-hydroxyphenyl)pyrazole, X⁻ = Cl⁻ (**1**), Br⁻ (**2**)) are synthesized as described in Chapter 2.⁸

Physical Measurements. Electronic absorption spectra were recorded on a Varian Cary 50 UV-visible spectrophotometer using cuvettes of 1 cm path length. HFEPR spectra were recorded using the EMR Facility at the National High Magnetic Field Laboratory in Tallahassee, Florida. The experimental setup utilizes a variety of solid-state sources and a superconducting 15/17 T magnet.¹⁰ Detection was provided with an InSb hot-electron bolometer (QMC Ltd., Cardiff, UK). Modulation for detection purposes was provided by modulating the magnetic field, which delivered a first derivative shape. A Stanford Research Systems SR830 lock-in amplifier converted the modulated signal to DC voltage. Polycrystalline manganese(III) compounds frequently experience field-induced torquing phenomena; as a result the crystallites tend to align their easy axis with the direction of the magnetic field and the perpendicular transitions are thereby suppressed. To avoid this phenomenon, immobilization with KBr and pressing into a pellet was done for compounds **1** and **2**. Spectra were also collected for **1** and **2** in a low-temperature methanol glass. Often the compounds are dissolved in an inert solvent or non-coordinating solvent. In this case, methanol was chosen as a solvent for solubility reasons. HFEPR spectra were recorded in a 146–619 GHz range using a locally constructed-type multifrequency instrument.¹⁰

Theory for EPR spectra. To analyze the EPR spectra, the most general spin Hamiltonian has been applied for an $S = 2$ spin state including both the Zeeman, and the second-order terms of the zero-field splitting (ZFS):

$$H = \beta B g S + B_2^0 O_2^0 + B_2^2 O_2^2 \quad (3)$$

Commonly the second-order ZFS parameters are written as $D = 3B_2^0$ and $E = B_2^2$ and the spin Hamiltonian can be expressed as:

$$H = \beta B g S + D(S_z^2 - S(S+1)/3) + E(S_x^2 - S_y^2) \quad (4)$$

The zero-field energy levels resulting from the spin Hamiltonian for $S = 2$ are shown in Figure A.1 in zero and non-zero applied magnetic field.

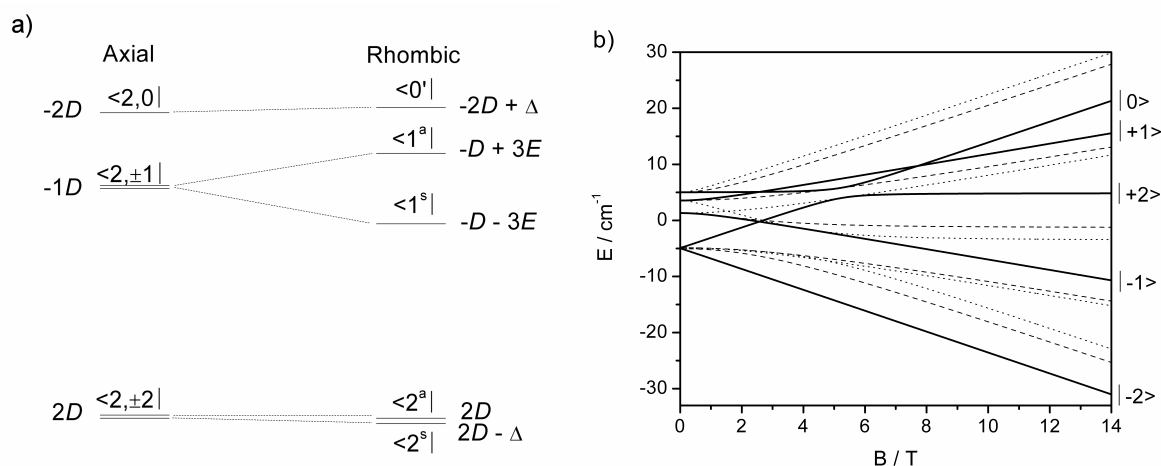


Figure A.1. a) Effect of particular zero-field splitting terms of the spin Hamiltonian for $S = 2$ with $D = -2.43 \text{ cm}^{-1}$, $E = -0.37 \text{ cm}^{-1}$, $g_{\text{iso}} = 2$, being $\Delta = 3E^2/D$. b) Energy level diagram for such system under applied magnetic field. Solid lines are for B_z ; dash lines are for B_x ; dotted lines are for B_y . The spin functions of the B_z levels are indicated.

A.3. Results and Discussion

HFEPR of solid-state $[\text{Mn}(\text{HphpzH})_2\text{X}]$ ($\text{X}^- = \text{Cl}^-$ (1), Br^- (2)). HFEPR spectra were recorded at different frequencies in the 4–30 K temperature range for compounds **1** and **2**. Figure A.2 shows the HFEPR spectra obtained at 5 and 10 K for **1** (a) and **2** (b), respectively at different frequencies. The dominant signal observed in these conditions is assigned to the parallel $|S, M_S\rangle = |2, -2\rangle \rightarrow |2, -1\rangle$ transition, as is the case for other $S = 2$ systems with negative D . The main signal shifts to higher fields with increasing frequency. As shown in the insets of Figure A.2, this field-frequency dependence can be fitted to the linear relationship $g\beta B_r = h\nu - 3D$,¹¹ in which $3D$ corresponds to the difference between the $-2\rangle$ to $-1\rangle$ energy levels for an axial system with $D < 0$ (Figure A.1a). Using this very approximate method, the zero-field splitting parameters can be estimated as: $D = -2.52 \text{ cm}^{-1}$ and -1.76 cm^{-1} , with $g = 2.04$ and $g = 2.00$, for **1** and **2**, respectively.

The magnetic properties of compounds **1** and **2** can be described by the spin Hamiltonian for a single ion (see equation 4). Therefore, depending on the zero-field splitting parameters, the energy levels will split in the presence of the magnetic field with x , y and z orientations in different ways. In Figure A.1b, the energy level diagram is shown for an $S = 2$ system with $D = -2.43 \text{ cm}^{-1}$, $E = -0.37 \text{ cm}^{-1}$, $g_{\text{iso}} = 2$ for the three different orientations of the field. In case of a powder, one has to average over the three directions. To determine better the zero-field splitting parameters and to characterize the peaks of smaller intensities, simulations were performed and compared with the experimental data using the SPIN program by A. Ozarowski. As a result in Figure A.5, the relationship between the frequency and the

resonance field is shown. Depending on the frequency used, the quality of the spectra varies (see Figure A.2). The sign of D is very difficult to assign at low frequencies for compounds **1** and **2**, due to the poor quality of the spectra. However at high frequencies, a clear negative sign of D is found. Simulated spectra with positive and negative D for compounds **1** and **2** are shown in Figure A.3, with the zero-field splitting parameters being $D = -2.43 \text{ cm}^{-1}$, $E = -0.37 \text{ cm}^{-1}$, $g_{\text{iso}} = 2$ and $D = -1.64 \text{ cm}^{-1}$, $E = -0.33 \text{ cm}^{-1}$, $g_{\text{iso}} = 2$ for compounds **1** and **2**, respectively. As shown in Figure A.3, a dominant resonance appears at 5.7 T and 7.9 T for compounds **1** and **2**, respectively, which can be assigned to the parallel $|S, M_S\rangle = |2, -2\rangle |2, -1\rangle$ transition. Due to the high rhombicity of compounds **1** and **2** and the low quality of the spectra, the assignment of other peaks is very difficult.

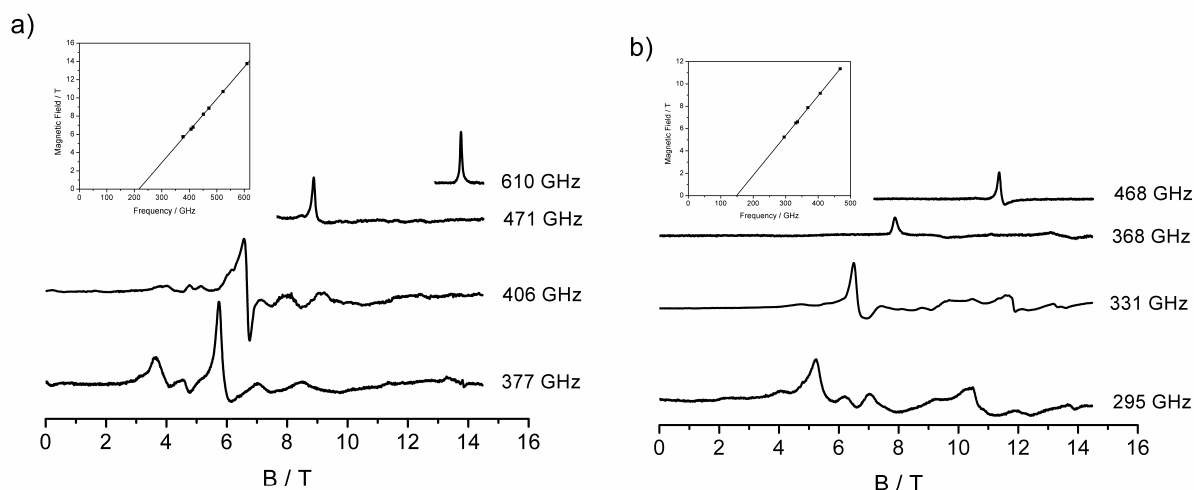


Figure A.2. HFEPN spectra of a solid polycrystalline **1** (a) and **2** (b) at 5 and 10 K, respectively at indicated frequencies. Insets, resonance field vs frequency dependence of the dominating transition.

To gain further information, measurements at higher temperatures were performed, where the excited spin levels become populated. Although the signal-to-noise ratio becomes worse at higher temperatures, no unusual changes were observed for both compounds in terms of spectral shape (Figure A.4). For compounds **1** and **2**, the signal assigned to the $|2, -2\rangle |2, -1\rangle$ transition become broader at higher temperatures, as often observed due to the population of the excited states. At 30 K, the intensity of the dominant signal decreases and the resonance corresponding to the transition $|2, -1\rangle |2, 0\rangle$ that appears around 11 T for compound **2**, becomes more intense due to the population of the excited states.

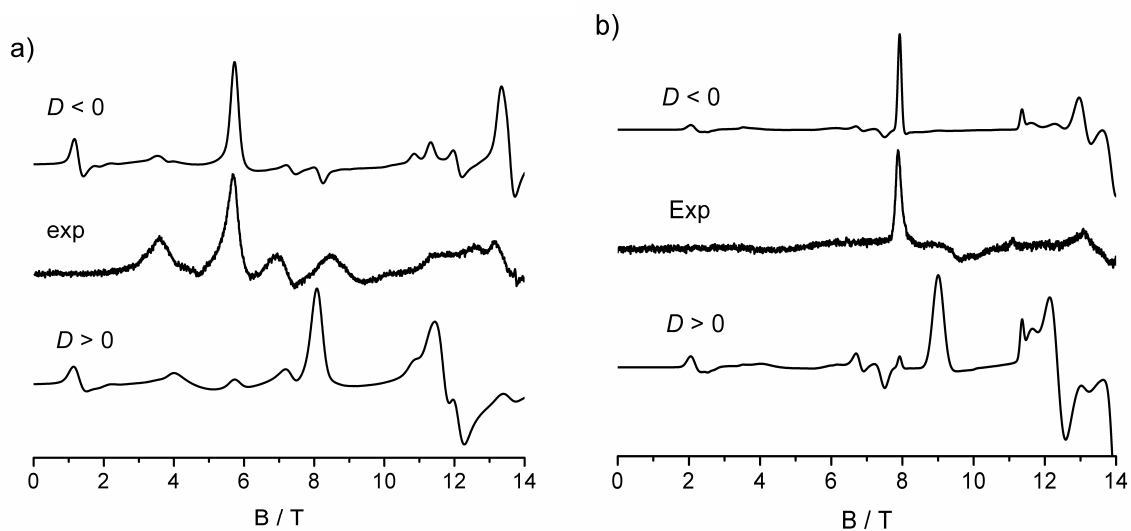


Figure A.3. HFEPR spectra of the solid polycrystalline **1** (a) at 377 GHz and 5 K and the solid polycrystalline **2** (b) at 368 GHz and 10 K. Simulated spectra were obtained using spin Hamiltonian parameters $D = -2.43 \text{ cm}^{-1}$, $E = -0.37 \text{ cm}^{-1}$, $g_{\text{iso}} = 2$ and $D = -1.64 \text{ cm}^{-1}$, $E = -0.33 \text{ cm}^{-1}$, $g_{\text{iso}} = 2$ for compounds **1** and **2**, respectively, and the simulations with the same zero-field splitting parameters with a positive D are also included.

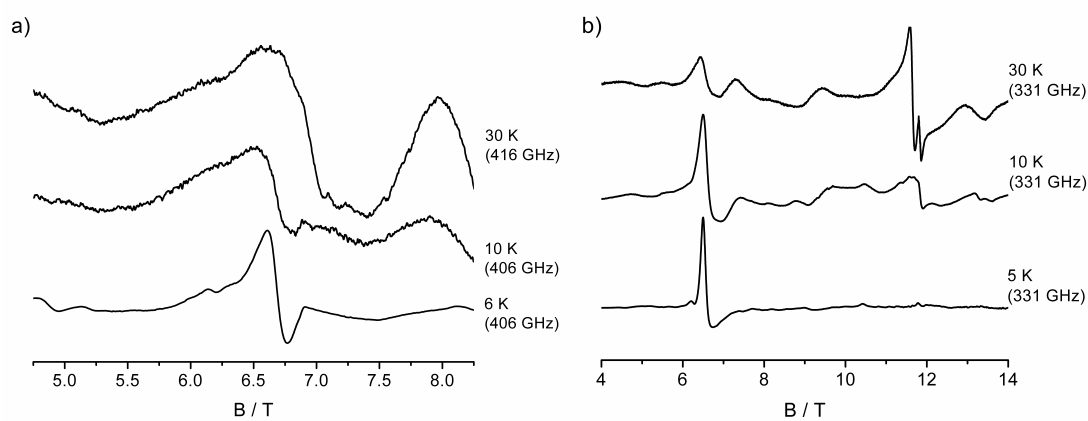


Figure A.4. HFEPR spectra of a solid polycrystalline **1** (a) and **2** (b) at indicated frequencies and temperatures.

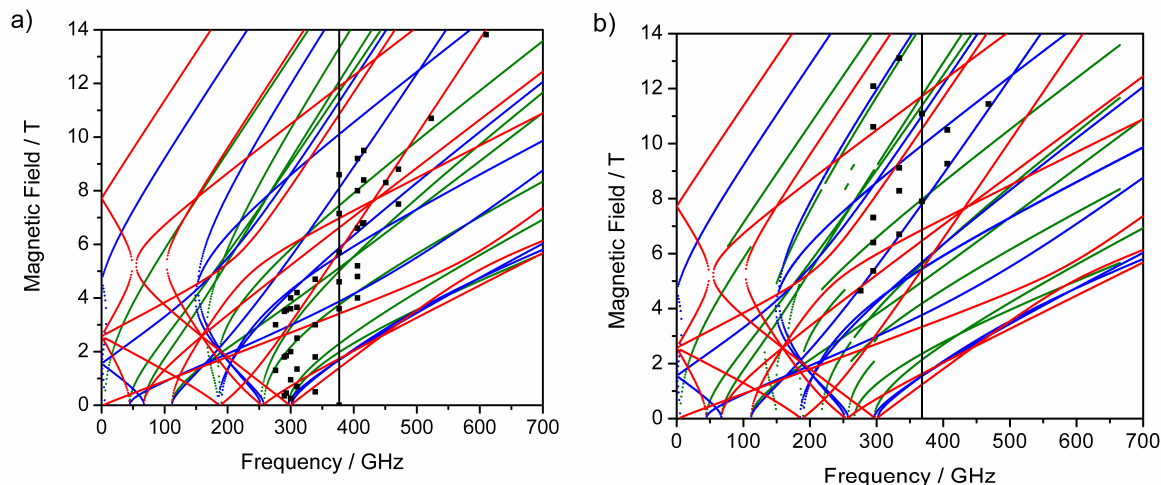


Figure A.5. a) Resonance field vs frequency dependence of HF-EPR signals for $S = 2$, $D = -2.43 \text{ cm}^{-1}$, $E = -0.37 \text{ cm}^{-1}$ and $g_{\text{iso}} = 2$. b) Resonance field vs frequency dependence of HF-EPR signals for $S = 2$, $D = -1.64 \text{ cm}^{-1}$, $E = -0.33 \text{ cm}^{-1}$ and $g_{\text{iso}} = 2$. Green lines, turning points with for $B_{\parallel x}$; blue lines, turning points with for $B_{\parallel y}$; red lines, turning points with for $B_{\parallel z}$. Line parallel to the y axis indicates the frequency 377 GHz. The square points represent the experimental points for solid compounds **1** (a) and **2** (b).

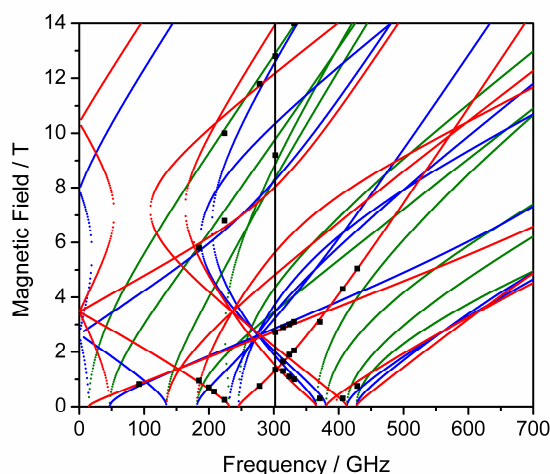


Figure A.6. Resonance field vs frequency dependence of HF-EPR signals for $S = 2$, $D = -3.32 \text{ cm}^{-1}$ and $E = -0.75 \text{ cm}^{-1}$. Green lines, turning points with for $B_{\parallel x}$; blue lines, turning points with for $B_{\parallel y}$; red lines, turning points with for $B_{\parallel z}$. Line parallel to the y axis indicates the frequency 377 GHz. The square points represent the experimental points for compounds **1** and **2** in solution.

HF-EPR of frozen solutions. The magnetic properties of the molecules can be influenced by intermolecular exchange effects which in EPR introduce line broadening.¹² A frozen solution spectrum can eliminate these unwanted effects, often resulting in a nicer spectrum. HF-EPR spectra at different frequencies were thus recorded in methanol glass for compounds **1** and **2**. Although it is not an inert solvent, it was chosen for solubility reasons. Both spectra

for compounds **1** and **2** turned out to be identical. The spectra are shown in Figure A.7. Significant differences were observed between the solid and the frozen solution. For example, at 302 GHz, a strong signal appears at 1.26 T, ascribed to the parallel $|S, M_S\rangle = |2, -2\rangle |2, -1\rangle$ transition, which is not present in the solid-state spectra (Figure A.7). This shows that methanol is not an “innocent solvent”, and as a result, the spin Hamiltonian parameters differ from the solid spectra, being $D = -3.32 \text{ cm}^{-1}$, $E = -0.75 \text{ cm}^{-1}$, $g_{\text{iso}} = 2$ for compounds **1** and **2**. The low stability of these compounds in solution has been confirmed by electronic absorption spectroscopy.

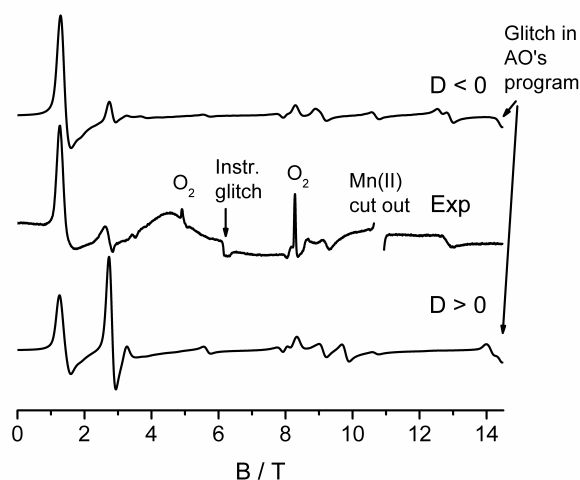


Figure A.7. HFEPR spectra of a solution of **1** in methanol at 302 GHz and 10 K. Simulated spectra were obtained using spin Hamiltonian parameters $D = -3.32 \text{ cm}^{-1}$, $E = -0.75 \text{ cm}^{-1}$, $g_{\text{iso}} = 2$; and the simulation with the same zero-field splitting parameters with a positive D are also included.

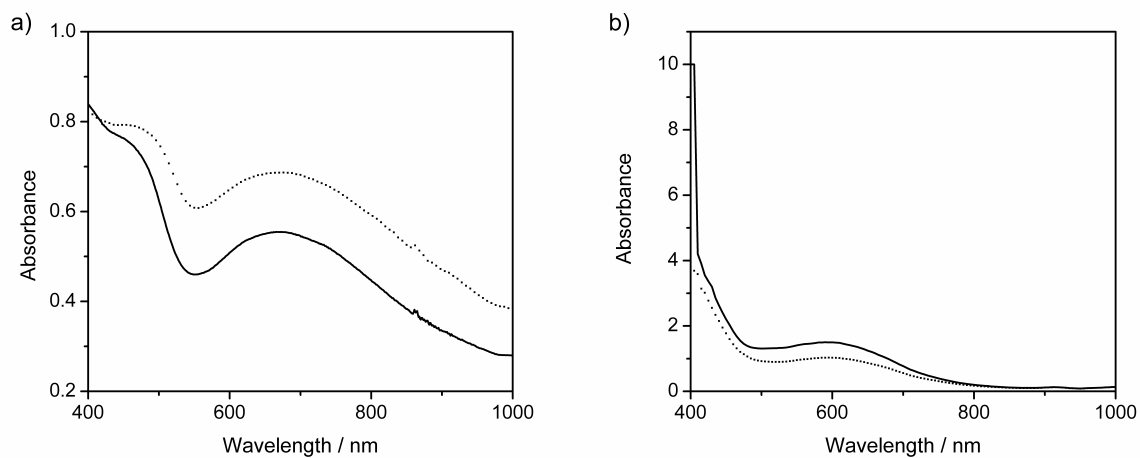


Figure A.8. Electronic absorption spectra of **1** (solid line) and **2** (dashed line) in solid state (a) and in methanol solution (b).

Electronic absorption spectra. Electronic absorption spectra were recorded in solid and in a methanol solution for compounds **1** and **2**. In solution both spectra were identical for compounds **1** and **2**. However, as shown in Figure A.8, the electronic spectrum of **1** and **2** dissolved in methanol differ from the solid. A shift of the maximum in the d–d band from *ca.* 675 nm in the solid to 590 nm in the solution indicates that compounds **1** and **2** do not retain the same coordination sphere in solution. Probably the halogen is very labile and it leaves the coordination sphere of the manganese(III) ion. Because of the empty position of the coordination sphere of the manganese(III) ion and the lability of the halogen in solution, these compounds have been used as starting materials (see Chapter 3).

Relation of structure to spin Hamiltonian parameters. Spin Hamiltonian parameters are in general closely related to the electronic and geometric structure.¹ The ability of EPR, and particularly HFEPN, to obtain these parameters, particularly the magnitude and sign of zero-field splitting, with high accuracy and precision, gives it a distinct advantage over bulk techniques such as magnetometry or calorimetry. However, the experimental data obtained for compounds **1** and **2** are somewhat disappointing in terms of quality, which is much below that achieved in other HFEPN studies of mononuclear compounds of manganese(III) ion such as those in ref.13. The reasons for this deficiency can be only speculated upon but in all likelihood are due to the same interactions that make these compounds so interesting, *i.e.* intermolecular hydrogen bonds and other similar interactions, which broaden the resonances in the solid state to the point where there is practically no baseline observed. This makes the spectral interpretation difficult, and the obtained parameter values inaccurate, at least in comparison with other HFEPN studies on similar manganese(III) systems.

Despite the above caveat, the estimates of the zero-field splitting parameters were obtained, and in particular a negative sign of D for compounds **1** and **2** established beyond much doubt. The negative sign of D is the usual case observed in mononuclear manganese(III) compounds, with very few exceptions.¹⁴⁻¹⁶ On the other hand, from the previous analysis of the magnetic susceptibility and the specific heat data a positive sign of D was obtained. As discussed in Chapter 2, the magnetic susceptibility and specific heat data of compounds **1** and **2** were modelled for an anisotropic Heisenberg chain using the following spin Hamiltonian:

$$\hat{H} = -2J \sum_{i=1}^{n-1} \{S_i S_{i+1}\} + D \sum_{i=1}^n S_{iz}^2 \quad (5)$$

The experimental data for both compounds, especially those obtained at low temperatures, made better fits using the theoretical models predicted by Blöte with $|D/J| = 2$, $D > 0$ (planar

anisotropy) and J antiferromagnetic. The big difference between HFEP R and bulk methods, however, is related to the fact that the E parameter was not included in the spin Hamiltonian (equation 5). HFEP R spectroscopy reveals a significant E value for compounds **1** and **2** with the rhombicity factor E/D ranging between 0.15 and 0.2. Since the maximum possible value for E/D is 0.33, both systems display a high rhombicity. This large ratio does not result from a low magnitude of D ; indeed, the D values that are observed are of similar magnitude as in other pentacoordinated manganese(III) compounds with an halogen atom at the axial position as discussed below.^{17,18} The omission of the E term in the theoretical analysis of the specific heat data might well be the cause of the discrepancies in the sign of the D term between different techniques. Unfortunately, appropriate predictions for biaxial anisotropy are not available in the literature.

The large rhombicity factor in **1** and **2** deserves some remarks. Speaking qualitatively, this reflects the site symmetry of these complexes. Given the square-pyramidal coordination in both complexes, one would intuitively expect either the situation of $D/E = 0$, or some small value, as is the case in porphyrin-based manganese(III) complexes.¹⁹ However, as shown convincingly in ref. 20, even the very high coordination symmetry in the hexaqua manganese(III) cation does not prevent it from showing a measurable D/E factor of *ca.* 0.06. Evidently, the rhombic parameter E is extremely sensitive to small deviations from an ideally symmetric environment, sometimes at a significant distance from the metal ion (in the case of the $[\text{Mn}(\text{H}_2\text{O})_6]^{3+}$ ion it was attributed to a small twist in the coordinated water molecules). Its calculation or prediction is a very difficult task and only rarely successful. The quality of the present EPR data does not justify such an effort.

The zero-field splitting parameters D and E of compounds **1** and **2** obtained by HFEP R spectroscopy can be compared to those reported for other mononuclear manganese(III) compounds in the literature, which have been extensively studied. The spin Hamiltonian parameters are summarized in Tables A.1 and A.2. The g values for mononuclear manganese(III) compounds are all in the range 1.96–2.03, with very small differences between anisotropic g -values, whereas the zero-field splitting parameters depend on the structure of the compound, in the first place on the coordination sphere of the metal ion. One distinct group is formed by compounds with an often distorted octahedral geometry, in which the O_6 is the common coordination sphere.^{12,20-24} These compounds display a D value between -4.52 and -4.35 cm^{-1} and a rhombic component, E , around 0.25 cm^{-1} . Also a compound with N_2O_4 sphere can be in this group with a large value of D .¹³ Two exceptions can be found in which one case is not a molecular compound.^{23,25} When the coordination sphere does not contain O-donors, a decrease of the absolute value of D is generally seen ($3.29 \leq |D| \leq 3.82 \text{ cm}^{-1}$). In addition rhombicity is present, with E varying between $0.30 \leq E \leq 0.70$, due to the

low symmetry of these complexes.^{14,16,26,27} A correlation can be found *i.e.* that tetragonally elongated octahedra present a negative value for D , while a compression results in a positive D value.^{14,16,25,28} The distortions of the coordination sphere around the manganese(III) ion, *i.e.* the angles, are also important.²⁸ An exception to the correlation of the elongation/compression of the Jahn-Teller axes can be found with the elongated octahedral compound [Mn(cyclam)I₂]I that presents a D equal to +0.604 cm⁻¹, resulting from a substantial contribution of a ligand-to-metal charge transfer.¹⁵ Moreover two compounds do not follow this trend of the zero-field splitting parameters values, apparently ascribed to a significant distortion of the octahedral geometry.^{29,30}

In macrocycle compounds with porphyrin-based ligands, the zero-field splitting parameters usually have a value of $-3 \leq D \leq -2$ cm⁻¹ and $E \approx 0$.^{11,17,19,31,32} The change of the porphyrin macrocyclic ligand by corrole-based ligand in mononuclear manganese(III) compounds induces a small rhombic component, $E \neq 0$.³²⁻³⁵ A significant E value ($E = 0.61$ cm⁻¹) is reported for a compound described as a N-confused porphyrin.³⁶ The large rhombic component is ascribed to the equatorial field produced for the C donor atom of the porphyrin ligand.³⁶

Compounds with square-pyramidal geometry, with O-donor ligands and/or N-donor ligands, possess zero-field splitting parameters with values of $-2.45 \leq D \leq -1.40$ cm⁻¹.^{17,18} Compounds **1** and **2** can be included in this group. The axial ligand determines the value of D . The chloride ligand imposes higher $|D|$ value. This trend has also been for other compounds with other geometries, *i.e.* manganese(III) porphyrinic compounds.^{18,37} Apparently, the presence of heavy atoms induces changes on the D term, due to the significant spin-orbit coupling. It may even bring D to a near-zero value.¹⁸ However, compounds **1** and **2** contain a larger E parameter as compared with the other square-pyramidal type of compounds.^{17,18} This value might arise from the different donor atoms in the plane that are also placed in *trans*-N₂O₂ configuration.

Table A.1. Spin Hamiltonian parameters for manganese(III) complexes obtained with HFEPR and related techniques.

Coord. sphere	Compound	D / cm^{-1}	$E / \text{cm}^{-1}{}^a$	E/D	g_x	g_y	g_z	Ref
O ₆	Mn ³⁺ doped in TiO ₂	-3.4(1)	0.116(1)	0.034	2.00(2)	2.00(2)	1.99(1)	25
O ₆	CsMn(SO ₄) ₂ ·12H ₂ O	-4.431(9)	0.258(8)	0.058	2.001(5)	1.997(7)	1.966(12)	20
O ₆	CsMn(SO ₄) ₂ ·12D ₂ O	-4.524(1)	0.276(1)	0.061				22
O ₆	CsMn(SO ₄) ₂ ·12D ₂ O	-4.491(7)	0.248(5)	0.055	1.981(5)	1.993(5)	1.988(5)	20
O ₆	Mn(H ₂ O) ₆ ³⁺ in CsGa(SO ₄) ₂ ·12H ₂ O	-4.514(1)	0.161(5)	0.036	2.000(1)	2.000(1)	1.988(6)	24
O ₆	Mn(dbm) ₃	-4.35	0.26	0.060	1.99	1.99	1.97	21
O ₆	Mn(acac) ₃	-4.52(2)	0.25(2)	0.055	1.99(1)	1.99(1)	1.99(1)	12
O ₆	[Mn(dbm) ₂ (CH ₃ OH) ₂]Br	-3.46	0.13	0.037	1.99	1.99	1.99	23
O ₄ N ₂	[Mn(dbm) ₂ (py) ₂](ClO ₄)	-4.504(2)	0.425(1)	0.094	1.993(1)	1.994(1)	1.983(1)	13
O ₂ N ₄	[Mn(bpia)(OAc)(OCH ₃)] [PF ₆]	+3.526(3)	0.588(6)	0.167	1.98(1)	1.952(6)	1.978(2)	16
N ₆	[Mn(terpy)(N ₃) ₃]	-3.29(1)	0.51(1)	0.155	2.000(5)	1.980(5)	2.010(5)	26
N ₆	[Mn(bpea)(N ₃) ₃]	+3.50(1)	0.82(1)	0.234	2.02(1)	1.98(1)	1.95(1)	14
N ₆	[Mn(taa)]	-5.90	0.50	0.085	2.0	2.0	2.0	29
N ₄ F ₂	[Mn(py ₂ (NMe) ₂)F ₂](PF ₆)	≈ 4						38
N ₄ Br ₂	[Mn(cyclam)Br ₂]Br	-	0.0135(6)	0.011	2.005(4)	2.036(2)	2.015(2)	30
		1.1677(7)						
N ₄ I ₂	[Mn(cyclam)I ₂]	+0.604	0.034	0.056	2.00	2.00	1.99	15
N ₃ F ₃	[Mn(terpy)(F) ₃]	-3.82(2)	0.75(2)	0.196	1.97(2)	2.04(1)	1.96(1)	14
N ₃ F ₃	[Mn(bpea)(F) ₃]	-3.67(2)	0.70	0.191	1.96(1)	1.98(1)	1.98(1)	14
N ₃ Cl ₃	[Mn(terpy)(Cl) ₃]	-3.46(4)	0.43(3)	0.124	1.96(1)	2.00(1)	2.00(1)	27
N ₃ Cl ₃	[Mn(Phterpy)(Cl) ₃]	-3.53(3)	0.30(2)	0.085	1.98(1)	2.00(1)	1.95(1)	27
N ₅	[Mn(DPDME)(N ₃) ₃]	-3.1(1)	<0.12	0.039	n.r	n.r	n.r	37
N ₄ Cl	[Mn(DPDME)Cl]	-2.53(2)	<0.013	0.005	n.r	n.r	n.r	37
N ₄ Cl	[Mn(TPP)Cl]	-2.290(5)	0.00(1)	-	2.005(5)	2.005(5)	1.98(2)	19,32
N ₄ Cl	[Mn(Pc)Cl]	-2.31(1)	0.00(1)	-	2.005(5)	2.005(5)	2.00(2)	11,19,32
N ₄ Cl	[Mn(ODMAPz)Cl]	-2.33(1)	0.00(1)	-			1.984	11
N ₄ Cl	[Mn(TSP)Cl]	-3.12(2)	0.00(1)	-	2.00(2)	2.00(2)	2.00(2)	17
N ₄ Cl	[Mn(OEP)Cl]	-2.40(1)	<0.02(1)	0.008	2.00(1)	2.00(1)	2.00(1)	18
N ₄ Br	[Mn(OEP)Br]	-1.07(1)	0.00(1)	-	2.01(1)	2.01(1)	1.98(1)	18
N ₄ Br	[Mn(DPDME)Br]	-1.1(1)	0	-	n.r	n.r	n.r	37
N ₅ C	[Mn(NCTPP)(py) ₂]	-3.08	0.61	0.198	2	2	2	36
N ₄ O	[Mn(tpfc)(OPPh ₃) ₃]	-2.69(2)	0.030(3)	0.011	1.994(4)	1.994(4)	1.980(4)	33
N ₄ O	(TBP ₈ Cz)Mn·CH ₃ OH	-2.60(2)	0.015(5)	0.006	2.00(1)	2.00(1)	2.00(1)	35
N ₅	[Mn(cor)(py)]	-2.78(1)	0.030(5)	0.011	2.02(1)	2.02(1)	2.00(1)	34
N ₄	[Mn(cor)]	-2.64(1)	0.015(5)	0.006	2.02(1)	2.02(1)	2.00(1)	32,34

^a By convention, the sign of E normally is the same of the D parameter; n.r = not reported.

Table A.2. Spin Hamiltonian parameters for manganese(III) complexes obtained with HFEP R and related techniques (continuation).

Coord. sphere	Compound	D / cm^{-1}	$E / \text{cm}^{-1}{}^a$	E/D	g_x	g_y	g_z	Ref
N ₂ O ₂ Br	[Mn(2-NCH ₃ NCTPP)Br]	-2.4	0.0013	-	n.r	n.r	n.r	31
O ₄ Cl	[Mn(Me ₂ dbm)Cl]	-2.45(3)	0.00(1)	-	2.03(2)	2.03(2)	2.02(2)	18
O ₄ Br	[Mn(Me ₂ dbm)Br]	-1.40(2)	0.00(1)	-	1.98(2)	1.98(2)	1.98(2)	18
N ₂ O ₂ Cl	Mn(salen)	-2.47(2)	0.17(1)	0.0688	2.00(2)	2.00(2)	2.00(2)	17
N ₂ O ₂ Cl	[Mn(HphpzH) ₂ Cl] (1)	-2.43	0.37	0.15	2.00	2.00	2.00	This work
N ₂ O ₂ Br	[Mn(HphpzH) ₂ Br] (2)	-1.64	0.33	0.2	2.00	2.00	2.00	This work

^a By convention, the sign of E normally is the same of the D parameter; n.r = not reported.

A.4. Conclusions

In this appendix, HFEP R studies have been performed as a complementary understanding of the magnetic susceptibility and heat capacity data. HFEP R spectroscopy has been used to determine the zero-field splitting parameters of the mononuclear manganese(III) compounds with the formula [Mn(HphpzH)₂X] (X⁻ = Cl⁻ (**1**), Br⁻ (**2**)) (Chapter 2). A negative zero-field splitting parameter, D has been found for both compounds. The discrepancies from the analysis of the heat capacity that reveal a positive D parameter might arise from the omission of the rhombicity term in such study, which is large, as established by the HFEP R spectroscopy. A relation of the structure with the spin Hamiltonian parameters has been described with the mononuclear manganese(III) compounds found in the literature. For both compounds, the HFEP R spectrum in solid differs from the solution. As a consequence, it indicates the high reactivity of these compounds; as a result, they have been used as building blocks for the synthesis of compounds with higher-nuclearity, as shown in Chapter 3.

A.5. References

1. Abragam, A.; Bleaney, B., *Electron Paramagnetic Resonance of Transition Ions*. Dover Publications: New York, 1986.
2. Drago, R. S., *Physical methods in chemistry*. W. B. Saunders Company: Philadelphia, 1992.
3. Smith, G. M.; Riedi, P. C., *Electron Paramagnetic Resonance*. Gilbert, B. C.; Davies, M. J.; Mc Lauchlan, A., Eds. Royal Society of Chemistry: Cambridge, 2000.
4. Smith, G. M.; Riedi, P. C., *Electron Paramagnetic Resonance*. Gilbert, B. C.; Davies, M. J.; Mc Lauchlan, A., Eds. Royal Society of Chemistry: Cambridge, 2002.
5. Boča, R., *Coord. Chem. Rev.*, **2004**, 248, 757-815.
6. Hagen, W. R., *Coord. Chem. Rev.*, **1999**, 192, 209-229.
7. Krzystek, J.; Ozarowski, A.; Telser, J., *Coord. Chem. Rev.*, **2006**, 250, 2308-2324.
8. Viciano-Chumillas, M.; Marqués-Giménez, M.; Tanase, S.; Evangelisti, M.; Mutikainen, I.; Turpeinen, M.; Smits, J. M. M.; de Gelder, R.; de Jongh, L. J.; Reedijk, J., *J. Phys. Chem. C*, **2008**, 112, 20525-20534.

9. Viciano-Chumillas, M.; Tanase, S.; Mutikainen, I.; Turpeinen, U.; de Jongh, L. J.; Reedijk, J., *Inorg. Chem.*, **2008**, 47, 5919-5929.
10. Hassan, A. K.; Pardi, L. A.; Krzystek, J.; Sienkiewicz, A.; Goy, P.; Rohrer, M.; Brunel, L. C., *J. Magn. Reson.*, **2000**, 142, 300-312.
11. Goldberg, D. P.; Telser, J.; Krzystek, J.; Montalban, A. G.; Brunel, L. C.; Barrett, A. G. M.; Hoffman, B. M., *J. Am. Chem. Soc.*, **1997**, 119, 8722-8723.
12. Krzystek, J.; Yeagle, G. J.; Park, J. H.; Britt, R. D.; Meisel, M. W.; Brunel, L. C.; Telser, J., *Inorg. Chem.*, **2003**, 42, 4610-4618.
13. Aromí, G.; Telser, J.; Ozarowski, A.; Brunel, L. C.; Stoeckli-Evans, H. M.; Krzystek, J., *Inorg. Chem.*, **2005**, 44, 187-196.
14. Mantel, C.; Hassan, A. K.; Pecaut, J.; Deronzier, A.; Collomb, M. N.; Duboc-Toia, C., *J. Am. Chem. Soc.*, **2003**, 125, 12337-12344.
15. Mossin, S.; Weihe, H.; Barra, A. L., *J. Am. Chem. Soc.*, **2002**, 124, 8764-8765.
16. Scheifele, Q.; Riplinger, C.; Neese, F.; Weihe, H.; Barra, A. L.; Juranyi, F.; Podlesnyak, A.; Tregenna-Piggott, P. L. W., *Inorg. Chem.*, **2008**, 47, 439-447.
17. Krzystek, J.; Telser, J., *J. Magn. Reson.*, **2003**, 162, 454-465.
18. Krzystek, J.; Telser, J.; Knapp, M. J.; Hendrickson, D. N.; Aromí, G.; Christou, G.; Angerhofer, A.; Brunel, L. C., *Appl. Magn. Reson.*, **2001**, 21, 571-585.
19. Krzystek, J.; Telser, J.; Pardi, L. A.; Goldberg, D. P.; Hoffman, B. M.; Brunel, L. C., *Inorg. Chem.*, **1999**, 38, 6121-6129.
20. Tregenna-Piggott, P. L. W.; Weihe, H.; Barra, A. L., *Inorg. Chem.*, **2003**, 42, 8504-8508.
21. Barra, A. L.; Gatteschi, D.; Sessoli, R.; Abbati, G. L.; Cornia, A.; Fabretti, A. C.; Uytterhoeven, M. G., *Angew. Chem.-Int. Edit. Engl.*, **1997**, 36, 2329-2331.
22. Basler, R.; Tregenna-Piggott, P. L. W.; Andres, H.; Dobe, C.; Gudel, H. U.; Janssen, S.; McIntyre, G. J., *J. Am. Chem. Soc.*, **2001**, 123, 3377-3378.
23. Gatteschi, D.; Sorace, L.; Sessoli, R.; Barra, A. L., *Appl. Magn. Reson.*, **2001**, 21, 299-310.
24. Krivokapic, I.; Noble, C.; Klitgaard, S.; Tregenna-Piggott, P.; Weihe, H.; Barra, A. L., *Angew. Chem.-Int. Edit.*, **2005**, 44, 3613-3616.
25. Gerritsen, H. J.; Sabisky, E. S., *Phys. Rev.*, **1963**, 132, 1507-1512.
26. Limburg, J.; Vrettos, J. S.; Crabtree, R. H.; Brudvig, G. W.; de Paula, J. C.; Hassan, A.; Barra, A. L.; Duboc-Toia, C.; Collomb, M. N., *Inorg. Chem.*, **2001**, 40, 1698-1703.
27. Mantel, C.; Chen, H. Y.; Crabtree, R. H.; Brudvig, G. W.; Pecaut, J.; Collomb, M. N.; Duboc, C., *ChemPhysChem*, **2005**, 6, 541-546.
28. Tregenna-Piggott, P. L. W., *Inorg. Chem.*, **2008**, 47, 448-453.
29. Kimura, S.; Otani, T.; Narumi, Y.; Kindo, K.; Nakano, M.; Matsubayashi, G., *J. Magn. Magn. Mater.*, **2004**, 272, 1102-1103.
30. Mossin, S.; Stefan, M.; ter Heerdt, P.; Bouwen, A.; Goovaerts, E.; Weihe, H., *Appl. Magn. Reson.*, **2001**, 21, 587-596.
31. Hung, S. W.; Yang, F. A.; Chen, J. H.; Wang, S. S.; Tung, J. Y., *Inorg. Chem.*, **2008**, 47, 7202-7206.
32. Krzystek, J.; Pardi, L. A.; Brunel, L. C.; Goldberg, D. P.; Hoffman, B. M.; Licoccia, S.; Telser, J., *Spectroc. Acta Pt. A-Molec. Biomolec. Spectr.*, **2002**, 58, 1113-1127.
33. Bendix, J.; Gray, H. B.; Golubkov, G.; Gross, Z., *Chem. Commun.*, **2000**, 1957-1958.
34. Krzystek, J.; Telser, J.; Hoffman, B. M.; Brunel, L. C.; Licoccia, S., *J. Am. Chem. Soc.*, **2001**, 123, 7890-7897.
35. Lansky, D. E.; Mandimutsira, B.; Ramdhanie, B.; Clausén, M.; Penner-Hahn, J.; Zvyagin, S. A.; Telser, J.; Krzystek, J.; Zhan, R. Q.; Ou, Z. P.; Kadish, K. M.; Zakharov, L.; Rheingold, A. L.; Goldberg, D. P., *Inorg. Chem.*, **2005**, 44, 4485-4498.
36. Harvey, J. D.; Ziegler, C. J.; Telser, J.; Ozarowski, A.; Krzystek, J., *Inorg. Chem.*, **2005**, 44, 4451-4453.
37. Brackett, G. C.; Richards, P. L.; Caughey, W. S., *J. Chem. Phys.*, **1971**, 54, 4383-4401.
38. Albela, B.; Carina, R.; Policar, C.; Poussereau, S.; Cano, J.; Guilhem, J.; Tchertanov, L.; Blondin, G.; Delroisse, M.; Girerd, J. J., *Inorg. Chem.*, **2005**, 44, 6959-6966.

Appendix B

Crystallographic information for compounds 16, 17 and 18 (Chapter 5)

More detailed crystallographic information for compounds $[\text{Mn}_8(\mu_4\text{-O})_4(\text{phpzH})_8(\text{thf})_4]$ (**16a**), $[\text{Mn}_8(\mu_4\text{-O})_4(\text{phpzH})_8(\text{EtOH})_4]\cdot 2\text{EtOH}$ (**17**) and $[\text{Mn}_6(\mu_3\text{-O})_4(\mu_3\text{-Br})_2(\text{HphpzEt})_6(\text{phpzEt})]$ (**18**) presented in Chapter 5 is shown here.

B.1. Crystallographic information

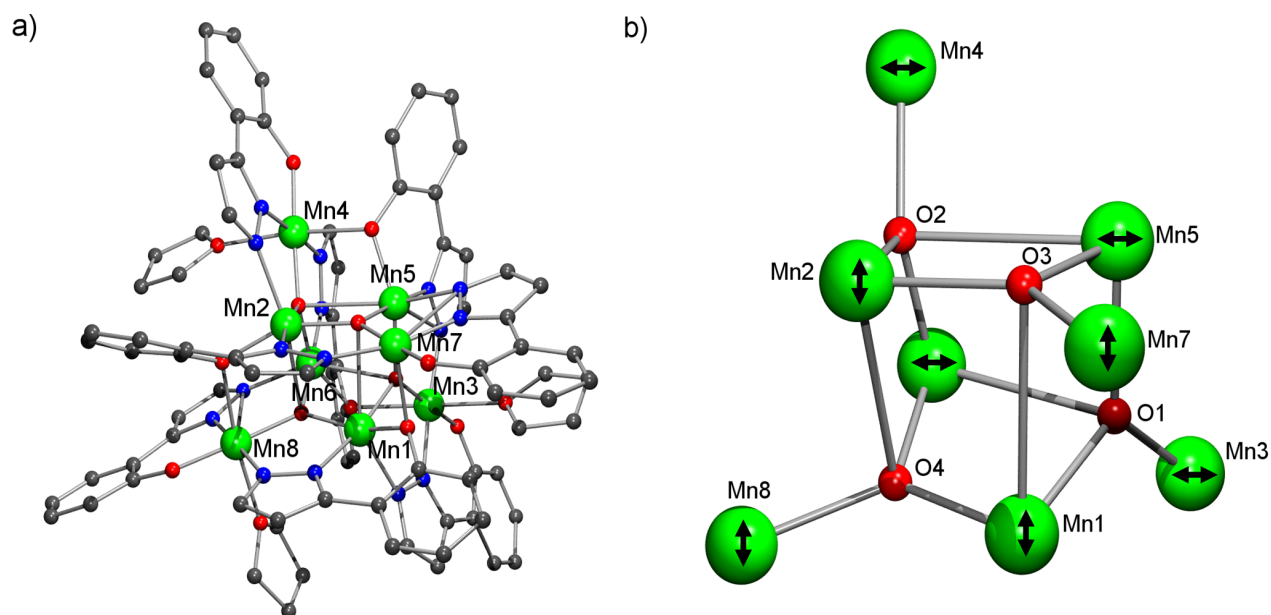


Figure B.1. a) Pluton projection of the compound [Mn₈(μ₄-O)₄(phpzH)₈(thf)₃] (**16a**). b) The [Mn₈(μ₄-O)₄]¹⁶⁺ core in which the Jahn-Teller axes are indicated by arrows. Hydrogen atoms are omitted for clarity. Colour code: green, manganese; blue, nitrogen; red, oxygen; grey, carbon.

Table B.1. Crystal data and structure refinements for $[\text{Mn}_8(\mu_4\text{-O})_4(\text{phpzH})_8(\text{thf})_3]$ (**16a**).

16a	
Formula	$\text{C}_{84}\text{H}_{72}\text{Mn}_8\text{N}_{16}\text{O}_{15}$
Formula mass $[\text{g mol}^{-1}]$	1985.10
Crystal system	Triclinic
Space group	P-1
a [\AA]	14.139(6)
b [\AA]	15.162(5)
c [\AA]	20.726(5)
α [$^\circ$]	78.212(18)
β [$^\circ$]	86.77(2)
γ [$^\circ$]	70.32(3)
V [\AA^3]	4095(2)
Z	2
D_{calc} [g cm^{-3}]	1.610
Crystal size	0.28×0.06×0.04
Number of collected reflections (unique)	70380 (14388)
Number of observed reflections ($I_o > 2\sigma(I_o)$)	6952
Internal R factor	0.1847
Number of parameters	1108
Goodness-of-fit S on F^2	1.066
μ [mm^{-1}]	1.268
R_1 ^[a] [$I > 2.0\sigma(I)$]	0.1161
wR_2 ^[b] [all data]	0.2332
T [$^\circ\text{C}$]	208
^[a] $R_1 = \sum F_o - F_c / \sum F_o $. ^[b] $wR_2 = \{ \sum [w(F_o^2 - F_c^2)^2] / \sum w(F_o^2)^2 \}^{1/2}$.	

Table B.2. Selected bonds lengths [Å] and angles [°] for the compound [Mn₈(μ₄-O)₄(phpzH)₈(thf)₃] (**16a**).

Bond Lengths					
Mn(1)–O(1)	1.938(7)	Mn(1)–O(161)	1.924(7)	Mn(1)–O(4)	1.889(7)
Mn(1)–N(152)	1.977(8)	Mn(1)–N(11)	2.115(10)	Mn(2)–O(2)	1.913(7)
Mn(2)–O(3)	1.895(7)	Mn(2)–O(141)	1.922(7)	Mn(2)–N(31)	2.155(10)
Mn(2)–N(132)	1.938(9)	Mn(3)–O(1)	1.891(7)	Mn(3)–O(1A)	2.286(8)
Mn(3)–O(21)	1.825(7)	Mn(3)–O(121)	2.302(8)	Mn(3)–N(12)	1.935(9)
Mn(3)–N(91)	1.990(9)	Mn(4)–O(1B)	2.272(8)	Mn(4)–O(2)	1.914(7)
Mn(4)–O(41)	1.856(8)	Mn(4)–O(101)	2.299(8)	Mn(4)–N(32)	1.936(9)
Mn(4)–N(111)	1.974(9)	Mn(5)–O(1)	1.924(7)	Mn(5)–O(3)	1.910(6)
Mn(5)–O(101)	1.921(8)	Mn(5)–N(51)	2.145(9)	Mn(5)–N(92)	1.941(8)
Mn(6)–O(2)	1.911(7)	Mn(6)–O(4)	1.910(7)	Mn(6)–O(121)	1.917(7)
Mn(6)–N(71)	2.152(10)	Mn(6)–N(112)	1.965(9)	Mn(7)–O(3)	1.886(7)
Mn(7)–O(61)	1.820(9)	Mn(7)–O(161)	2.193(8)	Mn(7)–N(52)	1.931(10)
Mn(7)–N(131)	1.999(11)	Mn(8)–O(1C)	2.294(9)	Mn(8)–O(4)	1.907(7)
Mn(8)–O(81)	1.842(8)	Mn(8)–O(141)	2.271(8)	Mn(8)–N(72)	1.934(10)
Mn(8)–N(151)	1.982(9)				
Bond Angles					
O(1)–Mn(1)–O(3)	66.6(3)	O(1)–Mn(1)–O(4)	87.9(3)	O(1)–Mn(1)–O(161)	96.7(3)
O(1)–Mn(1)–N(11)	88.5(3)	O(1)–Mn(1)–N(152)	171.0(4)	O(2)–Mn(2)–O(3)	88.9(3)
O(2)–Mn(2)–O(4)	67.6(3)	O(2)–Mn(2)–O(141)	97.7(3)	O(2)–Mn(2)–N(31)	88.6(3)
O(2)–Mn(2)–N(132)	173.6(4)	O(1)–Mn(3)–O(1A)	92.6(3)	O(1)–Mn(3)–O(21)	175.8(3)
O(1)–Mn(3)–O(121)	82.5(3)	O(1)–Mn(3)–N(12)	93.1(4)	O(1)–Mn(3)–N(91)	87.0(3)
O(2)–Mn(4)–N(32)	93.1(4)	O(2)–Mn(4)–O(41)	176.5(4)	O(2)–Mn(4)–O(101)	80.7(3)
O(2)–Mn(4)–N(111)	87.4(4)	O(1)–Mn(5)–O(2)	87.3(3)	O(1)–Mn(5)–O(3)	87.4(3)
O(1)–Mn(5)–O(101)	156.5(3)	O(1)–Mn(5)–N(51)	105.4(3)	O(1)–Mn(5)–N(92)	88.1(3)
O(1)–Mn(6)–O(2)	86.7(3)	O(1)–Mn(6)–O(4)	69.3(3)	O(1)–Mn(6)–O(121)	73.3(3)
O(1)–Mn(6)–N(71)	151.8(3)	O(1)–Mn(6)–N(112)	108.9(3)	O(3)–Mn(7)–O(61)	173.9(4)
O(3)–Mn(7)–O(161)	89.3(3)	O(3)–Mn(7)–N(52)	93.0(3)	O(3)–Mn(7)–N(131)	85.6(4)
O(4)–Mn(8)–O(81)	175.5(3)	O(4)–Mn(8)–O(141)	82.8(3)	O(4)–Mn(8)–N(72)	93.3(4)
O(4)–Mn(8)–N(151)	86.6(3)	O(4)–Mn(8)–O(1C)	91.0(3)		

Table B.3. Selected bond lengths (Å) and angles (°) for the compound $[\text{Mn}_8(\mu_4\text{-O})_4(\text{phpzH})_4(\text{EtOH})_4]\cdot 2\text{EtOH}$ (**17**).

Bond Lengths					
Mn(1)–O(1)	1.909(3)	Mn(1)–O(101)	2.347(3)	Mn(1)–O(312)	2.343(3)
Mn(1)–O(412)	1.849(3)	Mn(1)–N(41)	1.947(3)	Mn(1)–N(52)	1.992(3)
Mn(2)–O(1)	1.917(3)	Mn(2)–O(2)	2.709(3)	Mn(2)–O(4)	1.919(2)
Mn(2)–O(512)	1.911(3)	Mn(2)–N(51)	1.955(3)	Mn(2)–N(62)	2.171(3)
Mn(3)–O(1)	1.915(3)	Mn(3)–O(3)	1.916(3)	Mn(3)–O(4)	2.690(3)
Mn(3)–O(112)	1.906(3)	Mn(3)–N(11)	1.945(3)	Mn(3)–N(42)	2.155(3)
Mn(4)–O(1)	2.669(3)	Mn(4)–O(2)	1.926(3)	Mn(4)–O(3)	1.913(3)
Mn(4)–O(312)	1.939(3)	Mn(4)–N(22)	2.141(3)	Mn(4)–N(31)	1.958(3)
Mn(5)–O(3)	1.907(3)	Mn(5)–O(212)	1.843(3)	Mn(5)–>O(401)	2.39(2)
Mn(5)–O(712)	2.336(3)	Mn(5)–N(12)	2.001(3)	Mn(5)–N(21)	1.958(3)
Mn(5)–<O(41A)	2.29(3)	Mn(6)–O(4)	1.918(2)	Mn(6)–O(112)	2.353(3)
Mn(6)–O(201)	2.273(3)	Mn(6)–O(612)	1.862(3)	Mn(6)–N(61)	1.952(3)
Mn(6)–N(72)	1.990(3)	Mn(7)–O(2)	1.900(3)	Mn(7)–O(301)	2.3065
Mn(7)–O(512)	2.386(3)	Mn(7)–O(812)	1.850(3)	Mn(7)–N(32)	1.995(3)
Mn(7)–N(81)	1.955(3)	Mn(8)–O(2)	1.936(3)	Mn(8)–O(3)	2.665(3)
Mn(8)–O(4)	1.915(2)	Mn(8)–O(712)	1.926(3)	Mn(8)–N(71)	1.971(3)
Mn(8)–N(82)	2.157(3)				
Bond Angles					
O(1)–Mn(1)–O(101)	84.35(11)	O(1)–Mn(1)–O(312)	80.80(10)	O(1)–Mn(1)–O(412)	175.83(13)
O(1)–Mn(1)–N(41)	94.60(13)	O(1)–Mn(1)–N(52)	86.30(13)	O(1)–Mn(2)–O(2)	87.65(10)
O(1)–Mn(2)–O(4)	88.54(12)	O(1)–Mn(2)–O(512)	156.15(12)	O(1)–Mn(2)–N(51)	86.40(13)
O(1)–Mn(2)–N(62)	102.80(12)	O(1)–Mn(3)–O(3)	87.66(11)	O(1)–Mn(3)–O(4)	68.74(10)
O(1)–Mn(3)–O(112)	95.74(11)	O(1)–Mn(3)–N(11)	175.04(12)	O(1)–Mn(3)–N(42)	89.65(12)
O(1)–Mn(4)–O(2)	88.65(10)	O(1)–Mn(4)–O(3)	68.51(10)	O(1)–Mn(4)–O(312)	72.12(10)
O(1)–Mn(4)–N(22)	153.81(11)	O(1)–Mn(4)–N(31)	108.60(11)	O(3)–Mn(5)–O(212)	176.91(12)
O(3)–Mn(5)–>O(401)	86.0(6)	O(3)–Mn(5)–O(712)	81.60(11)	O(3)–Mn(5)–N(12)	87.17(12)
O(3)–Mn(5)–N(21)	92.90(13)	O(3)–Mn(5)–<O(41A)	85.0(7)	O(4)–Mn(6)–O(112)	82.36(11)
O(4)–Mn(6)–O(201)	93.27(12)	O(4)–Mn(6)–O(612)	175.24(13)	O(4)–Mn(6)–N(61)	93.40(12)
O(4)–Mn(6)–N(72)	87.21(12)	O(2)–Mn(7)–O(301)	95.76	O(2)–Mn(7)–O(512)	81.43(11)
O(2)–Mn(7)–O(812)	174.56(13)	O(2)–Mn(7)–N(32)	87.84(13)	O(2)–Mn(7)–N(81)	92.62(13)
O(2)–Mn(8)–O(3)	68.06(10)	O(2)–Mn(8)–O(4)	89.01(11)	O(2)–Mn(8)–O(712)	97.39(11)
O(2)–Mn(8)–N(71)	174.56(12)	O(2)–Mn(8)–N(82)	87.87(12)		

Table B.4. Hydrogen bond details (distances [Å] and angles [°]) for $[\text{Mn}_8(\mu_4\text{-O})_4(\text{phpzH})_4(\text{EtOH})_4]\cdot 2\text{EtOH}$ (**17**).

Donor–H···Acceptor	D–H	H···A	D···A	D–H···A
O(501)–H(50A)···O(201)	0.8399	2.0174	2.727(6)	141.71
O(601)–H(60A)···O(301)	0.8404	2.1723	2.8245	134.36

Table B.5. Selected bond lengths (Å) and angles (°) for [Mn₆(μ₃-O)₄(μ₃-Br)₂(HphpzEt)₆(phpzEt)] (**18**).

Bond Lengths					
Mn(1)–O(112)	1.874(4)	Mn(3)–Br(2)	2.7353(11)	Mn(6)–O(2)	1.910(3)
Mn(1)–O(2)	1.876(3)	Mn(3)–O(612)	2.577(3)	Mn(6)–O(4)	1.916(3)
Mn(1)–O(1)	1.901(3)	Mn(4)–O(1)	1.898(3)	Mn(6)–N(71)	1.978(4)
Mn(1)–N(11)	1.989(5)	Mn(4)–O(4)	1.903(3)	Mn(6)–Br(1)	2.8517(11)
Mn(1)–Br(1)	2.7488(10)	Mn(4)–O(412)	1.908(4)	Mn(6)–O(612)	2.294(3)
Mn(1)–Br(2)	3.0076(10)	Mn(4)–N(41)	2.000(5)	Mn(1)···Mn(2)	3.250
Mn(2)–O(3)	1.878(3)	Mn(4)–N(52)	2.260(4)	Mn(1)···Mn(4)	3.239
Mn(2)–O(212)	1.888(3)	Mn(4)–Br(1)	2.9014(11)	Mn(1)···Mn(6)	3.228
Mn(2)–O(1)	1.924(3)	Mn(5)–O(4)	1.901(3)	Mn(2)···Mn(3)	3.171
Mn(2)–N(21)	1.987(4)	Mn(5)–O(512)	1.923(3)	Mn(2)···Mn(4)	3.225
Mn(2)–Br(2)	2.7305(11)	Mn(5)–N(51)	1.975(4)	Mn(2)···Mn(5)	3.470
Mn(3)–O(3)	1.863(3)	Mn(5)–O(612)	1.994(3)	Mn(3)···Mn(5)	3.288
Mn(3)–O(2)	1.905(3)	Mn(5)–O(3)	2.158(3)	Mn(3)···Mn(6)	3.221
Mn(3)–O(312)	1.904(3)	Mn(5)–N(61)	2.221(4)	Mn(5)···Mn(6)	3.057
Mn(3)–N(31)	2.035(4)	Mn(6)–O(712)	1.875(4)		
Bond Angles					
Br(1)–Mn(1)–Br(2)	165.11(4)	Br(1)–Mn(1)–O(1)	87.75(10)	Br(1)–Mn(1)–O(2)	87.02(10)
Br(1)–Mn(1)–O(112)	95.05(12)	Br(1)–Mn(1)–N(11)	93.32(13)	Br(2)–Mn(2)–O(1)	90.05(10)
Br(2)–Mn(2)–O(3)	84.08(11)	Br(2)–Mn(2)–O(212)	96.70(11)	Br(2)–Mn(2)–N(21)	107.47(13)
Br(2)–Mn(2)–N(52)	161.42(9)	Br(2)–Mn(3)–O(2)	89.58(10)	Br(2)–Mn(3)–O(3)	84.22(10)
Br(2)–Mn(3)–O(312)	92.19(11)	Br(2)–Mn(3)–O(612)	154.42(8)	Br(2)–Mn(3)–N(31)	109.84(12)
Br(1)–Mn(4)–O(1)	83.42(10)	Br(1)–Mn(4)–O(4)	82.61(10)	Br(1)–Mn(4)–O(412)	93.88(11)
Br(1)–Mn(4)–N(41)	93.14(13)	Br(1)–Mn(4)–N(52)	167.87(12)	O(3)–Mn(5)–O(4)	91.88(13)
O(3)–Mn(5)–O(512)	87.19(13)	O(3)–Mn(5)–O(612)	83.42(13)	O(3)–Mn(5)–N(51)	88.99(15)
O(3)–Mn(5)–N(61)	165.68(15)	Br(1)–Mn(6)–O(2)	83.47(10)	Br(1)–Mn(6)–O(4)	83.79(10)
Br(1)–Mn(6)–O(612)	156.82(9)	Br(1)–Mn(6)–O(712)	104.05(13)	Br(1)–Mn(6)–N(71)	91.33(13)
Mn(1)–Br(1)–Mn(4)	69.90(3)	Mn(1)–Br(1)–Mn(2)	70.37(3)	Mn(4)–Br(1)–Mn(6)	70.13(3)
Mn(2)–Br(2)–Mn(3)	70.92(3)	Mn(1)–O(1)–Mn(2)	116.37(16)	Mn(1)–O(1)–Mn(4)	117.01(16)
Mn(2)–O(1)–Mn(4)	115.07(17)	Mn(1)–O(2)–Mn(3)	118.19(17)	Mn(1)–O(2)–Mn(6)	117.01(16)
Mn(3)–O(2)–Mn(6)	115.21(17)	Mn(2)–O(3)–Mn(3)	115.89(18)	Mn(2)–O(3)–Mn(5)	118.40(16)
Mn(3)–O(3)–Mn(5)	109.49(15)	Mn(4)–O(4)–Mn(5)	122.04(17)	Mn(4)–O(4)–Mn(6)	119.87(18)
Mn(5)–O(4)–Mn(6)	106.46(15)				

Samenvatting

Dit laatste hoofdstuk bevat een kort overzicht en evaluatie van het in het proefschrift beschreven onderzoek en tevens enkele conclusies en suggesties voor verder onderzoek.

In het recente verleden zijn diverse pogingen ondernomen om nieuwe moleculaire magnetische materialen te ontwikkelen.¹ Om dit te bereiken is het noodzakelijk de magnetische eigenschappen op nanoschaal te begrijpen. In de verbindingen uit de coördinatiechemie ligt de oorsprong van het magnetisch moment in de ongepaarde elektronen van overgangsmetaalionen of zeldzame-aard-ionen. Bovendien is de aanwezigheid van organische liganden nodig om de metaalionen te bruggen en het molecuul als geheel te stabiliseren. Daarom hangen de magnetische eigenschappen over het algemeen af van het karakter van het paramagnetisch metaalion, van de mogelijkheid van het ligand om magnetische interacties te propageren tussen de metaalionen en van de verschillende structurele topologieën opgelegd door de metaal-ligand-interacties.

In dit proefschrift is het mangaan(III)-ion geselecteerd om zijn coördinatiechemie te bestuderen vanwege zijn paramagnetisch gedrag in combinatie met een variëteit van nieuwe fenol-pyrazool-liganden. Het mangaan(III)-ion vertoont meestal een negatieve anisotropie van het Ising-type, hetgeen vaak leidt tot interessante magnetische eigenschappen.¹ Carboxylaten en Schiff-basen zijn bekende bruggende liganden die het mangaanion in verschillende oxidatietoestanden in polymere clusters kunnen stabiliseren.^{2,3} Daarom zijn verschillende pogingen ondernomen in de zoektocht naar nieuwe ligandtypes die bij voorkeur leiden tot nieuwe polymetallische systemen met interessante magnetische eigenschappen. De selectie van bruggende liganden is cruciaal voor de synthese van nieuwe moleculen met de gewenste topologie en magnetische eigenschappen. Daarom wordt in Hoofdstuk 1 een gedetailleerd bibliografisch onderzoek gepresenteerd, waarin de mogelijkheid van het pyrazool om op te treden als een bruggend ligand dat de magnetische uitwisselingsinteracties kan propageren in polymetallische verbindingen, wordt uiteengezet. In dit proefschrift is een fenolgroep geïntroduceerd als substituent op een pyrazoolring teneinde het aantal mogelijke bindingsplaatsen voor metaalionen te verhogen vanwege de zuurstofdonorplaats. Daartoe is een serie van fenol-pyrazool-liganden gesynthetiseerd met variaties op de 5-positie van de pyrazoolring, zoals waterstof, methyl, ethyl en fenyl, om de rol van het ligand in de vorming van nieuwe complexen te bestuderen. Samengevat is het doel van dit onderzoek dan ook het verkennen van de coördinatiechemie van deze nieuwe, op fenol-pyrazool gebaseerde liganden, en wel voornamelijk in combinatie met het mangaan(III)-ion, alsmede het bestuderen van de vorming van nieuwe complexen en hun magnetische eigenschappen.

In Hoofdstuk 2 wordt een familie gepresenteerd van mononucleaire mangaan(III)-verbindingen met de algemene formule $[\text{Mn}(\text{HphpzR})_2\text{X}]$ ($\text{R} = \text{H}, \text{Me}, \text{Et}, \text{Ph}$ en $\text{X}^- = \text{Cl}^-$,

Br⁻). Al deze verbindingen bevatten een vierkant-pyramidale geometrie voor mangaan(III). Er wordt aangetoond hoezeer de keuze van het ligand het type kristalrooster bepaalt; zo leidt de aanwezigheid van kleine substituenten op de 5-positie van de pyrazoolring tot de vorming van 1-D-ketens, gestabiliseerd door waterstofbindingen, terwijl grote substituenten, zoals fenyl op deze 5-positie, de vorming van dergelijke ketens blijken uit te sluiten. Magnetische en thermische eigenschappen zijn bestudeerd, die duidelijk het belang van het type kristalrooster op deze eigenschappen laten zien. Ook is het effect op de magnetische uitwisselingsinteracties van het verwisselen van het halide-ion (van chloride naar bromide) geanalyseerd voor dit type verbindingen. Verbindingen met de formule [Mn(HphpzH)₂X] (X⁻ = Cl⁻, Br⁻) vormen ketens, die gestabiliseerd worden door sterke waterstofbindingen, aangezien de afstanden tussen de mangaan(III)-ionen klein genoeg zijn om magnetische ketens te vormen. De analyse van de magnetische data en de thermische studies, zoals gerapporteerd in Hoofdstuk 2, resulteerde in Heisenberg-achtige ketens met een (vlakke) anisotropie (XY; een positieve uniaxiale anisotropieparameter *D*). De aanwezigheid van lange-afstandsordening is waargenomen bij ongeveer 1.5 K in metingen van de soortelijke warmte. De vondst van een XY-type anisotropie was enigszins verrassend, omdat het mangaan(III)-ion in de meeste gevallen een Ising-type anisotropie vertoont (negatieve *D*).⁴ Zoals in Appendix A is beschreven, is daarom HFEPN-spectroscopie uitgevoerd om betrouwbaarder het teken en de grootte van de anisotropieparameters te bepalen. De gevonden waarden van de uniaxiale anisotropieparameter *D* en de orthorhombische anisotropieparameter *E* van deze twee verbindingen zijn gerapporteerd in Hoofdstuk 2. De HFEPN-spectra van deze verbindingen in hun poedervorm laten inderdaad een negatieve *D* zien met daarbij een aanzienlijke waarde voor de *E*-parameter. Waarschijnlijk is daarom de afwezigheid van de *E* term in de theoretische modellen die beschikbaar waren voor de analyse van de soortelijke warmte data de oorzaak van de discrepantie in het teken van de *D*-term gevonden in de twee experimenten. Verder lieten additionele HFEPN-spectra die in oplossing werden genomen drastische veranderingen zien in de waarden van deze anisotropieparameters, hetgeen wijst op een lage stabiliteit van deze verbindingen in oplossing. In Appendix A wordt verder een discussie gepresenteerd over het teken en de grootte van de anisotropieparameters voor andere in literatuur gerapporteerde mononucleaire mangaan(III)-verbindingen, met name in relatie tot hun kristalstructuur. Het teken en de grootte van de parameter *D* blijken voornamelijk af te hangen van het type liganden op de axiale positie.

Zoals hierboven al vermeld, vormen de verbindingen [Mn(HphpzMe)₂X] (X⁻ = Cl⁻, Br⁻) ook 1-D ketens, zij het met een toename van de afstand tussen de mangaan(III)-ionen langs de keten die wordt veroorzaakt door het (meer omvangrijke) ligand H₂phpzMe. Deze toename verklaart waarom zwakkere antiferromagnetische interacties worden waargenomen in

vergelijking met de verbindingen $[\text{Mn}(\text{HphpzH})_2\text{X}]$ ($\text{X}^- = \text{Cl}^-, \text{Br}^-$). Dit verklaart waarom in deze complexen geen 1-D magnetische ordeningsverschijnselen worden waargenomen in het onderzochte temperatuurgebied (boven 2 K).

De introductie van een “bulky” substituent in de pyrazoolring, zoals fenyl, sluit de vorming van 1-D-ketens geheel uit, zoals is waargenomen in de verbindingen $[\text{Mn}(\text{HphpzPh})_2\text{X}]$ ($\text{X}^- = \text{Cl}^-, \text{Br}^-$). Aangezien de afstanden tussen de mangaan(III)-ionen groot zijn, wordt een bijna volledig paramagnetisch gedrag vertoond. Daarbij kunnen de $[\text{Mn}(\text{HphpzR})_2\text{X}]$ verbindingen gebruikt worden voor de synthese van polynucleaire verbindingen, zoals weergegeven in Hoofdstuk 3, door de labiliteit van het halide, de lege positie in het coördinatiegebied van het mangaan(III)-ion en de nog steeds lege coördinatiebindingsplaats van de N-H-groep van de pyrazoolring.

Hoofdstuk 3 en 4 gaan over oxide-gecentreerde trinucleaire mangaan(III)-complexen.^{5,6} Deze bevatten alle de trinucleaire kern $[\text{Mn}_3(\mu_3\text{-O})(\text{phpzR})_3]^+$, waarin de drie fenol-pyrazool-liganden in het vlak liggen dat gevormd wordt door de drie mangaan(III)-ionen en de axiale posities bezet zijn door oplosmiddelmoleculen (methanol en ethanol) en bruggende liganden (carboxylaat en azide). In deze hoofdstukken is de invloed van het type fenol-pyrazool-liganden en van het co-ligand op de structurele symmetrie van $[\text{Mn}_3(\mu_3\text{-O})(\text{phpzR})_3]^+$ en op de magnetische eigenschappen zorgvuldig bestudeerd. Blijkbaar is de keuze van het fenol-pyrazool-ligand in deze verbindingen bepalend voor het type kristalstructuur dat gevormd wordt, namelijk ofwel een geordende structuur van geïsoleerde trinucleaire eenheden, ofwel een rangschikking van deze eenheden in 1-D ketens.⁵⁻¹⁰ In deze 1-D-ketens kunnen de trinucleaire eenheden met elkaar verbonden zijn door een bruggende groep, door acetaat of azide, of door waterstofbrug-interacties. Substituenten op de 4-positie van de fenolring creëren geen verstoring van de $[\text{Mn}_3(\mu_3\text{-O})]^{7+}$ -kern en 1-D-ketens worden gevormd.⁷⁻¹⁰ Deze substituenten kunnen wellicht de scheiding controleren tussen de 1-D-ketens. Echter, substituenten in de 5-positie van de pyrazoolring,^{5,6} zoals methyl of fenyl dwingen het carboxylaat-ligand om te binden aan twee mangaan(III)-ionen van dezelfde trinucleaire mangaan(III)-eenheid, in plaats van de trinucleaire eenheden te bruggen. Als het carboxylaat-ligand klein is, zoals acetaat, kunnen deze trinucleaire eenheden ketens vormen, vanwege de waterstofbruggen die ontstaan tussen het carboxylaat-anion en het oplosmiddelmolecuul (verbinding **11** en **13**). Als het carboxylaat-ligand groter is, zoals bij benzoaat, binden er twee carboxylaten aan de twee mangaan(III)-ionen van dezelfde trinucleaire eenheid (verbindingen **14** en **15**) en raken de trinucleaire eenheden geïsoleerd. In al deze gevallen wordt gevonden dat de Mn–O–Mn-hoek in de brug waarmee het carboxylaat-ligand de mangaan(III)-ionen bindt kleiner wordt dan 120° , terwijl de overige hoek(en) verstoord worden in de richting van grotere waarden. De gecoördineerde oplosmiddelmoleculen blijken ook een belangrijke

oorzaak te zijn voor het stabiliseren van het type structuur. Het aantal oplosmiddelmoleculen gebonden aan mangaan(III)-ionen kan variëren. In verbinding **13** bijvoorbeeld is slechts één oplosmiddelmolecuul gecoördineerd (ethanol), in plaats van drie methanolmoleculen (verbinding **11**), waarbij de trinucleaire eenheden dichter bij elkaar worden gedwongen dan wanneer methanol aanwezig is. In al deze verbindingen met fenol-pyrazoolliganden worden voornamelijk antiferromagnetische interacties gevonden tussen de mangaan(III)-ionen in de trinucleaire eenheid.⁵⁻¹⁰ Voor een gelijkbenige driehoek zijn de Mn–O–Mn-hoeken 120° en de oxidebrug ligt in het vlak dat gevormd wordt door de drie mangaan(III)-ionen. In deze geometrie worden antiferromagnetische interacties inderdaad verwacht. Wanneer echter een verstoring in de $[\text{Mn}_3(\mu_3\text{-O})]^{7+}$ -kern aanwezig is, bijvoorbeeld wanneer de Mn–O–Mn hoeken kleiner worden dan 120° en een verplaatsing plaatsvindt van de $\mu_3\text{-O}^{2-}$ uit het vlak gevormd door de drie mangaan(III)-ionen, kan het type van magnetische interacties tussen de mangaan(III)-ionen drastisch veranderen. Dergelijke voorbeelden zijn waargenomen in de verbindingen $\text{Mn}_3(\mu_3\text{-O})(\text{phpzMe})_3(\text{MeOH})_3(\text{OAc}) \cdot 1.5\text{MeOH}$ (**11**) en $[\text{Mn}_3(\mu_3\text{-O})(\text{phpzMe})_3(\text{O}_2\text{CMe})(\text{EtOH})] \cdot \text{EtOH}$ (**13**), waarin een ferromagnetische interactie wordt gevonden voor de (enige) Mn–O–Mn brug met een verkleinde Mn–O–Mn hoek. Om nu ook voor de twee andere Mn–O–Mn bruggen een ferromagnetisch interactie tot stand te brengen zou dus een verstoring nodig zijn, waarbij alle drie Mn–O–Mn hoeken een waarde kleiner dan 120° krijgen. Naast deze (meestal dus antiferromagnetische) interacties die worden waargenomen binnen in de trinucleaire eenheden blijkt verder dat de kristalstructuur van deze verbindingen, met name de stapeling van de trinucleaire eenheden daarin, bepalend zijn voor de verschillende magnetische uitwisselingsinteracties die optreden tussen de trinucleaire mangaan(III)-eenheden. In de meeste 1-D-ketens worden (zwakke) ferromagnetische interacties waargenomen tussen de trinucleaire eenheden die de ketens vormen.⁶⁻¹⁰ Daarmee samenhangend wordt verschillend magnetisch gedrag gezien dat varieert van enkel-keten-magneet tot magnetische ordening over lange-afstand.⁵⁻¹⁰

Hoofdstuk 5 behandelt de synthese en karakterisering van mangaan(III)-verbindingen met een hoge nucleariteit. Appendix B bevat de kristallografische informatie over deze verbindingen. De verbinding $[\text{Mn}_8(\mu_4\text{-O}_4)(\text{phpzMe})_8(\text{thf})_4]$ was al eerder gerapporteerd in onze groep.¹¹ Als vervolg daarop zijn in de huidige studie de invloed van verschillende oplosmiddelen op de stabiliteit van de $[\text{Mn}_8(\mu_4\text{-O}_4)(\text{phpzR})_8]$ -kern nader onderzocht. De $[\text{Mn}_8(\mu_4\text{-O}_4)(\text{phpzR})_8]$ -kern wordt behouden wanneer de liganden H_2phpzH of de H_2phpzMe gebruikt worden, zelfs met oplosmiddelen als ethanol of acetontril. Echter, het gebruik van een meer bulky ligand, zoals H_2phpzEt , induceert onder geschikte synthetische condities de vorming van een nieuw type kern, waarschijnlijk vanwege sterische effecten opgelegd door de

ethylgroep. In dit geval is een hexanucleaire verbinding verkregen, $[\text{Mn}_6(\mu_3\text{-O})_4(\mu_3\text{-Br})_2(\text{HphpzEt})_6(\text{phpzEt})]$ (**18**). In de octanucleaire mangaan(III)-verbindingen, hierboven genoemd, zijn sterke antiferromagnetische interacties aanwezig tussen de mangaan(III)-ionen (Hoofdstuk 5 en ref 11), wat leidt tot een grondtoestand met spin $S_T = 0$. Het oplosmiddel modificeert noch het type structuur, noch de magnetische eigenschappen, aangezien het sterke antiferromagnetisme principieel veroorzaakt wordt door de magnetische uitwisselingsinteractie tussen de mangaan(III)-ionen in de kern en in de periferie, terwijl slechts zwakke antiferromagnetische interacties worden verwacht aanwezig te zijn tussen de mangaan(III)-ionen in de kern. Echter, in de hexanucleaire verbinding zijn zwakke ferromagnetische interacties waargenomen. Klaarblijkelijk worden zij verkozen door deze nieuwe kern, waarin de Jahn-Teller-assen verschillende richtingen hebben en aanzienlijke spin-canting mogelijk aanwezig zou kunnen zijn.

Hoofdstuk 6 presenteert de coördinatiechemie van het ligand H_2phpzMe met andere overgangsmetaalionen, zoals kobalt(III), koper(II) and nikkel(II). De keuze van het overgangsmetaalion kan leiden tot verschillende producten vanwege ligandvoorkeuren en de kinetiek van het overgangsmetaal. In het geval van het kobalt(III)-ion is een dinucleaire verbinding gevormd door oxidatie aan de lucht van het kobalt(II)-ion. Deze verbinding is diamagnetisch en de vier verschillende bindingsmogelijkheden van het ligand aan het kobalt(III)-ion benadrukken de coördinatieve veelzijdigheid van de fenol-pyrazool-liganden. In het geval van nikkel(II)- en koper(II)-ionen worden isostructurele vlak-vierkante mononucleaire verbindingen gevormd. Deze verbindingen zijn bereid via verscheidene synthetische routes, hetgeen hun hoge stabiliteit illustreert. Echter, onder specifieke condities kunnen ook clusters gevormd worden.^{12,13} Daarom kunnen geschikte synthetische condities leiden tot de vorming van andere nieuwe verbindingen.

References

1. Gatteschi, D.; Sessoli, R.; Villain, J., *Molecular Nanomagnets*. Oxford University Press: UK, 2006.
2. Christou, G., *Polyhedron*, **2005**, 24, 2065-2075.
3. Miyasaka, H.; Saitoh, A.; Abe, S., *Coord. Chem. Rev.*, **2007**, 251, 2622-2664.
4. Krzystek, J.; Ozarowski, A.; Telser, J., *Coord. Chem. Rev.*, **2006**, 250, 2308-2324.
5. Viciano-Chumillas, M.; Tanase, S.; Mutikainen, I.; Turpeinen, M.; de Jongh, L. J.; Reedijk, J., *Inorg.Chem.*, **2008**, 47, 5919-5929.
6. Viciano-Chumillas, M.; Tanase, S.; Mutikainen, I.; Turpeinen, U.; de Jongh, L. J.; Reedijk, J., *Dalton Trans.*, **2009**.
7. Bai, Y. L.; Tao, J.; Wernsdorfer, W.; Sato, O.; Huang, R. B.; Zheng, L. S., *J. Am. Chem. Soc.*, **2006**, 128, 16428-16429.
8. Liu, C. M.; Zhang, D. Q.; Zhu, D. B., *Chem. Commun.*, **2008**, 368-370.
9. Liu, C. M.; Zhang, D. Q.; Zhu, D. B., *Inorg.Chem.*, **2009**.
10. Tao, J.; Zhang, Y. Z.; Bai, Y. L.; Sato, O., *Inorg. Chem.*, **2006**, 45, 4877-4879.

11. Tanase, S.; Aromí, G.; Bouwman, E.; Kooijman, H.; Spek, A. L.; Reedijk, J., *Chem. Commun.*, **2005**, 3147-3149.
12. Aromí, G.; Bouwman, E.; Burzuri, E.; Carbonera, C.; Krzystek, J.; Luis, F.; Schlegel, C.; van Slageren, J.; Tanase, S.; Teat, S. J., *Chem.-Eur. J.*, **2008**, 14, 11158-11166.
13. Bai, Y. L.; V., T.; Huang, R. B.; Zheng, L. S.; Tao, J., *Chem.-Eur. J.*, **2009**, 15, 2377-2383.

Resumen

Este resumen en español está realizado con el fin de explicar a un lector sin experiencia en este campo, el trabajo doctoral realizado durante estos últimos cuatro años. Por eso puede contener algunas generalizaciones que a priori podrían crear imprecisiones. El objetivo de esta tesis es sintetizar y caracterizar imanes moleculares. Antes de exponer qué se ha realizado en el transcurso de este trabajo, es necesario explicar algunos conceptos básicos.

Un imán es un material que tiene la capacidad de producir un campo magnético en su exterior, capaz de atraer o repeler. Los imanes tradicionales están formados por metales y óxidos. Sin embargo, se están realizando numerosos esfuerzos para disminuir y controlar el tamaño de los imanes creando nuevos materiales a niveles nanoscópicos. Una manera de conseguirlo, es desarrollando sistemas moleculares, es decir, moléculas que puedan funcionar como imanes. Las aplicaciones de estos imanes moleculares pueden ser muy diversas, desde la biomedicina, ya que podrían guiar medicamentos y dirigirlos a determinados órganos, o la informática, ya que se podría aumentar la densidad o capacidad de información almacenada en el imán, llegándose a construir ordenadores cuánticos.

Un imán está formado por momentos magnéticos, es decir, electrones. Normalmente, esos momentos magnéticos están desordenados, debido a la agitación térmica. Cuando la temperatura disminuye, los momentos magnéticos o electrones empiezan a interactuar y a ordenarse. Hay diferentes tipos de orden, antiferromagnético, en el que los electrones se ordenan antiparalelamente, pudiéndose anular los momentos magnéticos, y ferromagnético, donde los electrones se ordenan paralelamente, con lo que, los momentos magnéticos están orientados en la misma dirección. Una vez, el sistema está ordenado, no necesariamente funciona como imán, ya que necesita un momento magnético neto o magnetización, es decir, que no se anulen todos los momentos magnéticos a través de la red molecular.

En química inorgánica, se busca esa fuente de momentos magnéticos o electrones en los iones de los metales de transición o tierras raras, que contienen electrones desapareados, pero se necesitan unos ligandos, que son unas moléculas orgánicas que se unen a dichos iones metálicos, para estabilizar la molécula, formando el llamado también complejo de coordinación. Dependiendo del diseño de los ligandos que se emplee, se pueden formar complejos de distintas nuclearidades, es decir, con diferente número de iones metálicos, así como diferentes topologías. Para desarrollar imanes moleculares, los ligandos tienen que presentar dos características, que sean capaces de unir diferentes metales y que sean capaces de propagar las interacciones magnéticas entre los metales de transición o tierras raras.

El trabajo de esta tesis ha consistido en sintetizar complejos de coordinación, principalmente de manganeso(III) con ligandos fenol-pirazólicos, y estudiar sus propiedades

magnéticas. Para conocer el tipo de comportamiento magnético, el compuesto se mide con un instrumento llamado SQUID, variando el campo magnético aplicado y la temperatura.

En el Capítulo 1, se explican brevemente los objetivos de la tesis. El manganeso se ha escogido como metal de transición, porque tiene diferentes estados de oxidación accesibles que son paramagnéticos, es decir, con electrones desapareados. Se ha realizado una búsqueda bibliográfica en la cual se describen los clústeres metálicos que contienen ligandos pirazólicos, demostrando que son buenos ligandos puentes capaces de transmitir las interacciones magnéticas entre iones metálicos. Así pues, se han sintetizado derivados pirazólicos con la fórmula H_2phpzR , con un fenol, y diferentes sustituyentes (hidrógeno, metil, etil y fenil) en el pirazol como ligandos.

En el Capítulo 2, se presenta una familia de compuestos mononucleares de manganeso(III) con la fórmula general $[Mn(HphpzR)_2X]$ ($R = H, Me, Et, Ph$ y $X = Cl, Br$). Se ha podido comprobar que el tipo de ligando fenol-pirazólico H_2phpzR , no influye en la obtención de compuestos con la misma geometría pero sí en el empaquetamiento cristalino, es decir, en cómo están organizados los distintos compuestos mononucleares de manganeso(III) en la red. Ante la presencia de ligandos H_2phpzR pequeños, como $R = H, Me$, se forman cadenas que están formadas por los compuestos mononucleares unidos por puentes de hidrógeno. Sin embargo cuando existen ligandos H_2phpzR con sustituyentes voluminosos, como $R = Ph$, la formación de cadenas no es posible. El tipo de organización o empaquetamiento cristalino determina las propiedades magnéticas. La influencia del halógeno en las propiedades magnéticas también ha sido estudiada en los compuestos con la fórmula $[Mn(HphpzR)_2X]$ ($R = H, Me, Et, Ph$ y $X = Cl, Br$), sintetizando compuestos con dos tipos de halógenos, cloro y bromo. Desde el punto de vista magnético, se observa que los compuestos $[Mn(HphpzH)_2X]$ son los más interesantes, porque los iones de manganeso(III) están muy próximos, y son capaces de interaccionar magnéticamente. Se observa que cada cadena se ordena antiferromagnéticamente a temperaturas de alrededor de 5 K (ordenamiento magnético 1-D), y todas las cadenas se ordenan entre ellas alrededor de 1.5 K (ordenamiento magnético 3-D). Esto ha sido observado con un instrumento (PPMS) que mide el calor específico que desprende la muestra cuando se ordena. Como cabe de esperar, las interacciones en el compuesto que contiene cloro son más fuertes que en el compuesto que contiene bromo. Para ver el tipo de ordenamiento que tienen las cadenas, los datos experimentales de susceptibilidad magnética (medidos con el SQUID) y calor específico (medidos con el PPMS) se comparan con modelos teóricos. Los análisis indican que el tipo de interacción como cadenas de Heisenberg, con anisotropía en el plano XY , es decir, los espines (los electrones del ion de manganeso(III)) en la cadena prefieren estar posicionados en dirección XY . Sin embargo los compuestos de manganeso(III), tienen anisotropía de tipo Ising, $D < 0$, es decir,

los electrones prefieren estar en la dirección z . Para cuantificar la anisotropía y para confirmar el tipo de anisotropía, se estudiaron los compuestos por espectroscopía de resonancia paramagnética electrónica a campos magnéticos muy altos (HFEPN). Estos estudios (Apéndice A) revelaron una anisotropía de tipo Ising ($D < 0$) con un alto componente rómbico (E). Probablemente la ausencia del componente rómbico es el origen de las discrepancias en el signo de D . Los compuestos $[\text{Mn}(\text{HphpzMe})_2\text{X}]$ ($\text{X} = \text{Cl}, \text{Br}$) también forman cadenas 1-D. Sin embargo, el ligando H_2phpzMe induce que los iones de manganeso(III) estén más distanciados y como consecuencia, las interacciones antiferromagnéticas son más débiles que las observadas en $[\text{Mn}(\text{HphpzH})_2\text{X}]$ ($\text{X} = \text{Cl}, \text{Br}$), y no se observa ordenamiento a temperaturas superiores a 2 K. En el caso de $[\text{Mn}(\text{HphpzPh})_2\text{X}]$ ($\text{X} = \text{Cl}, \text{Br}$), la formación de cadenas está impedida y como la distancia entre los iones de manganeso(III) es grande, éstos no interactúan magnéticamente. Son paramagnéticos. En esta familia de compuestos $[\text{Mn}(\text{HphpzR})_2\text{X}]$ ($\text{R} = \text{H}, \text{Me}, \text{Et}, \text{Ph}$ y $\text{X} = \text{Cl}, \text{Br}$), el halógeno es lábil y hay una posición en la esfera de coordinación del ión de manganeso(III) que no está ocupada. Así que se han utilizado como reactivos para la síntesis de compuestos de mayor nuclearidad (Capítulo 3).

En el Capítulo 3, se describe cómo se han obtenido varios compuestos trinucleares de manganeso(III) con el núcleo $[\text{Mn}_3(\mu_3\text{-O})(\text{phpzR})_3]^+$. Los tres iones de manganeso(III) forman triángulo con un puente oxido en el que tres ligandos doblemente desprotonados H_2phpzR están en el plano formado por los tres iones de manganeso(III). En las posiciones axiales del ión de manganeso(III), se encuentran moléculas de disolventes y ligandos puente como acetatos o azidas. En el Capítulo 4, se ha estudiado el impacto en el núcleo $[\text{Mn}_3(\mu_3\text{-O})(\text{phpzR})_3]^+$ de las moléculas presentes en las posiciones axiales. Para ello se han reemplazado las moléculas de disolventes y los ligandos puente. Así pues, se observa cómo el tipo de ligandos pirazólicos determina el número de moléculas de disolventes y también el número y la manera de coordinación de los ligandos puente, pudiéndose observar diferentes topologías de trinucleares, desde cadenas, cadenas formadas por puentes de hidrógeno o moléculas aisladas. Las propiedades magnéticas de estos compuestos se han medido y analizado con el SQUID. Se ha observado que los iones de manganeso(III) en el triángulo interactúan antiferromagnéticamente de forma dominante. Pero aparentemente una distorsión en el núcleo $[\text{Mn}_3(\mu_3\text{-O})]^{7+}$, en la que los ángulos Mn-O-Mn son menores de 120° , inducen una interacción ferromagnética. Así pues para conseguir una interacción ferromagnética en el triángulo, se deberían distorsionar los tres ángulos hacia valores menores. Cuando los complejos trinucleares están formando cadenas 1-D gracias a los ligandos puentes o a enlaces de puente de hidrógeno, en la mayoría de los casos, existen interacciones ferromagnéticas entre los trinucleares.

En el Capítulo 5 (y en el apéndice B), se describen dos compuestos octanucleares con la fórmula general $[\text{Mn}_8(\mu_4\text{-O}_4)(\text{phpzH})_8(\text{disolvente})_4]$ (disolvente = tetrahidrofurano y etanol) y un hexanuclear $[\text{Mn}_6(\mu_3\text{-O})_4(\mu_3\text{-Br})_2(\text{HphpzEt})_6(\text{phpzEt})]$. El tipo de disolvente no influye en la formación de los compuestos octanucleares en la que se preserva el núcleo $[\text{Mn}_8(\mu_4\text{-O}_4)(\text{phpzH})_8]$. Ambos compuestos interaccionan fuerte antiferromagnéticamente, ya que la principal interacción magnética es dada por los iones de manganeso(III) entre el núcleo y la periferia. Sin embargo, el uso de sustituyentes de ligandos pirazólicos con grupos funcionales más grandes, impide la formación de compuestos octanucleares en determinadas condiciones sintéticas, y se observa la formación del compuesto hexanuclear $[\text{Mn}_6(\mu_3\text{-O})_4(\mu_3\text{-Br})_2(\text{HphpzEt})_6(\text{phpzEt})]$, en el cual interacciones ferromagnéticas están presentes.

En el Capítulo 6 se utilizan iones metálicos diferentes al manganeso(III), como cobalto(III), cobre(II) o níquel(II). Según el tipo de iones metálicos se pueden formar diferentes tipos de productos. En este caso, se observa la preferencia estructural del ión cobre(II) o el níquel(II) para formar compuestos plano cuadrados, $[\text{M}(\text{HphpzMe})_2]$. Con el uso de sales de cobalto(II), se observa como este tipo de ligando estabiliza el estado de oxidación 3, que es diamagnético, es decir, no tiene electrones desapareados. Lo interesante de este compuesto es que el ligando tiene cuatro maneras de coordinarse, mostrando su versatilidad y sus amplias posibilidades en la química de coordinación.

Finalmente, en el séptimo capítulo se resume el trabajo de investigación de esta tesis, analizando los resultados obtenidos, en los cuales se demuestra la versatilidad de los ligandos fenol-pirazólicos para la formación de clústeres de iones de manganeso con interesantes propiedades magnéticas. También se explican sugerencias para futuros trabajos.

Curriculum Vitae

Marta Viciano Chumillas was born in Valencia (Spain) on the 10th of June 1980. She started the chemistry degree in September 1998 and she graduated from the Universitat de València on September 2003. The last year of her degree she was granted an Erasmus fellowship to work in Leiden University, The Netherlands. The work studied was based on cross metathesis in allyl C-glycosides under the supervision of Dr. M.S.M. Timmer and Prof. H. S. Overkleeft in the Bio-organic Synthesis group.

From September 2004 to August 2005 she was working at the Packaging, Transport and Logistics Research Institute (ITENE). She left the job there to become a PhD student in the Coordination and Bioinorganic Chemistry group (CBAC) at Leiden University under the supervision of Prof. Dr. J. Reedijk, Prof. Dr. L. J. de Jongh and Dr. S. Tanase-Grecea. The research described in her PhD thesis has been supported by a Marie Curie scholarship (QueMolNa) and by the European Network of Excellence Magmanet. Part of the work was performed in collaboration with Dr. M. Evangelisti (Universidad de Zaragoza) on the specific heat measurements and Dr. J. Krzystek (Florida State University, National High Magnetic Field Laboratory) on the HFEPR studies. During her PhD studies, a research stage was carried out in the group of Prof. M. Julve and Prof. F. Lloret at the Universitat de València.

Part of the work has been presented at several conferences, among at several national conferences as the Netherlands Catalysis and Chemistry Conference (NCCC) (2006–2009) and the HRSMC Autumn School “Advanced Metal-Organic Chemistry” in 2006, and also at international conferences, as the European Congress on Molecular Magnetism in Tomar (Portugal) in 2006, the European Material Research Society (E-MRS) Spring Meeting in Strasbourg (France) in 2007, the 11th International Conference on Molecule-based Magnets (ICMM) in Florence (Italy) in 2008 and the 1st European Molecular Nanoscience School (EsMolNa) in Gandia (Spain) in 2008.

List of Publications

Timmer M. S. M., Viciano Chumillas M., Donker-Koopman W. E., Aerts J. M. F. G., van der Marel G.A., Overkleef H.S., van Boom J.H., “**Selective cross metathesis of C-allyl glucosides**”, *J. Carbohydr. Chem.*, **2005**, 24, 335–351.

Youngme S., Chotkhun T., Leelasubcharoen S., Chaichit N., van Albada G.A., Viciano-Chumillas M., Reedijk J., “**A unique trinuclear triply bridged Cu(II) compound containing double acetato and single azido bridges: synthesis, X-ray structure and magnetism of $[\text{Cu}_3(\text{dpyam})_2(\mu_{1,1}\text{-N}_3)_2(\mu\text{-CH}_3\text{COO-}\kappa\text{-O}^1)_2(\mu\text{-CH}_3\text{COO-}\kappa\text{-O}^1, \text{O}^2)] \cdot 2\text{H}_2\text{O}$ (dpyam = di-2-pyridylamine)**”, *Inorg. Chem. Commun.*, 2007, 10, 109–113.

Viciano-Chumillas M.; Tanase, S.; Aromí, G.; Smits, J. M. M.; de Gelder, R.; Solans, X.; Bouwman, E.; Reedijk, J., “**Coordination versatility of 5(3)-(2-hydroxyphenyl)-3(5)-methylpyrazole: synthesis, crystal structure and properties of Co^{III} , Ni^{II} and Cu^{II} complexes**”, *Eur. J. Inorg. Chem.*, **2007**, 2635–2640.

Bruijninx P.C.A., Viciano-Chumillas M., Lutz M., Spek A.L., Reedijk J., van Koten G., Gebbink R.J.M.K., “**Oxidative double dehalogenation of tetrachlorocatechol by a bio-inspired Cu^{II} complex: formation of chloranilic acid**”, *Chem. Eur. J.*, **2008**, 14, 5567–5576.

van Albada, G.A., Dominicus I., Viciano-Chumillas M., Mutikainen I., Turpeinen U., Reedijk J., “**A unique chain of trinuclear Cu(II) units containing both neutral and anionic N-(pyrimidin-2-yl) acetamide (Haapm, resp. aapm) as a ligand and dicyanamide (dca): synthesis, characterization, X-ray structure and magnetism of $[\text{Cu}_3(\mu\text{-aapm})_2(\mu\text{-dca})_2(\text{Haapm})_2](\text{CF}_3\text{SO}_3)_2$** ”, *Polyhedron*, **2008**, 27, 617–622.

Viciano-Chumillas M., Tanase S., Mutikainen I., Turpeinen U., de Jongh L.J., Reedijk J., “**Mononuclear manganese(III) complexes as building blocks for the design of trinuclear manganese clusters: study of the ligand influence on the magnetic properties of the $[\text{Mn}_3(\mu_3\text{-O})]^{7+}$ core**”, *Inorg.Chem.*, **2008**, 47, 5919–5929.

Viciano-Chumillas M., Giménez-Marqués M., Tanase S., Evangelisti M., Mutikainen I., Turpeinen U., Smits J.M.M., de Gelder R., de Jongh L. J., Reedijk J., “**Manganese(III) compounds of phenol-pyrazole-based ligands: synthesis, crystal structure, magnetic, and thermal properties**”, *J.Phys.Chem. C*, **2008**, 112, 20525–20534.

Tanase S., Viciano-Chumillas M., Smits J.M.M., de Gelder R., Reedijk J., “**Copper(II) and lanthanoid(II) complexes of a new β -diketonate ligand with an appended non-coordinating phenol group**”, *Polyhedron*, **2009**, 28, 457–460.

Viciano-Chumillas M., Tanase S., Mutikainen I., Turpeinen U., de Jongh L.J., Reedijk J., “**Manganese(III) compounds with phenol-pyrazole based-ligands: impact of the co-ligand and the carboxylate ligand on the trinuclear core $[\text{Mn}_3(\mu_3\text{-O})(\text{phpzR})_3(\text{O}_2\text{CR}')_n]^{1-n}$** ”, *Dalton Trans.*, **2009**, 7445–7453.

Viciano-Chumillas M., Marino N., Sorribes I., Vicent C., Lloret F., Julve M., “ **$[\text{Cr}(\text{dmbipy})(\text{ox})_2]^-$: a new bis-oxalato building block for metal assembling. Crystal structures and magnetic properties of $\text{XPh}_4[\text{Cr}(\text{dmbipy})(\text{ox})_2] \cdot 5\text{H}_2\text{O}$ (X = P and As), $\{\text{Ba}(\text{H}_2\text{O})_2[\text{Cr}(\text{dmbipy})(\text{ox})_2]_2\}_n \cdot 17/2n\text{H}_2\text{O}$ and $\{\text{Ag}(\text{H}_2\text{O})[\text{Cr}(\text{dmbipy})(\text{ox})_2]\}_n \cdot 3n\text{H}_2\text{O}$** ”, *Cryst EngComm*, accepted.

Acknowledgements

After these four years, this journey has finished and now it is time to acknowledge all the people who have contributed to this work. On y va...

First of all, I would like to acknowledge the LIC and LION for giving me the opportunity to conduct this thesis project.

Thanks to the group CBAC for sharing a lot of good moments, volleyball matches, barbecues, movie nights, beers, etc. It was nice to meet so many people!! I would like to give thanks to “my guys”, Joris, Raja, Jimmy (bedankt voor de samenvating!) and Tiddo. I really enjoyed sharing the office with all of you. Although some time I missed some girls around!!. Dank je wel, “peopleilla”. Lies, thank you for letting me being part of the “catalysis office”. Patricia, Ferry, Núria and Eva, you have been very special to me. We spent great times together, all these trips, discussions about science and life, dinners, etc. I will never forget them! en fin, por vuestra amistad!!.

I would like to mention my students: Mónica, you were my first one. We made a good team! Gracias por tu energía y por tus ánimos constantes. Ahora me toca dárteles a ti!!. Graham and Demis, I learnt a lot with both of you!!.

I also would like to acknowledge Gé for the helium fillings, for your help with the EPR machine and for your copper samples, in which I performed my first magnetic fits. Thank you Jos for your elemental analysis measurements and for your permanent smile. Jopie and John, you did all the ESI-MS, even at the last moment!. John, I really appreciated your immediate help every time I came to you with “do you have one moment?”. Thanks to the secretaries, Yvonne, Ingrid and Daniëlle for your help with the administrative issues.

Part of the scientific work presented here would not been possible without the help of a number of people. Ilpo, Jan and René, you determine all these crystal structures. Marco, thank you for your specific heat measurements. Perdón, gracias!. Jurek, you helped me to understand that these doodles are the science of HFEPR.

Moltes gràcies al labo de València. Gràcies Miguel per acollir-me dins del teu grup. I per les fruites tan bones! Miguel i Paco, feu una immillorable parella! Gràcies als dos per transmetre la il·lusió per la ciència, vostra sabiduria i el bon ambient. Gràcies també a Diana, Chelo i Jesús, i als demés.

Edo, I enjoyed all these conversations we had every time I went to physics for Squid measurements.

Thank to all the people that I have met in Leiden and all these old friends I met again. All of you made my life outside the lab nicer.

Plácido, Begoña y los peques, Laura y Dani, sois mi “familia holandesa” Por esos cafés y algunas cosas más!! Merche, esta aventura holandesa la hemos compartido juntas casi desde el principio. Y ahora la hacemos acompañadas. Grazie mille Orlando.

Gracias a mi gente de Valencia, a la “peña Sagrado”, en especial, a María A., Teresa, María V., Sheila (¡gracias por la portada!) y Víctor. También a Rosa y a Mamen, y a Javi. Porque a pesar de la distancia, estáis siempre ahí. Los verdaderos amigos se cuentan con las manos...

Aunque creo que todo esto no hubiese sido posible a mi familia. Yaya, por ¿y cuándo vuelves?, tus cartas y muchas cosas más. A mi hermano, porque está ahí cuando menos te lo esperas. Y como no, a mis padres, por todo vuestro apoyo incondicional y por compartir conmigo todo tipo de momentos. ¡¡Os quiero!!.

Oli, qu'est ce que je peux dire que tu ne sais pas?. Pour toutes les choses que nous avons partagées et toutes celles qu'il nous reste à partager. Mille mercis!!.

And the journey continues!

Bedankt!!

Marta